Inhibition of iNOS and eIF4A prevents cachexia-mediated muscle wasting

Jason Sadek

Department of Biochemistry

McGill University, Montreal

September 2022

Thesis submitted to McGill University in partial fulfillment of the requirements of the degree of Doctor of Philosophy

Table of Contents

List of Figures and Tables 5
List of Abbreviations 7
Abstract – English 11
Abstract – French 13
Acknowledgements 15
Author Contributions 16
Original Contributions to Knowledge 18
1 Literature Review and Introduction 20
1.1 Relevance of Cachexia 20
1.1.1 What is cachexia and what is its clinical impact? 20
1.1.2 Clinical Definition of Cachexia and Diagnostic Criteria 23
1.1.3 Current management Options Against Cachexia 28
1.2 Molecular Mechanisms and Biochemical Signatures of Cachexia-induced Muscle Wasting 30
1.2.1 Cachexia-Induced Suppression of Muscle Protein Synthesis 30
1.2.2 Cachexia-Induced Catabolic Pathways 34
1.2.2.1 Proteasome-Mediated Degradation 34
1.2.2.2 Autophagy 36
1.2.3 Metabolic Defect, Energetic Stress, and Oxidative Stress in Cachexia 38
1.2.3.1 Metabolite Biomarkers of Cachexia 40
1.2.3.2 Cachexia-Mediated Metabolome Derangement 42
1.2.3.3 Impairment of Energy Production and Downstream Effects of Energy Crisis 48
1.3 Initiation of Cachexia: Systemic and Intracellular Factors 52
1.3.1 Initiators of Pro-Cachectic Signaling 54
1.3.1.1 Tumor Necrosis Factor Alpha and Interferon Gamma 54
1.3.1.2 Interleukin 6 and Leukemia Inhibitory Factor 56
1.3.1.3 Interleukin 1 59
1.3.1.4 Myostatin, Activin A, and Growth Differentiation Factor 11 60
1.3.2 Pro-Cachectic Transcription Factors 62
1.3.2.1 SMAD2, SMAD3, and FOXO 63
1.3.2.2 NF-κB 64
1.3.2.3 STAT3 66
1.3.3 Inducible Nitric Oxide Synthase and Cachexia 69

1.3.3.1 Role of Reactive Oxygen/Nitrogen Species in Impairing Energy Metabolism....75
1.4 Rationale 79
2 Pharmacological or genetic inhibition of iNOS prevents cachexia-mediated muscle wasting and its associated metabolism defects....82
2.1 Genetic deletion of the iNOS gene prevents inflammation-induced muscle wasting....82
2.2 Ablation of iNOS gene prevents sepsis-induced energy crisis....92
2.3 The iNOS inhibitor GW274150 prevents inflammation-induced muscle wasting....96
2.4 The iNOS inhibitor GW274150 prevents cancer-mediated disruption of energy production in wasting muscle....103
2.5 iNOS activity causes wasting of myotubes treated with pro-cachectic cytokines and disrupts the mitochondrial Electron Transport Chain....108
2.6 iNOS disrupts the mitochondrial structure in wasting skeletal muscle 116
3 eIF4A inhibition prevents the onset of cytokine-induced muscle wasting by blocking the STAT3 and iNOS pathways 119
3.1 The eIF4A allosteric inhibitor Hippuristanol recapitulates the actions of Pateamine A on cytokine-induced muscle wasting and the iNOS/NO pathway. 119
3.2 Hippuristanol reduces cytokine-induced activation of the STAT3 pathway. 123
3.3 Pateamine A and Silvestrol decrease activation of the STAT3 pathway in cytokine-treated myotubes. 126
4 Materials and Methods....129
4.1 Reagents 129
4.2 Antibodies....129
4.3 Cell Culture....130
4.4 Immunoblotting 131
4.5 Detection of media nitrite levels and IL-6 132
4.6 Reverse Transcription Quantitative PCR (RT-qPCR) 133
4.7 GC-MS metabolomic analysis....133
4.8 Cellular ATP content....134
4.9 Extracellular flux and bioenergetics analysis....134
4.10 Animal models 135
4.11 Grip strength....137
4.12 Fluorescence-activated cell sorting (FACS) 137
4.13 Muscle freezing and sectioning....138
4.14 Histological analysis of muscle cross-sectional area....138

4.15 Immunofluorescence....138
4.16 Transmission electron microscopy....139
4.17 Statistics and data processing....140
5 General Discussion....142
5.1 Overview....142
5.2 How does iNOS disrupt mitochondrial function and overall metabolism?....145
5.3 How does iNOS impair the myogenic program?....149
5.4 How does iNOS and eIF4A inhibition affect inflammatory signaling?....152
5.5 Does eIF4A inhibition affect STAT3 translation?....153
5.6 Conclusion: Repurposing GW274150 and developing eIF4A inhibitors for the treatment of cachexia in clinic....154
Appendices....158
References....173

List of Figures and Tables

Figure 1.1: Stages of cancer cachexia and management algorithm for cancer cachexia. 25
Figure 1.2 Invasiveness of interventions relative to expected survival. 29
Figure 1.3 Maintenance of Muscle Energy Metabolism Prevents Muscle Wasting. 33
Figure 1.4: Mitochondrial dysfunction in skeletal muscle negatively regulates muscle mass. 40
Table 1.1: Summary of muscle metabolites altered in cachectic muscle 47
Figure 1.5: Mitochondrial Fusion and Fission. 51
Figure 1.6: Signaling pathways leading to muscle atrophy. 53
Figure 1.7: Active NF-κB pathway is required for the rapid translocation of pY-STAT3 to the nucleus during IFNγ/TNFα-induced muscle wasting. 70
Figure 1.8: iNOS regulates glucose and lipids metabolism under inflammatory conditions. 72
Figure 1.9: Mechanisms of oxidative stress-induced muscle wasting. 77
Figure 2.1: iNOS knockout mice are resistant to LPS-driven muscle wasting. 85
Figure 2.2: Characterization of the LPS-induced effects on muscle integrity/composition in WT and iNOS KO mice. 87
Figure 2.3: Characterization of the LPS-induced immune response in WT and iNOS KO mice. 90
Figure 2.4: Genetic ablation of iNOS prevents LPS-driven deregulation of the TCA cycle and energy production. 94
Figure 2.5: Effect of GW on the immune response as well as muscle integrity/composition in C26-tumor bearing mice. 99
Figure 2.6: GW274150 treatment reduces muscle wasting in the C26 model. 101
Figure 2.7: Pharmacological inhibition of iNOS reduces C26-induced derangement of amino acids and impairment of energy production. 106
Figure 2.8: Cytokine treatment of C2C12 myotubes alters the levels of TCA cycle intermediates and activates AMPK in an iNOS-dependent manner. 110
Figure 2.9: GW274150 prevents a cytokine-induced shift to aerobic glycolysis in C2C12. 114
Figure 2.10: Inflammation-mediated loss of Complex II and IV integrity are reversed with GW274150. 115
Figure 2.11: Inflammation-mediated loss of mitochondrial integrity are reversed with genetic and pharmacological inhibition of iNOS. 117
Figure 3.1: Hippuristanol (Hipp), an eIF4A inhibitor, prevents IT-induced muscle wasting. 121
Figure 3.2: Hippuristanol (Hipp) prevents IT-mediated activation of the pro-cachectic iNOS/NO pathway. 122

Figure 3.3: Hippuristanol (Hipp) decreases IL-6 mRNA expression and secretion in IT-treated myotubes. 124
Figure 3.4: Hippuristanol (Hipp) inhibits STAT3 protein, but not STAT3 mRNA levels, in IT-treated myotubes. 125
Figure 3.5: Pateamine A recapitulates the impact of Hippuristanol on IL-6 secretion and STAT3 protein levels. 127
Figure 3.6: Silvestrol perturbs iNOS and STAT3 protein expression. 128
Figure 5.1: Schematic depicting the role of the iNOS/NO pathway in promoting energy crisis during cachexia-induced muscle wasting. 144
Figure 5.2*: In vitro* analysis of HuR nitration. 151

List of Abbreviations

3NT	3-nitrotyrosine
4E-BP1	4E-binding protein 1
ACC	acetyl-CoA carboxylase
ActRIIB	Activin Type II B
AICAR	5-aminoimidazole-4-carboxamide ribonucleotide
AKG	α-ketoglutarate
AMG	aminoguanidine
AMPK	AMP-activated protein kinase
APR	acute phase response
ASCO	American Society of Clinical Oncology
BCAA	branched chain amino acids
C/EBPδ	CAAT/enhancer-binding protein δ
C26	colon-26 adenocarcinoma
CASCO	Cachexia Score
CAT1	cationic amino acid transporter 1
CHF	chronic heart failure
CKD	chronic kidney disease
CNS	central nervous system
COPD	chronic obstructive pulmonary disorder
CPT	carnitine palmitoyltransferase
CRP	C reactive protein
CSA	cross-sectional area
CSS	cachexia staging score
DRP-1	dynamin-related protein 1
ECAR	extracellular acidification rate
eIF4A	eukaryotic initiation factor-4A
eIF4E	eukaryotic initiation factor 4E

EMSO	European Society for Medical Oncology
eNOS	endothelial Nitric oxide synthase
ETC	electron transport chain
EV	extracellular vesicles
FOXO	forkhead box protein O
GDF11	Growth Differentiation Factor 11
gp130	glycoprotein 130
GW	GW274150
Hipp	Hippuristanol
HK	hexokinase
HuR	Human antigen R
IDH	isocitrate dehydrogenase
IFNγ	interferon gamma
IGF-1	Insulin-like Growth Factor 1
IKK	IkB kinase
IL-1	interleukin 1
IL-6	interleukin 6
IMM	inner mitochondrial membrane
iNOS	inducible nitric oxide synthase
IκB	Inhibitor of κB
JAK	Janus Kinase
J-ATP	rate of ATP production
KO	knockout
LCADH	long-chain Acyl-CoAs dehydrogenase
LIF	Leukemia Inhibitory Factor
LPS	lipopolysaccharide
MCASCO	MiniCASCO
MFN	mitofusin

MnSOD	manganese SOD
MRF	myogenic regulatory factors
mTOR	mammalian target of rapamycin
MyHC	myosin heavy chain
NF-κB	nuclear factor-κB
nNOS	neuronal nitric oxide synthase
NO	nitric oxide
NOS	nitric oxide synthase
Nox	NADPH oxidase
NRF-1	nuclear response factor-1
NSCLS	non-small cell lung cancer
OCR	oxygen consumption rate
OPA1	optic atrophy protein 1
OXPHOS	oxidative phosphorylation
PatA	Pateamine A
Pax7	paired box 7
PDH	pyruvate dehydrogenase
PDK	PDH kinase
PFK	phosphofructokinase
PGC-1α	peroxisome proliferator–activated receptor-γ coactivator-1α
PI3K	phosphoinositide 3-kinase
PIF	proteolysis-inducing factor
PLS-DA	partial least squares discriminant analysis
PTM	post-translational modifications
RBP	RNA binding protein
RNS	reactive nitrogen species
ROS	reactive oxygen species
RRM	RNA recognition motif

S6	ribosomal protein S6
S6K	ribosomal protein S6 kinase
SDH	succinate dehydrogenase
SIRT-1	sirtuin 1
SOD	superoxide dismutase
STAT3	Signal Transducer and Activator of Transcription 3
TA	tibialis anterior
TCA	tricarboxylic acid
TEM	transmission electron microscopy
Tfam	mitochondrial transcription factor A
TGFβ	transforming growth factor-β
TNFα	tumor necrosis factor alpha
UPP	ubiquitin proteasome pathway
UTR	untranslated region
WT	wildtype

Abstract – English

Cachexia syndrome is a co-morbidity that can arise in several late-stage diseases such as cancer, chronic heart failure, and chronic obstructive pulmonary disease. This syndrome is characterized by the severe, excessive loss of mass due, in part, to the wasting of skeletal muscle. Although the syndrome is a major contribution to patient frailty and mortality, there are no effective treatments for this condition. In recent decades, our understanding of the etiology and pathology of cachexia has advanced significantly. Numerous targets involved in the initiation and progression of this condition have been identified. However, due to the overlapping function of these targets and the complex nature of the condition, previous attempts to cure cachexia have been unsuccessful. Therefore, a new approach to cachexia treatment is needed. In this thesis I have studied the therapeutic potential of targeting the function of two proteins, inducible nitric oxide synthase (iNOS) inhibition and eukaryotic initiation factor-4A (eIF4A) as treatment options for cachexia-induced muscle wasting. In Chapter 2, I focused on iNOS which is a main downstream effector of cachexia. In this work, I showed that genetic ablation of iNOS or direct inhibition of iNOS with a drug named GW274150 (GW), which was previously used in Phase 2 clinical trials for the treatment of migraines and rheumatoid arthritis, protects against atrophy in preclinical models of cachexia. Furthermore, I demonstrated that iNOS promotes wasting by disrupting cellular metabolism in cachectic skeletal muscle by impairing mitochondrial processes. I also show that these metabolic disturbances can be reversed by inhibition of iNOS. This work demonstrated mechanistically how iNOS promotes muscle wasting and provides a proof of principle for the repurposing of the iNOS inhibitor GW for the treatment of

cachexia-induced muscle loss. Work from our lab has also shown that perturbation of iNOS expression is also a potential therapeutic strategy to prevent cachexia-induced muscle wasting. Notably, one of these studies demonstrated that pateamine A, an eIF4A inhibitor, prevented muscle wasting by blocking the translation of the iNOS mRNA. In Chapter 3, I provided additional proof demonstrating that targeting eIF4A can be envisioned as a therapeutic strategy to prevent muscle wasting. We demonstrate that the compound hippuristanol, which inhibits eIF4A with a distinct mechanism of action from pateamine, prevents muscle wasting. Furthermore, I showed that hippuristanol can inhibit the translation of other pro-cachectic factors such as the key pro-cachectic transcription factor, Signal Transducer and Activator of Transcription 3 (STAT3), thereby perturbing the activation of the STAT3 pathway and expression of pro-cachectic STAT3-gene targets including Interleukin-6. Taken together this thesis proposes two promising treatment options against cachexia and offers mechanistic insight into how these drugs prevent muscle wasting through their modulation of key metabolic processes and inflammatory signaling.

Abstract – French

Le syndrome de la cachexie est une comorbidité qui peut surgir dans plusieurs maladies de niveaux avancés, tel que le cancer, l'insuffisance cardiaque chronique, et la maladie pulmonaire obstructive chronique. Ce syndrome est caractérisé par une perte sévère de masse excessive, partiellement due à la fonte de muscles squelettiques. Quoique ce syndrome contribue de façon majeure à la fragilité et la mortalité des patients, il n'existe pas de traitements efficaces pour cette condition. Durant les récentes décennies, notre compréhension de l'étiologie et la pathologie de cette condition ont significativement avancé. De nombreuses cibles impliquées dans l'initiation et la progression de cette condition ont été identifiées. Cependant, due au recoupement des fonctions de ces cibles, et la nature complexe de cette condition, les tentatives précédentes pour guérir la cachexie ont échoué. Ainsi, une nouvelle approche est nécessaire pour le traitement de la cachexie. Dans cette thèse, j'ai étudié le potentiel thérapeutique de cibler la fonction de deux protéines, la synthétase d'oxide nitrique inductible (iNOS) et le facteur d'initiation eucaryotique 4A (eIF4A), comme étant une option de traitement pour la fonte musculaire induite par la cachexie. Dans le chapitre 2, je me suis concentré sur iNOS, qui est un effecteur principal en aval de la cachexie. Dans ce travail, je montre que l'ablation génétique de iNOS ou l'inhibition directe de iNOS à l'aide d'un médicament nommé GW274150 (GW), qui a précédemment été utilisé dans des essais cliniques de Phase 2 pour le traitement de migraine et de la polyarthrite rhumatoïde, protège contre l'atrophie dans des modèles précliniques de la cachexie. De plus, je démontre que iNOS promeut la fonte musculaire en perturbant le métabolisme cellulaire des muscles squelettiques

cachectiques en altérant des procès mitochondriaux. Également, je montre que ces perturbations métaboliques peuvent être inversées par l'inhibition de iNOS. Ce travail démontre le mécanisme par lequel iNOS promeut la fonte musculaire et fournit une preuve de principe pour la réaffectation de l'inhibiteur de iNOS GW au traitement de la perte musculaire induite par la cachexie. D'autres travaux de notre laboratoire ont montré que la perturbation de l'expression de iNOS est une autre stratégie thérapeutique potentielle pour empêcher la fonte musculaire induite par la cachexie. Notamment, une de ces études démontre que pateamine A, un inhibiteur de eIF4A, a empêché la fonte musculaire en bloquant la traduction de l'ARNm de iNOS. Dans le chapitre 3, j'ai fourni des preuves additionnelles qui démontrent que cibler eIF4A peut-être envisagé comme étant une stratégie thérapeutique pour empêcher la fonte musculaire. Nous démontrons que le composé hippuristanol, qui inhibe eIF4A à l'aide d'un mécanisme d'action distinct de celui de pateamine A, empêche la fonte musculaire. De plus, je démontre que l'hippuristanol peut inhiber la traduction d'autres facteurs pro-cachectiques tel que le facteur de transcription pro-cachectique principal, capteur de signal et activateur de transcription 3 (STAT3), perturbant ainsi l'activation de la voie de STAT3 et l'expression de gènes pro-cachectiques cibles de STAT3, incluant l'interleukine-6. En somme, cette thèse propose deux options de traitements prometteurs contre la cachexie et offre un aperçu mécanistique de comment ces médicaments peuvent empêcher la fonte musculaire en modulant des procès métaboliques et les signalements inflammatoires principaux.

Acknowledgements

I am incredibly lucky to have such wonderful family, friends, and mentors who have supported me on my journey to completing my doctoral studies. First and foremost, I would like to thank Imed. Thank you for welcoming me to your lab many years ago and guiding me to develop from the undergraduate volunteer I began as to the scientist I am today. You have instilled in me a strong determination and an enthusiasm for science which will drive me forward in my future pursuits. I am forever grateful for what I have achieved under your supervision. Thank you, Sergio, you have been instrumental in my training as a mentor, helping me succeed in my goals, and I appreciate your friendship along with those unexpected pranks that can strike from even 500 miles away. A big thanks to Derek and Amr, in the lab you set strong examples for me and encouraged my growth as a scientist. I have enjoyed working with you so much and I treasure your friendship and our great experiences in and out the lab. To Anne-Marie and Souad, I hold dearly our many good times together and I will miss our big collection days and our chats on our commutes home. Brenda, Xian, Kholoud, Philippe, Bianca, Pauline, Sandrine, and Romane you have been a joy to work with and I am so happy to have gotten to know all of you. Thank my committee members Dr. Danuta Radzioch, Dr. Colin Crist, and Dr. Natasha Chang for their invaluable advice over the years.

Lastly, I would like to thank my family. To my fiancée Hayley, your love, support, and care has helped me overcome every challenge I've faced, and I've cherished these last five years with you with many more to come. Thank you to my Mom, my Dad, and my brother Jack. I could not have asked for a better family. Your shining examples have been an ideal to strive for and your love has driven me forward.

Author Contributions

The specific contributions of co-authors for this traditional thesis are highlighted below. This thesis is comprised of results from two published articles in Chapter 2 and Chapter 3 which were modified for the traditional thesis format.

Chapter 2: Pharmacological or genetic inhibition of iNOS prevents cachexia-mediated muscle wasting and its associated metabolism defects

Jason Sadek, Derek T Hall, Bianca Colalillo, Amr Omer, Anne-Marie K Tremblay, Virginie Sanguin-Gendreau, William Muller, Sergio Di Marco, Marco Emilio Bianchi, and Imed-Eddine Gallouzi

I was responsible for experimental design, conducting all the experimental investigations with the assistance from the co-authors, and performing the formal analysis and visualization of experimental findings. Dr. Derek Hall assisted with sample collection and preparation in animal studies utilizing the C26 adenocarcinoma model, conducted *in vitro* Seahorse studies, and assisted with characterization of the *in vitro* model used. Bianca Colalillo assisted with sample collection and processing for western blot analyses for *in vitro* studies and assisted with the animal studies utilizing the LPS sepsis model. Dr. Amr Omer assisted with RT-qPCR analyses, preparing muscle sections for immunofluorescence microscopy, and assisted with the animal studies in the LPS model. Anne-Marie Tremblay assisted with animal studies performing collection and preparation of mouse samples analyzed. Virginie Sanguin-Gendreau performed flow cytometry sample processing and data analysis. Dr. William Muller assisted with the interpretation of the flow cytometry data. Dr. Sergio Di Marco assisted with experimental design, data analysis, and data interpretation. Dr. Marco Emilio Bianchi

assisted with data interpretation. Dr. Imed-Eddine Gallouzi supervised the experimental design, execution, data interpretation, and progress of the project.

Chapter 3: eIF4A inhibition prevents the onset of cytokine-induced muscle wasting by blocking the STAT3 and iNOS pathways

Zvi Cramer, Jason Sadek, Gabriela Galicia Vazquez, Sergio Di Marco, Arnim Pause, Jerry Pelletier, and Imed-Eddine Gallouzi

I was responsible for design of key experiments assessing the role of Hippuristanol, Pateamine A, and Silvestrol on the iNOS/NO pathway, STAT3 Pathway, and IL-6 expression. I participated in carrying out all experiments in the chapter with the assistance from the co-authors. In addition, I performed formal analysis and visualization of experimental findings. Zvi Cramer assisted with conception and design of experiments characterizing the *in vitro* model as well as analyzing and visualizing experimental findings. Dr. Sergio Di Marco assisted with key experiments and helped with data analyses and interpretation. Gabriela Galicia Vazquez assisted with characterization of the *in vitro* model. Dr. Arnim Pause helped in the conceptualization of the original idea and data interpretation. Dr. Jerry Pelletier provided key reagents and helped with data interpretation. Dr. Imed-Eddine Gallouzi conceptualized, established, and supervised the execution of research goals and data analysis and interpretation.

Chapter 5: General Discussion

I conceptualized, performed, analyzed, and interpreted experimental results shown in the discussion under the supervision of Dr. Imed-Eddine Gallouzi.

Original Contributions to Knowledge

Chapter 2: Pharmacological or genetic inhibition of iNOS prevents cachexia-mediated muscle wasting and its associated metabolism defects

- Identified a new mechanism by which iNOS mediates cachexia-induced muscle wasting through disruption of skeletal muscle metabolism and energy homeostasis.
- Demonstrated that genetic ablation of the iNOS enzyme or its inhibition with the drug GW274150 protects mice against cachexia-induced muscle wasting and metabolic defect initiated by either LPS-mediated inflammation or C26 adenocarcinoma tumors.
- Showed that iNOS disrupts mitochondrial content, morphology, and energy production processes in sepsis- and cancer-induced cachexia.
- Determined that iNOS impairs oxidative phosphorylation and causes energetic stress, leading to wasting.
- Provided proof of principle for the repurposing of the iNOS inhibitor GW274150 for the treatment of cachexia-induced muscle wasting.

Chapter 3: eIF4A inhibition prevents the onset of cytokine-induced muscle wasting by blocking the STAT3 and iNOS pathways

- Identified the potential use of drugs that target eIF4A to prevent cachexia induced muscle wasting by inhibiting the expression and subsequent activation of eIF4A-responsive pro-cachectic factors, such as STAT3 or iNOS.
- Demonstrated that Hippuristanol, a chemical inhibitor of eIF4A, prevents cachectic muscle wasting *in vitro*.

- Showed that hippuristanol prevents the activation of the pro-cachectic STAT3 and iNOS signaling pathways by preventing the expression, at the translational level, of STAT3 and iNOS, respectively.
- Determined that the effect of Hippuristanol is specific to inhibition of eIF4A since these results were recapitulated using additional eIF4A inhibitors Pateamine A and silvestrol.

1 Literature Review and Introduction

1.1 Relevance of Cachexia

1.1.1 What is cachexia and what is its clinical impact?

Cachexia is a severe wasting syndrome which develops as a result of multiple chronic, pro-inflammatory conditions (Baracos *et al*, 2018; Evans *et al*, 2008; Peixoto da Silva *et al*, 2020; Scherbakov & Doehner, 2018; Springer *et al*, 2006). These conditions include cancer, infections (e.g., sepsis, tuberculosis, and AIDS), chronic organ diseases (e.g., heart, lung, and kidney), and auto-immune conditions (e.g., rheumatoid arthritis) (Baracos *et al.*, 2018; Evans *et al.*, 2008; Peixoto da Silva *et al.*, 2020; Scherbakov & Doehner, 2018; Springer *et al.*, 2006). The prevalence of cachexia accompanying these diseases is variable, most frequently arising in later stages of disease progression (Baracos *et al.*, 2018; Peixoto da Silva *et al.*, 2020; Scherbakov & Doehner, 2018; von Haehling *et al*, 2016). Furthermore, the occurrence of cachexia in disease is often imprecisely estimated due to inconsistencies in defining the syndrome which are highlighted in the following section (Springer *et al.*, 2006). Considering this discrepancy in diagnosis, estimates on the prevalence of cachexia in these chronic diseases range from 5 to 90% depending on the condition (Scherbakov & Doehner, 2018; von Haehling *et al.*, 2016). Within cancers themselves, the prevalence varies widely, with pancreatic cancers having the highest prevalence and prostate cancers having the lowest (Baracos *et al.*, 2018).

Cachexia causes a variety of symptoms which contribute to important clinical outcomes including increased frailty, lower quality of life, and decreased survival(Baracos *et al.*, 2018; Peixoto da Silva *et al.*, 2020). Cachectic patients have

significantly increased mortality rates compared to non-cachectic counterparts suffering from similar diseases. For example, cachexia increases 18-month mortality rates of heart failure patients from 17% to 50%(Anker *et al*, 1997; Springer *et al.*, 2006). In advanced cancer, weight stable patients also had significantly higher median survival compared to cachectic patients that experienced severe weight loss (Martin *et al*, 2015). A very significant symptom contributing to lower survival is the irreversible and involuntary loss of muscle and, in many cases, adipose tissue that results in extreme weight loss (Baracos *et al.*, 2018; Kazemi-Bajestani *et al*, 2016; Scherbakov & Doehner, 2018). A defining characteristic of cachectic weight loss is that it cannot be reversed by nutritional supplementation which distinguishes it from other wasting conditions such as malnutrition(Evans *et al.*, 2008; Fearon *et al*, 2011). In patients suffering from late-stage disease, this loss of mass can be a primary contributor to mortality for several reasons. Decreased mass can lower patient tolerance to treatments against their primary disease (Kazemi-Bajestani *et al.*, 2016). This has a dual effect in that it increases drug toxicity or decreases tolerance to surgical intervention, and it allows the primary condition to progress leading to negative patient outcomes (Kazemi-Bajestani *et al.*, 2016). Alternatively, decreased mass and impaired function of critical muscles (i.e., heart and diaphragm) can also lead to death (Kalantar-Zadeh *et al*, 2013). Indeed, cachexia has been associated with cardiac dysfunction, heart failure and sudden cardiac death (Kalantar-Zadeh *et al.*, 2013). Furthermore, decreased diaphragm function contributes to respiratory difficulties (Kalantar-Zadeh *et al.*, 2013). Reduced skeletal muscle mass can also lead to significant reduction in overall physical performance in cachectic patients (Scherbakov & Doehner, 2018). This is commonly manifested in lower activity

levels and strength in cachectic patients compared to non-cachectic counterparts, which lead to further functional deconditioning and deterioration (Argilés *et al*, 2017; Evans *et al.*, 2008; Fearon *et al.*, 2011; Muscaritoli *et al*, 2010).

In addition to wasting, nutritional deficiencies are prominent in cachectic patients who frequently display loss of appetite and malabsorption (Evans *et al.*, 2008; Fearon *et al.*, 2011; Peixoto da Silva *et al.*, 2020). Cachectic patients often suffer from secondary anorexia, which is the loss of appetite resulting from chronic inflammatory responses, due to the high levels of inflammation driving the cachectic process (Peixoto da Silva *et al.*, 2020). In patients suffering from anorexia and cachexia, the normal function of neuronal pathways that regulate satiety and feeding responses are disrupted leading to suppression of appetite (Nicolini *et al*, 2013; Peixoto da Silva *et al.*, 2020). To compound the caloric deficit inflicted by anorexia, inflammation-mediated reduction in gut barrier function and alteration of gut microbiota can further reduce macronutrient absorption and energy levels in cachectic patients (Kalantar-Zadeh *et al.*, 2013; Peixoto da Silva *et al.*, 2020). Although not being solely responsible for the wasting observed in cachexia, nutritional deficiencies cannot be neglected. They have pervasive and multifactorial effects on quality of life and mental health and are associated with patient mortality.

The large body of work characterizing the signs and symptoms of cachexia is crucial in defining and diagnosing this deadly syndrome. Understanding the contribution of various manifestations of the cachexia syndrome is key in identifying targets for therapy. Due to the diversity of the causes and the symptomology of the condition, it is important

to develop an internationally standardized method of diagnosis to advance the treatment of the condition.

1.1.2 Clinical Definition of Cachexia and Diagnostic Criteria

A widely agreed upon step in combating and developing new therapeutics against cachexia is the formation of a consensus clinical definition and an effective classification system to grade the syndrome (Argilés *et al*, 2011; Blum *et al*, 2014; Evans *et al.*, 2008; Fearon *et al.*, 2011; Garcia *et al*, 2022; Martin *et al.*, 2015; Vigano *et al*, 2017; Zhou *et al*, 2018). Establishing a uniform system that can be used to classify/grade the syndrome will enable future clinical trials to have consistent inclusion criteria. It will also allow regulatory agencies to better assess the efficacy of candidate drugs (Argilés *et al.*, 2011; Baracos *et al.*, 2018; Blum *et al.*, 2014; Evans *et al.*, 2008; Fearon *et al.*, 2011; Garcia *et al.*, 2022). Although the definition of cachexia is generally agreed upon, the criteria in diagnosing cachexia, especially cancer cachexia, are debated with various scoring systems in place. The generally accepted unifying definition of cachexia was developed during the “Cachexia Consensus Conference” in 2006 (Evans *et al.*, 2008). Leaders in the field agreed on the following base definition: ‘‘Cachexia is a complex metabolic syndrome associated with underlying illness and characterized by loss of muscle with or without loss of fat mass. The prominent clinical feature of cachexia is weight loss in adults (corrected for fluid retention) or growth failure in children (excluding endocrine disorders). Anorexia, inflammation, insulin resistance, and increased muscle protein breakdown are frequently associated with cachexia. Cachexia is distinct from starvation, age-related loss of muscle mass, primary depression, malabsorption, and hyperthyroidism, and is associated with increased morbidity (Evans *et al.*, 2008).” This

initial system designated patients as cachectic when they exhibited weight loss of at least 5% in 12 months or less in the presence of underlying illness, in addition to three of the following symptoms: decreased muscle strength, fatigue, anorexia, low fat-free mass index, and abnormal biochemistry (increased inflammatory markers (e.g., the acute phase reactant protein C reactive protein (CRP), interleukin-6), anemia, low serum albumin) (Evans *et al.*, 2008). Although these experts came to a consensus on defining and diagnosing the syndrome, the application of these metrics was refined for the diagnosis of cancer cachexia.

Between the development of the consensus definition of cachexia in 2006 to the present, several additional classification systems have been proposed to score the presence and severity of cancer cachexia. These systems have focused on scoring the stage of cachexia progression and its severity. In 2011, Fearon et al. published an international consensus on the definition and classification of cancer cachexia that expanded upon the 2006 consensus by proposing 3 stages of cachexia: precachexia, cachexia, and refractory cachexia (Fearon *et al.*, 2011). This cancer cachexia-focused consensus suggested clinical characteristics on how to stratify and treat patients in each stage (Figure 1.1). Importantly, it provided a framework to facilitate the design of clinical trials, new treatment regiments based on stage, and routine clinical management (Fearon *et al.*, 2011).

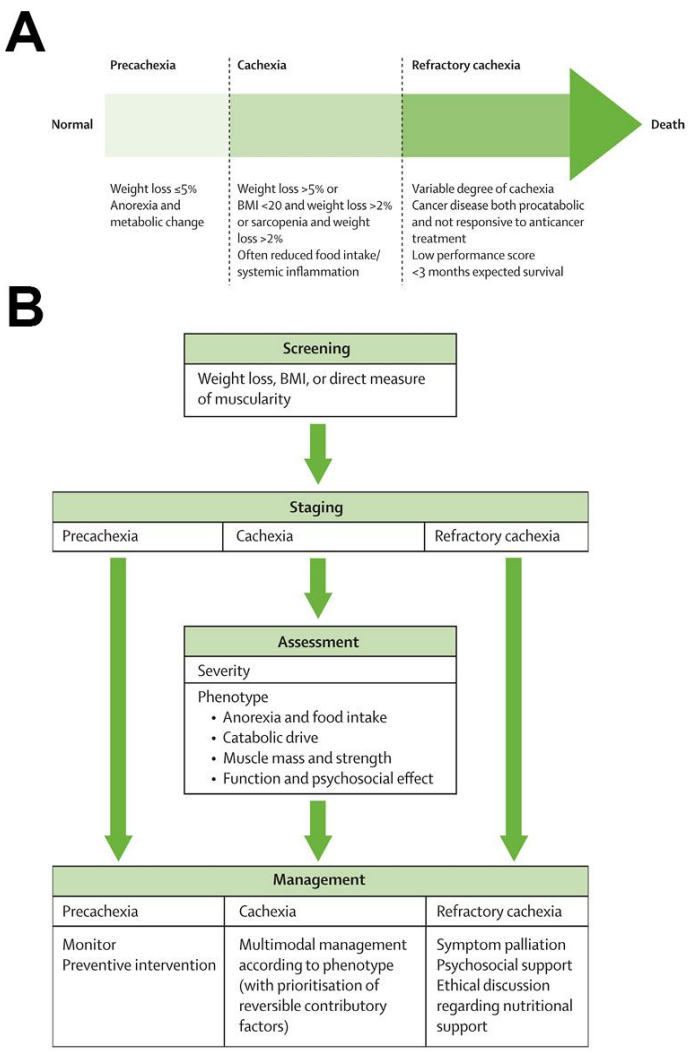

Figure 1.1: Stages of cancer cachexia and management algorithm for cancer cachexia.

(A) Cachexia represents a spectrum through which not all patients will progress. At present there are no robust biomarkers to identify those precachectic patients who are likely to progress further or the rate at which they will do so. Refractory cachexia is defined essentially on the basis of the patient's clinical characteristics and circumstances. BMI=body-mass index. (B) Patients should be screened for cachexia, then undergo detailed assessment. All patients require optimum oncological and general medical management. Once patients with cachexia have been phenotyped, a detailed multimodal management plan (including nutrition, exercise, anti-inflammatory strategies, and other adjuncts) can be established. BMI=body-mass index. *Reprinted from Fearon K, Strasser F, Anker SD, Bosaeus I, Bruera E, Fainsinger RL, Jatoi A, Loprinzi C, MacDonald N, Mantovani G (2011) Definition and classification of cancer cachexia: an international consensus. The lancet oncology 12: 489-495 with permission from Elsevier.*

In 2014 a validation study of the consensus framework was published, which stratified the cachexia stages by weight loss and BMI (Blum *et al.*, 2014). They were able to distinguish between cachectic and non-cachectic patients, but ultimately more parameters were needed to discriminate precachectic patients from non-cachectic patients (Blum *et al.*, 2014). Additional assessment of CRP levels and appetite loss for identification of precachexia resolved this issue highlighting the benefit of adding biomarkers in classification systems (Blum *et al.*, 2014). In line with this, studies by Vigano in 2012 and 2017 evaluated the relevance of the four stages of cachexia and proposed added criteria to apply them to clinical practice (Vigano *et al*, 2012; Vigano *et al.*, 2017). However, these criteria were unable to demarcate precachectic and cachectic patients suggesting that more work is needed to define supporting criteria to weight loss (Vigano *et al.*, 2012; Vigano *et al.*, 2017).

In 2011 an alternative cancer cachexia staging tool was proposed called the Cachexia Score or CASCO (Argilés *et al.*, 2011). Unlike other classification systems (described above) this tool scored cachexia severity on a numerical scale based on body weight loss, lean body mass loss, various inflammation markers, markers of metabolic disruption, markers of immunosuppression, physical performance, anorexia, and quality of life assessments (Argilés *et al.*, 2011). This study also proposed a tentative method of detecting precachexia in patients not presenting loss of body weight to address the growing attention to this stage (Argilés *et al.*, 2011; Muscaritoli *et al.*, 2010). In 2017, CASCO's ability to classify the severity of cachexia was validated and its parameters were simplified in the MiniCASCO (MCASCO) tool (Argilés *et al.*, 2017). The ability of CASCO and MCASCO to predict patient survival was not tested though

and should be a critical aspect of future studies to prove its effectiveness over body composition focused scoring systems.

Accounting for the wide range of BMI seen in cancer patients, an alternative classification system for cancer cachexia was developed and validated by Martin *et al.* (Martin *et al.*, 2015). In this system, 5 grades of cachexia severity (0 – 4) were developed based on median survival of patients in relation to their % weight loss and BMI. A strong correlation between low BMI, high % weight loss, and low median survival time was identified without the use of other biochemical factors or lean muscle mass measurements emphasizing the utility of in-depth assessment of weight loss in cachexia diagnosis (Martin *et al.*, 2015).

Lastly, the cachexia staging score (CSS) published in 2018 addressed the limitations of the previously described diagnostic tools (Zhou *et al.*, 2018). The CSS developed by Zhou et al. scored patients from 0 (no cachexia) to 12 (refractory cachexia) based off weight loss, performance status, appetite loss, and abnormal biochemistry markers. To simplify assessment, sarcopenia was assessed with a previously validated questionnaire replacing resource intensive methods such as CT imaging (Zhou *et al.*, 2018). CSS was able to discriminate the different stages of cachexia effectively based on clinical outcomes (e.g., quality of life and survival) (Zhou *et al.*, 2018). Further validation of the CSS tool is needed on larger patient groups to apply this promising tool on an international scale.

With several proposed diagnostic tools/classification systems in place, it is well understood within the cachexia research community that there is a need for robust and unified system in defining and diagnosing cachexia (Garcia *et al.*, 2022). Furthermore,

leaders in the field recognize the need to bridge the gap between the research community and clinicians to apply advancements of cachexia classification and detection into clinical practice (Garcia *et al.*, 2022). Expanding education and awareness of cachexia to clinicians, patients, and caregivers is essential to improving patient care in the future (Garcia *et al.*, 2022). Moving towards standardizing assessment and management of cachexia internationally, current clinical practice guidelines from American Society of Clinical Oncology (ASCO) and European Society for Medical Oncology (ESMO) utilize principles of the 2011 cancer cachexia consensus definition in diagnosis (Arends *et al*, 2021; Garcia *et al.*, 2022; Roeland *et al*, 2020). With our understanding of markers of cachexia evolving, international groups are actively revising the 2011 consensus definition which can further guide how cachexia is identified and managed (Garcia *et al.*, 2022).

1.1.3 Current management Options Against Cachexia

At this time, there are no clinically approved, effective therapies that can completely reverse the debilitating effects associated to cachexia (Arends *et al.*, 2021; Roeland *et al.*, 2020). The primary method of reversing cachexia is curing the overlying disease (Solheim *et al*, 2018). This task is easier said than done as cachexia is often undiagnosed or detected in terminal stages of disease progression and cachexia complicates treating the overlying disease (Garcia *et al.*, 2022; Kazemi-Bajestani *et al.*, 2016). Furthermore, in the case of cancer, therapies often contribute to cachexia (Garcia *et al.*, 2022; Solheim *et al.*, 2018). Clinicians are left with limited number of options to manage symptoms, which only delay the progression of these symptoms and do not improve patient survival (Arends *et al.*, 2021; Roeland *et al.*, 2020).

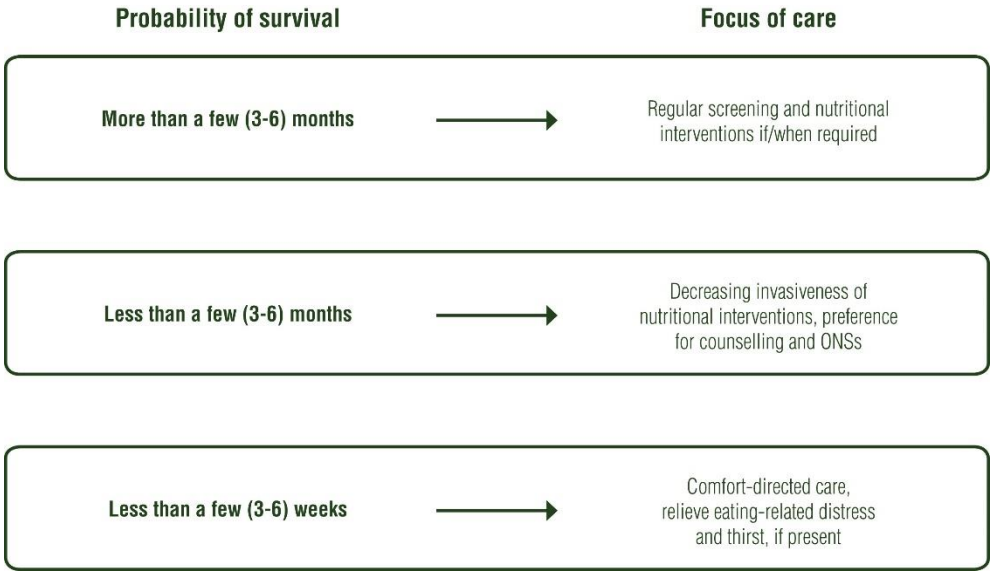

Figure 1.2 Invasiveness of interventions relative to expected survival.
Reprinted from Arends J, Strasser F, Gonella S, Solheim T, Madeddu C, Ravasco P, Buonaccorso L, de van der Schueren M, Baldwin C, Chasen M (2021) Cancer cachexia in adult patients: ESMO Clinical Practice Guidelines☆. ESMO open 6 with permission from Elsevier.

Current cachexia management strategies are highlighted in the ASCO and ESMO guideline on Cancer Cachexia (Arends *et al.*, 2021; Roeland *et al.*, 2020). Initial clinical assessment of cachexia focuses on changes in nutritional status and body weight (Arends *et al.*, 2021; Fearon *et al.*, 2011; Roeland *et al.*, 2020). The treatment guidelines focus on nutritional, psychosocial, pharmacologic as well as exercise interventions (Arends *et al.*, 2021; Roeland *et al.*, 2020). Due to the lack of pharmacological interventions to reverse cachexia, the ASCO and EMSO guidelines do not endorse any drugs to cure cachexia. However, they recommend short term treatments with progesterone analogs, most notably megestrol acetate, or a corticosteroid to increase appetite and promote weight gain primarily in adipose tissue despite a lack of effect on patient survival (Arends *et al.*, 2021; Roeland *et al.*, 2020). The EMSO guidelines also suggest the use of an antipsychotic drug called olanzapine to treat appetite and nausea thereby improving patient quality of life (Arends *et al.*,

2021). Both guidelines advocate for development of multimodal interventions which combine nutritional support with exercise and other interventions although trials are still ongoing (Arends *et al.*, 2021; Solheim *et al.*, 2018). The above management strategies, although improving patient nutritional status and quality of life, do not definitively combat muscle wasting and the increased mortality associated with cachexia. Further work is needed to test the efficacy of exercise interventions and multimodal therapies, which include novel drug treatments, to potentially address the diverse symptomology of cachexia.

1.2 Molecular Mechanisms and Biochemical Signatures of Cachexia-induced Muscle Wasting

The initiation of cachexia is a complex, multifactorial process making treatment of this deadly condition challenging. In general, the loss of muscle mass, which is the primary cause of morbidity in cachexia patients, is believed to be associated with an increase in the inhibition of anabolic pathways (that promote the synthesis of proteins) and/or the activation of catabolic pathways (that decrease protein content in muscle).

1.2.1 Cachexia-Induced Suppression of Muscle Protein Synthesis

Translation-mediated protein synthesis is a highly regulated process that is controlled at multiple levels (i.e., initiation, elongation, termination, and recycling) (Dufner & Thomas, 1999; Hershey *et al*, 2012; Mamane *et al*, 2006). In cachectic muscle the synthesis of proteins (which helps mediate protein content) is generally decreased due to the inhibition of the initiation step of the translational process (Fearon *et al*, 2012; Hardee *et al*, 2017; Peixoto da Silva *et al.*, 2020; Webster *et al*, 2020). Translation initiation is a critical step of the protein synthesis process that is regulated by several

signaling pathways. A focal point of this regulatory program is the mammalian target of rapamycin (mTOR) protein, which promotes protein synthesis when active (Dufner & Thomas, 1999; Hershey *et al.*, 2012; Mamane *et al.*, 2006). mTOR controls anabolic signaling through two primary mechanisms. mTOR promotes protein synthesis through the activation of the ribosomal protein S6 kinase (S6K) that subsequently activates ribosomal protein S6 (S6), and the inactivation of the 4E-binding protein 1 (4E-BP1) that is known to inhibit the eukaryotic initiation factor 4E (eIF4E) (Dufner & Thomas, 1999; Mamane *et al.*, 2006).

In muscle, the levels and availability of nutrients are key stimuli that control mTOR activation (Hardee *et al.*, 2017; Mamane *et al.*, 2006). Within muscle, notable regulators of mTOR include AKT and AMP-activated protein kinase (AMPK) that activate or repress mTOR activity, respectively (Hardee *et al.*, 2017; Mamane *et al.*, 2006). AKT and AMPK activity are both stimulated by their phosphorylation. AKT activation is normally promoted by anabolic growth factors such as Insulin-like Growth Factor 1 (IGF-1) and it can also be induced by exercise (Mamane *et al.*, 2006; Webster *et al.*, 2020). On the other hand, AMPK is most notably activated during energetic crisis where energy must be preserved, which is marked by decreased ATP levels and accumulation of AMP (Hardee *et al.*, 2017; Mamane *et al.*, 2006).

During cachexia, a decrease in anabolic pathways is known to occur due to inhibition of translation of proteins as a result of the impairment of mTOR activity (Ábrigo *et al*, 2018; Hardee *et al.*, 2017; White *et al*, 2013). This has been attributed to alterations of AKT and AMPK signaling as well as dysregulation of mTOR activation in response to nutrients and physical activity all of which promote anabolic resistance (Fearon *et al.*,

2012; Hardee *et al.*, 2017; Webster *et al.*, 2020). In response to feeding, cachectic patients have been observed to mount significantly impaired anabolic responses supporting the presence of anabolic resistance (Hardee *et al.*, 2017). Anorexia which often accompanies cachexia also likely contributes to the lower anabolic signaling in cachectic muscle through decreased food intake (Peixoto da Silva *et al.*, 2020). Interestingly, high protein foods that are rich in specific amino acids such as leucine have been shown to improve anabolic responses (Hardee *et al.*, 2017). However, these strategies have not yet been successfully employed to prevent cachectic muscle wasting in the long term likely since the activation of catabolic pathways (described below) supersedes protein production (Fearon *et al.*, 2012). Regarding exercise responses, limited studies have shown positive benefits to improving protein synthesis; nonetheless, these responses appear to be disrupted by cachexia and need to be further explored (Hardee *et al.*, 2017). In wasting muscle, AKT signaling can be repressed through decreased activity of growth factors and insulin resistance leading to anabolic resistance (Peixoto da Silva *et al.*, 2020; Sakuma *et al*, 2017; Webster *et al.*, 2020). In addition, well established negative regulators of AKT phosphorylation, including the SMAD2/SMAD3 pathway (described in later sections), that decrease AKT activation are induced in cachectic muscle(Sartori *et al*, 2009; Sartori *et al*, 2021). Further contributing to mTOR deactivation, AMPK phosphorylation is markedly increased during muscle wasting (Hall *et al*, 2018; Stana *et al*, 2017; White *et al.*, 2013). This AMPK activation has been associated with disruption of energy production in cachectic muscle (Hall *et al.*, 2018; Hardee *et al.*, 2017; VanderVeen *et al*, 2017). Interestingly work from our lab has shown that correction of muscle energy metabolism

can restore anabolic signaling in cachectic muscle suggesting the importance of metabolic dysfunction in causing cachexia-induced anabolic defects (Figure 1.3) (Hall *et al.*, 2018). Overall, these effects generally result in decreased phosphorylation of AKT, mTOR, S6, and 4E-BP1 in cachectic muscle leading to the inhibition of protein synthesis (Fearon *et al.*, 2012; Hardee *et al.*, 2017; Peixoto da Silva *et al.*, 2020; Webster *et al.*, 2020; White *et al.*, 2013). Cachexia therefore causes an imbalance in protein homeostasis that is due, in part, to a decrease in anabolic pathways.

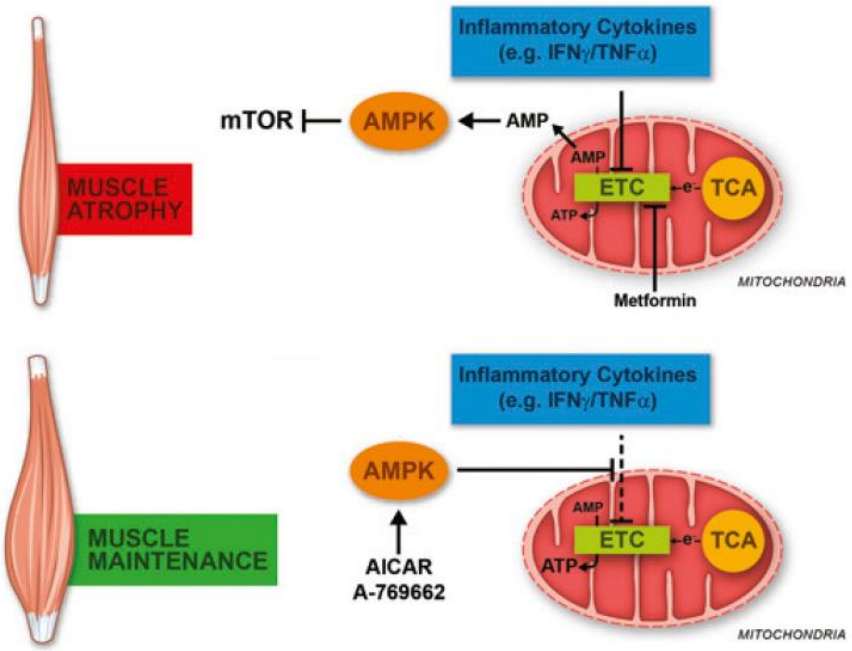

Figure 1.3 Maintenance of Muscle Energy Metabolism Prevents Muscle Wasting. (Top) Pro-inflammatory cytokines IFNγ/TNFα, which are known inducers of cachectic muscle wasting (described below) as well as metformin impair mitochondrial oxidative respiration in muscle causing energetic stress. This leads to suppression of protein synthesis and muscle wasting. (Bottom) AMPK agonists such as AICAR restore mitochondrial function in cytokine treated muscle preventing energetic stress and allowing for maintenance of muscle mass. *Adapted from Hall DT, Griss T, Ma JF, Sanchez BJ, Sadek J, Tremblay AMK, Mubaid S, Omer A, Ford RJ, Bedard N et al (2018) The AMPK agonist 5-aminoimidazole-4-carboxamide ribonucleotide (AICAR), but not metformin, prevents inflammation-associated cachectic muscle wasting. EMBO Molecular Medicine 10: e8307 with permission from John Wiley and Sons.*

1.2.2 Cachexia-Induced Catabolic Pathways

Several studies have highlighted cachexia-induced protein degradation as a major contributor to muscle wasting by enacting a negative protein balance. Elevated protein degradation can be achieved through activation of the ubiquitin proteasome (UPP) and autophagy pathways. While the proteasome can process individual proteins (Lecker *et al*, 2006), autophagy complements this process by degrading macromolecules and whole organelles (Sandri, 2016). While the role of UPP in cachexia-induced muscle wasting has been the subject of a large body of work, only recently has autophagy been appreciated as a major mechanism of cachexia-induced negative protein balance (Sakuma *et al.*, 2017; Sandri, 2016).

1.2.2.1 Proteasome-Mediated Degradation

Proteasome-mediated degradation of proteins is a targeted process which is regulated at multiple levels (Lecker *et al.*, 2006; Sandri, 2016). Proteins targeted for breakdown are marked by post-translational addition of poly-ubiquitin which is mediated by proteins named E1, E2, and E3. Upon polyubiquitination, targeted proteins are degraded into small peptides by the 26S proteasome, a multiprotein complex with protease activity that is responsible for the majority of protein degradation in the cell (Lecker *et al.*, 2006; Sandri, 2016). The initial step in the degradation of proteins by the UPP involves the activation of ubiquitin by E1 which then facilitates its transfer to E2 enzymes. E2 enzymes act as a carrier of ubiquitin to E3 ubiquitin ligases. E3 ligases then catalyze the transfer of ubiquitin from the E2 to the protein target. Specificity of protein targets is determined by pairs of E2 and E3 enzymes each having a unique set of targets. Since there is approximately 20 to 100 different E2 enzymes and up to 1000

different E3 ligases, there is a broad diversity of E2/3 combinations which can exist to mediate the selective degradation of proteins in different cells/tissues including muscle. Despite this, the muscle specific E3 ligases, Murf1 and atrogin-I, have been identified to play a prominent role in regulating UPP-mediated degradation of proteins during cachexia-induced muscle wasting (Lecker *et al.*, 2006; Sakuma *et al.*, 2017; Sandri, 2016).

Several laboratories have shown that Murf1 and atrogin-I are strongly induced during cachexia-mediated muscle wasting. Importantly, while overexpression of atrogin-I has been shown to induce atrophy *in vitro* (Bodine *et al*, 2001) knockout of these E3 ligases in mice prevents muscle atrophy induced due to cachexia, denervation, glucocorticoid treatment, or starvation (Bodine *et al.*, 2001; Cohen *et al*, 2015; Sandri, 2016). The central importance of these factors has been questioned though as knocking out these atrogenes only partially prevents wasting in animals (Sandri, 2016; Shyh-Chang, 2017). Furthermore, there is conflicting evidence on whether protein degradation by the UPP is elevated in cachexia, although this is likely attributed to the diverse etiology of cachexia from different stimuli (Porporato, 2016; Sakuma *et al.*, 2017; Shyh-Chang, 2017).

It is believed that the targeted degradation of specific key muscle factors, rather than a general increase in degradation, is responsible for the atrophic effects seen during cachexia (Cohen *et al.*, 2015; Sandri, 2016; Tisdale, 2009). In line with this, Murf1 has been associated with the ubiquitination and degradation of sarcomeric and structural proteins such as myosin heavy chain (MyHC) and myosin light chains (Cohen *et al.*, 2015; Glass, 2010; Sandri, 2016; Tisdale, 2009). Atrogin-I has also been found to associate to sarcomere components such as myosin, although this interaction has not

been proven to result in degradation. Complimenting the breakdown of sarcomere factors, atrogin-I is linked to degradation of myogenic regulatory factors (MRF) that are involved in muscle growth and maintenance. To this end, studies have found that atrogin-I promotes breakdown of the MRF MyoD and the translation initiation factor eIF3-f, potentially exacerbating impairment of muscle repair and protein synthesis to allow for accumulation of muscle damage (Cohen *et al.*, 2015; Glass, 2010; Sandri, 2016; Tisdale, 2009). This differential targeting demonstrates the unique function of these atrogenes in causing wasting. Due to their role in impairing key muscle processes, targeting the function of E3 ligases could prove beneficial in cachexia treatment. A recent study has shown that impairment of Murf1 by small molecules partially protects against melanoma-induced cachexia (Adams *et al*, 2020). This partial effect can potentially be attributed to compensation by other E3 ligases, such as TRIM3, that can also target sarcomere proteins during wasting (Cohen *et al.*, 2015). This compensatory effect, therefore, suggests that targeting multiple E2 enzymes and/or E3 ligases may be required to produce an effective therapeutic against wasting. Additionally, identifying factors/pathways involved in the expression of components of the UPP can also prove fruitful as the level of several of these have been shown to increase in cachectic muscle (Sakuma *et al.*, 2017; Sandri, 2016; Tisdale, 2009).

1.2.2.2 Autophagy

As described in the section detailing repression of protein synthesis, cachectic stimuli often impair AKT-mTOR signaling. This impairment can arise from changes in the extracellular signaling environment or from intracellular sensing of energy stress. AKT-mTOR axis inhibition can promote catabolic signaling pathways as well through

induction of autophagy (Franco-Romero & Sandri, 2021). Autophagy is a multistep process (i.e., induction and activation, autophagosome formation, and lysosome fusion) (Franco-Romero & Sandri, 2021; Sartori *et al.*, 2021) where damaged organelles, misfolded proteins, protein aggregates, or macromolecules that are marked for degradation are enveloped in cytoplasmic vesicles called autophagosomes that are subsequently fused into lysosomes to degrade their contents (Franco-Romero & Sandri, 2021). Interestingly, under non-cachectic, normal conditions, skeletal muscle extensively utilizes the autophagy pathway to maintain muscle homeostasis. Alterations of autophagy flux in either direction is noted to have negative effects in muscle. Increases in autophagy have been linked to muscle fiber atrophy, while decreases in autophagy are associated with deterioration of muscle function due to accumulation of damage (Franco-Romero & Sandri, 2021; Penna *et al*, 2019a; Sartori *et al.*, 2021). Several studies have reported an increase in the activation of autophagy in both animal models of cachexia as well as cachectic patients (Mofarrahi *et al*, 2012; Porporato, 2016; Sandri, 2016; Stana *et al.*, 2017). Overactivation of autophagy under these conditions was shown to exacerbates the pathological consequences associated to the onset of this condition (Penna *et al.*, 2019a; Penna *et al*, 2019b). Interestingly, however, inhibition of autophagy does not appear to be a successful therapeutic strategy as it does not improve wasting or survival (Penna *et al.*, 2019a; Penna *et al.*, 2019b). It is suggested that autophagy might be a protective response in wasting to clear damaged organelles (Penna *et al.*, 2019a). Therefore, maintaining a balance of autophagy in cachectic muscle appears to be necessary despite its pro-atrophic effects.

Of particular interest in cachexia is the subtype of autophagy termed mitophagy that targets mitochondria. During cachexia, mitochondria are damaged as a result of their extensive to oxidative stress (Fukawa *et al*, 2016; Owen *et al*, 2019). Under normal conditions, damaged mitochondria are removed by the mitophagic process. Under cachectic conditions the accumulation of dysfunctional mitochondria, due to impaired mitophagy, can contribute to decreased muscle performance and function (Franco-Romero & Sandri, 2021). Indeed, this phenomenon has also been reported in age related muscle loss (Sakuma *et al.*, 2017). Studies have shown that the accumulation of defective muscle mitochondria during cachexia and ageing can be addressed through overexpression of the key mitophagy factor Parkin that maintains muscle mitochondria (Gouspillou *et al*, 2018; Leduc-Gaudet *et al*, 2020; Leduc-Gaudet *et al*, 2019). In these works, Parkin overexpression not only improved mitochondrial quality and contents, but also protected against sepsis-induced muscle wasting and age-related loss of muscle mass and strength(Leduc-Gaudet *et al.*, 2020; Leduc-Gaudet *et al.*, 2019). Taken together, the evidence suggests that strategies which manipulate autophagy in cachectic muscle should improve mitochondrial quality and maintain normal mitochondrial levels.

1.2.3 Metabolic Defect, Energetic Stress, and Oxidative Stress in Cachexia

Cachexia-mediated metabolic dysfunction in target tissues is increasingly recognized as a key driver of atrophy. Skeletal muscle function is highly energy dependent utilizing vast reserves of energy for contraction and repair of damage from exercise and environmental pressures. Under cachectic conditions, cellular energy production is disrupted causing energetic stress through mechanisms described below. This

energetic stress, consequently, contributes to the induction of catabolic pathways leading to breakdown of muscle protein to bolster energy reserves. In order to preserve energy, this energetic stress also induces inhibition of anabolic pathways to prevent the energy intensive synthesis of proteins that is normally required for the maintenance, function, and repair of skeletal muscle. These metabolic stresses thereby lead to loss of muscle mass and decreased muscle performance, two defining characteristics of cachectic muscle. The following section will highlight the progress made to characterize and understand the metabolic defects which promote these cachectic phenotypes.

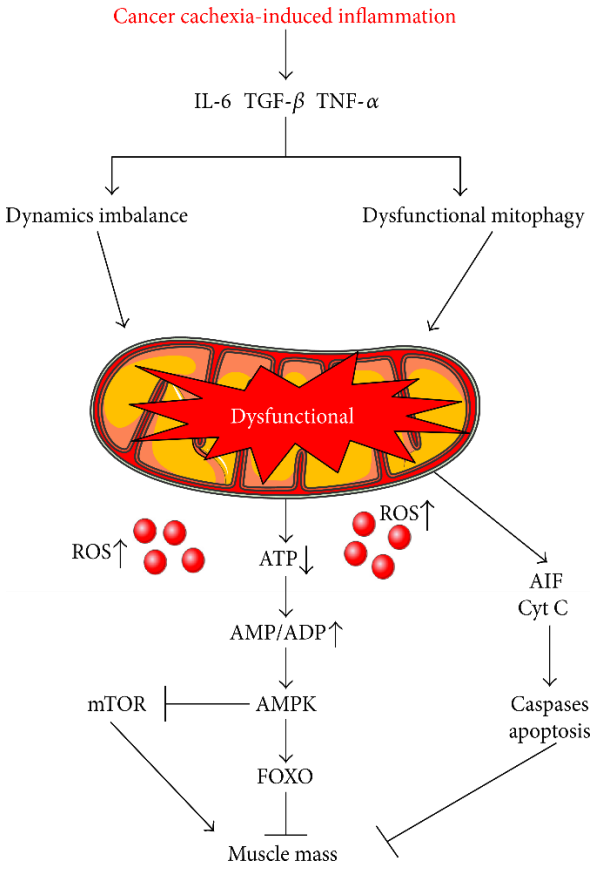

Figure 1.4: Mitochondrial dysfunction in skeletal muscle negatively regulates muscle mass.
Elevated levels of pro-inflammatory factors such as IL-6, TNF-α, and TGF-β during cancer cachexia disrupt mitochondrial homeostasis leading to dysfunction mitochondria. Dysfunctional mitochondria release aberrant amounts of reactive oxygen species (ROS) and decrease ATP production. This leads to chronic activation of AMPK to negatively regulate protein synthesis causing decreased muscle mass. The figure was made with Servier Medical Art (http://www.servier.com/Powerpoint-image-bank). *Reprinted from VanderVeen BN, Fix DK, Carson JA (2017) Disrupted skeletal muscle mitochondrial dynamics, mitophagy, and biogenesis during cancer cachexia: a role for inflammation. Oxidative medicine and cellular longevity 2017 under the Creative Commons Attribution License.*

1.2.3.1 Metabolite Biomarkers of Cachexia

Reviewed in (Cui *et al*, 2022), metabolomics is an increasingly recognized tool used in cachexia research to investigate cachexia biomarkers and metabolic defects within target tissues. Studies assessing metabolite biomarkers of cachexia have identified

various candidate metabolic signatures associated with adipose wasting, energy metabolism, or muscle protein breakdown. Investigations on amino acid levels in serum and plasma have found classes of amino acids altered in cachectic subjects. In general, decreases in branched chain amino acids (BCAA) levels from cachectic animals and patients have been noted (Cala *et al*, 2018; Der-Torossian *et al*, 2013a; Ni *et al*, 2021; Pin *et al*, 2019a; Pötgens *et al*, 2021; QuanJun *et al*, 2015; Yang *et al*, 2018). A consistent pattern was also found in levels of 3-carbon glycogenic amino acids alanine and glycine that were shown to decrease and increase, respectively, in blood during cachexia, (Cala *et al.*, 2018; Cui *et al*, 2019a; QuanJun *et al.*, 2015; Yang *et al.*, 2018). Studies evaluating the potential of urine amino acids and muscle breakdown products as biomarkers reported conflicting results as the collection of the altered metabolites was inconsistent between reports (Eisner *et al*, 2011; Stretch *et al*, 2012; Yang *et al.*, 2018). A similar challenge was faced by studies focusing on lipid profiles in serum and plasma that detected markers of lipid mobilization (e.g., lipolysis or hyperlipidemia), but no consensus on markers that can be utilized in cachexia detection (Cala *et al.*, 2018; Cui *et al.*, 2019a; Der-Torossian *et al.*, 2013a; Miller *et al*, 2019; O'Connell *et al*, 2008; Pin *et al.*, 2019a; Stretch *et al.*, 2012). These discrepancies can potentially be attributed to variations in inclusion criteria, protocols for standardizing sample collection, and cachexia models used (Cui *et al.*, 2022; Fujiwara *et al*, 2014). Nevertheless, decreases in serum and plasma BCAAs and alterations of 3-carbon glycogenic amino acids levels during cachexia were a common finding and warrant further assessment in larger studies to cement their importance.

1.2.3.2 Cachexia-Mediated Metabolome Derangement

As highlighted above, the study of biomarker in urine and blood isolated from cachectic patients indicated cachexia-induced defects in amino acid and lipid metabolism. Although the breakdown of glucose by glycolysis and the tricarboxylic acid (TCA) cycle is a significant supplier of energy within cells, non-sugar metabolites (amino acids, lipids, and ketone bodies) can support these pathways through a process called anaplerosis that feeds these alternative energy sources into the TCA cycle for oxidation (Brunengraber & Roe, 2006; Vander Heiden *et al*, 2009). As cachexia is believed to impair energy production to cause energy deficit and wasting, a primary focus of metabolomics studies in target tissues was to elucidate the mechanisms responsible for this defect.

Disruption of energy metabolism through dysregulation of glucose metabolism in cachectic muscle was suggested in a seminal metabolomics-based cachexia study. This study discovered alterations in the levels of glycolysis metabolites and TCA cycle intermediates reminiscent of the Warburg effect (Der-Torossian *et al*, 2013b). Notably, these defects were believed to be, in part, a result of oxidative stress in cachectic muscle. The Warburg effect in cachectic muscle could lead to energetic stress as it results in the decreased utilization of the glycolysis/oxidative phosphorylation (OXPHOS) process (which is more efficient for energy production) and increased dependence on anaerobic glycolysis (Der-Torossian *et al.*, 2013b; Hall *et al.*, 2018; Vander Heiden *et al.*, 2009). The above observations have since been corroborated by other groups. Indeed, studies suggested increases in glycolysis in wasting muscle due to depletion of glucose, glycogen, and glycolysis intermediates (Cui *et al.*, 2019a; Cui *et*

al, 2019b; QuanJun *et al.*, 2015; Tseng *et al*, 2015). Within the TCA cycle, increases in α-ketoglutarate (AKG) and decreases in its downstream metabolite succinate have been reported suggesting a blockage in the TCA cycle (Chiocchetti *et al*, 2021; Cui *et al.*, 2019a; Pin *et al.*, 2019a). These alterations to glycolysis and the TCA cycle were accompanied by energetic stress, decreases in anabolic signaling, and expression of atrogenes (described above in sections 1.2.1 and 1.2.2) supporting the notion that there is a lack of energy production (Cui *et al.*, 2019b). Decreased levels of glycolytic and TCA cycle metabolites in serum and plasma of patients further supports the signature described above indicating a dysregulation of glucose metabolism in cachectic subjects (Lautaoja *et al*, 2019; Pin *et al.*, 2019a; Pötgens *et al.*, 2021).

It is possible that cachectic muscles compensate for lower glucose-dependent energy production by enhancing oxidation of amino acids, lipids, and ketone bodies. Indeed, muscle proteolysis and increased levels of anapleurotic amino acids in wasting muscle have been identified to potentially supplement energy production. Hyperlipidemia in serum, signs of mobilization of lipids, increase of ketone bodies to enter the TCA cycle have also been reported in cachexia to support this. However, due to defects in TCA cycle and impaired energy production through OXPHOS in cachectic muscle, hyperlipidemia and accumulation of amino acids could be result of incomplete oxidation of these substrates (Cui *et al.*, 2019b; Pin *et al.*, 2019a).

Increases in the levels of the cationic amino acids arginine and lysine which can feed into the TCA cycle through AKG and acetyl-CoA, respectively, have been consistently reported in cachectic muscle (Cui *et al.*, 2019a; Cui *et al.*, 2019b; Der-Torossian *et al.*, 2013b; Kunzke *et al*, 2020; Lautaoja *et al.*, 2019). Arginine is catabolized for entry into

the TCA cycle through conversion to ornithine by arginase enzymes that can be further metabolized. Funneling of arginine into AKG has been shown to accelerate OXPHOS and benefit cellular energetics (Xu *et al*, 2016). Critical steps of arginine and lysine catabolism/anaplerosis occurs in the mitochondria, and their accumulation in cachectic muscle is suggested to be a result of decreased expression of their mitochondrial transporter cationic amino acid transporter 1 (CAT1) (Kunzke *et al.*, 2020). The defective shuttling of cationic amino acids, in particular arginine, was therefore suggested to contribute to energy production deficits (Kunzke *et al.*, 2020).

Similar to cationic amino acids, BCAAs, lipids, and ketone bodies can feed into the TCA cycle through mitochondrial processes. These processes produce acetyl-CoA or succinyl-CoA which can enter the TCA cycle (Brunengraber & Roe, 2006; Ye *et al*, 2020). Several studies have found that BCAAs accumulate in cachectic muscle likely due to muscle protein breakdown and are unsuccessfully directed to anapleurotic reactions (Chiocchetti *et al.*, 2021; Cui *et al.*, 2019a; Cui *et al.*, 2019b; Lautaoja *et al.*, 2019; Tseng *et al.*, 2015; Zhou *et al*, 2021). Similarly, ketone bodies are also reported to accumulate in cachectic muscle and their accumulation was attributed to decreased expression of key ketone body oxidation enzymes required for their anaplerosis (QuanJun *et al.*, 2015; Zhou *et al.*, 2021). Several studies have also investigated the catabolism of acyl-CoAs that are broken down to acetyl-CoA by β-oxidation. Long-chain acyl-CoAs enter the mitochondria through conversion to acylcarnitine species and are subsequently reconverted to acyl-CoAs after entry (Li *et al*, 2019). Once converted back to their CoA analog, fatty acids enter β-oxidation through long-chain Acyl-CoAs dehydrogenase (LCADH). The transport step is noted as the rate-limiting steps of β-

oxidation and is mediated by two carnitine palmitoyltransferase (CPT) enzymes CPT1 and CPT2. The levels of acylcarnitines, therefore, are used to gauge levels of β-oxidation (Fukawa *et al.*, 2016; Li *et al.*, 2019). Acute exposure to cachectic conditions has also been shown to trigger mobilization of lipid stores into acylcarnitines to increase β-oxidation in human primary myotubes(Fukawa *et al.*, 2016). This increase in β-oxidation was noted to cause severe oxidative stress which triggers wasting (Fukawa *et al.*, 2016). In contrast, this accumulation of acylcarnitines was not recapitulated in the C26 animal model of cancer cachexia although this may indicate that in chronic, late-stage cachexia, lipid stores are exhausted (Pin *et al.*, 2019a). Interestingly, saturated long-chain fatty acids are associated with inducing pro-inflammatory pathways (Ye *et al.*, 2020). Therefore, accumulation of acylcarnitine species in early stages could indicate that although β-oxidation is increased, cachectic muscle mitochondria are overloaded leading to propagation of saturated fatty acid-induced inflammatory signaling and oxidative stress (Fukawa *et al.*, 2016; Ye *et al.*, 2020).

Although not directly related to energy production pathways, inefficient utilization of amino acids freed from muscle protein breakdown can also contribute to energetic stress. During energetic crisis, amino acids released from muscle proteolysis can be shunted to the liver for gluconeogenesis to bolster systemic glucose metabolism in what is called the Cori cycle. Indeed, decreases in 3-carbon glucogenic amino acids in cachectic muscle with concurrent elevation in livers have been reported suggesting the mobilization of these amino acids to the liver (Cui *et al.*, 2019a; Cui *et al.*, 2019b; Der-Torossian *et al.*, 2013b; Lautaoja *et al.*, 2019; Pötgens *et al.*, 2021). However, hepatic function of these amino acids during cachexia may not be glucogenic, as key

gluconeogenic enzymes are reportedly downregulated in cachectic livers (Pötgens *et al.*, 2021). Pötgens *et al.* suggested that these amino acids are instead directed to acute phase response (APR) protein production (Pötgens *et al.*, 2021). Elevated APR protein production has been previously reported in cachectic muscle and liver (Bonetto *et al*, 2012; Bonetto *et al*, 2011; Zimmers *et al*, 2016). Rerouting of amino acids from muscle proteins to APR proteins is inefficient due to amino acid mismatch between the protein types requiring high proportions of muscle to supply low yields of APR proteins (Pötgens *et al.*, 2021; Stephens *et al*, 2008). Therefore, this inefficient protein conversion adds to the negative protein balance in cachectic muscle.

Table 1.1: Summary of muscle metabolites altered in cachectic muscle

Metabolites	Function	Alteration in Cachexia	Cause of shift and effect on muscle wasting	Reference
Glucose and glycolysis intermediates	Glycolysis	Decrease	Cause: increased glycolysis to compensate for decreased OXPHOS Effect: insufficient energy production in muscle	(Cui *et al.*, 2019a; Cui *et al.*, 2019b; Der-Torossian *et al.*, 2013b; QuanJun *et al.*, 2015; Tseng *et al.*, 2015)
AKG	TCA cycle	Increase	Cause: disruption of TCA cycle flux Effect: decreased aerobic energy production	(Chiocchetti *et al.*, 2021; Cui *et al.*, 2019a; Pin *et al.*, 2019a)
Succinate	TCA cycle	Decreased	Cause: disruption of TCA cycle flux Effect: decreased aerobic energy production	(Chiocchetti *et al.*, 2021; Cui *et al.*, 2019a; Pin *et al.*, 2019a)
Cationic amino acids (arginine, lysine)	Protein synthesis, TCA cycle anapleurosis, NO generation (arginine)	Increased	Cause: increased muscle protein breakdown and impaired mitochondrial shuttling Effect: decreased anapleurosis into TCA cycle	(Cui *et al.*, 2019a; Cui *et al.*, 2019b; Der-Torossian *et al.*, 2013b; Kunzke *et al.*, 2020; Lautaoja *et al.*, 2019)
BCAAs (leucine, isoleucine, valine)	Protein synthesis, TCA cycle anapleurosis,	Increased	Cause: increased muscle protein breakdown and impaired mitochondrial shuttling Effect: decreased anapleurosis into TCA cycle	Cui, 2019 #166;Cui, 2019 #153;Cui, 2019 #166;Zhou, 2021 #170;Lautaoja, 2019 #161;Chiocchetti, 2021 #169;Tseng, 2015 #165;Tseng, 2015 #165}
Ketone bodies	TCA cycle anapleurosis	Increased	Cause: decreased levels of processing enzymes Effect: decreased anapleurosis into TCA cycle	(QuanJun *et al.*, 2015; Zhou *et al.*, 2021)
Acylcarnitine	Transport of acyl-CoA into mitochondria, β-oxidation	Increased (acute) Decreased (chronic)	Cause: increased mobilization of lipid stores Effect: increased oxidative stress and damage in muscle	(Fukawa *et al.*, 2016; Pin *et al.*, 2019a)
Serine, glycine, alanine	Protein synthesis, gluconeogenesis	Decrease	Cause: secretion from muscle to either enter Cori cycle or support synthesis of APR proteins Effect: inefficient utilization of amino acids leading to negative protein balance	(Cui *et al.*, 2019a; Cui *et al.*, 2019b; Der-Torossian *et al.*, 2013b; Lautaoja *et al.*, 2019; Pötgens *et al.*, 2021)

1.2.3.3 Impairment of Energy Production and Downstream Effects of Energy Crisis

Metabolomics studies have offered much insight into the metabolic pathways affected by cachectic conditions which culminate in diminished energy production. These metabolic outcomes are achieved through alterations to expression and/or activity of proteins required for the function of energy production pathways. As highlighted above, a prominent defect is the altered flux of metabolites into the TCA cycle from glycolysis and other energy reserves. Normally in differentiated tissue, glycolysis converts glucose into pyruvate, which is converted to acetyl-CoA in the mitochondria and can then feed into the TCA cycle (Vander Heiden *et al.*, 2009). However, during cachexia glucose metabolism for OXPHOS-based energy production in muscle appears to be hindered, due to a Warburg-like shift.

A contributing factor to the observed Warburg-like shift is the blockade of pyruvate conversion to acetyl-CoA (Pin *et al*, 2019b). The conversion of pyruvate to acetyl-CoA is catalyzed by the pyruvate dehydrogenase (PDH) complex, which can be negatively regulated by PDH kinases (PDK) (Zhang *et al*, 2014). Cachectic conditions increase PDK4 expression in muscle, leading to decreased PDH activity and energetic defects, which could be prevented by PDK4 blockade (Constantinou *et al*, 2011; Pin *et al.*, 2019b). Overexpression of PDK4 can cause wasting without the surrounding inflammatory signaling found in cachexia (Pin *et al.*, 2019b). Together these data indicate the importance of glucose oxidation through the TCA cycle for energy status and muscle maintenance. (Pin *et al.*, 2019b). Further contributing to impaired glucose oxidation in cachectic muscle is the reduced expression and/or activity of various TCA

cycle enzymes and electron transport chain (ETC) proteins including AKG dehydrogenase, aconitase, succinate dehydrogenase (SDH) (a component of complex II), and complex IV thereby preventing TCA cycle flux and OXPHOS-linked ATP generation (Brown *et al*, 2017; Cui *et al.*, 2019a; Fontes-Oliveira *et al*, 2013; Owen *et al.*, 2019; Penna *et al.*, 2019b; Pin *et al.*, 2019a; Pin *et al*, 2022; Pin *et al.*, 2019b; Remels *et al*, 2010; Wyart *et al*, 2022). Due to impaired flux of glucose metabolism into the TCA cycle, wasting muscle is noted to increase glycolysis rates to compensate for lower energy production, albeit unsuccessfully (Hall *et al.*, 2018; Pin *et al.*, 2019b). This has been demonstrated by metabolomic measurements of glycolysis intermediates and increased expression of hexokinase (HK) and phosphofructokinase (PFK), two of the major rate-limiting enzymes in glycolysis (Cui *et al.*, 2019a; Remels *et al.*, 2010). Furthermore, observed elevations of extracellular acidification and lactate release suggest increased glycolysis in cachectic muscle cells (Hall *et al.*, 2018; Pin *et al.*, 2022).

With many of these metabolic disruptions occurring in the mitochondria, cachexia's effect on mitochondrial structure, dynamics, and damage have been the focus of many studies. Several structural defects appear in mitochondria of cachectic muscle (Fontes-Oliveira *et al.*, 2013; Owen *et al.*, 2019; Shum *et al*, 2012). Notably, loss of cristae in the inner mitochondrial membrane (IMM), which is the site of oxidative phosphorylation, is likely a major contributor to diminished ETC complex function (Shum *et al.*, 2012). This membrane disruption could be a result of oxidative damage as well as changes to mitochondrial phospholipid composition (Antunes *et al*, 2014; Fontes-Oliveira *et al.*, 2013). Cachexia-driven mitochondria swelling, loss of IMM function, and multiple

vesicle-like bodies suggest that cachexia negatively alters the balance of mitochondrial turnover (mitophagy versus biogenesis) and dynamics (fission versus fusion) (Mofarrahi *et al.*, 2012; Romanello & Sandri, 2022; VanderVeen *et al.*, 2017). Work in models of cachexia show that expression of mitochondrial biogenesis factors decreases with concomitant increases in mitophagy factor expression (Brown *et al.*, 2017; Franco-Romero & Sandri, 2021; Mofarrahi *et al.*, 2012; Penna *et al.*, 2019b; Pin *et al.*, 2022; Remels *et al.*, 2010; White *et al*, 2012). Furthermore, differential expression of fusion and fission factors is suggested to cause deleterious mitochondrial fragmentation (Brown *et al.*, 2017; Franco-Romero & Sandri, 2021; VanderVeen *et al.*, 2017; White *et al.*, 2012). Taken together, the disruption of mitochondria and upregulation of glycolysis factors is unable to meet the energy needs of muscle thereby causing energetic crisis. A significant downstream outcome of cachexia-induced energy crisis is decreased functionality and strength (Murphy *et al*, 2012; Owen *et al.*, 2019; VanderVeen *et al*, 2019; VanderVeen *et al*, 2018; Wyart *et al.*, 2022). Cachexia-mediated muscle dysfunction is therefore likely caused by inflammation- and energetic stress that, through the repression of anabolism and induction of catabolic pathways, leads to a decrease in muscle contractile protein content/quality and energy levels. This, consequently, results in the reduced function of muscles and their ability to sustain muscle contractions (which normally requires high energy demands and the expression of muscle contractile proteins).

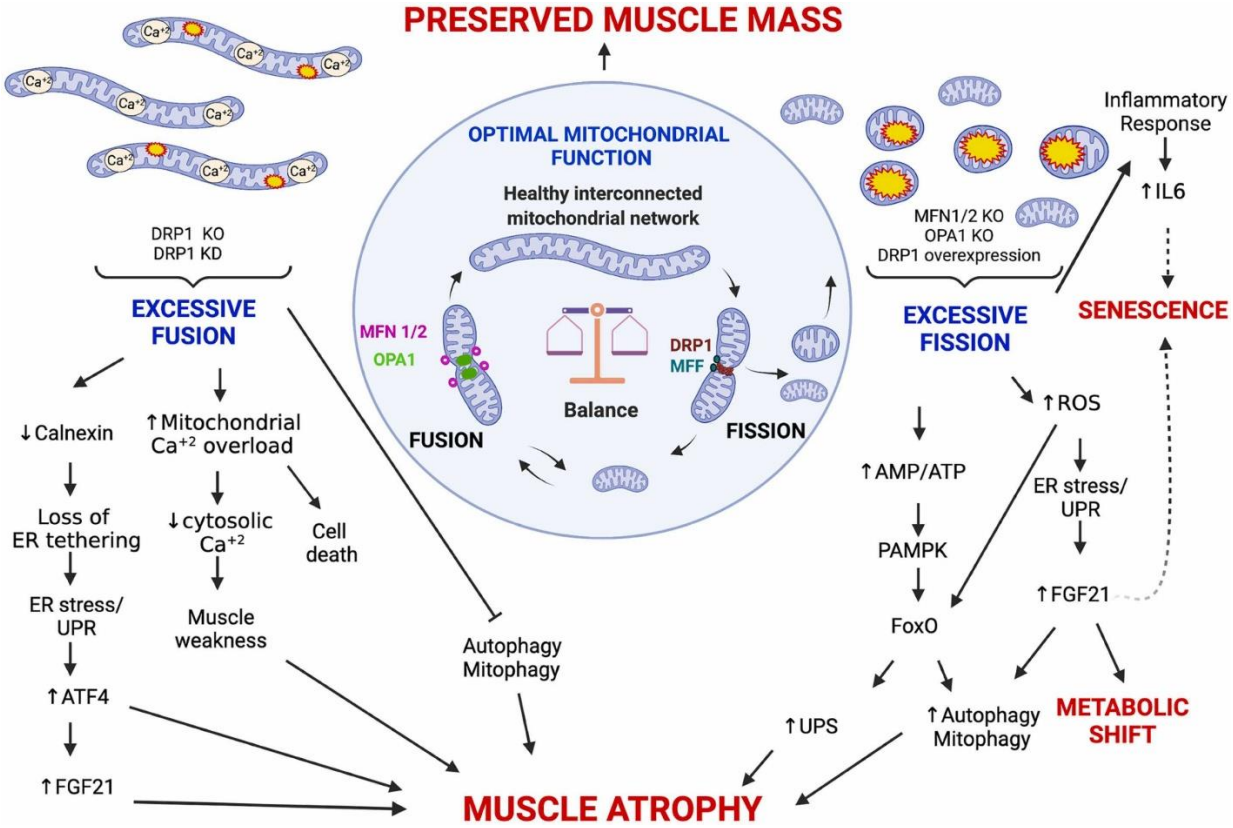

Figure 1.5: Mitochondrial Fusion and Fission.

Scheme representing the effects of unbalanced mitochondrial fusion and fission on the activation of signaling pathways controlling muscle mass. Dashed lines indicate mechanisms that needs more studies. KO: Knockout, KD: Knockdown. Figures were created with BioRender.com. *Reprinted from Romanello V, Sandri M, 2022. Implications of mitochondrial fusion and fission in skeletal muscle mass and health, Seminars in Cell & Developmental Biology. Elsevier. with permission from Elsevier.*

1.3 Initiation of Cachexia: Systemic and Intracellular Factors

Cachexia is recognized as a metabolic disorder driven by inflammatory responses (Evans *et al.*, 2008; Fearon *et al.*, 2011). Due to our incomplete understanding of the etiology of cachexia, the mechanisms behind metabolic dysfunction and the factors responsible for initiating cachexia remain unknown. Expanding our understanding of the multiple molecular mechanisms that cause cachexia can aid in the identification of drug targets for its prevention or treatment. This may involve the development of pharmacological or nonpharmacological therapeutics (Baracos *et al.*, 2018; Peixoto da Silva *et al.*, 2020). As muscle is the principal affected tissue, research into how pro-cachectic signaling induces muscle wasting is crucial.

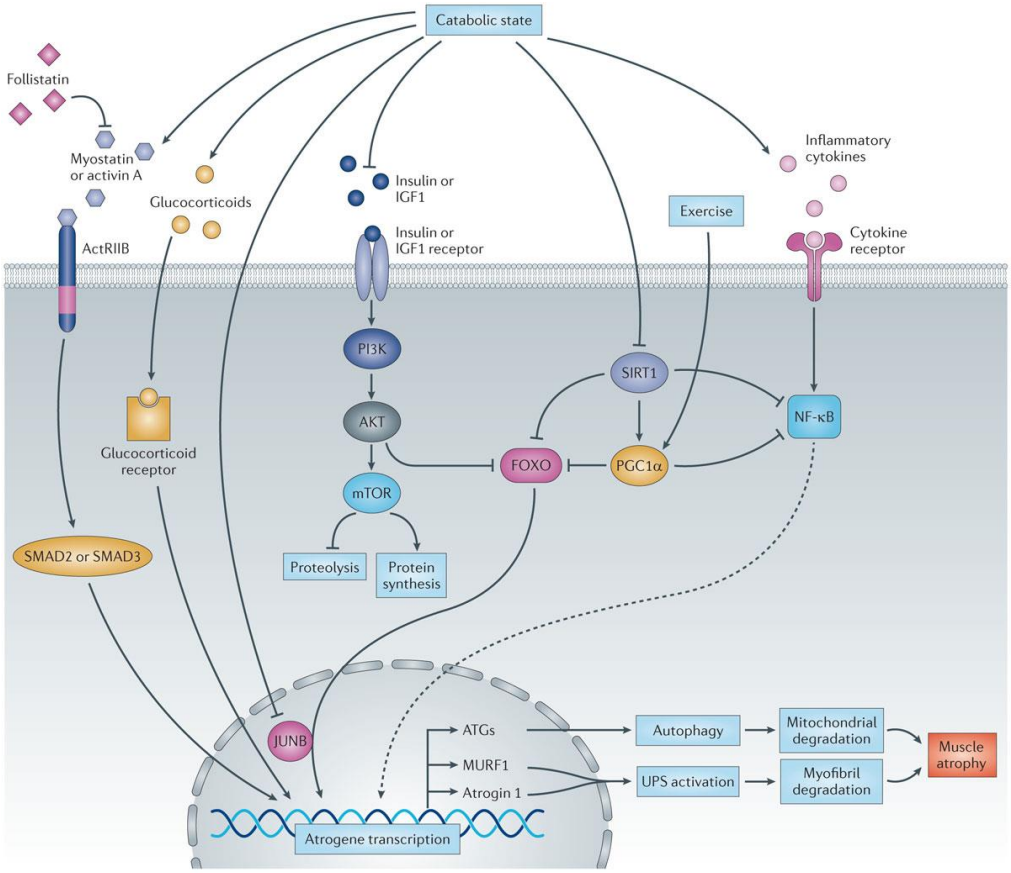

Figure 1.6: Signaling pathways leading to muscle atrophy.
In diverse catabolic states, multiple intracellular signalling pathways stimulate the expression of atrogenes and thus protein degradation via the proteasome and autophagy. These catabolic effects in muscle are mediated by specific transcription factors, including forkhead box protein O (FOXO) proteins, nuclear factor-κB (NF-κB) and SMAD2 or SMAD3. The activation of these transcription factors results from extracellular stimuli and/or from a decrease in phosphoinositide 3-kinase (PI3K)–AKT–mammalian target of rapamycin (mTOR) signalling. This reduction in PI3K–AKT signaling activity results in inhibition of mTOR and protein synthesis, and together with the accelerated proteolysis leads to muscle atrophy. The dashed line indicates that the evidence for NF-κB-mediated induction of atrogene expression is tentative. ActRIIB, activin A receptor, type IIB; ATGs, autophagy-related genes; IGF1, insulin-like growth factor 1; JUNB, transcription factor JunB; MURF1, muscle-specific RING-finger 1; PGC1α, peroxisome proliferator-activated receptor-γ coactivator 1α; SIRT1, NAD-dependent protein deacetylase sirtuin 1; UPS, ubiquitin–proteasome system. *Reprinted from Cohen S, Nathan JA, Goldberg AL (2015) Muscle wasting in disease: molecular mechanisms and promising therapies. Nature reviews Drug discovery 14: 58-74 with permission from Springer Nature.*

1.3.1 Initiators of Pro-Cachectic Signaling

1.3.1.1 Tumor Necrosis Factor Alpha and Interferon Gamma

Tumor Necrosis Factor Alpha (TNFα) was one of the first discovered inflammatory factors to induce cachexia (Beutler & Cerami, 1986; Fearon *et al.*, 2012). Originally identified in early reports in the 1980s as the secreted factor cachectin, TNFα has been shown to drive lethal septic shock (which is associated to cachexia-induced muscle wasting) (Beutler & Cerami, 1986; Beutler *et al*, 1985). At pathologically high levels, TNFα is associated with weight loss, anorexia, activation of protein degradation by the proteasome, and dysregulation of lipid metabolism by lipoprotein lipase inhibition and induction of lipolysis (Beutler & Cerami, 1986; Patel & Patel, 2017; Tisdale, 1997, 2008). In muscle, several studies demonstrated that TNFα promoted negative protein balance by inducing activation of the UPP through upregulation of ubiquitin and E3 ligase expression and by, furthermore, impairing protein synthesis through repression of translation initiation (Fearon *et al.*, 2012; Lang *et al*, 2002; Li *et al*, 2005; Llovera *et al*, 1998; Tisdale, 2008). TNFα was also found to strongly dysregulate cellular energy production through impairment of oxidative metabolism (Remels *et al.*, 2010). Contrary to its established role in myogenesis, high concentrations of TNFα additionally impaired the muscle differentiation process and regeneration (Chen *et al*, 2007; Guttridge *et al*, 2000; Tisdale, 2008). Due to these pervasive pro-cachectic effects, it was believed that TNFα blockade could cure cachexia (Jatoi *et al*, 2010). Work in animal models of cachexia suggested the efficacy of TNFα impairment in cachexia prevention (Jatoi *et al.*, 2010). Despite past successes in preclinical models, clinical trials using infliximab, a monoclonal antibody that blocks TNFα, in non-small cell lung cancer (NSCLS) showed

that TNFα inhibition did not improve patient outcome, with no effects on patient weight or survival. Surprisingly, patients treated with infliximab experienced a worse quality of life and fatigue (Jatoi *et al.*, 2010; Wiedenmann *et al*, 2008). Nevertheless, the role of TNFα in cachexia should not be discounted as cachexia is often described as a multifactorial condition with various inflammatory mediators contributing to its pathology. In patients suffering from chronic diseases that are known inducers of cachexia (i.e., chronic heart failure (CHF), chronic kidney disease (CKD), chronic obstructive pulmonary disorder (COPD), malaria, leishmaniasis, and AIDS), serum TNFα levels are often increased (Remels *et al.*, 2010; Webster *et al.*, 2020). However, circulating TNFα levels are not always increased in cancer patients and elevated TNFα levels does not always result in cachexia (Kayacan *et al*, 2006; Socher *et al*, 1988; Tisdale, 1997, 2008). It remains possible that the inefficaciousness of TNFα blockade in humans is due to cooperation of TNFα with other cytokines and redundancy in cytokine function in cachectic patients.

Often observed working in conjunction with TNFα, Interferon Gamma (IFNγ) is another prominent cytokine implicated in cachexia. In the context of cancer, studies have shown that IFNγ is able to induce severe cachexia (Matthys *et al*, 1991a). Interestingly in murine models of cachexia, IFNγ blockade was shown to prevent wasting and impair tumor growth(Matthys *et al.*, 1991a; Matthys *et al*, 1991b). Despite its evident role in driving wasting in these models, it does not appear that IFNγ can cause cachexia alone and requires other tumor-derived factors such as TNFα to drive its effects (Matthys *et al.*, 1991a; Tisdale, 1997). Indeed, several studies have shown that TNFα and IFNγ have synergistic effects on promoting wasting by decreasing the

expression of the muscle protein myosin heavy chain as well as the myogenic factor MyoD. It has also been shown to induce activation of the UPP (Acharyya *et al*, 2004; Di Marco *et al*, 2005; Guttridge *et al.*, 2000; Ma *et al*, 2017; Peixoto da Silva *et al.*, 2020). Due to the cooperative nature of pro-cachectic cytokines, elucidating the downstream targets of TNFα and IFNγ can unveil targets where inflammatory signals converge to promote wasting.

1.3.1.2 Interleukin 6 and Leukemia Inhibitory Factor

A large body of work suggests that interleukin 6 (IL-6) is a major promoter of cachexia (Carson & Baltgalvis, 2010). IL-6 has been proposed, in the animal models of cachexia, to promote wasting of both adipose tissue and skeletal muscle, as well as causing anorexia (Baltgalvis *et al*, 2008; Baltgalvis *et al*, 2009; Bonetto *et al.*, 2011; Han *et al*, 2018; Petruzzelli *et al*, 2014; Siddiqui *et al*, 2020; Soda *et al*, 1995; Strassmann *et al*, 1992). IL-6 induces activation of the innate immune system's APR, which is commonly observed in cancer cachexia patients and is linked to poor outcome (Bonetto *et al.*, 2011; Stephens *et al.*, 2008). In addition, IL-6 promotes muscle proteolysis by stimulating the expression of the E3 ubiquitin ligase atrogin-1 (Baltgalvis *et al.*, 2009). IL-6, furthermore, promotes adipose wasting by inducing lipolysis causing the mobilization of triglycerides in the blood resulting in the browning of adipose tissues and an increase in energy expenditure (Han *et al.*, 2018; Petruzzelli *et al.*, 2014).

IL-6 has been associated with disease progression in cancer patients correlating with reduced patient survival (Fearon *et al.*, 2012; Ramsey *et al*, 2019). Due to its prominence in late-stage disease and ability to promote cachexia, IL-6 was studied as a target for therapy and diagnosis as a biomarker (Kayacan *et al.*, 2006; Kuroda *et al*,

2007; Ramsey *et al.*, 2019; Riccardi *et al*, 2020; Tisdale, 1997). Similar to TNFα, IL-6 elevation has been noted in cachectic patients suffering from CHF, CKD, or COPD (Webster *et al.*, 2020). However, the correlation between the induction of IL-6 and cachexia remains controversial as there are conflicting reports regarding its elevation in relation to weight loss and its use as a biomarker (Fearon *et al.*, 2012; Kayacan *et al.*, 2006; Kuroda *et al.*, 2007; Ramsey *et al.*, 2019; Riccardi *et al.*, 2020). Clinical trials using a humanized anti-IL-6 antibody in cachectic lung cancer patients suggested limited efficacy of IL-6 blockade in treating cachexia contrary to observations in animal models using similar strategies. Indeed, studies using prominent animal models of cancer cachexia, such as the colon-26 (C26) adenocarcinoma model and the $APC^{Min/+}$ mouse model, demonstrated that muscle wasting is driven by IL-6 elevation and activity (Baltgalvis *et al.*, 2008; Baltgalvis *et al.*, 2009; Bonetto *et al*, 2016; Carson & Baltgalvis, 2010; Soda *et al.*, 1995; Strassmann *et al.*, 1992). Although impairment of IL-6 in clinical trials reversed symptoms such as anorexia, fatigue, and anemia, it did not prevent loss of lean body mass in clinic (in contrast to the animal models described above) (Baltgalvis *et al.*, 2008; Bayliss *et al*, 2011; Carson & Baltgalvis, 2010; Strassmann *et al.*, 1992). Nevertheless, the importance of IL-6 should not be ignored as other factors could have compensated for its activity in the IL-6 antibody treated patients (Bayliss *et al.*, 2011). Indeed IL-6 is a member of a larger family of cytokines which are classified by their use of a common receptor subunit glycoprotein 130 (gp130) (Rose-John, 2018). Approaching IL-6 inhibition by blocking the receptor could prove more fruitful as it would also impair other family members which also have pro-cachectic functions such as Leukemia Inhibitory Factor (LIF) (Ando *et al*, 2013; Zhang *et al*, 2021).

Several recent studies have highlighted the role of LIF in driving cachexia and its ability to potentiate pro-cachectic mechanisms associated with IL-6 (Jorgensen & de la Puente, 2022; Zhang *et al.*, 2021). Studies on LIF have focused on its role in promoting cachexia in mouse models (mainly the C26) of the syndrome (Zhang *et al.*, 2021), (Arora *et al*, 2020; Arora *et al*, 2018; Kandarian *et al*, 2018; Seto *et al*, 2015). In the C26 model, tumor-mediated elevation of LIF is involved in many cancer-driven cachectic effects. *In vitro* studies using conditioned media of C26 cells showed that LIF is a primary factor involved in promoting wasting of cultured myotubes (Seto *et al.*, 2015). In addition, *in vivo* experiments using the C26 model demonstrated that LIF signaling is critical in the induction of systemic inflammation in these tumor bearing mice (Kandarian *et al.*, 2018). Systemic LIF elevation, either released by the tumor or by injection of recombinant protein, was shown to cause atrophy of muscles, anorexia, and lipolysis that drives adipose tissue wasting (Arora *et al.*, 2020; Arora *et al.*, 2018; Kandarian *et al.*, 2018). Interestingly, LIF was able to promote these effects in IL-6 knockout mice, suggesting its ability to compensate for IL-6 blockade (Arora *et al.*, 2020). In these studies, methods to impair LIF activity were utilized and included LIF neutralizing antibodies (Arora *et al.*, 2018; Kandarian *et al.*, 2018; Seto *et al.*, 2015), antibodies that neutralize the LIF receptor subunit gp130 (Arora *et al.*, 2018), introduction of miRNA miR-29c (that downregulates LIF expression) (Xie *et al*, 2021), and inhibiting downstream LIF signaling with small molecules (Arora *et al.*, 2020; Seto *et al.*, 2015). Utilization of such strategies in future translational studies focused on cachexia in humans offer an interesting alternative to IL-6 blockade which has been shown to not be sufficient to reverse wasting and improve patient survival (Bayliss *et al.*, 2011).

1.3.1.3 Interleukin 1

A prominent factor in systemic inflammatory responses, interleukin 1 (IL-1) has been studied as a potential biomarker and driver of cachexia (McDonald *et al*, 2018; Porporato, 2016). Elevation of IL-1 has been associated with cancer cachexia as well as CHF-induced cachexia (Laird *et al*, 2021; Peixoto da Silva *et al.*, 2020; Porporato, 2016; Sadeghi *et al*, 2018; Webster *et al.*, 2020). IL-1 has two isoforms with mainly redundant functions, IL-1α and IL-1β, which both promote inflammation by stimulating the expression of various cytokines (Laird *et al.*, 2021; McDonald *et al.*, 2018). The expression of these isoforms is differentially regulated, with IL-1β being only expressed upon inflammation while IL-1α being constitutively expressed (although it's expression can also upregulated with inflammation) (Voronov *et al*, 2013). IL-1 has been implicated in promoting tumor metastasis, which could contribute to its pro-cachectic effects as cancer cachexia is often associated with late-stage, metastatic disease (McDonald *et al.*, 2018; Tomasin *et al*, 2019). IL-1 is believed to contribute to muscle wasting by also disrupting the ability of the central nervous system (CNS) to regulate systemic metabolism. Shown to have anorexigenic effects, IL-1 causes hypothalamic dysfunction through increases in systemic tryptophan and serotonin levels that trigger early satiety. In addition, IL-1 has been associated with stimulation of hypothalamic neuronal populations which initiate muscle proteolysis and adipose tissue lipolysis (Laird *et al.*, 2021; McDonald *et al.*, 2018). Despite these pro-cachectic effects, the causative relationship between IL-1 and cachexia has been questioned as there are studies showing that IL-1 antagonism in animal models of cachexia is ineffective at reversing muscle wasting and that physiological doses of IL-1 do not affect food intake or weight

(Albrecht, 1996; Peixoto da Silva *et al.*, 2020; Porporato, 2016; Tisdale, 1997). As the primary pro-cachectic effects of IL-1 target the CNS, these past attempts at deducing the role of IL-1 in the etiology of cachexia and treating the condition in animal models may have failed due to their inability to impair IL-1 that has crossed the blood-brain barrier. To offer a better chance of success, future studies assessing the therapeutic potential of IL-1 blockade should consider the limitations of many drugs which cannot enter the brain from circulation.

1.3.1.4 Myostatin, Activin A, and Growth Differentiation Factor 11

Myostatin, Activin A, and Growth Differentiation Factor 11 (GDF11) belong to the transforming growth factor-β (TGFβ) family of factors that maintain muscle function by regulating their development, growth, and differentiation (Egerman & Glass, 2014, 2019; Suh & Lee, 2020). These “myokines” limit muscle growth by negatively affecting muscle mass and signal through the Activin Type II B (ActRIIB) receptor (Elkina *et al*, 2011). Interestingly, genetic depletion of myostatin or inhibition of the ActRIIB receptor causes hypertrophy in animal models (Elkina *et al.*, 2011; Lach-Trifilieff *et al*, 2014). Despite sharing redundant functions, these myokines are likely distinct in their roles. GDF11 and Activin A are believed to have higher potencies compared to myostatin (Egerman & Glass, 2019; Hammers *et al*, 2017; Suh & Lee, 2020). Furthermore, the expression of GDF11 and myostatin is differentially regulated throughout the lifespan of an organism as increase of GDF11 with age has been associated with sarcopenia despite the concurrent decrease of myostatin (Brun & Rudnicki, 2015; Egerman *et al*, 2015; Egerman & Glass, 2019). Due to their pervasive role as negative regulators of muscle growth and links to sarcopenia, these myokines therefore represent attractive subjects

of study in cachexia. Indeed, administration of excess levels of myostatin, Activin A, or GDF11 cause significant muscle atrophy and dysfunction (Chen *et al*, 2014; Hammers *et al.*, 2017; Zimmers *et al*, 2002; Zimmers *et al*, 2017). Recombinant GDF11 administration has also been shown to induce anorexia through its upregulation of the anorexigenic factor GDF15 (Jones *et al*, 2018). Despite these pro-cachectic effects, the clinical relevance of these myokines in causing cachexia is still under debate. It is unclear how the expression of these myokines is altered in cachectic patients. Activin A is reported to be elevated in inflammatory diseases which can cause cachexia (Fearon *et al.*, 2012; Loumaye & Thissen, 2017). In line with this, limited reports in cancer patients suggest that Activin A is upregulated in cachectic patients and patients with poor prognosis, while myostatin levels are decreased (Loumaye *et al*, 2015; Loumaye *et al*, 2017; Loumaye & Thissen, 2017). Conversely, the expression of myostatin was shown to be increased in cachectic patients suffering from AIDS and COPD suggesting that each condition has a unique set of myokines responsible for promoting wasting (Argilés *et al*, 2012). Work in preclinical models support this notion and emphasize the importance of cachexia-induced alteration of the balance between myokines and negative regulators such as follistatin causing an overall increase in ActRIIB signaling to promote wasting (Argilés *et al.*, 2012; Costelli *et al*, 2008; Fearon *et al.*, 2012; Loumaye & Thissen, 2017).

Studies using preclinical models of cachexia indicated that inhibition of these myokines either individually or through blockade of the ActRIIB receptor was a promising therapeutic strategy (Argilés *et al.*, 2012; Busquets *et al*, 2012; Chen *et al*, 2017; Gallot *et al*, 2014; Hatakeyama *et al*, 2016; Klimek *et al*, 2010; Lach-Trifilieff *et al.*,

2014; Smith *et al*, 2015; Zhou *et al*, 2010). Antibody-mediated inhibition of the ActRIIB receptor was shown to prevent muscle wasting and improve survival of mice affected by cachexia inducing cancers (Busquets *et al.*, 2012; Hatakeyama *et al.*, 2016; Klimek *et al.*, 2010; Zhou *et al.*, 2010). With this body of evidence suggesting the efficacy of impairing ActRIIB signaling in curing cachectic muscle wasting, antibody therapies against myostatin (LY2495655, Landogrozumab) and ActRIIB (BYM338, Bimagrumab) were tested in clinic (Cohen *et al.*, 2015; Golan *et al*, 2018; Nielsen *et al*, 2021; Smith *et al.*, 2015). Despite the success of LY2495655 in preserving muscle mass and strength in C26 tumor-bearing mice, human trials in pancreatic cancer patients showed no clinical benefit to myostatin inhibition (Golan *et al.*, 2018; Smith *et al.*, 2015). Similarly, ActRIIB inhibition with BYM338 failed to prevent cachexia in patients with lung or pancreatic cancer (Nielsen *et al.*, 2021; Shyh-Chang, 2017). Like the setbacks faced by TNFα and IL-6 blockade, myostatin and ActRIIB inhibition may potentially be compensated for by other factors which trigger similar downstream pathways that lead to wasting.

1.3.2 Pro-Cachectic Transcription Factors

As highlighted above, muscle wasting is associated with many pro-inflammatory cytokines whose primary function is to initiate various downstream signaling pathways in target tissues. The effects of activation of pro-cachectic signaling pathways are marked by transcriptional changes in muscle. These alterations in gene expression are driven by several key, pro-cachectic transcription factors, notably forkhead box protein O (FOXO) family proteins, SMAD2 and 3, Nuclear Factor kappa B (NF-κB), and Signal

Transducer and Activator of Transcription 3 (STAT3). A description of each and their role during cachexia-induced muscle wasting is presented below.

1.3.2.1 SMAD2, SMAD3, and FOXO

Downstream signaling of the TGFβ family members myostatin, Activin A, and GDF11 is primarily mediated by members of the Smad family of transcription factors, SMAD2 and SMAD3 (Egerman & Glass, 2014; Elkina *et al.*, 2011; Sartori *et al.*, 2009). Similar to inhibition of myostatin and ActRIIB, inhibition of SMAD2/3 causes hypertrophy (Sartori *et al.*, 2009). On the other hand, activation of SMAD2/3 signaling decreases protein synthesis (by inhibiting AKT phosphorylation) and increases protein degradation to block muscle growth (Chen *et al.*, 2014; Cohen *et al.*, 2015; Zhou *et al.*, 2010). SMAD2/3 signaling promotes protein degradation by preventing AKT-mediated inhibition of FOXO transcription factors, which are key activators of muscle-specific protein degradation pathway (Chen *et al.*, 2017; Chen *et al.*, 2014; Cohen *et al.*, 2015; Zhou *et al.*, 2010). FOXO proteins are known to translocate to the nucleus and induce the expression of the E3 ligases Murf1 and atrogin-1, which promote proteasome degradation during muscle wasting. They have also been implicated in stimulating the expression of genes involved in autophagy (Fearon *et al.*, 2012; Franco-Romero & Sandri, 2021). Some of the downstream effects of SMAD2/3 signaling in cachectic conditions, such as FOXO induction and atrogene expression, are not unique products of SMAD2/3 activity as several pro-cachectic stimuli have been noted to activate these factors (Baracos *et al.*, 2018; Cohen *et al.*, 2015; Egerman & Glass, 2014; Webster *et al.*, 2020). Therefore, elucidating the points of convergence of the many pro-cachectic pathways can allow for the development of novel therapeutic strategies that target the

final executors of cachexia that drive muscle wasting, which have the advantage of avoiding upstream redundancies.

1.3.2.2 NF-κB

NF-κB is often described as a major regulator of inflammatory signaling, integrating the extracellular stimuli of cytokines including TNFα, IL-1, and proteolysis-inducing factor (PIF) and intracellular stimuli such as oxidative stress (Peixoto da Silva *et al.*, 2020; Tisdale, 2009; von Haehling *et al*, 2002). NF-κB activity is regulated through its sub-cellular localization. Under normal conditions, NF-κB is found in an inactive state in the cytoplasm due to its binding to the Inhibitor of κB (IκB) protein (Guttridge, 2004). During inflammatory conditions, however, activation of cells results in the phosphorylation of IκB by the IkB kinase (IKK) leading to its degradation. This thereby allows NF-κB to translocate from the cytoplasm to the nucleus where it can mediate the transcription of its target genes (Guttridge, 2004). NF-κB has been reported to contribute to the onset of cachexia through the induction of several, distinct mechanisms. The importance of this factor has been demonstrated in functional studies where NF-κB ablation prevented cachexia, while its overactivation induced wasting (Cai *et al*, 2004; Wysong *et al*, 2011). As a central node of inflammatory responses, NF-κB has been shown to promote the expression of TNFα and IL-6 during cachexia (Guttridge, 2004; Zhou *et al*, 2003). Interestingly, this function has been reported in other inflammatory contexts such as rheumatoid arthritis where NF-κB is associated with similar increases in TNFα, IL-6, and IL-1 expression (Liu *et al*, 2017; von Haehling *et al.*, 2002). The regulation of cytokine transcription by NF-κB suggests the presence of a positive feedback loop where NF-κB promotes the expression of TNFα and IL-1 that,

in turn, act in an autocrine manner to further activate NF-κB (Guttridge, 2004; Zhou *et al.*, 2003). Downstream of this pro-inflammatory effect, a well-documented mechanism in skeletal muscle by which NF-κB promotes wasting is through activation of FOXO, increased expression of muscle specific-E3 ligases, and increased expression of UPP factors to favor negative protein balance (Cai *et al.*, 2004; Fearon *et al.*, 2012; Webster *et al.*, 2020; Wyke & Tisdale, 2005). Indeed, NF-κB-induced protein degradation has been shown to target key muscle proteins such as the myogenic protein myosin heavy chain (MyHC) (Acharyya *et al.*, 2004; Fearon *et al.*, 2012; Li & Reid, 2000; Wyke & Tisdale, 2005).

NF-κB activity has also been implicated in disrupting the myogenic program that regulates the differentiation and maintenance of skeletal muscle (Di Marco *et al.*, 2005; Guttridge *et al.*, 2000). *In vitro* studies have shown that NF-κB is involved in downregulating the expression of several MRFs, including MyoD leading to muscle wasting (Di Marco *et al.*, 2005; Guttridge *et al.*, 2000). NF-κB-mediated increase in the expression of the transcription factor paired box 7 (Pax7) in muscle progenitor cells is another mechanism through which it affects the expression of MRFs (He *et al*, 2013). Pax7 regulates myogenesis at multiple levels and stimulates the proliferation and survival of muscle progenitor cells (Kuang *et al*, 2006). Pax7 depletion allows for the induction of the MRFs MyoD and myogenin, permitting proper determination and fusion of muscle progenitor cells into muscle fibers (He *et al.*, 2013). The sustained elevation of Pax7 and impairment of MyoD and myogenin induction in cachectic muscle therefore disrupts muscle maintenance and allows for accumulation of muscle fiber damage

thereby enhancing wasting (He *et al.*, 2013). Nevertheless, the NF-κB-dependent factors that sustain Pax7 elevation have not been identified.

1.3.2.3 STAT3

STAT3 is a well-established downstream mediator of signaling from several pro-cachectic cytokines including IL-6, IL-6 family member cytokines, and IFNγ. STAT3, over the years, has increasingly been recognized as a central factor in muscle wasting (Zimmers *et al.*, 2016). Canonical STAT3 function is regulated through control of its dimerization. This regulatory switch is managed by Janus Kinase (JAK) mediated phosphorylation of STAT3 at the tyrosine residue Y705, which occurs when upstream receptors are activated and JAKs and STAT3 are recruited to them. Phosphorylation of Y705 allows for STAT3 to dimerize and amass in the nucleus where it can promote or negatively affect transcription of genes involved in inflammatory responses and several pro-tumorigenic functions in disease contexts (Zimmers *et al.*, 2016). Other modifications of STAT3 have been reported, such as the phosphorylation of serine S727 that promotes STAT3 association with cofactors, but the importance of these modifications in cachectic muscle are not established (Ma *et al.*, 2017; Zimmers *et al.*, 2016). Nevertheless, in mouse models of cancer cachexia, increased pY705-STAT3 levels in muscle and increased pS727-STAT in liver and adipose tissue have been reported (Zimmers *et al.*, 2016).

With a wide range of functions in tissues (e.g., muscle, liver, tumor, adipose, and hypothalamus) linked in the complex etiology of cachexia, the contribution of STAT3 to wasting is multifaceted (Zimmers *et al.*, 2016). Initial studies assessing the function of STAT3 in cachexia highlighted its role as a downstream effector of IL-6 in muscle and

liver. Activation of STAT3 in muscle caused wasting, while its inhibition prevented atrophy (Bonetto *et al.*, 2012; Bonetto *et al.*, 2011; Ma *et al.*, 2017; Mubaid *et al*, 2019). This has been corroborated by recent studies which demonstrated that tumor-derived and macrophage-derived factors induce STAT3 activation in muscle to promote wasting (Hu *et al*, 2019; Shukla *et al*, 2020). Interestingly work from our lab has shown that STAT3 induction and activation in cachectic muscle is regulated post-transcriptionally by the RNA binding protein (RBP) Human antigen R (HuR) (Mubaid *et al.*, 2019). In this study, HuR was found to bind the STAT3 mRNA and promote its translation by preventing miR-330-mediated translation inhibition (Mubaid *et al.*, 2019). Our lab has also shown that STAT3 has IL-6 independent functions during cachexia and is responsive to TNFα and IFNγ (Ma *et al.*, 2017). In characterizing these IL-6 independent functions, our lab identified a novel function of STAT3 in that it formed a complex with NF-κB to promote transcription of the pro-cachectic effector such as inducible nitric oxide synthase (iNOS) (Ma *et al.*, 2017). Impairment of this STAT3/NF-κB-mediated function importantly had anti-cachectic effects (Ma *et al.*, 2017). Another mechanism by which STAT3 promotes muscle loss is, in part, due to its activation of the UPP, which was postulated to supply amino acids for the production of APR proteins in both muscle and liver (Bonetto *et al.*, 2012; Bonetto *et al.*, 2011; Zimmers *et al.*, 2016). As STAT3 is an essential factor in the induction of the APR, STAT3-mediated protein degradation can positively regulate this function (Zimmers *et al.*, 2016). Indeed, work in animal models of cachexia associated STAT3 activation with increased expression of atrogenes in muscle and elevated levels of APR proteins in both skeletal muscle and liver (Bonetto *et al.*, 2012; Bonetto *et al.*, 2011; Zimmers *et al.*, 2016). In cancer and

CKD-induced cachexia, STAT3-mediated expression of the CAAT/enhancer-binding protein δ (C/EBPδ) transcription factor has been shown to contribute to increased atrogene expression. C/EBPδ facilitates this function by inducing myostatin expression, promoting FOXO activity and muscle catabolism (Silva *et al*, 2015; Zhang *et al*, 2013). The above observations on STAT3-mediated activation of C/EBPδ and IL-6 independent functions of STAT3 suggests that the crosstalk between pro-cachectic pathways can complicate the treatment of cachexia. Therapeutic strategies that target upstream factors can potentially be compensated for by redundant activation methods for master regulators of the syndrome.

Recent studies have highlighted the role of STAT3 in intercellular communication between muscle, adipose tissue, and tumors through extracellular vesicles (EVs) to drive wasting in target tissues (Fan *et al*, 2022; Hu *et al.*, 2019). With growing attention to the function of tumor derived EVs in cancer pathogenesis, assessing their role in cachexia could offer new insight into the etiology of the syndrome. In a series of studies, STAT3 was involved in not only the biogenesis of tumor derived EVs, but also the induction of atrogene expression in response to EV signals (Fan *et al.*, 2022; Hu *et al.*, 2019). Another potential means through which STAT3-mediated EV communication could promote wasting is through dysregulation of myogenesis and cellular metabolism in target tissues (Pin *et al.*, 2022).

With its wide-ranging pro-cachectic functions, targeting STAT3 activity remains an attractive target in the prevention of cachexia. Studies in preclinical animal models have utilized both direct (C188-9) (Silva *et al.*, 2015; Zhang *et al.*, 2013) and indirect inhibitors (through either IL-6 signaling blockade (Miller *et al*, 2017) or JAK1/2 inhibition

(ruxolitinib) (Arora *et al.*, 2020; Seto *et al.*, 2015)) to successfully treat cachexia. These findings suggest that employment of these drugs in treating cachexia in clinical trials could be promising. Indeed, ruxolitinib was shown to increase survival and quality of life in patients with myelofibrosis by preventing the onset of cachexia (Mesa *et al*, 2015; Verstovsek *et al*, 2017). Despite this, the use of ruxolitinib has proven unsuccessful in improving patient survival of pancreatic cancer where cachexia is very prevalent (Hurwitz *et al*, 2018). It is likely that the efficacy of JAK/STAT blockade in prevention of cachexia in myelofibrosis is due to treatment of the overlying condition which ruxolitinib did not accomplish in pancreatic cancer trials. Furthermore, differential regulation of JAK/STAT pathway activation between myeloproliferative cancers to pancreatic cancer could potentially explain this difference in effectiveness (Hurwitz *et al.*, 2018). Therefore, use of clinically viable STAT3 inhibitors may prove more efficacious to improve survival and alleviate cachexia in pancreatic cancer patients.

1.3.3 Inducible Nitric Oxide Synthase and Cachexia

An accumulating body of work from our group and others has shown that NF-κB/STAT3-dependent iNOS induction is strongly correlated with cachectic muscle wasting (Adams *et al*, 2003; Agusti *et al*, 2004; Buck & Chojkier, 1996; Di Marco *et al*, 2012; Di Marco *et al.*, 2005; Ma *et al.*, 2017). iNOS is one of three nitric oxide synthase (NOS) enzymes, distinguished by its robust induction during inflammation (Bogdan, 2001). Indeed, all three NOS isoforms (i.e., iNOS, endothelial NOS (eNOS), and neuronal NOS (nNOS)) can be expressed in skeletal muscle, however, iNOS is more strongly induced in response to cachectic stimuli such as lipopolysaccharide (El-Dwairi *et al*, 1998; Hussain *et al*, 1997). NOS enzymes produce a bioactive gas named nitric

oxide (NO) from the breakdown of L-arginine to L-citrulline, but iNOS in particular produces very high levels of NO compared to other NOS enzymes and physiologically iNOS derived NO is utilized to fight infection (Bogdan, 2001). However, our current understanding of the mechanisms behind iNOS-driven cachectic effects remains limited.

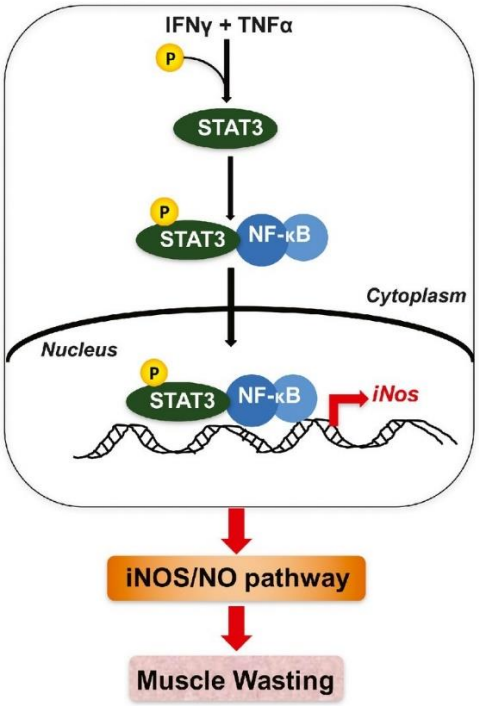

Figure 1.7: Active NF-κB pathway is required for the rapid translocation of pY-STAT3 to the nucleus during IFNγ/TNFα-induced muscle wasting.
Model depicting how STAT3 promotes cytokine-induced muscle wasting. The cytokines IFNγ and TNFα act synergistically by activating STAT3 via phosphorylation on its Y705 residue. Following the degradation of IκBα (not shown here), pY-STAT3 translocates to the nucleus as a complex with NF-κB and upregulates the expression of iNOS, leading to the activation of the iNOS/NO pathway, which in turn promotes muscle wasting. *Reprinted from Ma JF, Sanchez BJ, Hall DT, Tremblay AMK, Di Marco S, Gallouzi IE (2017) STAT 3 promotes IFN γ/TNF α-induced muscle wasting in an NF-κB-dependent and IL-6-independent manner. EMBO molecular medicine 9: 622-637 with permission from John Wiley and Sons.*

In wasting muscle, pro-inflammatory cytokine-stimulated iNOS expression results in pathologically high levels of NO (Anavi & Tirosh, 2020; Hall *et al*, 2011; Powers *et al*,

2016). Work from our group and others has demonstrated that iNOS function is vital in driving cachexia-induced muscle wasting. Initial work on iNOS demonstrated that its induction by TNFα and associated NO production/oxidative stress caused wasting, and importantly iNOS inhibition prevented this effect (Buck & Chojkier, 1996). Following this study, our group demonstrated that the previously observed NF-κB-mediated decay of the MyoD mRNA during cachexia requires iNOS expression (Di Marco *et al.*, 2005). Under these conditions, the increased expression of iNOS occurs due to the increased stability of the iNOS message as a result of the binding of HuR to an AU-rich element in the 3'untranslated region (UTR). (Di Marco *et al.*, 2005). This work also demonstrated that the downregulated expression of MyoD is dependent on the production of the free radical peroxynitrite ($ONOO^-$) which is formed from the reaction of NO with free oxygen radicals including superoxide (O_2^-) (Di Marco *et al.*, 2005). Noting the potential therapeutic benefit of iNOS impairment, further work by our group demonstrated that indirect means of iNOS impairment through inhibition of its expression prevented wasting both in *in vitro* and *in vivo* models of wasting (Di Marco *et al.*, 2012; Hall *et al.*, 2018; Ma *et al.*, 2017). The expression of iNOS has been shown to increase in several cachexia models and samples from heart failure, cancer, and COPD patients suggesting the pervasive action of iNOS in various types of cachexia (Adams *et al.*, 2003; Agusti *et al.*, 2004; Arneson-Wissink & Doles, 2021; Buck & Chojkier, 1996; Di Marco *et al.*, 2012; Di Marco *et al.*, 2005; Hall *et al.*, 2018; Ma *et al.*, 2017; Powers *et al.*, 2016; Ramamoorthy *et al*, 2009).

Although not studied in cachexia models, iNOS has been associated with the pathogenesis of several metabolic diseases reviewed in (Anavi & Tirosh, 2020).

Interestingly, a study printed after the publication of work presented in Chapter 2 has also linked iNOS-driven metabolic defects in myoblasts to impaired differentiation likely explaining previously described NF-κB-mediated disruption of muscle repair in cancer models of cachexia (Arneson-Wissink & Doles, 2021; He *et al.*, 2013). Therefore, with our current understanding of the metabolic dysfunctions occurring in cachexia, the importance of iNOS in cachexia progression, and the links between iNOS and metabolic disease, it is possible that iNOS disrupts differentiated skeletal muscle metabolism to cause muscle wasting.

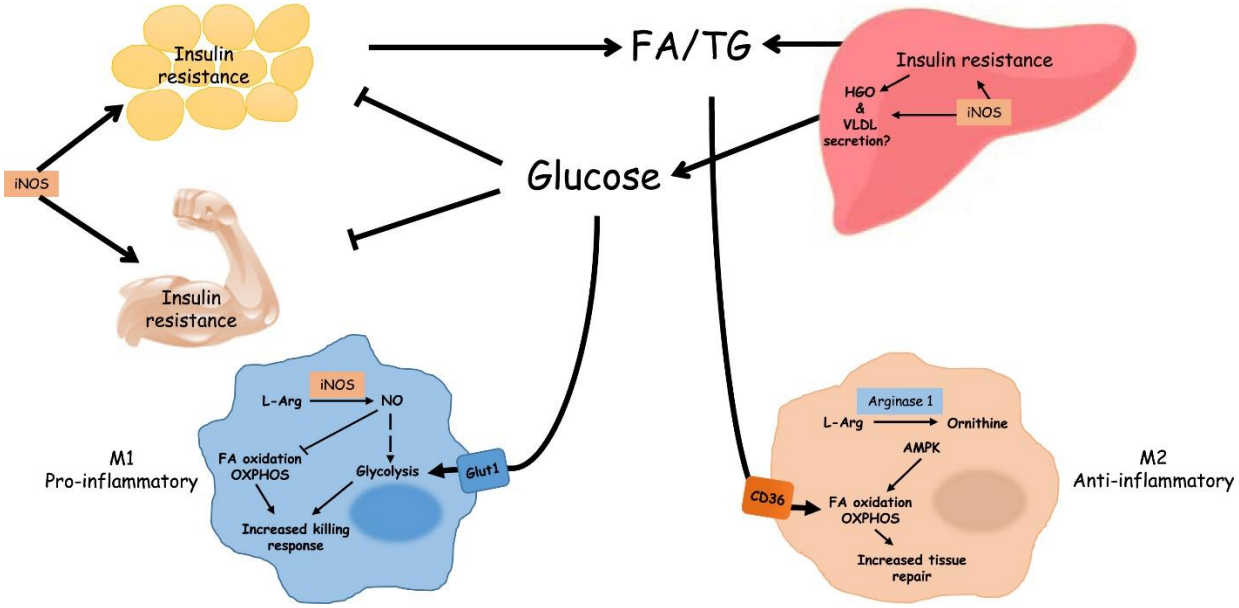

Figure 1.8: iNOS regulates glucose and lipids metabolism under inflammatory conditions.

iNOS activation promotes hepatic glucose output which diminishes muscle and adipose tissue glucose uptake. Subsequently, adequate glucose supply is available for pro-inflammatory immune cells utilization. Activation of iNOS further results in elevated blood fatty acids/triglycerides levels at least, in part, by stimulating adipose tissue lipolysis and/or hepatic VLDL secretion. FA, fatty acids; HGO, hepatic glucose output; L-Arg, L-Arginine; iNOS, inducible nitric oxide synthase; OXPHOS, oxidative phosphorylation; TG, triglycerides; VLDL, very low-density lipoprotein. *Reprinted from Anavi S, Tirosh O (2020) iNOS as a metabolic enzyme under stress conditions. Free Radical Biology and Medicine 146: 16-35 with permission from Elsevier.*

As mentioned above, several studies have shown that iNOS impairment has anti-cachectic effects in *in vitro* and *in vivo* models of cachexia (Arneson-Wissink & Doles, 2021; Buck & Chojkier, 1996; Di Marco *et al.*, 2012; Di Marco *et al.*, 2005; Hall *et al.*, 2018; Hall *et al.*, 2011; Ma *et al.*, 2017). A group of these studies utilized direct small molecule inhibitors including aminoguanidine (AMG), nitro-L-arginine, or 1400W to inhibit iNOS (Arneson-Wissink & Doles, 2021; Buck & Chojkier, 1996; Di Marco *et al.*, 2005). Despite their utility in discerning the therapeutic potential of iNOS inhibition in treating cachectic muscle wasting these drugs have not successfully undergone clinical development. An iNOS inhibitor called GW274150 (GW) has been tested up to phase II clinical trials to treat migraines, rheumatoid arthritis, and asthma showing efficient iNOS inhibition in clinical settings without major side effects (Høivik *et al*, 2010; Seymour *et al*, 2012; Víteček *et al*, 2012). Although the effectiveness of GW in treating these conditions was not an improvement compared to existing drugs (Høivik *et al.*, 2010; Seymour *et al.*, 2012; Víteček *et al.*, 2012), clinically viable iNOS inhibitors could hold promise in treating cachexia which currently has no effective therapies.

In addition to small molecule drugs targeting iNOS, indirect means of impairment have also been explored (Di Marco *et al.*, 2012; Hall *et al.*, 2018; Ma *et al.*, 2017). Of particular interest to the data presented in Chapter 3 is previous work by our lab using a eukaryotic initiation factor-4A (eIF4A) inhibitor called Pateamine A (PatA) in treating cachectic muscle wasting (Di Marco *et al.*, 2012). eIF4A is an ATP-dependent RNA helicase and is the most abundant member of the eIF4F complex that also contains eIF4G and eIF4E (Pelletier *et al*, 2015). eIF4A has two isoforms involved in mediating the initiation of translation which are nearly identical in humans and mice, eIF4AI and

eIF4AII (Chu & Pelletier, 2015; Pelletier *et al.*, 2015). eIF4A unwinds secondary structure in the 5'UTR of mRNAs allowing for recruitment of the 43S preinitiation complex (Pelletier *et al.*, 2015). PatA inhibits eIF4A by causing eIF4A to irreversibly clamp onto transcripts resulting in its depletion (Bordeleau *et al*, 2008). Our lab's work demonstrated that PatA prevented iNOS translation to deplete iNOS levels thereby preventing TNFα/IFNγ-induced loss of MyoD and myogenin mRNA expression (Di Marco *et al.*, 2012). Interestingly, eIF4A inhibitors are known to have anti-inflammatory and anti-cancer effects due to their ability to inhibit the selective translation of groups of pro-tumorigenic/inflammatory transcripts with secondary structure in their 5'UTR, which makes them sensitive to eIF4A depletion/inhibition (Bordeleau *et al.*, 2008; Chu & Pelletier, 2015; Romo *et al*, 2004; Singh *et al*, 2021; Zhang *et al*, 2020). Due to the irreversible nature of its mechanism of action, PatA is regarded as toxic therefore discouraging its use in clinical settings (Bordeleau *et al.*, 2008; Chu & Pelletier, 2015). Other inhibitors of eIF4A were proposed as promising therapeutic agents to treat cancer as well as inflammation-induced conditions. These include steroids such as Hippuristanol (Hipp) and rocaglates such as Silvestrol derivatives (Chu & Pelletier, 2015; Taroncher-Oldenburg *et al*, 2021). The rocaglate silvestrol has a similar mechanism of action to PatA where it depletes eIF4A by stimulating its association with mRNAs. This interaction is however reversible suggesting the potential of rocaglates as therapeutics to treat inflammatory induced conditions(Chu & Pelletier, 2015; Pelletier *et al.*, 2015). Indeed, very recently the rocaglate Zotatifin (eFT226) entered Phase I trials as an antiviral and is in Phase 1-2 trials against solid tumor cancers (Taroncher-Oldenburg *et al.*, 2021). In contrast to PatA and rocaglates, the steroid Hipp

allosterically inhibits eIF4A by shifting eIF4A into an inactive conformation (Chu & Pelletier, 2015; Pelletier *et al.*, 2015). Because of the high selectivity of Hipp for eIF4A compared to other related helicases and the more favorable therapeutic characteristics of Hipp compared to PatA, the use of this compound to treat cachexia-induced muscle wasting could prove fruitful (Chu & Pelletier, 2015).

1.3.3.1 Role of Reactive Oxygen/Nitrogen Species in Impairing Energy Metabolism

Highlighted in the previous sections above are a multitude of inflammatory and metabolic alterations that occur in cachexia. These pro-inflammatory and, importantly, metabolic insults are associated with oxidative stress causing dysfunction of key enzymes (e.g., ETC complexes, AKG dehydrogenase, aconitase) (Der-Torossian *et al.*, 2013b; Owen *et al.*, 2019; Penna *et al*, 2020; Wyart *et al.*, 2022). Oxidative stress and its subset nitrosative stress originate from two sources in cachectic muscle, reactive oxygen species (ROS) such as superoxide and reactive nitrogen species (RNS) such as NO and peroxynitrite (Hall *et al.*, 2011; Owen *et al.*, 2019). During inflammation, ROS can be produced through several means, including NADPH oxidase (Nox) activity and defective ETC complex activity, while NO is produced by iNOS (Ábrigo *et al.*, 2018; Powers *et al.*, 2016). ROS and RNS add post-translational modifications (PTM) to proteins leading to their dysfunction or degradation (Barreiro *et al*, 2005; Radi, 2018). ROS normally modify proteins through irreversible carbonylation, while NO mediates the S-nitrosylation of proteins producing labile nitrocysteine residues, and peroxynitrite irreversibly nitrates proteins on tyrosine residues producing 3-nitrotyrosine (3NT) (Agrawal *et al*, 2020; Barreiro *et al.*, 2005; Owen *et al.*, 2019). NO also can impair metal

centers (e.g., iron-sulfur (Fe-S) clusters) of proteins that are often essential for function (e.g., ETC complexes) (Radi, 2018). Regarding their role in cachexia, several studies have reported significant increases in total protein carbonylation and nitration in cachectic muscle, which are even able to persist in muscle after recovery from cachexia-causing illness for as long as 2-4 weeks causing long-term mitochondrial dysfunction and functional deficit (Barreiro *et al.*, 2005; Owen *et al.*, 2019; Wyart *et al.*, 2022). Furthermore, mitochondrial proteins specifically exhibit significant increases in carbonylation and nitration in cachectic muscle (Antunes *et al.*, 2014; McLean *et al*, 2014; Padrão *et al*, 2013). In line with this, a study on the role of NOS enzymes in muscle mitochondria found that endotoxemia led to increased production of mitochondrial NO, superoxide, and hydrogen peroxide which can lead to dysfunction through increased peroxynitrite formation (Alvarez & Boveris, 2004). Interestingly, similar observations have been made in aged rat cardiac muscle samples subjected to proteomic studies where a wide array of nitrated mitochondrial and metabolic proteins were identified (Kanski *et al*, 2005).

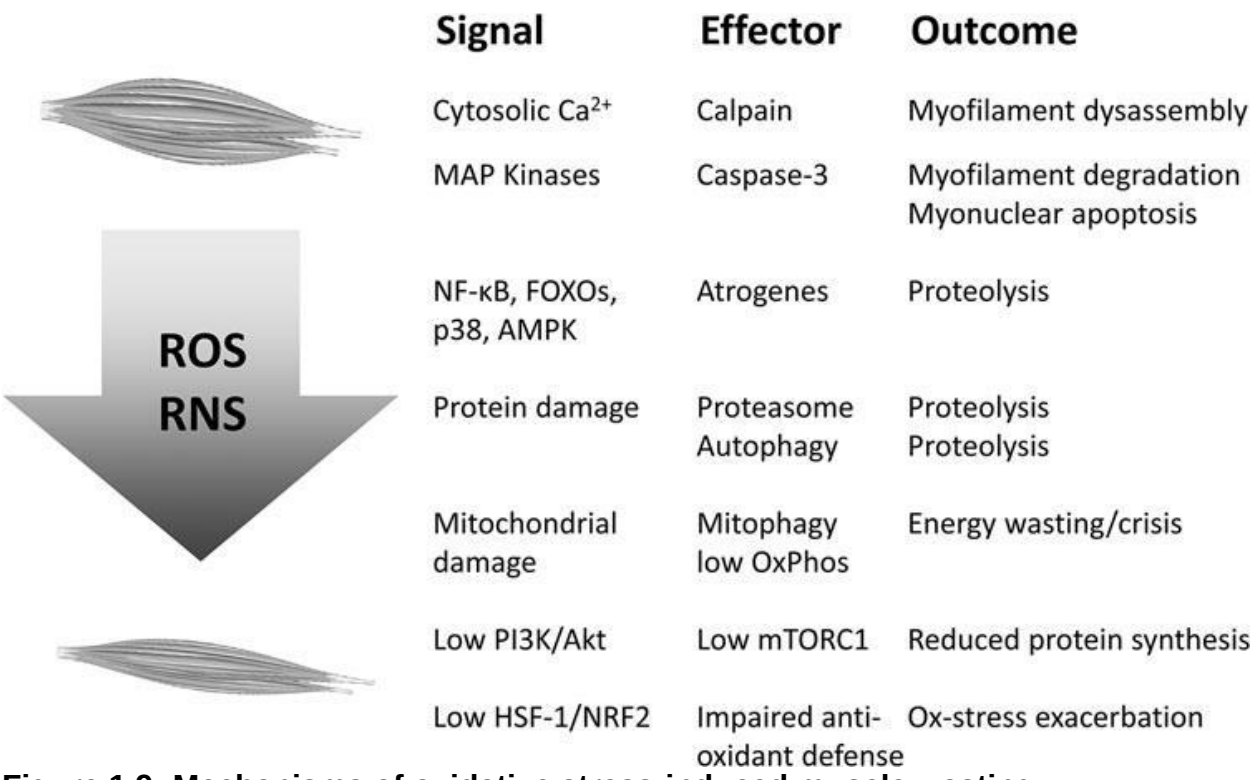

Figure 1.9: Mechanisms of oxidative stress-induced muscle wasting.
ROS/RNS imbalance, due to insufficient muscle cell adaptation, directly and indirectly generate distinct intracellular ‘‘Signals’’ that in turn activate ‘‘Effector’’ proteins/systems eventually leading to most of the alterations observed in cancer-induced muscle wasting (Outcome). NMJ, neuromuscular junction; OxPhos, oxidative phosphorylation; ox-stress, oxidative stress; RNS, reactive nitrogen species; ROS, reactive oxygen species. *Reprinted from Penna F, Ballaro R, Costelli P (2020) The redox balance: a target for interventions against muscle wasting in cancer cachexia? Antioxidants & Redox Signaling 33: 542-558 with permission from Mary Ann Liebert, Inc.*

In cachectic muscle, detrimental ETC complex function is suggested to be a major source of ROS associated with cytokine function (Powers *et al.*, 2016). Indeed, OXPHOS dysfunction can appear as soon as 2 hours after exposure to cachectic stimuli and is correlated with significant increases in oxidative stress over extended periods (McLean *et al.*, 2014). Drastic increases of β-oxidation in cachectic muscle can also contribute to early ROS production through a Complex III-mediated mechanism (Fukawa *et al.*, 2016; Rosca *et al*, 2012; Seifert *et al*, 2010). Interestingly, work in other systems has shown that NO production can inhibit ETC function through a two-phase

mechanism (Radi, 2018). First, NO can reversibly inhibit complex IV by outcompeting oxygen binding to its heme group leading to electron leakage and superoxide production. Next, peroxynitrite is formed by a reaction between NO and newly generated mitochondrial superoxide and can irreversibly inhibit complexes I and II through nitration, which are further impaired through modification by ROS and NO (Radi, 2018). However, the functional relevance of these OXPHOS inhibiting mechanisms and the importance of iNOS in driving them in cachectic muscle has not been demonstrated.

The iNOS/NO/$ONOO^-$ activity has also been shown to impair redox mechanisms in other systems (Radi, 2018). Under physiological conditions, superoxide is mainly processed by superoxide dismutase (SOD) enzymes to form hydrogen peroxide. SOD enzymes act in competition with NO though with basal levels of peroxynitrite being produced since the rate of reaction between NO and superoxide is much higher than superoxide and SODs (Radi, 2018). Under cachectic conditions where NO levels can drastically increase, NO likely outcompetes SOD enzymes allowing for accumulation of peroxynitrite and nitrosative stress. Interestingly, due to the kinetics of the reaction between NO or SODs with superoxide, induction of SOD expression cannot completely block peroxynitrite formation by NO as long as NO is continuously produced (Radi, 2018). To further impair oxidant defense, peroxynitrite can modify and inhibit the mitochondrial antioxidant protein manganese SOD (MnSOD) through nitration of tyrosine-34 within the active site (Demicheli *et al*, 2016; MacMillan-Crow *et al*, 1996). Examining the presence of these iNOS/NO/$ONOO^-$-mediated mechanism in cachectic muscle can enrich our understanding of redox homeostasis under these conditions.

1.4 Rationale

Cachexia is a deadly and debilitating syndrome that currently has no approved or effective treatments (Baracos *et al.*, 2018). It arises in several chronic, inflammation-mediated conditions such as cancer, COPD, HIV infection, and sepsis (Baracos *et al.*, 2018; Evans *et al.*, 2008; Peixoto da Silva *et al.*, 2020; Scherbakov & Doehner, 2018; Springer *et al.*, 2006). It is characterized by a dramatic, involuntary loss of muscle which negatively influences patient outcomes (Anker *et al.*, 1997; Baracos *et al.*, 2018; Kazemi-Bajestani *et al.*, 2016; Martin *et al.*, 2015; Peixoto da Silva *et al.*, 2020; Scherbakov & Doehner, 2018; Springer *et al.*, 2006). With its significant impacts, there is a pressing need to develop novel therapeutic strategies to combat cachexia. An effort has been made to delineate the mechanisms responsible for the initiation of cachexia. Various attempts to treat this condition by targeting upstream initiators have proven unsuccessful, likely due to the multifactorial nature of the syndrome (Bayliss *et al.*, 2011; Fearon *et al.*, 2012; Golan *et al.*, 2018; Jatoi *et al.*, 2010; Nielsen *et al.*, 2021; Wiedenmann *et al.*, 2008). Uncovering downstream effectors where pro-cachectic signaling converge, which are directly responsible for muscle atrophy may represent a more efficacious avenue for the development of therapies.

Cachectic muscle wasting is thought to result from pro-inflammatory cytokine-mediated alterations to both anabolic and catabolic pathways leading to muscle breakdown (Cohen *et al.*, 2015; Fearon *et al.*, 2012; Hardee *et al.*, 2017). Work in animal models and human cachexia patients have shown that pro-inflammatory signals disrupt muscle anabolism through impairment of protein synthesis and activate protein degradation pathways (Fearon *et al.*, 2012; Hall *et al.*, 2018; Hardee *et al.*, 2017;

Sandri, 2016; Tisdale, 2009; White *et al.*, 2013). These cytokines, further, have been shown to mediate cachexia-induced metabolic dysfunction that promotes imbalance of muscle protein homeostasis (Cui *et al.*, 2022; Hardee *et al.*, 2017; Shyh-Chang, 2017). Inflammation-associated perturbation of muscle energy production leads to energetic crisis, which simultaneously promotes protein degradation and inhibits anabolic pathways (Hardee *et al.*, 2017; VanderVeen *et al.*, 2017; White *et al.*, 2013). A suggested cause of this disruption of muscle energy metabolism is cachexia-induced mitochondrial dysfunction (Brown *et al.*, 2017; Hall *et al.*, 2018; Kunzke *et al.*, 2020; VanderVeen *et al.*, 2017; Wyart *et al.*, 2022).

Several pro-inflammatory cytokines have been implicated in causing these deleterious effects such as TNFα, IFNγ, and IL-6 (Fearon *et al.*, 2012; Tisdale, 2009). These extracellular signaling factors subsequently activate pro-inflammatory transcription factors such as STAT3 and NF-κB which mediate the expression of pro-cachectic effectors such as iNOS (Fearon *et al.*, 2012; Tisdale, 2009). In various systems, iNOS has been shown to affect cellular processes by disrupting mitochondrial energy production due to its ability to generate reactive nitrogen species that can damage mitochondrial macromolecules and electron transport chain proteins (Anavi & Tirosh, 2020; Bailey *et al*, 2019; Li *et al*, 2020; Palmieri *et al*, 2020; Radi, 2018). iNOS has previously been shown to be a driver of muscle wasting, but the mechanisms behind its pro-cachectic function remain elusive (Adams *et al.*, 2003; Agusti *et al.*, 2004; Buck & Chojkier, 1996; Di Marco *et al.*, 2012; Di Marco *et al.*, 2005; Ma *et al.*, 2017). My objective in Chapter 2 was to determine whether iNOS was a cause of metabolic defect in wasting muscle and whether iNOS inhibition is a viable therapeutic strategy to

prevent muscle loss in pre-clinical models of cachexia. To this end I showed that in cachectic muscle, iNOS is a trigger of energy crisis through mitochondrial dysfunction and that direct inhibition of iNOS protects against metabolic defects and atrophy.

Earlier work by our lab has shown that a drug called PatA, which inhibits eIF4A, can alleviate cachexia by silencing iNOS mRNA translation (Di Marco *et al.*, 2012). Interestingly, in other systems, eIF4A inhibition has been shown to have broader anti-inflammatory effects which could be beneficial in cachexia (Bordeleau *et al.*, 2008; Chu & Pelletier, 2015; Romo *et al.*, 2004; Singh *et al.*, 2021; Zhang *et al.*, 2020). Therefore, in Chapter 3, I tested the effectiveness of several eIF4A inhibitors in preventing the expression of iNOS, the activation of the iNOS/NO pathway and, consequently, muscle wasting. In doing so I aimed to confirm the anti-cachectic effects of eIF4A blockade and, furthermore, potentially identify other eIF4A sensitive pro-cachectic factors (in addition to iNOS). Here, I recapitulated previous observations where eIF4A inhibition effectively inhibited iNOS expression and protected against muscle wasting using Hipp, PatA, and Silvestrol which have distinct mechanisms of action against eIF4A. Furthermore, I showed that eIF4A inhibitors further interfered with cachectic signaling by preventing the translation of STAT3. Overall, this work presents the potential utility of direct iNOS inhibition and eIF4A inhibition in treating cachectic muscle wasting. In addition, this thesis reveals novel insight into how iNOS and eIF4A impair energy metabolism and inflammatory signaling, respectively.

2 Pharmacological or genetic inhibition of iNOS prevents cachexia-mediated muscle wasting and its associated metabolism defects

2.1 Genetic deletion of the iNOS gene prevents inflammation-induced muscle wasting

Induction of the pro-cachectic factor iNOS and pathological NO production has been associated with various metabolic disorders suggesting that it may have a role in cachexia-induced metabolic dysfunction (Anavi & Tirosh, 2020; Hall *et al.*, 2018; Hall *et al.*, 2011). To this end we assessed muscle loss and metabolic defects in mouse models of inflammation-induced muscle wasting.

We first used a lipopolysaccharide (LPS)-induced model of septic cachexia to assess these cachectic phenotypes in male wildtype (WT) and iNOS knockout (KO) C57BL/6 mice. Models of septic cachexia are capable of inducing muscle wasting over short periods of time (Leduc-Gaudet *et al.*, 2020; Moarbes *et al*, 2019; Mofarrahi *et al.*, 2012; Stana *et al.*, 2017). WT and iNOS KO mice were injected intraperitoneally with either saline or a low dose of LPS shown to induce mild muscle wasting after 18 hours (Braun *et al*, 2013; Hall *et al.*, 2018; Jin & Li, 2007). As LPS is known to significantly decrease food consumption in mice, we pair-fed the mice to match the food consumption of the LPS-treated WT mice accounting for variations resulting from different food intake (Braun *et al.*, 2013; Hall *et al.*, 2018). Skeletal muscle and tissues masses were normalized to the initial body weight to account for different starting sizes of mice as previously done in (Pin *et al.*, 2019a; Pin *et al.*, 2019b).

As a first step we verified proper induction of the cachectic phenotype in our LPS treated mice. We confirmed that the WT mice, but not the iNOS KO mice, expressed

iNOS protein in response to LPS (Figure 2.1A). We then measured iNOS activity in these muscles by assessing levels of 3NT modified proteins (Ahsan, 2013; Chatterjee *et al*, 2003) and observed that 3NT levels only increased in LPS-treated WT but not iNOS KO mice (Figure 2.1B). We next assessed the effect of iNOS KO on LPS-induced loss of body weight and muscle mass. We observed that both saline treated WT and iNOS KO mice experienced a 10-12% decrease in body weight due to pair feeding, and that LPS treatment did not significantly affect this loss of body weight in both genetic backgrounds (Figure 2.2A). Regarding muscle mass, we observed LPS-induced wasting of tibialis anterior (TA), soleus, and quadriceps muscles that, importantly, iNOS KO protected against (Figure 2.1C-F). We did not observe wasting in the gastrocnemius muscle (Figure 2.2B). Measurement of the minimum feret diameter (Figure 2.1G) and cross-sectional area (CSA) (Figure 2.2C) of the muscle fibers from the tibialis anterior muscle confirmed LPS-induced muscle wasting was prevented by genetic ablation of iNOS. In addition, we assessed whether there were differences in muscle fiber type composition (i.e., Type I, Type IIA and TypeIIB/IIX fibers) in the TAs of these mice. Importantly, muscle fiber type strongly influences muscle metabolism with Type I fibers depending on OXPHOS-mediated oxidative metabolism and Type II fibers mainly depending on glycolysis. Furthermore, Type I fibers are noted to be protected from wasting (Janice Sánchez *et al*, 2019). In our assessment, we observed no appreciable differences in fiber type composition between the four groups (Figure 2.2D). In order to assess the effect of inflammation-induced muscle wasting on muscle strength we next quantified changes in grip strength caused by LPS treatment (Murphy *et al.*, 2012). We observed that iNOS KO mice were protected from LPS-mediated loss of muscle

strength (Figure 2.1H). Together, these results demonstrate that genetic ablation of iNOS prevents LPS-induced muscle wasting.

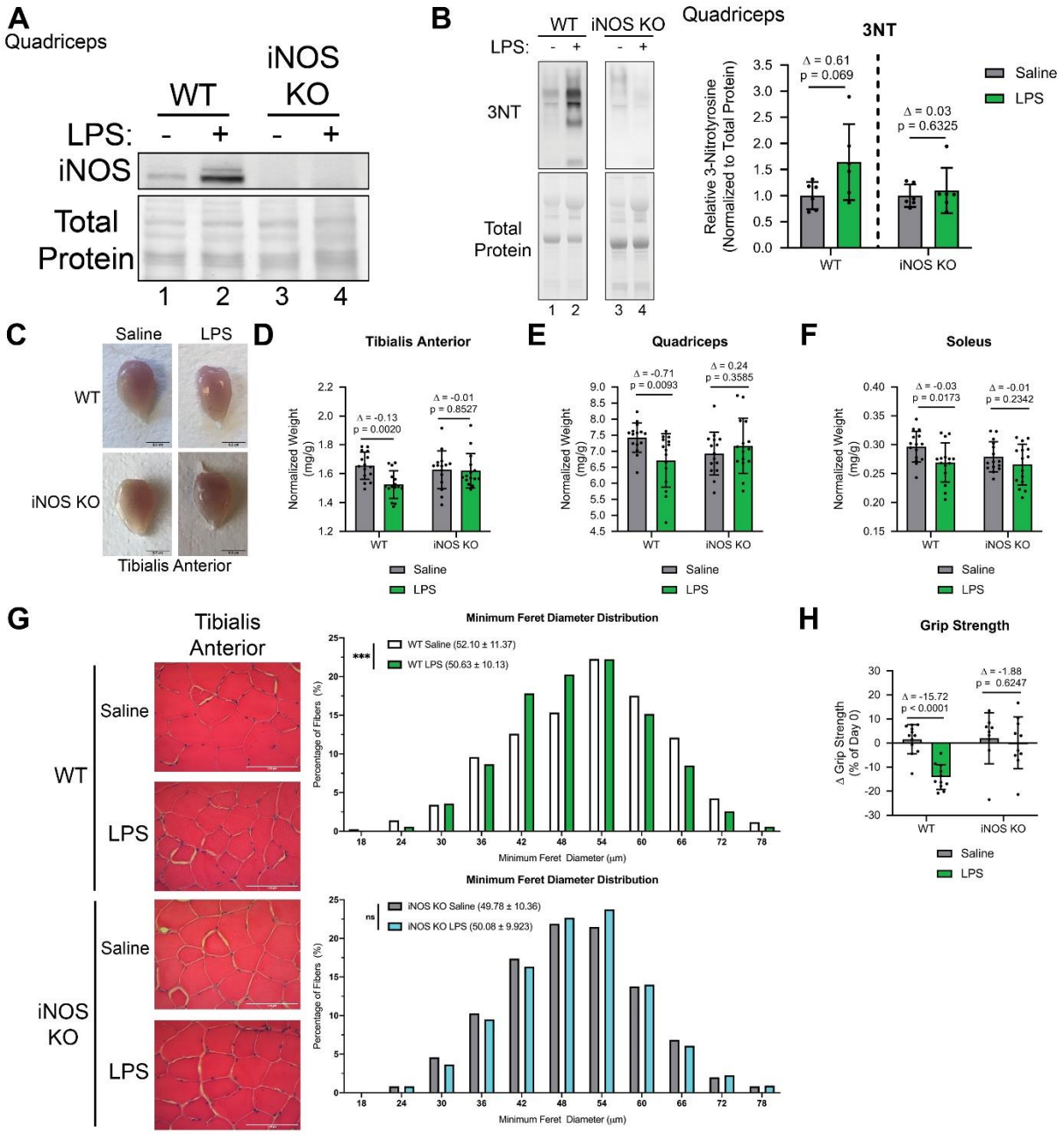

Figure 2.1: iNOS knockout mice are resistant to LPS-driven muscle wasting.

Male C57BL/6 wildtype (WT) and iNOS knockout (KO) mice were intraperitoneally injected with 1mg kg^{-1} LPS or an equivalent volume of carrier solution. Control WT, Control KO, and LPS-treated KO cohorts were pair-fed (PF) to the WT LPS-treated cohorts. After 18h, mice were euthanized, and tissue samples were analyzed.

(A) *Quadriceps* from saline or LPS treated, WT or iNOS KO mice, were isolated and used for western blot analysis with anti-iNOS (n=4). Ponceau S was used for total protein staining.

(B) *(left) Quadriceps* from saline or LPS treated, WT or iNOS KO mice, were isolated and used for western blot with anti-3NT (n=6). Total protein levels are also shown (*right*) Quantification of the 3NT to total protein ratio. Ratios are expressed relative to the saline treated controls.

(C) Representative images of tibialis anterior muscles. Scale bars represent 0.5 cm.

(D-F) Weight of *tibialis anterior* (D), *quadricep* (E) and *soleus* (F) muscle normalized to initial body weight (n=15).

(G) (*left*) representative photomicrographs of H&E stained *tibialis anterior* muscle sections from control and iNOS KO mice injected with or without LPS. Scale bars = 100 μm. (*right*) frequency histogram showing the distribution of muscle fiber minimum feret diameter in the *tibialis anterior* muscles from saline or LPS treated (*top*) WT control and (*bottom*) iNOS KO mice (n = 4). A total of 300 fibers per muscle were used for the analysis. Statistical comparisons, mean, and standard deviation of the mean are shown in the histogram legend.

(H) Change in grip strength between day of injection and endpoint of experiment. (WT saline n=12, WT LPS n=11, iNOS KO saline n=9, and iNOS KO LPS n=10).

Data information: Individual data points represent values from individual mice. Error bars represent the standard deviation (SD) of the mean. (B) Statistical comparisons were made between saline treated controls and LPS treated mice of same genotype. Plotted data was relativized to saline controls of corresponding genotype. Δ indicates the difference of mean values and p-values were calculated with a Student's T-test. (D-F and H) For statistical comparisons, Δ indicates the difference of mean values and p-values were calculated with an ANOVA followed by Fisher's LSD test. (G) p-values were calculated with a Kolmogorov-Smirnov test (***$P < 0.001$). Non statistically significant comparisons ($P > 0.05$) are indicated as non-significant (ns).

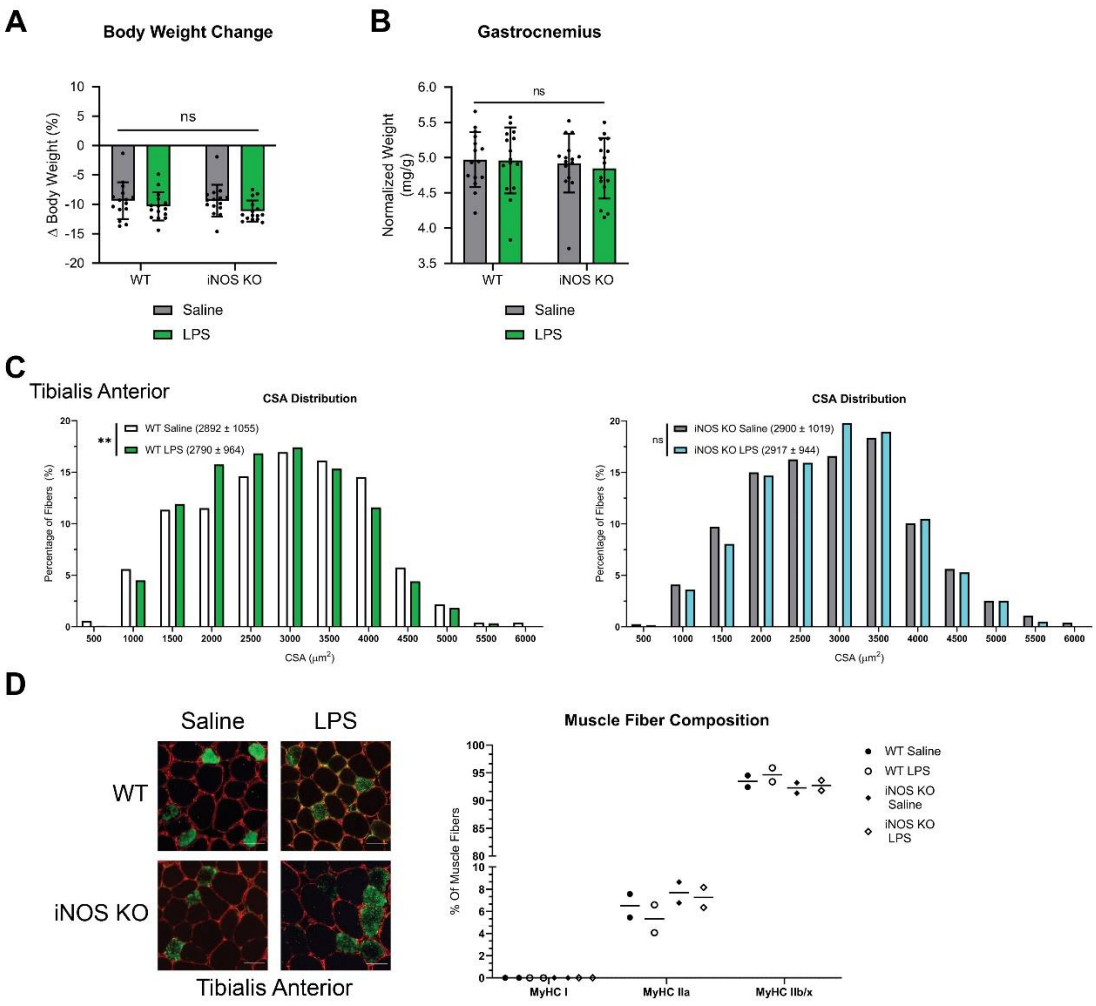

Figure 2.2: Characterization of the LPS-induced effects on muscle integrity/composition in WT and iNOS KO mice.

Male C57BL/6 wildtype (WT) and iNOS knockout (KO) mice were intraperitoneally injected with 1mg kg^{-1} LPS or an equivalent volume of carrier solution. Control WT, Control KO, and LPS-treated KO cohorts were pair-fed (PF) to the WT LPS-treated cohorts. After 18h, mice were euthanized, and tissue samples were analyzed.

(A) Percent body weight change from time of injection to endpoint of experiment. (n=15).

(B) *Gastrocnemius* weight normalized to initial body weight. (n=15).

(C) Frequency histogram showing the distribution of muscle fiber CSA in the *tibialis anterior* muscles from (*left*) WT control and (*right*) iNOS KO mice (n = 4). A total of 300 fibers per muscle were used for the CSA analysis. Statistical comparisons, mean, and standard deviation of the mean are shown in the histogram legend.

(D) (*left*) photomicrographs of immunofluorescence images of *tibialis anterior* muscle sections from WT control and iNOS KO mice injected with or without LPS. Sections were stained against MyHC I (Blue), MyHC IIa (Green), and Laminin (Red). Unstained fibers were classified as MyHC IIb/x. Scale bars = 50 μm. (*right*) percentage of Type I, Type IIa, and Type IIb/IIx fibers in the whole *tibialis anterior* muscles from control and iNOS KO mice (n = 2).

Data information: Individual data points represent values from individual mice. Error bars represent the standard deviation (SD) of the mean. (C) p-values were calculated with a Kolmogorov-Smirnov test (**P < 0.01). Non statistically significant comparisons (P > 0.05) are indicated as non-significant (ns).

In parallel to our phenotypic assessment of LPS-induced muscle wasting, we also evaluated the immune response of WT and iNOS KO mice. We first measured spleen enlargement (splenomegaly), splenic macrophage polarization, and macrophage levels in the spleen and skeletal muscle of the WT and iNOS KO mice. We found that LPS similarly altered the immune response in both WT and iNOS KO mice. Indeed, both mice had similar spleen enlargement (Figure 2.3A), increased M1 macrophages levels/decreased M2 macrophages levels in the spleen (Figure 2.3B-D), and increased levels of total muscle macrophages (Figure 2.3E). We then measure systemic levels of the pro-cachectic cytokines IL-1α, IL-1β, IL-6, and TNFα. We found that IL-1β and IL-1α were unaffected by LPS treatment (Figure 2.3F-G). However, although serum IL-6 and TNFα levels were increased in LPS-treated WT mice, the levels of these cytokines were significantly decreased iNOS KO (Figure 2.3H-I). Therefore, we show that iNOS affects the systemic secretion of the pro-inflammatory cytokines IL-6 and TNFα without affecting polarization or levels of macrophages.

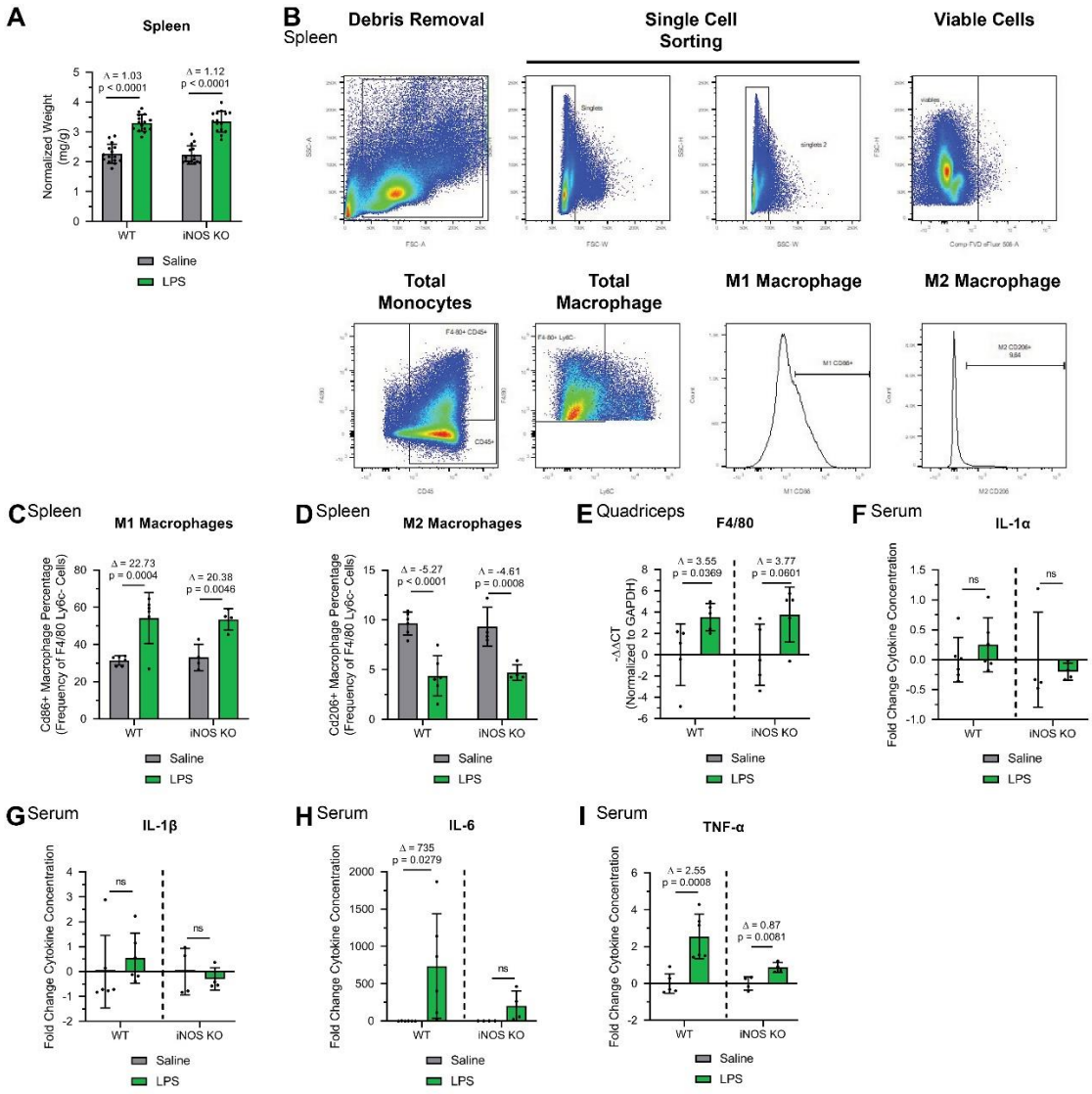

Figure 2.3: Characterization of the LPS-induced immune response in WT and iNOS KO mice.

Male C57BL/6 wildtype (WT) and iNOS knockout (KO) mice were intraperitoneally injected with 1mg kg^{-1} LPS or an equivalent volume of carrier solution. Control WT, Control KO, and LPS-treated KO cohorts were pair-fed (PF) to the WT LPS-treated cohorts. After 18h, mice were euthanized, and tissue samples were analyzed.

(A) Spleen weight normalized to initial body weight. (n=15).

(B) Gating strategy for flow cytometry analysis of spleen M1 and M2 macrophages.

(C) Percentage of CD86+ M1 splenic macrophages relative to the total F4/80+Ly6C- macrophage population (WT saline n=6, WT LPS n=6, iNOS KO saline n=4, and iNOS KO LPS n=4).

(D) Percentage of CD206+ M2 splenic macrophages relative to the total F4/80+Ly6C- macrophage population (WT saline n=6, WT LPS n=6, iNOS KO saline n=4, and iNOS KO LPS n=4).

(E) *Quadriceps* from saline or LPS treated, WT or iNOS KO mice, were isolated and used for RT-qPCR analysis for F4/80 mRNA expression. The - Δ Δ CT was plotted relative to the saline conditions of each background and normalized to GAPDH mRNA levels (n=5).

(F-I) Serum from saline or LPS treated, WT or iNOS KO mice was collected. Fold change of IL-1α (F), IL-1β (G), IL-6 (H) and TNF-α (I) levels in LPS-treated mice was plotted relative to saline condition (WT saline n=6, WT LPS n=6, iNOS KO saline n=4, and iNOS KO LPS n=4).

Data information: Individual data points represent values from individual mice. Error bars represent the standard deviation (SD) of the mean. (A, C, D) For statistical comparisons, Δ indicates the difference of mean values and p-values were calculated with an ANOVA followed by Fisher's LSD test. (E-I) Statistical comparisons were made between saline treated controls and LPS treated mice of same genotype. Plotted concentration data was relativized to saline controls of corresponding genotype. Δ indicates the difference of mean values and p-values were calculated with a Student's T-test.

2.2 Ablation of iNOS gene prevents sepsis-induced energy crisis

To determine if iNOS is involved in cachexia-induced metabolism defects in muscle we performed LC-MS/MS, in TA muscles collected from WT and iNOS KO mice treated or not with LPS. This analysis detected 119 metabolites including amino acids, acylcarnitines, glycerophospholipids, and organic acids. The raw metabolomics data was analyzed using the MetaboAnalyst 4.0 software to detect global trends. Using the multivariate analysis approach of partial least squares discriminant analysis (PLS-DA), we show that WT mice have a distinct metabolic profile compared to iNOS KO mice and that LPS causes metabolomic shifts in both mouse backgrounds (Figure 2.4A). Further comparison of relativized metabolite concentrations confirmed these observations comparing WT and iNOS KO mice (Appendix Figure 2.1). Next, we conducted pathway analysis using the Mus musculus KEGG library comparing Saline controls to LPS treated mice in both backgrounds. We identified several pathways that were altered in WT mice in response to LPS such as glycolysis and TCA cycle, which were not altered by LPS in iNOS KO mice (Figure 2.4B). Due to significant alterations to TCA cycle metabolites, iNOS was also likely involved in impairing amino acid anapleurosis into the TCA cycle. Indeed, there was an iNOS dependent effects on glutamine and glutamate metabolism and pathways involving arginine (Figure 2.4B). Due to the alterations in energy production pathways in WT mice, but not iNOS KO mice, we assessed the energetic status of LPS treated mice to see if iNOS activation disrupted these processes. To this end we quantified by Western blot AMPK activation by assessing phosphorylation at Thr172 (pAMPK), which when active would suggest the presence of energetic crisis (increase in the AMP/ATP ratio) in wasting muscles (Hardie *et al*, 2012;

Stein *et al*, 2000). We showed that LPS activates AMPK in WT but not iNOS KO mice (Figure 2.4C). Taken with the above global analyses, these data suggest that iNOS induction in response to LPS disrupts energy production prompting energetic stress in cachectic muscle.

To further understand how iNOS impairs energy production in wasting muscle, we analyzed the metabolite concentrations in glycolysis, the TCA cycle, anapleurotic and acylcarnitine metabolic pathways (Figure 2.4D, G). Most glycolysis and TCA cycle metabolites were altered by LPS treatment in WT mice, but not iNOS KO mice, suggesting that iNOS is responsible for these LPS-mediated alterations (Appendix Figure 2.2). Specifically, iNOS tended to increase glucose and decrease pyruvate, suggesting that glucose metabolism was reduced by iNOS (Figure 2.4D-E). Furthermore, iNOS caused increases in citrate with concurrent decreases in AKG and succinate suggesting that TCA cycle flux was impaired by iNOS (Figure 2.4D-E). iNOS activity also induced increases in arginine levels, the substrate of iNOS, which is also involved in anapleurosis (Figure 2.4F) (Kunzke *et al.*, 2020; Xu *et al.*, 2016). As acylcarnitine levels can be used to measure β-oxidation (Fukawa *et al.*, 2016), we then assessed their concentrations and estimated the activity of key enzymes involved in β-oxidation by calculating several ratios based on acylcarnitine levels as previously described (Li *et al.*, 2019). iNOS activity in WT mice caused a decrease in long, even-chained acylcarnitines suggesting an impairment of β-oxidation and associated enzymes (Appendix Figure 2.3). This was confirmed by our assessment of CPT1 and CPT2 activity where we found that iNOS tended to impair these enzymes that catalyze the rate limiting steps of β-oxidation (Figure 2.4H). These observations collectively

indicate that iNOS disrupts energy production through glycolysis and mitochondrial pathways in response to LPS.

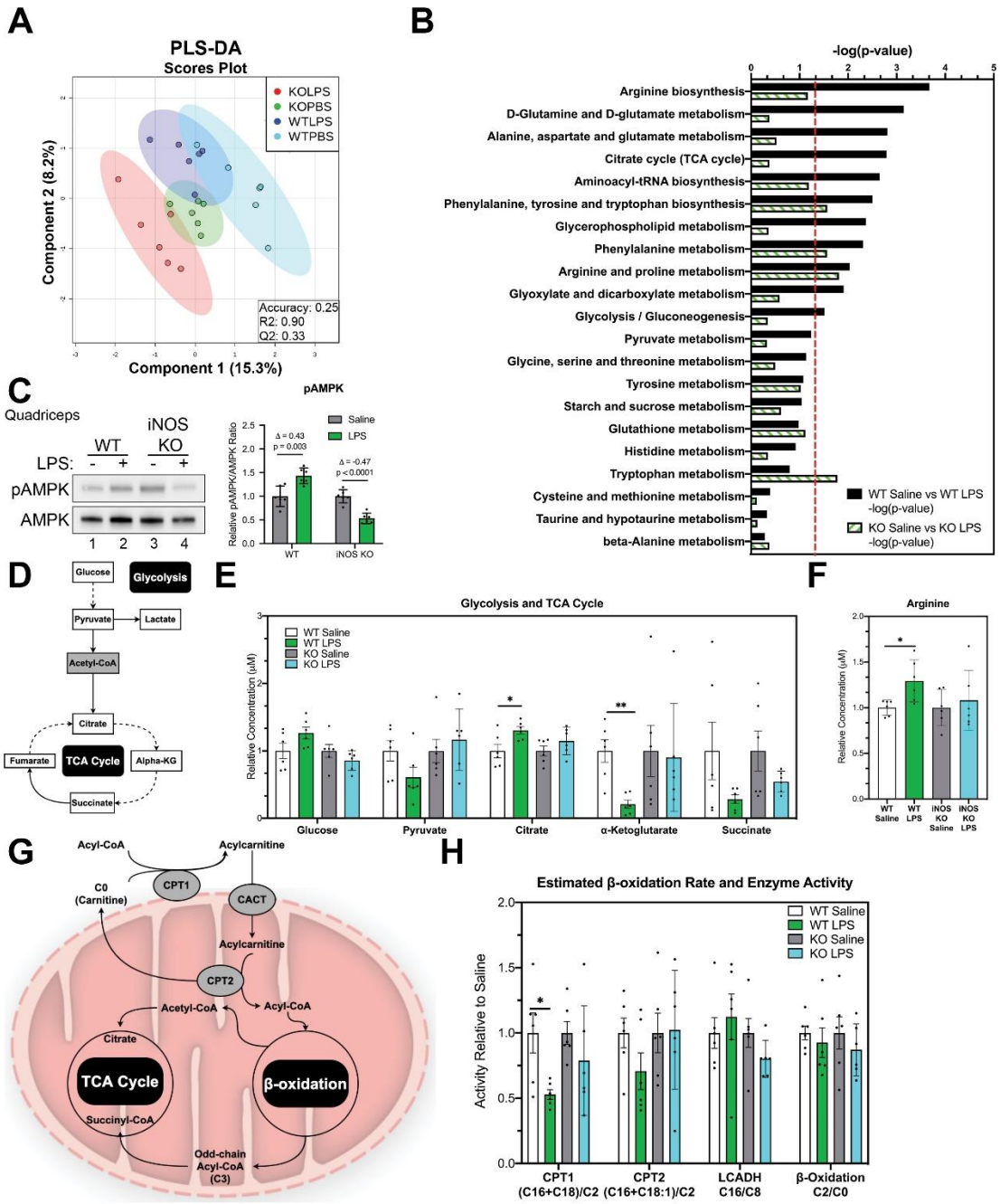

Figure 2.4: Genetic ablation of iNOS prevents LPS-driven deregulation of the TCA cycle and energy production.

Male C57BL/6 wildtype (WT) and iNOS knockout (KO) mice were intraperitoneally injected with 1mg kg^{-1} LPS or an equivalent volume of carrier solution. Control WT, Control KO, and LPS-treated KO cohorts were pair-fed (PF) to the WT LPS-treated

cohorts. After 18h, mice were euthanized, and the metabolome of tibialis anterior muscles was analyzed through LC-MS/MS.

(A) Scores scatter plot of partial least square discriminant analysis (PLS-DA) model of metabolites from WT and iNOS KO mice treated with or without LPS. Metabolomic data were range-scaled and mean-centered.

(B) Pathway Analysis using MetaboAnalyst 4.0 Software comparing significantly altered pathways from WT saline to LPS as well as iNOS KO saline to LPS. Pathways are ranked by their significance and filtered based on a Pathway Impact Score >0.1. Metabolomic data were range-scaled and mean-centered. P-values were obtained using GlobalTest and the -log(p-value) corresponding to a p-value of 0.05 is indicated by the red dashed line.

(C) (*left*) Western blot analysis of pThr172-AMPK (pAMPK) and total AMPK (AMPK) in *quadriceps* muscle. (*right*) Quantification of the pAMPK to AMPK ratio. Ratios are expressed relative to the saline treated controls.

(D) Schematic of Glycolysis and the TCA cycle. White boxes denote detected metabolites. Grey boxes denote undetected metabolites. Dashed arrows indicate presence of multiple reactions between metabolites.

(E) Relative concentrations of metabolites involved in glycolysis and TCA cycle.

(F) Relative concentration of arginine.

(G) Schematic of acylcarnitine metabolism. Grey circles denote key enzymes involved in metabolic processes highlighted.

(H) Relative estimated activity of CPT1, CPT2, LCADH, and β-oxidation.

Data information: Individual data points represent values from individual mice, with a total of six mice per cohort (n = 6). (B) P-values were obtained using GlobalTest. (C-H) Error bars represent the standard deviation (SD) of the mean. Statistical comparisons were made between saline treated controls and LPS treated mice of same genotype. Plotted concentration data was relativized to saline controls of corresponding genotype. p-values were calculated with a Student's T-test (*P < 0.05; **P < 0.01). (C) Δ indicates the difference of mean values.

2.3 The iNOS inhibitor GW274150 prevents inflammation-induced muscle wasting

The results above suggest that iNOS impairment could represent a viable therapeutic option to prevent cachectic muscle wasting. To investigate this possibility, we obtained a clinically tested iNOS inhibitor called GW274150 or GW that is efficient in an *in vivo* setting without having major side effects and is highly specific inhibitor for iNOS unlike other NOS enzymes. Using GW, we assessed the efficacy of this small molecule to directly inhibit iNOS to prevent inflammation-induced muscle wasting and associated metabolic defects.

We first tested whether GW could recapitulate the effects of iNOS KO in our LPS model of muscle wasting. We compared our results using GW to the results in Figures 2.1-2.3 from WT and iNOS KO mice treated with or without LPS. Indeed, this revealed that GW protected against LPS-induced muscle wasting similarly to what was observed in the iNOS KO (Appendix Figure 2.4). With GW able to recapitulate the anti-cachectic effects of iNOS KO, we next evaluated whether GW could prevent muscle wasting in the murine C26 adenocarcinoma model of cancer cachexia. We injected male BALB/C mice with C26 colon cancer cells which induces muscle wasting over the course of 14-19 days (Bonetto *et al.*, 2016; Di Marco *et al.*, 2012; Hall *et al.*, 2018). In our model mice were then treated with or without GW 5 days post-injection once the tumors were palpable since inhibition of iNOS has been shown to impair tumor growth (Garrido *et al*, 2017; Granados-Principal *et al*, 2015; Kostourou *et al*, 2011).

As with our verification of the cachexia phenotype conducted in our LPS model, we first confirmed that iNOS was expressed in muscle of C26-injected mice (Figure 2.5A).

We then, furthermore, characterized the immune response of these mice. We observed, in the C26 mice, an enlargement of the spleen and increase in muscle macrophage levels, which were not impacted by iNOS inhibition with GW (Figure 2.5B-C). Serum IL-6, TNFα and IL-1β increased in C26-injected mice, and GW treatment prevented the induction of these cytokines similar to what was observed in our LPS-treated iNOS KO (Figure 2.5E-G). As iNOS impairment could alter tumor growth, we measured final tumor weights and found no effect on final tumor burden (Figure 2.6A). To gauge the effectiveness of iNOS blockade by GW, we next measured 3NT levels in muscle as described above. C26-injection caused a significant increase in 3NT modification of proteins, which GW treatment reduced by approximately 50%, demonstrating that GW impaired iNOS activity in muscle (Figure 2.6B). We then assessed the effect of iNOS inhibition with GW on C26-mediated loss of body weight and tissue mass. We observed a C26-induced wasting of adipose tissue which was not affected by GW treatment (Figure 2.5H). However, C26-injection triggered significant body weight loss, which was slightly protected against with GW treatment (Figure 2.6C). We also found that GW partially protected against C26-induced wasting of the TA, gastrocnemius, quadriceps, and soleus (Figure 2.6D-G). As in the LPS model, these observations on muscle wasting were confirmed by analyses of muscle fiber minimum ferret diameter (Figure 2.6H) and CSA (Figure 2.5I). Similarly, assessment of muscle fiber type distribution showed no alteration to muscle fiber type specification caused by C26 tumors or GW treatment (Figure 2.5J). Lastly, we observed that although muscle strength was reduced in C26-treated mice, this effect was partially negated by treatment with GW (Figure 2.6I). Overall, these data suggest that GW-mediated inhibition of iNOS protects mice

from several cancer-induced effects including systemic inflammatory cytokine elevation, muscle atrophy, and loss of muscle function.

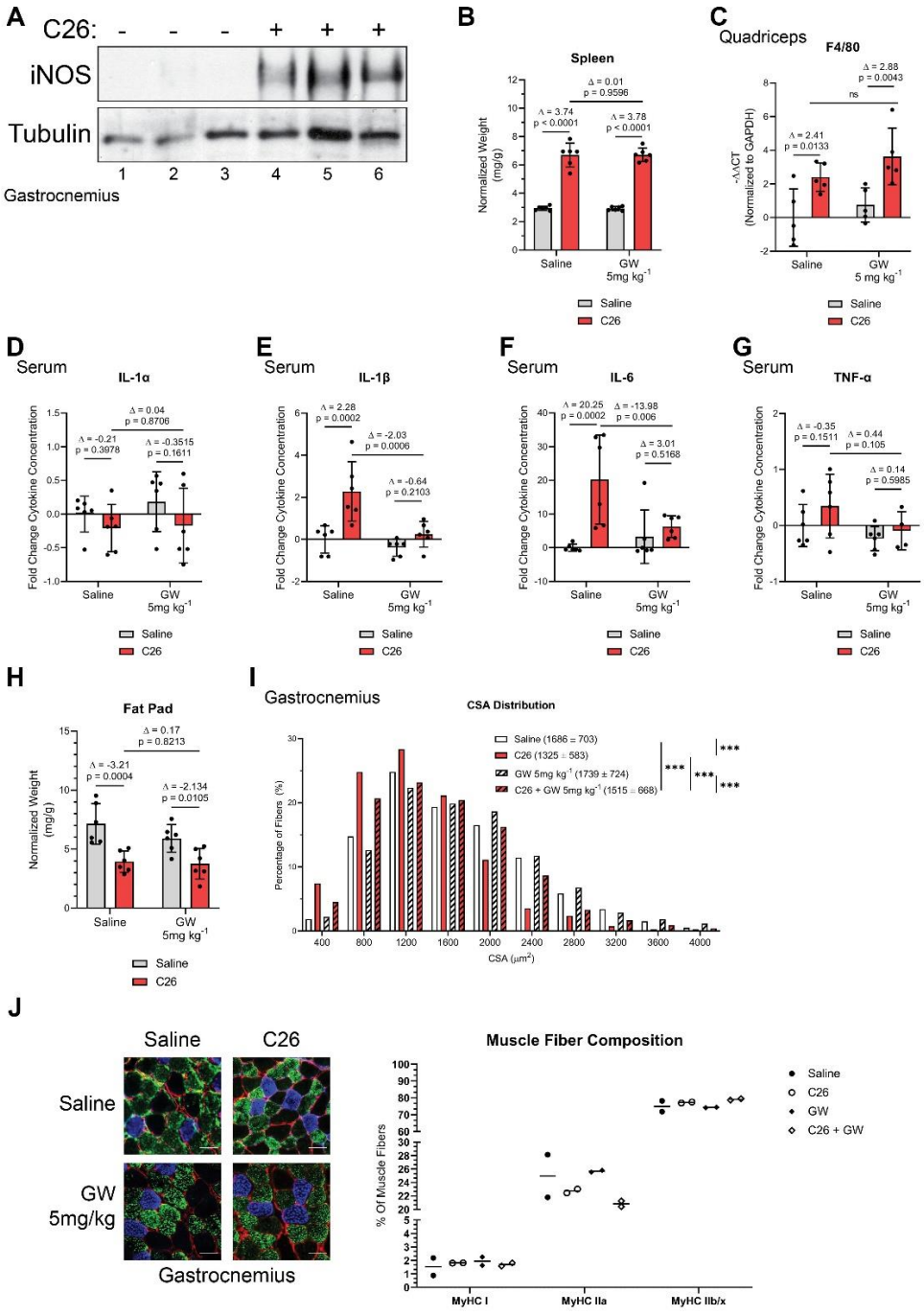

Figure 2.5: Effect of GW on the immune response as well as muscle integrity/composition in C26-tumor bearing mice.

Male BALB/C mice were injected subcutaneously with C26 cells ($1.25x10^6$ cells) or an equivalent volume of saline. After 5 days, and everyday thereafter, saline and C26 injected mice were treated with or without GW (5mg kg^{-1}). After 16 days, mice were euthanized, and tissue samples were analyzed.

(A) iNOS and Tubulin (loading control) protein levels in the *gastrocnemius* muscle was assessed by Western blot (n=3).

(B) Spleen weight normalized to initial body weight.

(C) *Quadriceps* from control and C26 mice treated with or without GW were isolated and used for RT-qPCR analysis for F4/80 mRNA expression. The - Δ Δ CT is plotted relative to the saline condition and normalized to GAPDH mRNA levels (n=5).

(D-G) Serum from saline and C26-tumor bearing mice treated with or without GW was collected. Fold change of IL-1α (D), IL-1β (E), IL-6 (F) and TNF-α (G, n=4 for C26 + GW) levels were plotted relative to saline condition.

(H) Inguinal fat pad weight normalized to initial body weight.

(I) Frequency histogram showing the distribution of muscle fiber CSA in the *gastrocnemius* muscles from control and C26 mice treated with or without GW (saline n=4, C26 n = 4, GW 5mg/kg n=3, and C26 GW 5mg/kg n=4). A total of 600-700 fibers per muscle were used for the CSA analysis. Statistical comparisons, mean, and standard deviation of the mean are shown in the histogram legend.

(J) (*left*) photomicrographs of immunofluorescence images of *gastrocnemius* muscle sections from control and C26 mice treated with or without GW. Sections were stained against MyHC I (Blue), MyHC IIa (Green), and Laminin (Red). Unstained fibers were classified as MyHC IIb/x. Scale bars = 50 μm. (*right*) percentage of Type I, Type IIa, and Type IIb/IIx fibers in the whole Gastrocnemius muscles from control and C26 mice treated with or without GW (n = 2).

Data information: Individual data points represent values from individual mice, with a total of six mice per cohort (n = 6) unless stated otherwise. Error bars represent the standard deviation (SD) of the mean. (B-H) For statistical comparisons, Δ indicates the difference of mean values and p-values were calculated with an ANOVA followed by Fisher's LSD test. (I) p-values were calculated with a Kolmogorov-Smirnov test (***$P < 0.001$).

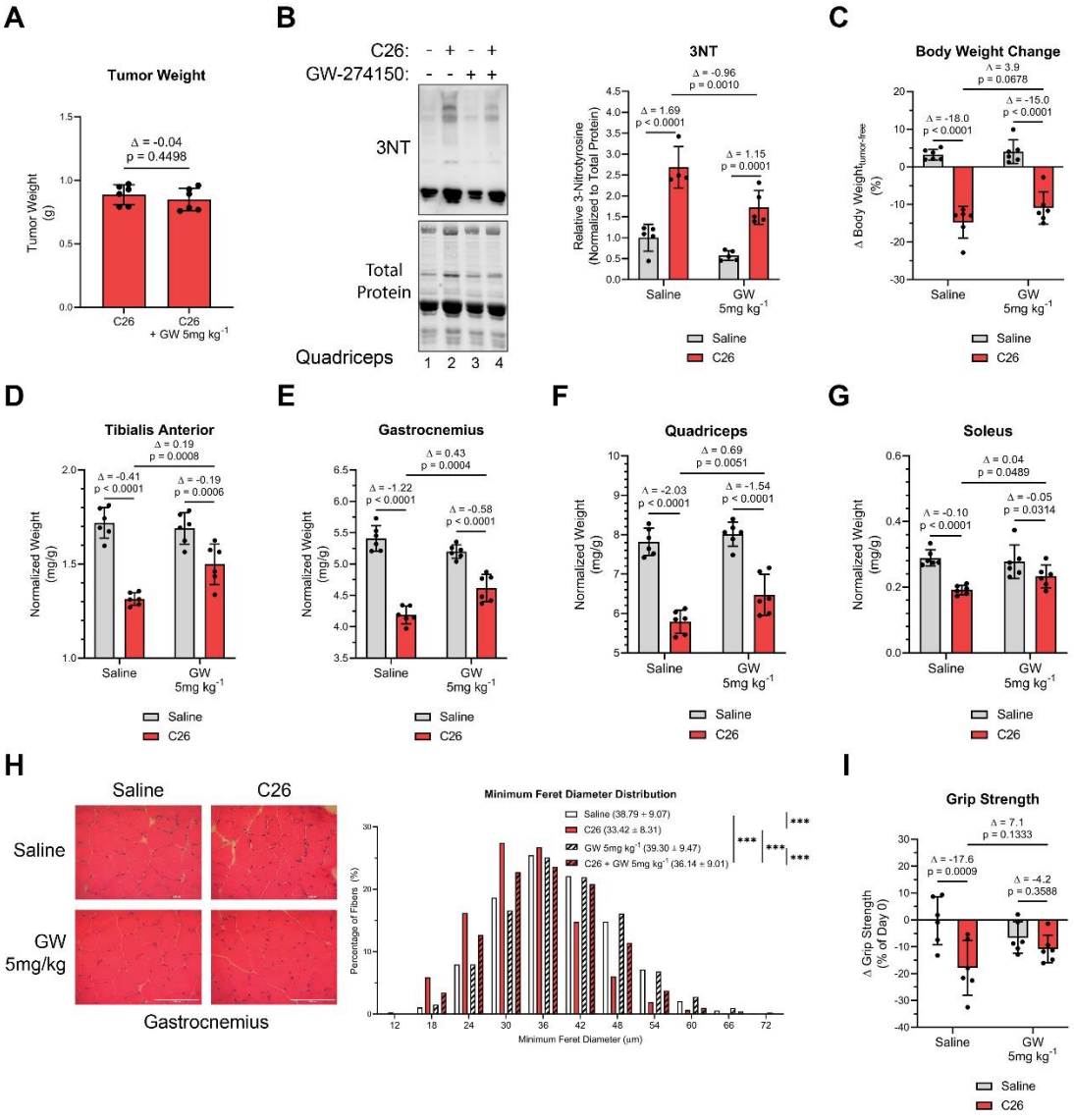

Figure 2.6: GW274150 treatment reduces muscle wasting in the C26 model.
Male BALB/C mice were injected subcutaneously with C26 cells ($1.25x10^6$ cells) or an equivalent volume of saline. After 5 days, and everyday thereafter, saline and C26 injected mice were treated with or without GW (5mg kg^{-1}). After 16 days, mice were euthanized, and tissue samples were analyzed.

(A) Effect of GW on tumor weight.

(B) (*left*) Representative image of Western blot analysis of 3NT staining and Stain Free imaged total protein levels from *quadriceps* muscle. (*right*) Quantification of the 3NT to total protein ratio (saline n=5, C26 n = 4, GW 5mg/kg n=5, and C26 GW 5mg/kg n=5).

(C) Percent body weight change from day 0 to day 16.

(D-G) Weight of *tibialis anterior* (D), *gastrocnemius* (E), *quadricep* (F) and *soleus* (G) muscle normalized to initial body weight.

(H) (*left*) Representative photomicrographs of *gastrocnemius* muscles sections from control and C26 mice treated with or without GW taken after H&E staining. Scale bars = 100 μm. (*right*) frequency histogram showing the distribution of muscle fiber minimum feret diameter in the *gastrocnemius* muscles from control and C26 mice treated with or without GW (saline n=4, C26 n = 4, GW 5mg/kg n=3, and C26 GW 5mg/kg n=4). A total of 600-700 fibers per muscle were used for the analysis. Statistical comparisons, mean, and standard deviation of the mean are shown in the histogram legend.

(I) Change in grip strength from before tumor cell injection (day 0) and before endpoint collection (day 16).

Data information: Individual data points represent values from individual mice, with a total of six mice per cohort (n = 6) unless stated otherwise. Error bars represent the standard deviation (SD) of the mean. (A) Δ indicates the difference of mean values and p-values were calculated with a Student's T-test. (B-G, I) For statistical comparisons, Δ indicates the difference of mean values and p-values were calculated with an ANOVA followed by Fisher's LSD test. (H) p-values were calculated with a Kolmogorov-Smirnov test (***P < 0.001).

2.4 The iNOS inhibitor GW274150 prevents cancer-mediated disruption of energy production in wasting muscle

To determine if GW can protect mice from metabolic dysfunction that is characteristic of C26-induced muscle wasting (Der-Torossian *et al.*, 2013b; Lautaoja *et al.*, 2019; Murphy *et al.*, 2012; Pin *et al.*, 2019a; Pin *et al.*, 2019b), we performed LC-MS/MS analysis to assess the metabolome of TA muscles in our model. We first determined the impact of GW on non-cachectic mice through pathway analysis. We demonstrated that GW had very minor alterations on metabolic pathways *in vivo* (Appendix Figure 2.5A). Indeed, although glucose metabolism appeared unaffected, arginine biosynthesis and D-glutamine/D-glutamate metabolism were markedly altered as demonstrated by the decrease in arginine and glutamate levels, respectively (Appendix Figure 2.5). We next assessed metabolomic alterations induced by C26 injection in TA muscles as well as how GW alters the metabolome of C26 tumor bearing mice. PLS-DA analysis showed global C26-induced shifts in the overall metabolome, with GW treatment of tumor bearing mice generating a distinct metabolic profile (Figure 2.7A). Pathway analysis confirmed these observations as the presence of C26 tumors caused alteration of energy production pathways (i.e., glycolysis and pyruvate metabolism) and amino acid metabolism (e.g., arginine and proline metabolism and arginine biosynthesis), while GW cotreatment further affected these same pathways (Figure 2.7B and Appendix Figure 2.6). To evaluate the impact of iNOS activity on cellular energy production we next measured AMPK activation. Although AMPK activation was strongly induced by in C26-tumor bearing mice (indicative of energetic stress) this effect was partially prevented by GW treatment (Figure 2.7C). Taken together with our observations in the LPS model,

these data indicate that iNOS disrupts energy production in several cachexia contexts and that iNOS impairment positively affects cellular energetic status.

Similar to our analysis in our sepsis model we assessed metabolite concentrations in key energy production and amino acid metabolism pathways. Regarding glycolysis and pyruvate metabolism, we found that although glucose levels were unaffected in C26 injected mice, there was an accumulation of pyruvate suggesting an impairment of pyruvate metabolism (Figure 2.7D). In C26-tumor bearing mice, GW significantly decreased glucose levels suggesting an increased utilization of glucose (Figure 2.7D). Regarding amino acid metabolism, aspartate tended to decrease in C26-tumor mice (Figure 2.7E). Furthermore, we found that C26-induced cachexia caused accumulation of arginine, lysine, methlyhistidine, and tryptophan (Figure 2.7E), which is consistent with recent studies assessing muscle amino acid levels in C26-injected mice and suggests increases in muscle protein breakdown (Der-Torossian *et al.*, 2013b; Kunzke *et al.*, 2020; Lautaoja *et al.*, 2019; QuanJun *et al.*, 2015; Tseng *et al.*, 2015). Importantly, iNOS impairment by GW prevented these amino acid alterations (Figure 2.7E). The recovery of amino acid levels by GW in C26-tumor bearing mice treated suggests a protective effect of iNOS inhibition against protein catabolism. As highlighted in Chapter 1, the accumulation of amino acids could also indicate the impairment of anapleurosis to supplement cellular energy production, therefore, the normalization of amino acid levels by GW can promote energy production imbuing positive effects on energetic status of these muscles (Figure 2.7C). To measure the contribution of lipids to energy production we assessed acylcarnitine levels in our model. As seen in our LPS-induced model of wasting, C26-induced cachexia caused a decrease in saturated, long,

even-chain acylcarnitines, which was either recovered to basal levels or increased from the basal concentration by GW (Appendix Figure 2.7). Estimations of activity levels of CPT1 and CPT2 showed their activity were not significantly affected by the C26 tumors, while they were strongly induced by GW (Figure 2.7F). In addition, activity of key the β-oxidation enzyme LCADH decreased and estimated overall β-oxidation increased in tumor bearing mice in iNOS-dependent manner as GW treatment reversed these effects (Figure 2.7F). Interestingly, GW treatment of control mice increased long-chain acylcarnitines and affected CPT1, CPT2 and LCADH activity and β-oxidation similarly to what was observed in the C26 + GW cohort, showing that iNOS impairment affects this process in non-cachectic contexts as well (Appendix Figure 2.8). In addition to β-oxidation, acylcarnitines, specifically short, odd-chain acylcarnitine species, can also feed into the TCA cycle through conversion into succinyl-CoA (Brunengraber & Roe, 2006). Interestingly, C26-induced wasting also decreased 3- (C3) and 5- (C5) carbon acylcarnitines which was recovered with GW treatment (Figure 2.7G). These observations indicate that C26-induced iNOS activity impairs energy production in the mitochondria by deregulating critical enzymes involved in acylcarnitine metabolism, β-oxidation, and anapleurosis.

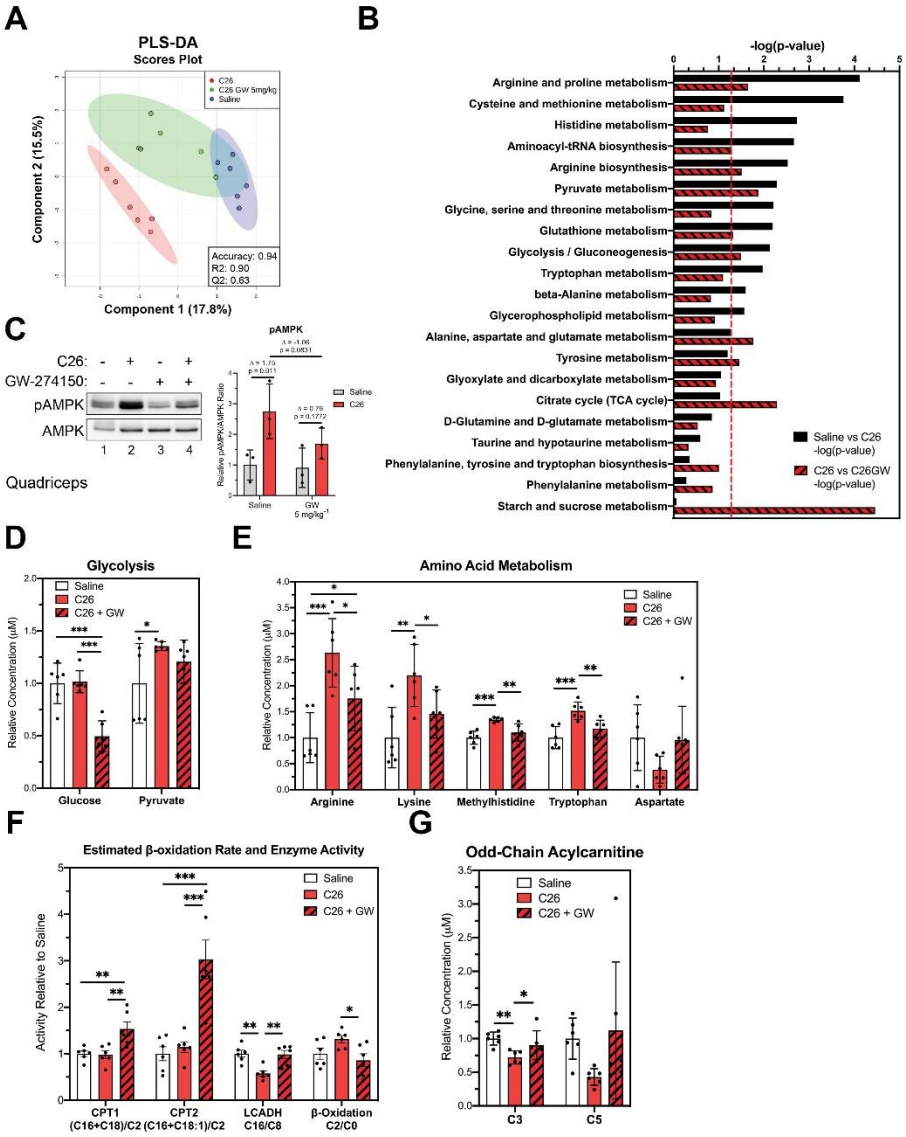

Figure 2.7: Pharmacological inhibition of iNOS reduces C26-induced derangement of amino acids and impairment of energy production.

Male BALB/C mice were injected subcutaneously with C26 cells ($1.25x10^6$ cells) or an equivalent volume of saline. After 5 days and everyday thereafter, the C26 tumor-bearing mice were injected with either saline or GW 5mg kg^{-1}. After 16 days, mice were euthanized, and the metabolome of tibialis anterior muscles was analyzed through LC-MS/MS.

(A) Scores scatter plot of partial least square discriminant analysis (PLS-DA) model of metabolites from saline, C26, and C26 + GW treated mice. Metabolomic data were range-scaled and mean-centered.

(B) Pathway Analysis using MetaboAnalyst 4.0 Software comparing significantly

altered pathways from saline to C26 as well as C26 to C26 + GW. Pathways are ranked by their significance and filtered based on a Pathway Impact Score >0.1. Metabolomic data were range-scaled and mean-centered. P-values were obtained using GlobalTest and the -log(p-value) corresponding to a p-value of 0.05 is indicated by the red dashed line.

(C) (*left*) Western blot analysis of pThr172-AMPK (pAMPK) and total AMPK (AMPK) in *quadriceps* muscle (n = 3). (*right*) Quantification of the pAMPK to AMPK ratio relative to the saline treated control (n = 3).

(D) Relative concentrations of metabolites involved in glycolysis.

(E) Relative concentrations of amino acids.

(F) Relative estimated activity of CPT1, CPT2, LCADH, and β-oxidation.

(G) Relative concentrations of odd-chain acylcarnitines.

Data information: Individual data points represent values from individual mice, with a total of six mice per cohort (n = 6) unless otherwise stated. (B) P-values were obtained using GlobalTest. (C-G) Error bars represent the standard deviation (SD) of the mean. p-values were calculated with an ANOVA followed by Fisher's LSD test (*P < 0.05; **P < 0.01; ***P < 0.001). (C) Δ indicates the difference of mean values.

2.5 iNOS activity causes wasting of myotubes treated with pro-cachectic cytokines and disrupts the mitochondrial Electron Transport Chain

As our above analyses suggested that iNOS impairs cellular energy production and mitochondrial processes to cause energy crisis, we sought to investigate how iNOS affects the ATP production rates of glycolysis and OXPHOS, two primary energy production mechanisms in the cell. We therefore utilized an *in cellulo* model of wasting to assess the mechanism behind iNOS-induced metabolic defect. In our analyses, we used IFNγ/TNFα treated C2C12 myotubes, which we have previously used to mimic the effect of cytokines on muscle fibers *in vivo* (Di Marco *et al.*, 2012; Di Marco *et al.*, 2005; Hall *et al.*, 2018; Ma *et al.*, 2017). To assess the role of iNOS in these processes we used GW to prevent inflammation-induced wasting. We, additionally, used another iNOS inhibitor AMG, to confirm our results with GW (Thornalley, 2003).

We began by characterizing the validity and relevance of the C2C12 myotubes compared to our *in vivo* models by assessing if iNOS similarly affected myotube size and metabolism after cytokine treatment. As previously shown, IFNγ/TNFα treated C2C12 myotubes wasted over 48 hours (Figure 2.8A-B) (Hall *et al.*, 2018; Mubaid *et al.*, 2019). In IFNγ/TNFα treated C2C12 myotubes, there were significant increases in iNOS protein expression and media nitrite levels as well as deregulation of the TCA cycle and anapleurotic metabolites that feed into it (Figure 2.8C-D). Consistent with the *in vivo* models and previous studies, iNOS inhibition by GW prevented IFNγ/TNFα-induced atrophy (Figure 2.8A-B) (Di Marco *et al.*, 2012; Di Marco *et al.*, 2005) and, similarly to AMG, impaired iNOS activity in a dose dependent manner, without affecting iNOS expression (Figure 2.8C and Appendix Figure 2.9). Myotube wasting was associated

with the presence of energy stress as IFNγ/TNFα treatment activated AMPK, which is sensitive to the ratio of ATP to AMP within the cell (Figure 2.8E-F). iNOS inhibition with GW or AMG, however, prevented AMPK activation under these conditions (Figure 2.8E-F and Appendix Figure 2.10A). We confirmed our results by also assessing phosphorylation of a downstream target of AMPK, acetyl-CoA carboxylase (ACC), and overall energy levels by measuring ATP levels in cytokine treated myotubes (Figure 2.8E-G). Indeed, we found that although IFNγ/TNFα treatment increased the phosphorylation of ACC and reduced cellular ATP levels, both AMG and GW prevented these effects (Figure 2.8E-G and Appendix Figure 2.10B). As AMPK activation is also associated with impairment of mTOR activity we assessed phosphorylation of ribosomal protein S6 kinase (S6K) and ribosomal protein S6 (S6), which are downstream targets of the pathway (Figure 2.8H-I). In line with our assessment of AMPK phosphorylation, IFNγ/TNFα treatment impaired S6K and S6 phosphorylation leading to inactivation of protein synthesis, while inhibition of iNOS restored their activity (Figure 2.8H-I). Overall, the above analyses showed the presence of iNOS-mediated metabolic defects in C2C12 with similar characteristics to our findings in *in vivo* models.

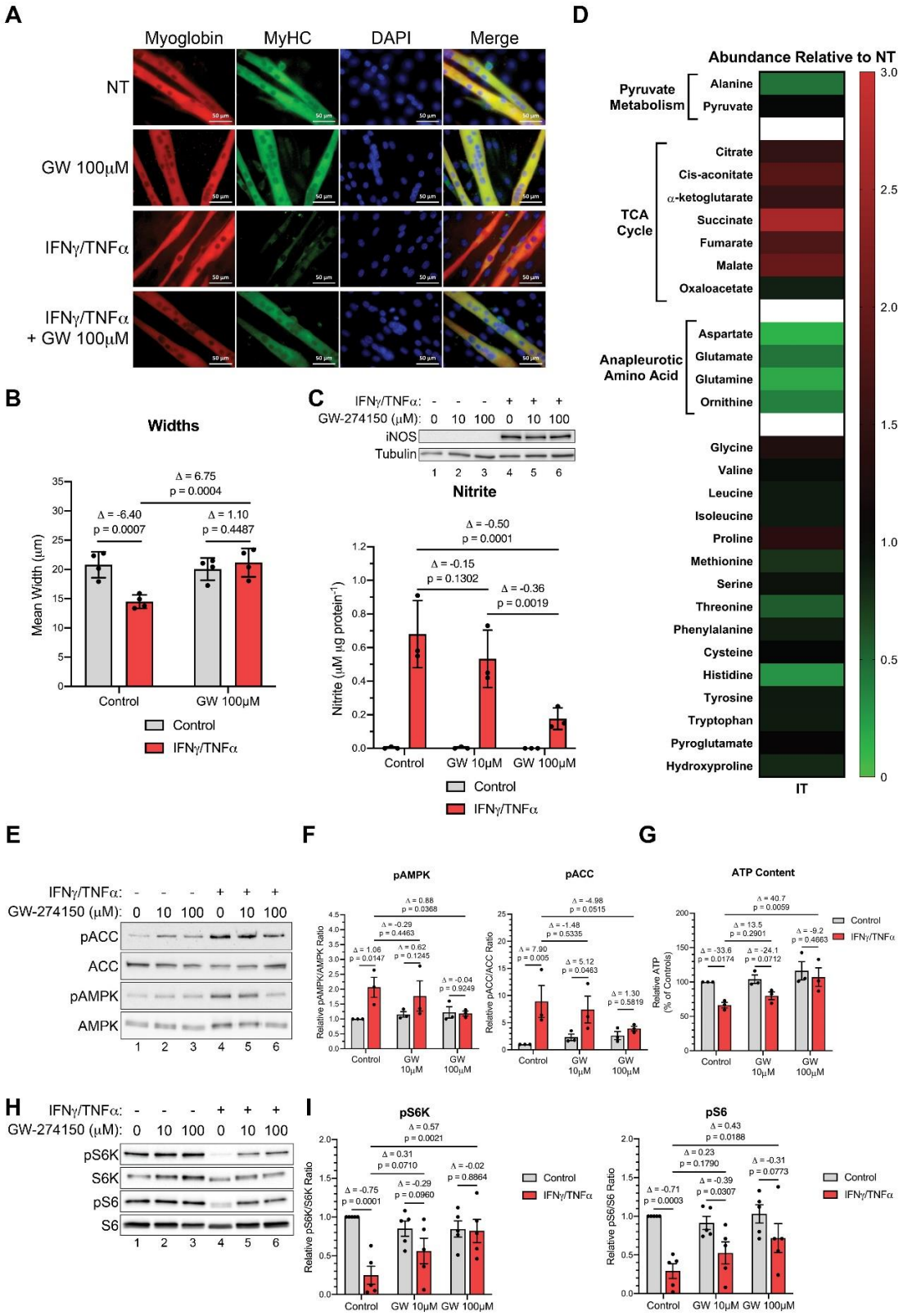

Figure 2.8: Cytokine treatment of C2C12 myotubes alters the levels of TCA cycle intermediates and activates AMPK in an iNOS-dependent manner.

C2C12 myotubes were treated with or without IFNγ (100U/mL) and TNFα (20ng/mL) and the indicated doses of GW. Protein content and metabolites were extracted from cells 24h after treatment and analyzed for AMPK phosphorylation, ACC phosphorylation, and total iNOS levels as well as GC-MS, respectively. Myotube integrity and widths as well as phosphorylation of S6 and S6K were assessed 48h after treatment.

(A) Representative immunofluorescence imaging for myoglobin and myosin heavy chain (MyHC) in not treated (NT) controls and IFNγ/TNFα (IT) samples treated with or without GW. Nuclei were visualized with DAPI staining (n=4).

(B) Quantification of mean fiber widths (n=4).

(C) (*top*) Western blot analysis for iNOS and tubulin (n=3). (*bottom*) Media nitrite levels (n=3).

(D) Heatmap visualizing mean concentration corresponding to metabolites of IFNγ/TNFα (IT) treated samples relative to not treated (NT) controls (n=3). Red and green indicate an increase or decrease in metabolite levels, respectively.

(E) Western blot analysis for pThr172-AMPK (pAMPK), total AMPK (AMPK), pSer79-ACC (pACC), and total ACC (ACC).

(F) Quantification of the pAMPK to AMPK ratio (*left*) and the pACC to ACC ratio (*right*) relative to the untreated control (n=3).

(G) Cellular ATP content quantified as a percentage of the untreated control (n=3).

(H) Western blot analysis for pThr389-S6K (pS6K), total S6K (S6K), pSer235/236-S6 (pS6), and total S6 (S6) (n=5).

(I) Quantification of the (*left*) pS6K to S6K ratio and the (*right*) pS6 to S6 ratio relative to the untreated control (n=5).

Data information: Individual data points represent independent experimental replicates. Error bars represent the standard deviation (SD) of the mean. For statistical comparisons, Δ indicates the difference of mean values and p-values were calculated with an ANOVA followed by Fisher's LSD test.

We next focused on our primary question of how iNOS during cytokine mediated muscle wasting by assessing energy production due to glycolysis and OXPHOS. To this end, we used the Seahorse Extracellular Flux analyzer to measure oxygen consumption rate (OCR) and extracellular acidification rate (ECAR), which are correlated to oxidative respiration and glycolysis, respectively (Appendix Figures 2.11 and 2.12). Using a method published by Mookerjee *et al.,* we calculated the theoretical basal and maximal rates of oxidative ($J\text{-}ATP_{oxidative}$), glycolytic($J\text{-}ATP_{glycolytic}$), and total ($J\text{-}ATP_{total}$) ATP production (J-ATP) of C2C12 myotubes treated or not with IFNγ/TNFα and iNOS inhibitors (Mookerjee *et al*, 2017, 2018). Calculation of basal J-ATP rate allowed us to determine the relative utilization of glycolysis or OXPHOS for ATP production at the initial state (Figure 2.9B and Appendix Figure 2.13B). The maximal J-ATP rates were determined after FCCP treatment for $J\text{-}ATP_{oxidative}$ and monensin treatment for $J\text{-}ATP_{glycolytic}$. Determination of the maximal rates allows for visualization of the bioenergetic profile of the myotubes (Figure 2.9A and Appendix Figure 2.13A). Furthermore, the maximal J-ATP rates can also be used to calculate the bioenergetic capacity of the cell, which represents the functional limit of glycolytic and oxidative processes (Figure 2.9D and Appendix Figure 2.13D). Our assessment of the bioenergetic and basal metabolic profile of C2C12 showed that while myotubes are highly oxidative in the untreated condition, cytokines strongly impair oxidative metabolism, resulting in an increase in glycolytic metabolism, and significantly decreased basal ATP production rates (Figure 2.9A-B and Appendix Figure 2.13A-B). The percentage of energy production from glycolysis, defined as the glycolytic index, between untreated and cytokine treated myotubes increased from 10% to 60-90%

(Figure 2.9C and Appendix Figure 2.13C). Furthermore, the bioenergetic capacity of cytokine-treated cells was significantly decreased (Figure 2.9D and Appendix Figure 2.13D), suggesting that collectively these cytokine-induced insults to ATP production likely cause the energetic stress observed. Importantly, the iNOS inhibitors GW and AMG restored normal bioenergetic profile, basal metabolism, and bioenergetic capacity (Figure 2.9A-D and Appendix Figure 2.13A-D). Overall, we show that iNOS activity strongly impairs oxidative energy production and shifts metabolic output towards glycolysis that cannot meet the energy needs of myotubes.

With the strong impairment of OXPHOS in IFNγ/TNFα treated C2C12, we investigated how iNOS is targeting this process. We probed for expression levels of ETC complex subunits that are labile when complexes are disassembled and nonfunctional. We found that cytokines targeted Complex II and Complex IV integrity, significantly reducing levels of their subunits (Figure 2.10, Appendix Figures 2.14 and 2.15). This detrimental disruption of ETC complex integrity was prevented with iNOS inhibitors indicating that iNOS compromises OXPHOS function in the context of muscle wasting by targeting complex II and IV integrity and function (Figure 2.10, Appendix Figure 2.15).

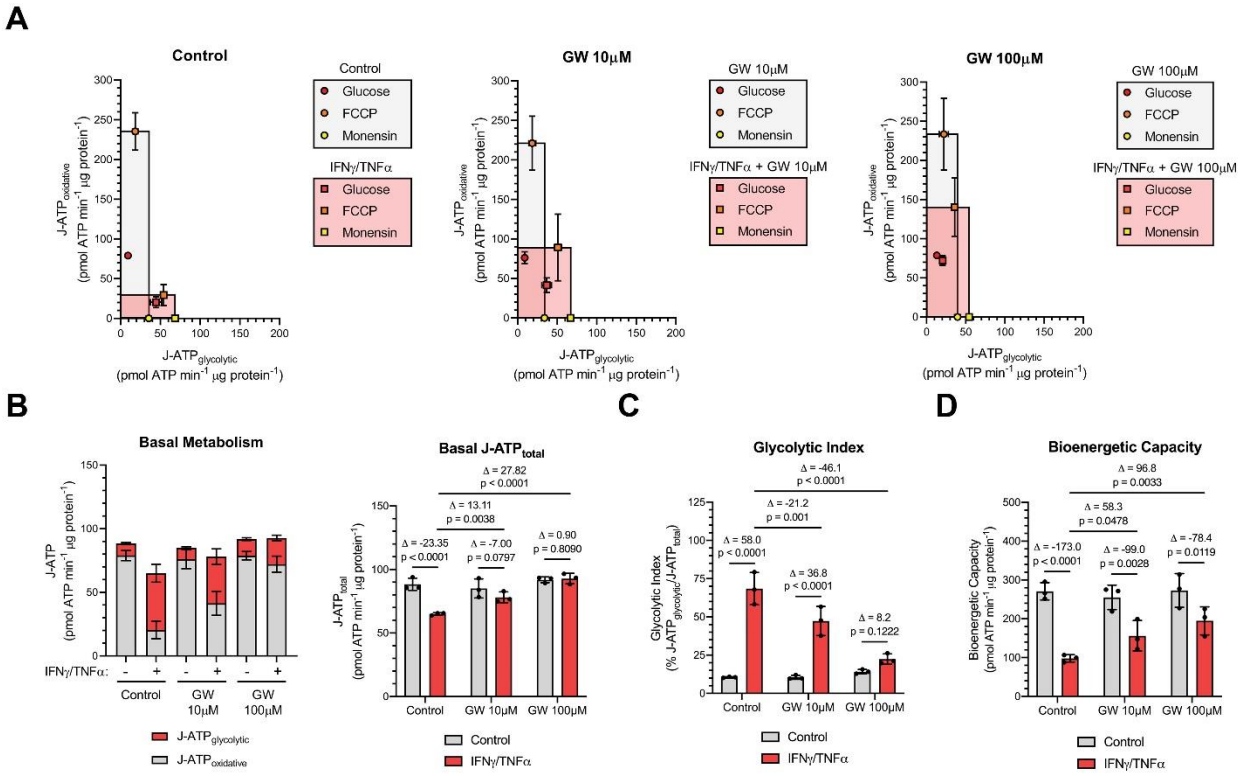

Figure 2.9: GW274150 prevents a cytokine-induced shift to aerobic glycolysis in C2C12.

C2C12 myotubes were treated with or without IFNγ (100U/mL) and TNFα (20ng/mL) and the indicated doses of GW. ATP production rates (J-ATP) from oxidative phosphorylation (oxidative) and glycolysis (glycolytic) were determined from measurements of extracellular flux 24h after treatment.

(A) Bioenergetic profiles. Highlighted squares are defined by the theoretical maximal $J\text{-}ATP_{oxidative}$ and $J\text{-}ATP_{glycolytic}$ rates.

(B) (*left)* Basal $J\text{-}ATP_{glycolytic}$ and $J\text{-}ATP_{oxidative}$ rates. (*right*) Total basal J-ATP rate.

(C) Glycolytic index of basal metabolism.

(D) Total bioenergetic capacity.

Data information: Individual data points represent three independent experiments (n = 3). The data points for each experiment are calculated from the average of technical triplicates. Error bars represent the standard deviation (SD) of the mean. For statistical comparisons, Δ indicates the difference of mean values and p-values were calculated with an ANOVA followed by Fisher's LSD test.

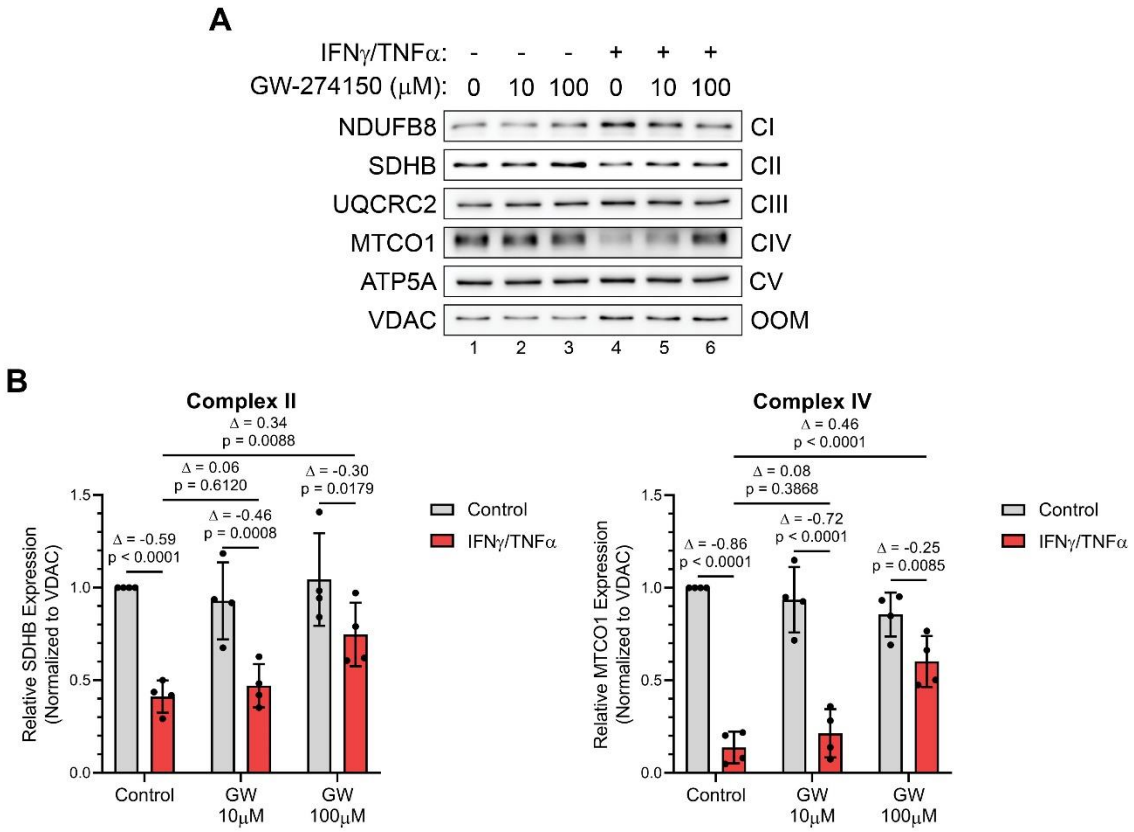

Figure 2.10: Inflammation-mediated loss of Complex II and IV integrity are reversed with GW274150.

C2C12 myotubes were treated with or without IFNγ (100U/mL) and TNFα (20ng/mL) and the indicated doses of GW. Protein content was extracted 24h after treatment.

(A) Western blot analysis for ETC protein complex subunits.

(B) (*left*) Quantification of SDHB (Complex II; CII) normalized to VDAC (Outer Mitochondrial Membrane; OMM) and relative to untreated control. (*right*) Quantification of MTCO1 (Complex IV; CIV) normalized to VDAC and relative to untreated control.

Data information: Individual data points are from four independent experimental replicates (n = 4). Error bars represent the standard deviation (SD) of the mean. For statistical comparisons, Δ indicates the difference of mean values and p-values were calculated with an ANOVA followed by Fisher's LSD test.

2.6 iNOS disrupts the mitochondrial structure in wasting skeletal muscle

To conclude our study, we assessed mitochondrial content and morphology in skeletal muscle collected from both our *in vivo* models of wasting using transmission electron microscopy (TEM) as these parameters are associated with mitochondrial function (Cogliati *et al*, 2016; Li *et al.*, 2020). We found that LPS treatment disrupted the cristae structures of the IMM in WT mice, but not iNOS KO mice (Figure 2.11A). In our C26 model, we observed that tumor bearing mice had decreased mitochondrial content in their muscle (Figure 2.11B left), with their remaining mitochondria being fragmented and without cristae (Figure 2.11B right). GW treatment of tumor bearing mice partially prevented loss of mitochondrial content and maintained cristae structure (Figure 2.11B). Interestingly, we found that GW treatment of control mice tended to increase the number of mitochondria in the muscles suggesting a role of iNOS in limiting mitochondrial biogenesis under normal conditions (Figure 2.11B). Mitochondrial fragmentation, depletion of mitochondria, and disruption of IMM cristae structures have all been previously observed in models of cachexia and are suggested to strongly impair OXPHOS-linked energy production (Brown *et al.*, 2017; Franco-Romero & Sandri, 2021; Shum *et al.*, 2012; VanderVeen *et al.*, 2017; White *et al.*, 2012). Therefore, the LPS and C26-mediated assaults to mitochondrial content and morphology suggest that oxidative energy production is impaired in these muscles in an iNOS-dependent manner. Together, our models of muscle wasting demonstrate that genetic ablation of iNOS or inhibition of its activity enhances mitochondrial function by preventing both the loss of IMM structure and capacity for oxidative phosphorylation.

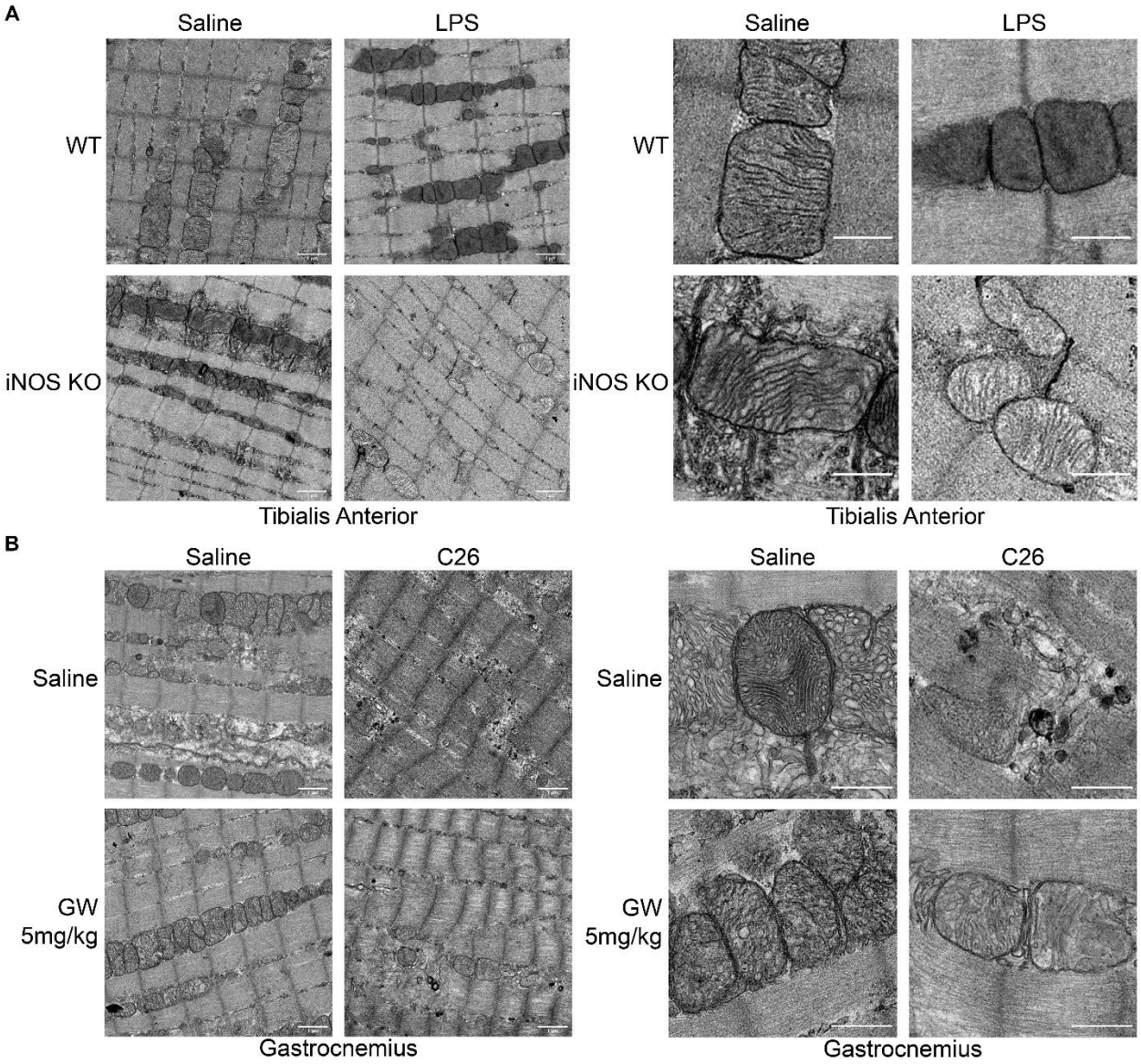

Figure 2.11: Inflammation-mediated loss of mitochondrial integrity are reversed with genetic and pharmacological inhibition of iNOS.

(A) Male C57BL/6 wildtype (WT) and iNOS knockout (KO) mice were intraperitoneally injected with 1mg kg^{-1} LPS or an equivalent volume of carrier solution. Control WT, Control KO, and LPS-treated KO cohorts were pair-fed (PF) to the WT LPS-treated cohorts. After 18h, mice were euthanized, and *tibialis anterior* muscles were imaged by transmission electron microscopy. (*left*) Representative micrograph of *tibialis anterior* muscle (n=2). Scale bar = 1 µm. (*right*) Zoomed section of representative image to highlight mitochondria. Scale bar = 0.5 µm.

(B) Male BALB/C mice were injected subcutaneously with C26 cells ($1.25x10^6$ cells) or an equivalent volume of saline. After 5 days, and everyday thereafter, saline and C26 injected mice were treated with or without GW (5mg $kg^{-1)}$. After 16 days, mice were euthanized, and *gastrocnemius* muscles were imaged by transmission electron microscopy. (*left*) Representative micrograph of *gastrocnemius* muscle (n=2). Scale bar = 1 µm. (*right*) Zoomed section of representative image to highlight mitochondria. Scale bar = 0.5 µm.

Data information: Images representative of 2 individual mice.

3 eIF4A inhibition prevents the onset of cytokine-induced muscle wasting by blocking the STAT3 and iNOS pathways

3.1 The eIF4A allosteric inhibitor Hippuristanol recapitulates the actions of Pateamine A on cytokine-induced muscle wasting and the iNOS/NO pathway.

As Chapter 2 provides strong evidence behind the efficacy of direct iNOS inhibition in the treatment of cachectic muscle wasting, in the following chapter, I sought to explore alternative means of impairing iNOS in wasting muscle. Indeed, several studies from our lab have shown that disruption of iNOS expression has similar anti-cachectic effects to direct inhibitors. Notably, one of our previous studies showed that the eIF4A inhibitor PatA prevents cytokine-induced muscle wasting, both *in vitro* and *in vivo,* by selectively disrupting iNOS mRNA translation (Di Marco *et al.*, 2012). This work suggested that targeting iNOS induction with PatA can potentially alleviate cachexia. The toxicity of PatA, however, hinders its ability to be translated to clinic. Alternative drugs targeting eIF4A should be investigated for their therapeutic potential in preventing cachexia-induced muscle wasting. To address this, we tested the effect of an eIF4A inhibitor Hipp in our *in vitro* models of cachexia-induced muscle wasting. Hipp inhibits eIF4A with a distinct mechanism of action from PatA and has more favorable therapeutic characteristics. Unlike PatA, its interaction with eIF4A is reversible, and consequently, is less toxicity. We therefore investigated if Hipp prevents, *in vitro,* the wasting of C2C12 myotubes treated with IFNγ and TNFα as described in Chapter 2.

We first confirmed if Hipp treatment prevents wasting similar to PatA by visualizing the integrity of myotubes and measuring their diameter 72 hours after treatment with or without IFNγ/TNFα. We demonstrated that Hipp, indeed, (Figure 3.1A) prevented the

wasting of myotubes which occurs due to cytokine treatment (Figure 3.1B-C). As the anti-cachectic effects of PatA were attributed to the inhibition of iNOS translation we next assessed whether different doses of Hipp (100 and 200 nM) affected IFNγ/TNFα-induced iNOS expression and activity. We showed that Hipp significantly decreased, in a dose dependent manner, iNOS protein expression (Figure 3.2A-B) with corresponding decreases in NO production (Figure 3.2C). These data suggest that Hipp recapitulates the anti-cachectic effects of PatA and confirm that these effects were specific to eIF4A inhibition.

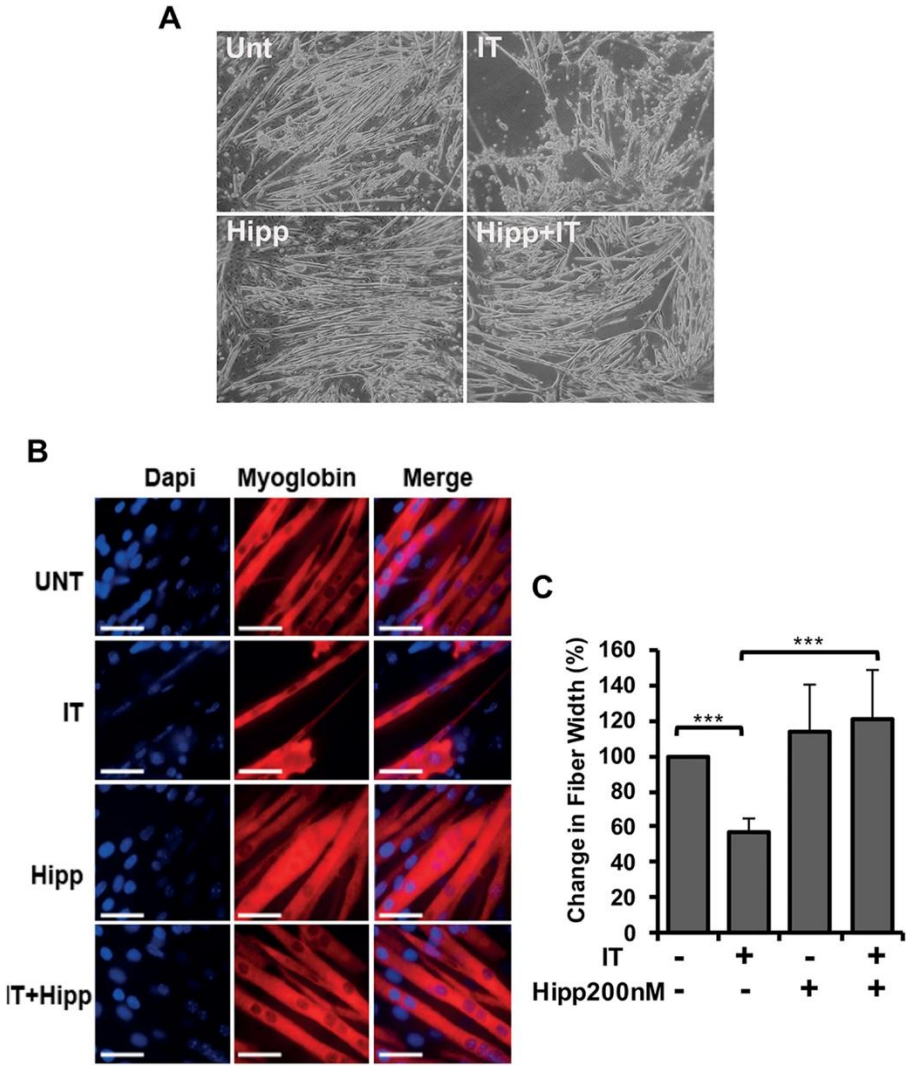

Figure 3.1: Hippuristanol (Hipp), an eIF4A inhibitor, prevents IT-induced muscle wasting.

C2C12 myotubes treated with or without IFNγ (100 U/mL) and TNFα (20 ng/mL) for 72 hours in the presence or absence Hipp (200 nM).

(A) Representative phase-contrast imaging of myotubes.

(B) Representative immunofluorescence imaging for myoglobin to visualize myotube integrity. Nuclei were visualized with DAPI staining.

(C) Quantification of myotube fiber width plotted as the percentage relative to untreated myotubes.

Data Information: Error bars represent the standard error of the mean (SEM) of three independent experiments (n = 3). For statistical comparisons P-values were calculated with Student's t-test (***$P < 0.001$).

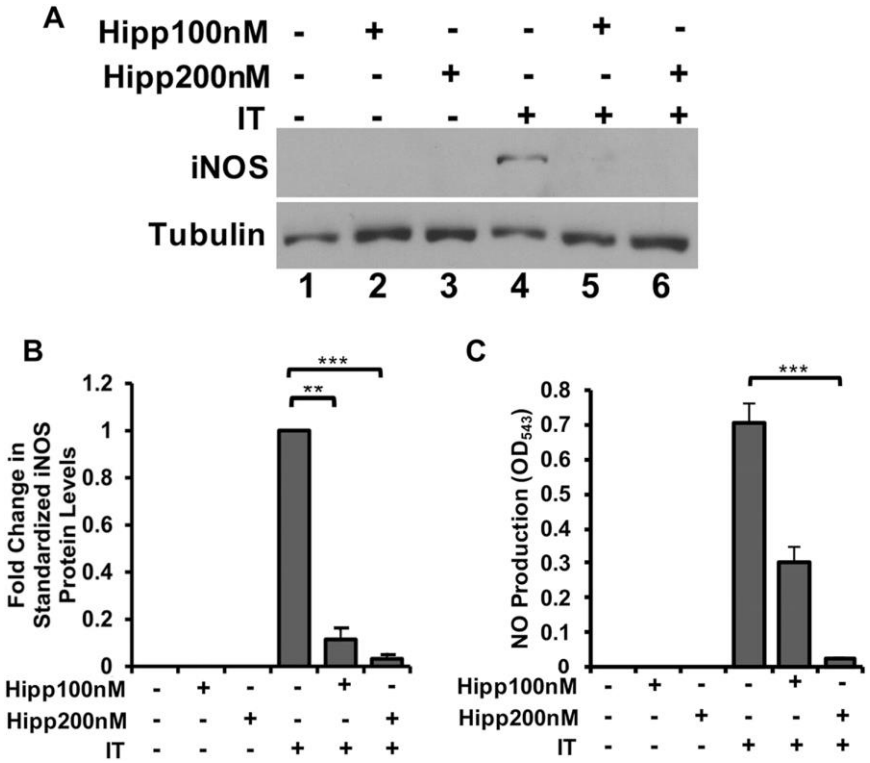

Figure 3.2: Hippuristanol (Hipp) prevents IT-mediated activation of the pro-cachectic iNOS/NO pathway.

C2C12 myotubes treated with or without IFNγ (100 U/mL) and TNFα (20 ng/mL) for 24 hours in the presence or absence Hipp (100 and 200 nM).

(A) Western blot analysis of iNOS protein levels in myotubes. Tubulin was included as a loading control.

(B) Quantification of iNOS protein levels and standardized to Tubulin levels plotted relative to IFNγ/TNFα-treated myotubes (n = 3).

(C) NO production in myotubes determined using the Griess assay (n = 4).

Data Information: Error bars represent the standard error of the mean (SEM) of three or four independent experiments as indicated above. For statistical comparisons P-values were calculated with Student's *t*-test (**P < 0.01; ***P < 0.001).

3.2 Hippuristanol reduces cytokine-induced activation of the STAT3 pathway.

Inhibition of eIF4A has been shown to have broad anti-inflammatory/anti-cancer effects. Since PatA is more effective in preventing cachexia than the iNOS inhibitor AMG (Bordeleau et al., 2008; Chu & Pelletier, 2015; Romo et al., 2004; Singh et al., 2021; Zhang et al., 2020)(Di Marco *et al.*, 2012), we investigated whether other pro-cachectic factors were dependent on eIF4A for their expression. First, we assessed if Hipp impacted secreted levels of the pro-cachectic cytokine IL-6 and its mRNA expression, as we have previously shown its expression is induced in C2C12 myotubes treated with IFNγ/TNFα (Ma *et al.*, 2017). Indeed, Hipp significantly decreased levels of secreted IL-6 in cytokine-treated myotubes (Figure 3.3A), in addition to impairing the expression of the IL-6 mRNA (Figure 3.3B). As both levels of mRNA and translated protein were decreased by Hipp, we could not conclude whether Hipp impaired IL-6 translation or whether this effect was due to impairment of an upstream factor responsible for IL-6 transcription. Therefore, we looked at the effect of Hipp on the expression of upstream pro-cachectic transcription factors that are involved in mediating the transcription of IL-6.

eIF4A was previously shown to regulate the expression of several oncogenic super enhancer-associated transcription factors (Wolfe *et al*, 2014). Since STAT3 is a super enhancer associated factor that was shown to regulate the expression of IL-6 (Ma *et al.*, 2017; Yoon *et al*, 2012; Yu *et al*, 2009; Zimmers *et al.*, 2016) (Hnisz *et al*, 2013), we assessed whether eIF4A impairment by Hipp was impacting the activation of the STAT3 pathway and the translation of STAT3 mRNA in our model. We demonstrate that Hipp indeed prevented the activation and total expression of STAT3 (as seen by measuring

the levels of phosphotyrosine-705 STAT3 (PY705-STAT3) and total STAT3 protein levels) (Figure 3.4A-C). Importantly, Hipp did not significantly affect STAT3 mRNA levels induced by IFNγ/TNFα (Figure 3.4D) suggesting that Hipp prevents activation of the STAT3 pathway and expression of its downstream targets by inhibiting STAT3 mRNA translation.

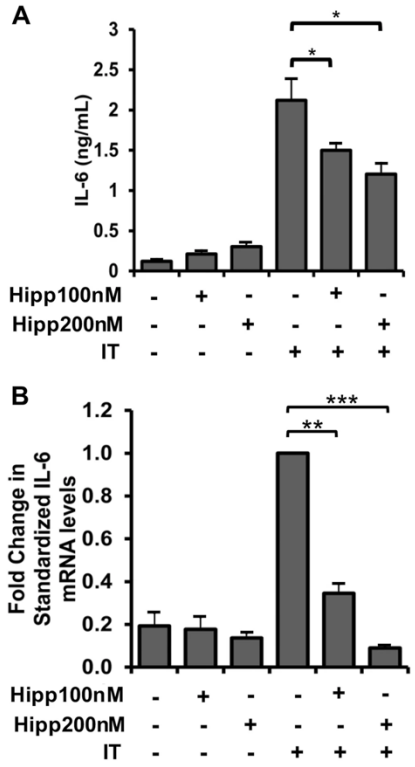

Figure 3.3: Hippuristanol (Hipp) decreases IL-6 mRNA expression and secretion in IT-treated myotubes.

C2C12 myotubes treated with or without IFNγ (100 U/mL) and TNFα (20 ng/mL) for 24 hours in the presence or absence Hipp (100 and 200 nM).

(A) IL-6 concentrations detected by ELISA in the supernatants from myotubes.

(B) RT-PCR analysis for IL-6 mRNA expression standardized to RPL32 housekeeping gene, normalized relative to IFNγ/TNFα-treated myotubes.

Data Information: Error bars represent the standard error of the mean (SEM) of three independent experiments (*n* = 3). For statistical comparisons P-values were calculated with Student's *t*-test (*p < 0.05; **P < 0.01; ***P < 0.001).

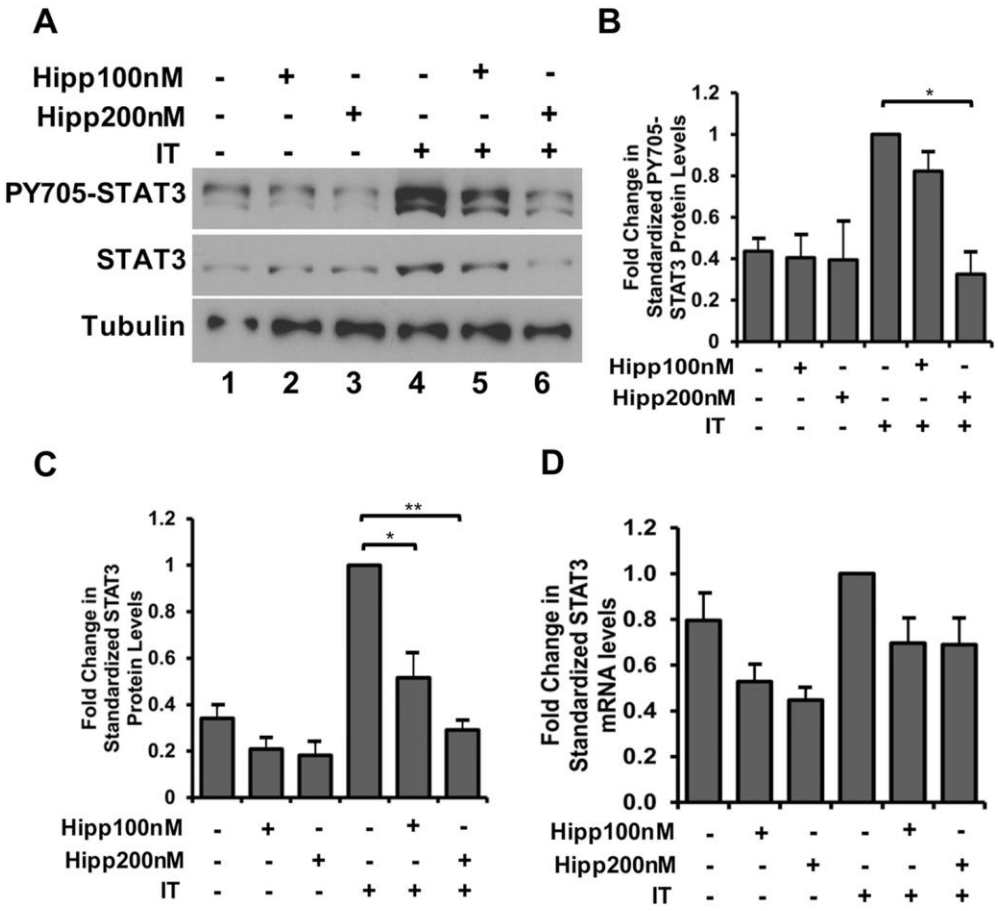

Figure 3.4: Hippuristanol (Hipp) inhibits STAT3 protein, but not STAT3 mRNA levels, in IT-treated myotubes.

C2C12 myotubes treated with or without IFNγ (100 U/mL) and TNFα (20 ng/mL) for 24 hours in the presence or absence Hipp (100 and 200 nM).

(A) Western blot analysis of PY705-STAT3 and STAT3 protein levels in myotubes. Tubulin was included as a loading control.

(B-C) Quantification of (B) PY705-STAT3 and (C) STAT3 protein levels and standardized to Tubulin levels plotted relative to IFNγ/TNFα-treated myotubes.

(D) RT-PCR analysis for STAT3 mRNA expression standardized to RPL32 housekeeping gene, normalized relative to IFNγ/TNFα-treated myotubes.

Data Information: Error bars represent the standard error of the mean (SEM) of three independent experiments (*n* = 3). For statistical comparisons P-values were calculated with Student's *t*-test (*p < 0.05; **P < 0.01).

3.3 Pateamine A and Silvestrol decrease activation of the STAT3 pathway in cytokine-treated myotubes.

As Hipp strongly reduced STAT3 expression and activation of the STAT3 pathway, we concluded our study by confirming that these effects were specific to eIF4A inhibition. To this end, we evaluated the effect of PatA and another eIF4A inhibitor silvestrol on the STAT3 pathway in cytokine-treated myotubes. First, we assessed the effect of PatA on IL-6 and STAT3 expression. As expected, PatA recapitulated the effects of Hipp on IL-6 induction in response to IFNγ/TNFα by decreasing both secreted levels of IL-6 and its mRNA expression (Figure 3.5A-B). PatA treatment of IFNγ/TNFα-treated myotubes also reduced protein levels of total STAT3 and its activated state PY705-STAT3 (Figure 3.5C-E), without affecting STAT3 mRNA levels (Figure 3.5F). Therefore, PatA impaired the STAT3 pathway by repressing STAT3 mRNA translation similar to Hipp. Lastly, we confirmed the anti-cachectic effects of eIF4A inhibition with silvestrol by measuring activation of the iNOS/NO and STAT3 pathways. As expected, silvestrol decreased NO production and iNOS protein levels in cytokine-treated myotubes in a dose dependent manner (Figure 3.6A-C). Silvestrol also significantly reduced STAT3 protein levels in a dose dependent manner, without affecting STAT3 mRNA levels (Figure 3.6B,D,E). Taken together, our results show that eIF4A inhibitors reduce the abundance of iNOS and STAT3 proteins at the translational level, thereby preventing cachexia-induced muscle wasting.

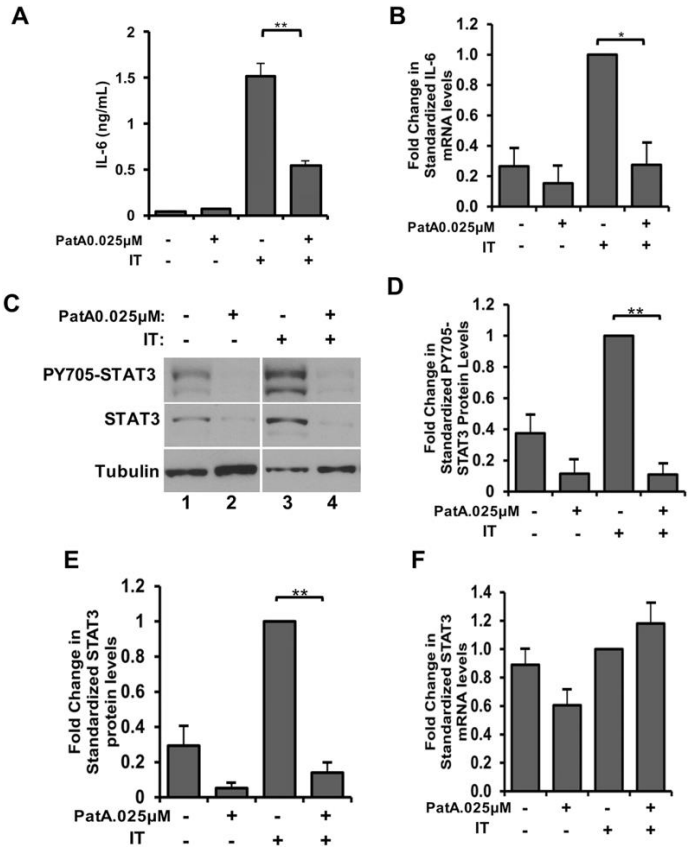

Figure 3.5: Pateamine A recapitulates the impact of Hippuristanol on IL-6 secretion and STAT3 protein levels.

C2C12 myotubes treated with or without IFNγ (100 U/mL) and TNFα (20 ng/mL) for 24 hours in the presence or absence of PatA (0.025 μM).

(A) IL-6 levels in the supernatant of myotubes determined by ELISA.

(B) RT-PCR analysis for IL-6 mRNA expression standardized to RPL32 housekeeping gene, normalized relative to IFNγ/ TNFα-treated myotubes.

(C) Western blot analysis of PY705-STAT3 and STAT3 protein levels in myotubes. Tubulin was included as a loading control.

(D-E) Quantification of (D) PY705-STAT3 and (E) STAT3 protein levels and standardized to Tubulin levels plotted relative to IFNγ/ TNFα-treated myotubes.

(F) RT-PCR analysis for STAT3 mRNA expression standardized to RPL32 housekeeping gene, normalized relative to IFNγ/ TNFα-treated myotubes.

Data Information: Error bars represent the standard error of the mean (SEM) of three independent experiments (n = 3). For statistical comparisons P-values were calculated with Student's t-test (*$p < 0.05$; **$P < 0.01$).

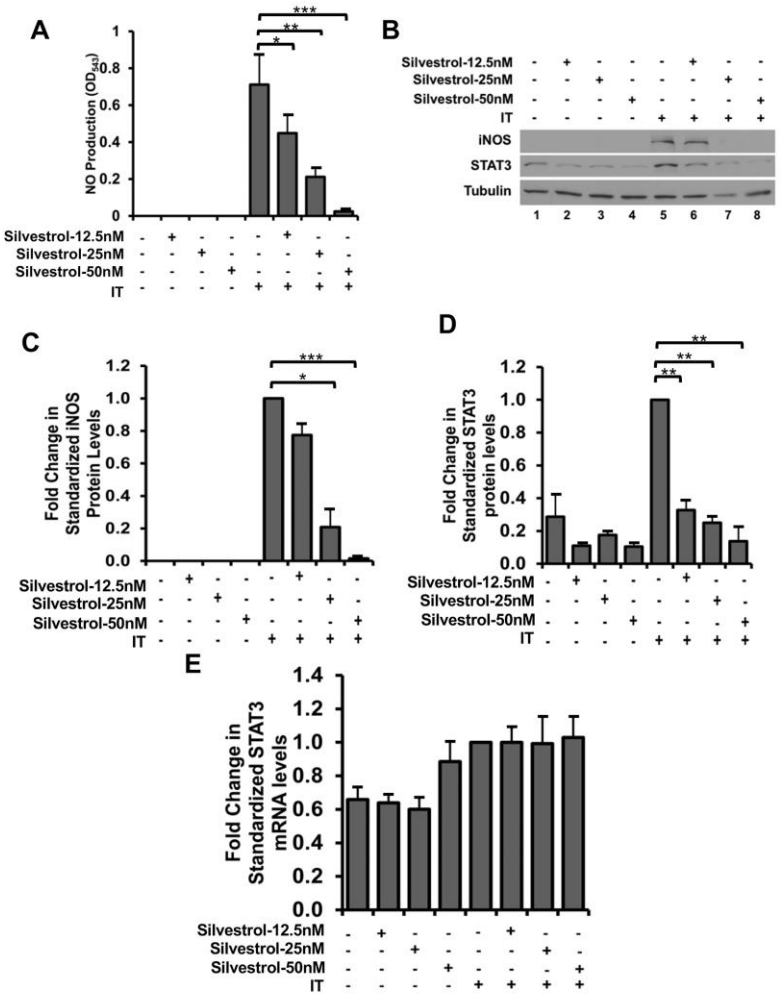

Figure 3.6: Silvestrol perturbs iNOS and STAT3 protein expression.

C2C12 myotubes treated with or without IFNγ (100 U/mL) and TNFα (20 ng/mL) for 24 hours in the presence or absence of Silvestrol (12.5, 25, and 50nM).

(A) NO production in myotubes determined using the Griess assay (*n* = 5).

(B) Western blot analysis of iNOS and STAT3 protein levels in myotubes. Tubulin is included as a loading control (*n* = 3).

(C-D) Quantification of (C) iNOS and (D) STAT3 protein levels and standardized to Tubulin levels plotted relative to IFNγ/TNFα-treated myotubes (*n* = 3).

(E) RT-PCR analysis for STAT3 mRNA expression standardized to RPL32 housekeeping gene, normalized relative to IFNγ/TNFα-treated myotubes (*n* = 3).

Data Information: Error bars represent the standard error of the mean (SEM) of three or five independent experiments as indicated above. For statistical comparisons P-values were calculated with Student's *t*-test (*p < 0.05; **P < 0.01; ***P < 0.001).

4 Materials and Methods

4.1 Reagents

lFNγ (485-MI) and TNF-α (410-MT) were obtained from R&D systems. GW274150 (HY-12119) was purchased from MedChemExpress. Hippuristanol, Silvestrol, and Pateamine A were kindly provided by Dr. Jerry Pelletier. Aminoguanidine (396494), DAPI (10236276001), oligomycin (75351), Rotenone (R8875), antimycin A (A8674), and monensin (M5273) were purchased from Sigma-Aldrich. ECL Western Blotting Detection Reagent (RPN2106) was bought from GE Healthcare Life Sciences.

4.2 Antibodies

The iNOS antibody (610431) was purchased from BD Transduction Laboratories. The CD45 conjugated to BV786 (564225) antibody was purchased from BD Horizon. VDAC (48665), pThr172-AMPKa (2535), total AMPKa (2603), pSer79-ACC (3661), total ACC (3662), pThr389-S6K (9205), total S6K (2708), pSer235/236-S6 (2211), S6 (2317), total STAT3 (9139), and pTyr705-STAT3 (9145) antibodies were purchased from Cell Signaling Technology. The myoglobin (ab77232), 3NT (ab61392), and Total OXPHOS Rodent Antibody Cocktail (ab110413) (containing five antibodies, one against a subunit of each ETC complex) antibodies were purchased from Abcam. The F4/80 conjugated to PE/Cy7 (123114), Ly6c conjugated to APC-fire750 (128046), CD206 conjugated to PE (141706), and CD86 conjugated to BV421 (105032) antibodies were purchased from BioLegend. Laminin (L9393) antibody was purchased from Sigma-Aldrich. The tubulin antibody (DSHB Hybridoma Product 6G7; deposited by Halfter, W.M.), myosin heavy chain (DSHB Hybridoma Product MF20; deposited by Fischman, D.A.), MyHC I (DSHB Hybridoma Product BA-D5; deposited by Schiaffino, S.), and MyHC IIa (DSHB

Hybridoma Product SC-71; deposited by Schiaffino, S.) antibodies were obtained from the Developmental Studies Hybridoma Bank (DSHB). Horseradish peroxidase (HRP)-conjugated goat secondary antibodies against mouse (315-035-003) and rabbit (111-035-003) primary antibodies were obtained from Jackson ImmunoResearch Laboratories. Alexa Fluor™ 488-conjugated goat anti-mouse secondary (A11029), Alex Fluor™ 594-conjugated goat anti-rabbit secondary (A11072), Alexa Fluor™ 594-conjugated goat antimouse secondary (A11032), Alexa Fluor™ 647-conjugated goat antirabbit secondary (A21244), Alexa Fluor™ 488-conjugated goat anti-mouse IgG1 secondary (A21121), and Alexa Fluor™ 594-conjugated goat anti-mouse IgG2b secondary (A21145) antibodies were purchased from Thermo Fisher Scientific.

4.3 Cell Culture

C2C12 myoblast cells (American Type Culture Collection (ATCC), Manassas, VA, USA) were cultured on 0.1% gelatin-coated (Sigma-Aldrich) culture dishes (Corning). C2C12 myoblasts were grown in DMEM (Thermo Fisher 11995-065 or Invitrogen) with high glucose, L-glutamine, and sodium pyruvate that was supplemented with 20% fetal bovine Serum (FBS) (Sigma-Aldrich F1051) and 1% penicillin/streptomycin (Sigma-Aldrich P0781). Cultured myoblasts were differentiated into myotubes upon reaching 90-100% confluence by switching medium to DMEM containing 2% horse serum (Invitrogen 16050122) and 1% penicillin/streptomycin. Cells were monitored for mycoplasma infection by DAPI staining.

Myotubes were treated with or without IFNγ (100 U mL^{-1}) and TNFα (20 ng mL^{-1}) (IT) for 24 to 72 hours after visibly forming which occurred three or four days after induction of differentiation. GW or Aminoguanidine treatments were conducted concurrently for

the duration of IT treatment. Myotubes treated with eIF4A inhibitors were incubated for 30 minutes with or without Hippuristanol (100 and 200 nM), Pateamine A (0.025 μM) or Silvestrol (12.5, 25 and 50 nM) at the beginning of IT treatment. Cells were then washed with PBS and re-incubated with media with or without IT.

4.4 Immunoblotting

Total protein extracts from C2C12 cells were prepared using a lysis buffer containing 50 mM HEPES pH 7.0, 150 mM NaCl, 10% glycerol, 1% Triton X-100, 10 mM sodium pyrophosphate, 100 mM NaF, 1 mM EGTA, 1.5 mM $MgCl_2$, 0.1 mM sodium orthovanadate, and complete EDTA-free protease inhibitors (Roche Applied Science). Skeletal muscle protein content was prepared by homogenizing muscle in ice-cold muscle protein extraction buffer containing PBS supplemented with 1% NP-40, 0.5% sodium deoxycholate, 50 mM NaF, 5 mM $Na_4P_2O_7$, 0.1% SDS, 0.1 mM sodium orthovanadate, and complete EDTA-free protease inhibitors. The soluble protein fraction was clarified by centrifugation at 12,000 g for 5 min at 4°C and diluted with Laemmli loading dye.

Laemmli diluted protein lysates were resolved on 7.5–12% acrylamide gels and transferred to nitrocellulose membranes using the Trans-Blot® Turbo™ system. Transfer efficiency and protein loading were visualized by either reversible Ponceau S staining or Stain-Free imaging. Membranes were blocked in 10% skim milk and washed three times in Tris-buffered saline containing 0.1% Tween (TBS-T). Membranes were incubated in primary antibodies diluted in either 5% skim milk or 5% BSA containing TBS-T overnight at 4˚C. Membranes were probed with antibodies against iNOS (1:5,000), VDAC (1:5,000), pThr172-AMPKa (1:5,000 – 1:1,000), total AMPKa (1:5000 –

1:1,000), pSer79-ACC (1:5000 – 1:1,000), total ACC (1:1,000), pThr389-S6K (1:2,000), total S6K (1:5,000), pSer235/236-S6 (1:5,000), S6 (1:1,000), tubulin (1:1,000), total STAT3 (1:1,000), and pTyr705-STAT3 (1:1,000), total OXPHOS Rodent antibody cocktail (1:1,000), and 3NT (1:2,000). Primary antibodies were washed off three times with TBS-T. Membranes were then incubated for 1 h at room temperature with the appropriate HRP-conjugated secondary antibodies (1:5,000 – 1:10,000) diluted in 5% skim milk. Secondary antibodies were washed off three times with TBS-T and exposed using ECL reagent. Chemiluminescent signal was detected using either photosensitive film or a Bio-Rad ChemiDoc™ imaging system. Densitometry quantification was performed using either ImageJ software or Bio-Rad Image Lab™ software.

4.5 Detection of media nitrite levels and IL-6

Quantification of NO released was achieved by measuring media nitrite levels with GRIESS reagent. GRIESS reagent 1 (1% sulphanilamide, 5% phosphoric acid) and GRIESS reagent 2 (0.1% N-(1-naphthyl)-ethylenediamine dihydrochloride) were mixed 1:1 to make GRIESS reagent. Nitrite concentration of unknown samples was determined by comparison against a standard curve established from a serial dilution of sodium nitrite solution. Standards and unknown media samples were mixed 1:1 with GRIESS reagent, incubated at room temperature for 5 min, and their absorbance of 543 nm wavelength was measured.

IL-6 in the supernatant of IT-treated myotubes was measured using the Mouse IL-6 ELISA Ready-SET-Go!® Kit (eBioscience, Inc.).

4.6 Reverse Transcription Quantitative PCR (RT-qPCR)

Total RNA was extracted using TRIzol® (Thermo Fisher 15596018) according to the manufacturer's instructions. RNA quality and quantity were determined using a Thermo Fisher NanoDropTM reader (ND-1000) and agarose gel electrophoresis. 1 µg of total RNA was reverse transcribed to cDNA using either the M-MuLV Reverse Transcriptase (New England Biolabs) or iScript cDNA Synthesis Kit (Bio-Rad 1708891). cDNA was analyzed by qPCR with SsoFastTM Evagreen® Supermix (Bio-Rad 1725200) using primers for F4/80 (F: 5'-GCA TCA TGG CAT ACC TGT TC-3' R: 5'-GAG CTA AGG TCA GTC TTC CT-3'), GAPDH (F: 5'-AAG GTC ATC CCA GAG CTG AA-3' R: 5'- AGG AGA CAA CCT GGT CCT CA-3'), STAT3 (F: 5'-GCT GCT TGG TGT ATG GCT CT-3', R: 5'-TAT CTT GGC CCT TTG GAA TG-3'), IL-6 (F: 5'-AACGATGATGCACTTGCAGA-3' R: 5'-CTC TGA AGG ACT CTG GCT TTG-3'), and RPL32 (F: 5'-TTC TTC CTC GGC GCT GCC TAC GA-3', R: 5'-AAC CTT CTC CGC ACC CTG TTG TCA-3'). All levels were normalized to GAPDH (Chapter 3) or RPL32 (Chapter 4) and relativized to controls.

4.7 GC-MS metabolomic analysis

Cells were lysed using sonication in dry ice chilled 80% methanol to collect soluble and insoluble fractions. Total genomic DNA (gDNA) was collected from the insoluble fraction by phenol:chloroform:isoamyl alcohol extraction to relativize metabolite concentrations to cell content. 750 ng of D-myristic acid was added to each sample's soluble fraction as an internal standard. Soluble fraction samples were dried and dissolved in 30 µl of methoxyamine hydrochloride (10 mg/ml) in pyridine. Samples were then derivatized using 70 µl of N-(tert-butyldimethylsilyl)-N-methyltrifluoroacetamide

(MTBSTFA) to generate tert-butyldimethylsilyl (TBDMS) esters. Metabolite levels were measured with an Agilent 5975C GC/MS equipped with a DB-5MS+DG (30 m × 250 μm × 0.25 μm) capillary column (Agilent J&W, Santa Clara, CA, USA). Electron impact was set at 70 eV, and a total of 1 μl of sample was injected in splitless mode with the inlet temperature of 280°C. As helium was used as a carrier gas with a flow rate of 1.5512 ml/min the myristic acid internal standard elutes at 17.94 min. Quadrupole was set at 150°C and the interface at 285°C. The oven program was started at 60°C for 1 min, then increased at a rate of 10°C/min until 320°C and held at 320°C for 10 min. Data were acquired with both in scan (1–600 m/z) and selected ion (SIM) modes (McGuirk *et al*, 2013). Mass isotopomer distribution and metabolite abundance were determined using a custom algorithm developed at McGill University (McGuirk *et al.*, 2013). Metabolite abundance was normalized to D-myristic acid levels and relativized to total gDNA content.

4.8 Cellular ATP content

Cellular ATP content was determined using the ATP Determination Kit (Invitrogen A22066). After removing media and washing quickly with room temperature PBS, cells were lysed in their plates ATP Assay Lysis Buffer (25 mM Tris–HCl, 2 mM DTT, 2 mM EDTA, 10% glycerol, and 1% Triton X-100) for 5 min at room temperature while agitated on a plate shaker. Plates were then placed on ice and ATP content was determined according to manufacturer instructions.

4.9 Extracellular flux and bioenergetics analysis

Oxygen consumption rate (OCR) and extracellular acidification rate (ECAR) were measured with an Agilent Seahorse XFe24 Analyzer. C2C12 myoblasts were plated and

differentiated to myotubes in XFe24 culture plates (1007777-004). Cells were switched to XF Base Medium (103575-100) supplemented with 10 mM D-glucose (Sigma G7528) and cultured in a CO_2-free incubator at 37°C, according to manufacturer instructions 1 h before assessment. A XFe24 sensor cartridge (102340-100) calibrated according to the manufacturer's instructions, was loaded with Oligomycin to 1 µM, FCCP to 1.5 µM, Rotenone to 1 µM, Antimycin A to 1 µM, and monensin to 20 µM. Basal extracellular flux was measured in three cycles and two measurement cycles were performed between drug injections. Measurement cycles occurred as follows: 3 min mix, 2 min wait, and 3 min measurement. During the experiment, media buffering capacity was determined using a sequential injection of HCl in two wells and ranged from 0.061 to 0.065 mpH pmol $H^{+\ -1}$. Well protein content was determined after the run as follows. Cells were washed three times in room temperature albumin-free Krebs-Ringer phosphate HEPES (KRPH) medium (2 mM HEPES, 136 mM NaCl, 2 mM NaH_2PO_4, 3.7 mM KCl, 1 mM $MgCl_2$, 1.5 mM $CaCl_2$, pH 7.4). Cells were then lysed for 30 min on ice using 25 µl of RIPA lysis buffer (150 mM NaCl, 50 mM Tris, 1 mM EGTA, 1 mM EDTA, 1% TritonX-100, 0.5% sodium deoxycholate, 0.1% SDS, pH 7.4) followed by agitation for 5 min. Protein content was lastly measured using a BCA assay (Thermo Fisher 23225) according to the manufacturer's instructions and extracellular flux rates were normalized to protein content. Bioenergetic profiling was determined as detailed by (Mookerjee *et al.*, 2017, 2018).

4.10 Animal models

Animal experiments were carried out with approval from the McGill University Faculty of Medicine Animal Care Committee and are in accordance with the guidelines set by

the Canadian Council of Animal Care. Mice were housed in a controlled environment in sterile cages with corn-cob bedding set on a 12-h light–12-h dark cycle. Mice were provided commercial laboratory food (Harlan #2018; 18% protein rodent diet; Madison, WI) and had free access to water.

For the LPS model of septic cachexia, male C57BL/6 wild-type and whole-body iNOS knockout mice on a C57BL/6 background ages 8–12 weeks were obtained from Jackson Laboratories. LPS was prepared in 0.5% BSA dissolved in sterile PBS to a concentration of 0.1 mg ml^{-1}. At the beginning of the dark cycle (18:30 h to 19:30 h), mice were intraperitoneally injected with 10 ml kg^{-1} LPS for a final concentration of 1 mg kg^{-1}. GW-injected mice were intraperitoneally injected with 5 mg kg^{-1} dose of GW 24 h before LPS injection and then a second time simultaneously with LPS injection. The dose of GW utilized (5 mg kg^{-1}) has previously been shown to reduce collagen-induced arthritis similar to that in iNOS knockout (Cuzzocrea *et al*, 2002). Mice were separated into individual cages to allow for pair-feeding compared to wild-type, LPS-injected mice. Wild-type, LPS-injected mice were fed *ad libitum*, and all other cohorts were fed the average amount of food consumed by LPS-injected mice. Mice were euthanized approximately 18h after injection, tissues were collected and weighed. Tissues were either snap-frozen in liquid nitrogen or prepared for sectioning as described below.

For the C26 model of cancer cachexia, male BALB/C mice ages 6–8 weeks were obtained from Jackson Laboratory. Cages were randomly assigned to each treatment group. C26 adenocarcinoma cells provided by Dr. Denis Guttridge were cultured in DMEM supplemented with 10% FBS and 1% penicillin/streptomycin. Cells were kept below 70% confluency and minimally passaged before injection. Injected C26 cells were

prepared at a concentration of 1.25×10^7 cells ml^{-1}. 100 µl was injected subcutaneously into the right flank of the mice for a final dose of 1.25×10^6 cells per mouse. For saline controls, an equivalent volume of PBS was injected. Tumor growth was monitored by manual measurement with calipers. GW was prepared to a final concentration of 0.5 mg ml^{-1} in sterile PBS. Five days after C26 injection and every day thereafter, mice were intraperitoneally injected with 10 ml kg^{-1} of either GW for a final dose of 5 mg kg^{-1} or PBS. On day 14–19 post-C26 injection, mice were anesthetized with isoflurane gas and exsanguinated by cardiac puncture. Following cervical dislocation, tissue was collected as described in the LPS experiment.

4.11 Grip strength

Forelimb grip strength was measured using a using a DFE II Series Digital Force Gauge (Ametek DFE II 2-LBF 10-N). Mice were allowed to acclimate the morning of injection. Mice were suspended by the tip of the tail, allowing them to establish a grip. Peak forelimb grip force was measured by gently pulling the mice parallel to the meter until their grip was broken. The mice were returned to their home cage for at least one minute before subsequent measurements. Four measurements were taken per mouse. This process was conducted before injection and the morning of euthanasia to determine the percent change in peak grip strength.

4.12 Fluorescence-activated cell sorting (FACS)

Spleens from saline or LPS-treated WT and iNOS KO mice were collected and passed through a strainer on ice to obtain single cells. Red blood cells were lysed using ACK buffer for 3 min at room temperature. Viability was assessed using fixable viability dye eFluorYM506 (Thermo Fisher/eBioscience 65-0866-14). Viable cells were then

analyzed using the CD45, F4/80, Ly6c, CD206, and CD86 antibodies. BD Cytofix/ Cytoperm™ (BD Bioscience, 554722) was used to fix the myeloid compartment according to the manufacturer instructions. The $CD86^+$ cells or $CD206^+$ cells were gated on viable cells that were $Cd45^+$, $F4/80^+$, and $Ly6c^-$. Flow cytometry was done in the BD LSR Fortessa 4 lasers (405/488/561/633 nm) flow cytometer, and the results were analyzed using Flowjo_v 10.7.1_CL (Treestar).

4.13 Muscle freezing and sectioning

Gastrocnemius and tibialis anterior muscles were mounted on 7% tragacanth gum and snap-frozen in liquid nitrogen-cooled isopentane. Samples were stored at -80°C before cryosectioning at 10 μm intervals.

4.14 Histological analysis of muscle cross-sectional area

Sections of muscles were stained with hematoxylin and eosin (H&E) staining. Stained samples were subsequently imaged by visible light microscopy. Muscle minimum Feret's diameter and cross-sectional areas were determined using ImageJ software to manually trace the circumference of individual fibers.

4.15 Immunofluorescence

For immunofluorescence of C2C12 myotubes to measure myotube diameter, cells were fixed in 3% paraformaldehyde for 30 min. Cells were permeabilized and blocked with 0.1%-0.5% Triton X-100, 1% goat serum in PBS (Thermo Fisher 16210-064). Cells were then incubated in primary antibodies against myosin heavy chain (MF-20; 1:1,000) and myoglobin (1:500) for 1 h. After washing, they were incubated in Alexa® Fluor secondary antibodies (1:500) for 1 h, stained with DAPI, and mounted on coverslips with VECTASHIELD® Antifade Mounting Medium (Vector Laboratories H-1000).

Samples were imaged with a Zeiss Observer Z1 microscope and AxioCam MRm digital camera. Myotube diameters were measured at two or three points along each fiber using the Carl Zeiss Zen2 (blue) software.

For immunofluorescence on sections of muscles to determine fiber type composition, frozen sections were first equilibrated to room temperature for 20 min. Sections were fixed in 3% paraformaldehyde for 30 min, blocked in 5% goat serum for 1 h, incubated in primary antibodies against MyHC I (1:50), MyHCIIa (1:500), and laminin (1:250) overnight. After washing, sections were incubated in Alexa® Fluor secondary antibodies in (1:500) for 1 h. The sections were then mounted on coverslips using VECTASHIELD® HardSet Antifade Mounting (Vector Laboratories H-1400). The entirety of the sections was imaged with a Zeiss Observer Z1 microscope and AxioCam MRm digital camera. The images of entire muscle sections were assembled using ImageJ software, and each fiber was then classified as type I or type IIa positive. Unstained fibers with no signal were classified as being type IIb/x.

4.16 Transmission electron microscopy

Tibialis anterior or gastrocnemius tissue samples were imaged at the Facility for Electron Microscopy Research at McGill University (Montreal, Quebec, Canada). The tissue samples were fixed overnight in 2.5% glutaraldehyde in 0.1 M sodium cacodylate buffer, then postfixed with 1% OsO_4 + 1.5% potassium ferrocyanide in 0.1 M sodium cacodylate buffer for 2 h at 4°C and washed three times with Milli-Q water. The tissues were dehydrated in a graded series of acetone-dH_2O up to 100%. Following dehydration, tissues were infiltrated with a graded series of Epon-acetone (1:1, 2:1, 3:1), embedded in 100% Epon, and polymerized at 65°C for 48 h. Ultrathin serial

sections (90–100 nm) were prepared using a Leica Microsystems EM UC6 ultramicrotome with a Diatome diamond knife, transferred to 200-mesh copper TEM grids, and poststained with 4% uranyl acetate for 6 min and Reynold's lead citrate for 5 min. Images were taken by an FEI Tecnai G2 Spirit120 kV TEM with a Gatan UltraScan 4000 CCD Camera Model 895. The proprietary Gatan Digital Micrograph 16-bit images (DM3) were then converted to unsigned 8-bit TIFF images.

4.17 Statistics and data processing

For *in vitro* studies, n indicates experimental replicates. Experimental replicates were excluded if the negative (non-treated) and positive (cytokine-treated) samples did not show an appropriate inflammatory response. For *in vivo* studies, n indicates the number of animals per treatment cohort. Mice were excluded if they developed complications (phenotypes unrelated to cachexia or humane-intervention endpoints such as ulceration of the tumor mass). Samples for measuring myotube diameter and minimum Feret's diameter/cross-sectional areas were blinded before imaging and during quantification. Bar graphs represent the mean, with error bars showing either the standard deviation of the mean for biological replicates, standard error of the mean, or the standard deviation for technical replicates as indicated in figure legends. In Chapter 2, significance P-values between means were computed using either one-way ANOVA with Fisher's LSD test for multiple treatments groups, Student's t-test for comparison of two groups, or Kolmogorov–Smirnov test for comparison of frequency distributions in GraphPad Prism version 7 or 8, GraphPad Software, La Jolla California USA, www.graphpad.com. The pathway analysis of the metabolomics data set was conducted using MetaboAnalyst 4.0, www.metaboanalyst.ca. P-values of significantly altered pathways were determined

using GlobalTest on MetaboAnalyst 4.0. In Chapter 3 significance P-values between means were computed using Student's t-test in Microsoft Excel.

5 General Discussion

5.1 Overview

Cachexia is a deadly syndrome that, to this day, has no treatment regimen that successfully reverses its deleterious consequences. Past attempts at treating cachexia by targeting upstream initiators of the cachectic phenotype have not succeeded due to the complex etiology of the syndrome. Identifying and targeting downstream effectors of multiple pro-cachectic signaling pathways might be the key to preventing wasting. iNOS is one such effector that is induced in wasting muscle and has long been hypothesized to be a major contributor to cachectic muscle wasting, although the mechanisms behinds its atrophic effects are poorly understood. A goal of this thesis was to address this gap and expand our understanding of the mechanisms behind iNOS-mediated muscle wasting. Work from our group and others has also suggested the therapeutic potential of targeting the iNOS/NO pathway, through either direct chemical inhibition or indirect means of impairing iNOS expression, in preventing cachectic muscle wasting. Indeed, our lab has presented several distinct methods of impairing iNOS expression or activity in cachectic muscle such as through the early activation of AMPK, inhibition of STAT3/NF-κB-mediated transcription of iNOS, and inhibition of eIF4A; all of which recapitulated or exceeded the anti-cachectic effects of direct inhibitors of iNOS (Di Marco *et al.*, 2012; Di Marco *et al.*, 2005; Hall *et al.*, 2018; Ma *et al.*, 2017). Therefore, this thesis also sought to provide a proof of principle for the efficacy of clinically translatable strategies that impair iNOS to combat cachexia and to elucidate the mechanisms behind the anti-cachectic effects of these potential therapeutics.

iNOS is increasingly recognized as a regulator of cellular metabolism in inflammatory diseases, suggesting it may also promote metabolic dysfunction in cachectic muscle. To this end, in Chapter 2 I uncovered a novel function of iNOS as a driver of metabolic defect and energetic crisis in wasting muscle. iNOS activity decreased mitochondrial content, disrupted the cristae on the IMM, and decreased OXPHOS activity leading to insufficient energy production and a catabolic state in muscle (Figure 5.1). This work also provided evidence supporting the repurposing of the clinically tested iNOS inhibitor GW274150 as GW prevented cachexia-induced muscle wasting and metabolic dysfunction in preclinical models of the syndrome (Figure 5.1). Chapter 3 solidified our understanding of the anti-cachectic effects of eIF4A inhibition. The work presented in this chapter proved that the previously described PatA-mediated disruption of iNOS mRNA translation is specific to its impairment of eIF4A as two other eIF4A inhibitors, Hipp, which has a distinct mechanism of action, and Silvestrol, similarly affected iNOS protein expression. Furthermore, this work identified a broader anti-cachectic effect of eIF4A inhibition as Hipp, PatA, and Silvestrol prevented STAT3 translation and, furthermore, activation of the STAT3 pathway leading to the reduced production of IL-6. Collectively, these results support the therapeutic potential of targeting iNOS and eIF4A in preventing cachexia induced muscle wasting. However, new questions remain unanswered such as the molecular targets of iNOS in cachexia and how these potential drugs can be translated into clinic.

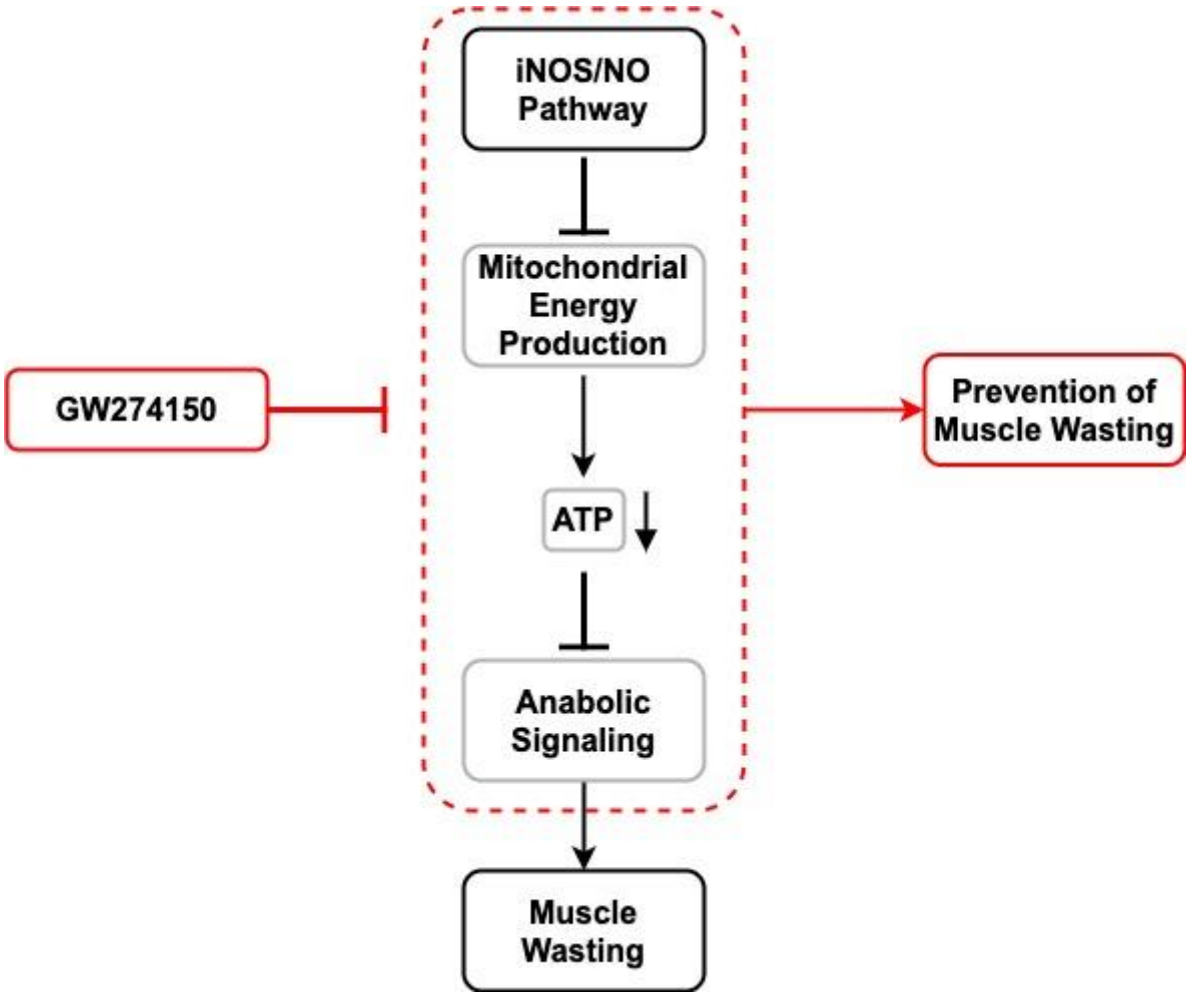

Figure 5.1: Schematic depicting the role of the iNOS/NO pathway in promoting energy crisis during cachexia-induced muscle wasting.
(*Outlined in black and grey*) Upon activation by underlying diseases such as cancer, the iNOS/NO pathway is activated. In turn, iNOS inhibits mitochondrial energy production in skeletal muscles reducing ATP production which leads to muscle wasting. As a result of these effects, anabolic signaling is reduced and muscle loss is induced. (*Highlighted in red*) On the hand, pharmacological inhibition of iNOS activity with drugs such as GW274150 reverses these effects, preventing muscle wasting.

5.2 How does iNOS disrupt mitochondrial function and overall metabolism?

The iNOS-driven metabolic insults described in Chapter 2 such as the disruption of OXPHOS-dependent ATP production, the impairment of ETC Complex II and IV, and the induction of energetic crisis are in line with previously observed cachexia-mediated impairment of oxidative metabolism and mitochondrial dysfunction (Brown *et al.*, 2017; Der-Torossian *et al.*, 2013b; Julienne *et al*, 2012; Kunzke *et al.*, 2020; McLean *et al.*, 2014; Padrão *et al.*, 2013; Pin *et al.*, 2019a; VanderVeen *et al.*, 2019; VanderVeen *et al.*, 2018; White *et al.*, 2012). Nevertheless, our mechanistic analysis did not identify the complete collection of metabolic factors which iNOS targets. Although we observed drastic iNOS-mediated alterations to mitochondrial morphology and dynamics, how iNOS alters these parameters is a pressing question. In addition, several iNOS-driven alterations to metabolic pathways including glycolysis, TCA cycle, and amino acid metabolism were found. Identifying which factors iNOS targets to influence these pathways can further our understanding of the extensive metabolic remodeling caused by iNOS.

This work identified a signature of amino acids, comparable to previous metabolomics studies, indicative of increased muscle protein breakdown and impaired anapleurosis that was correlated with iNOS activity and iNOS-induced energetic crisis (Der-Torossian *et al.*, 2013b; Kunzke *et al.*, 2020; Lautaoja *et al.*, 2019; QuanJun *et al.*, 2015; Tseng *et al.*, 2015). Notably, iNOS-dependent accumulation of arginine levels in both the C26 and LPS models was observed. This accumulation is significant as arginine is the substrate of iNOS and has also been shown to promote iNOS protein synthesis (Chaturvedi *et al*, 2007; El-Gayar *et al*, 2003; Lee *et al*, 2003). Dissecting the

relationship between iNOS and arginine levels can provide insight into how the iNOS/NO pathway is maintained in cachectic muscle. As iNOS also altered glycolysis and the TCA cycle, a future direction from this work is identifying which metabolic enzymes are regulated by iNOS. Recent work in M1 polarized macrophages has shown that iNOS disrupts glucose catabolism through glycolysis and TCA cycle by impairing the enzymes PDH, isocitrate dehydrogenase (IDH), and aconitase (Bailey *et al.*, 2019; Palmieri *et al.*, 2020). Interestingly, PDH and aconitase inhibition have been reported in cachectic muscle suggesting that iNOS could mediate these effects in cachexia too (Pin *et al.*, 2019b; Wyart *et al.*, 2022). With reports of increased expression of the key glycolysis enzymes HK and PFK in wasting muscle (Cui *et al.*, 2019a; Remels *et al.*, 2010), also assessing how iNOS affects these enzymes could explain the observed iNOS-dependent increases in glycolysis in wasting C2C12.

Our reported reduction of mitochondrial content in the C26 model of cachexia is likely due to regulation of mitochondrial turnover by iNOS. Inflammation-induced cachexia has been associated with decreased expression and activity of biogenesis factors (Remels *et al.*, 2010; VanderVeen *et al.*, 2017; White *et al.*, 2012). The deacetylase sirtuin 1 (SIRT-1), which targets several transcription factors such as NF-κB and the mitochondrial biogenesis promoter peroxisome proliferator–activated receptor-γ coactivator-1α (PGC-1α), has been shown to be downregulated in wasting muscle (Lee & Goldberg, 2013; Shinozaki *et al*, 2014; VanderVeen *et al.*, 2017). Interestingly, in other systems, inflammation-induced iNOS expression and activity has been associated with SIRT-1 inactivation leading to increased acetylation of transcription factors (Nakazawa *et al*, 2017; Shinozaki *et al.*, 2014). iNOS-derived NO was shown to S-

nitrosylate SIRT-1 during inflammation leading to its inactivation (Nakazawa *et al.*, 2017; Shinozaki *et al.*, 2014). This impairment of SIRT-1-mediated deacetylation led to activation of NF-κB and deactivation of PGC-1α (Nakazawa *et al.*, 2017; Shinozaki *et al.*, 2014). Indeed, PGC-1α and downstream factors nuclear response factor-1 (NRF-1) and mitochondrial transcription factor A (Tfam), all of which promote biogenesis, are also typically downregulated in cachectic muscle (Remels *et al.*, 2010; VanderVeen *et al.*, 2017; White *et al.*, 2012). It remains possible, therefore, that iNOS impairs mitochondria biogenesis in cachexia-induced muscle wasting through SIRT-1 S-nitrosylation thereby promoting catabolism (though activation of NF-κB and mitochondria dysfunction due in part to the downregulation of PGC-1α activity).

Alternatively, iNOS activity in the C26 model may reduce mitochondrial content by increasing mitophagy. Mitophagy is increased in cachectic muscle, likely caused by loss of mitochondrial function (e.g., depolarization and disruption of the IMM) and increased expression of circulating pro-cachectic factors (Brown *et al.*, 2017; Franco-Romero & Sandri, 2021; Penna *et al.*, 2019a; VanderVeen *et al.*, 2017). Our results demonstrated that iNOS impairs OXPHOS through disruption of Complex II and IV integrity and the IMM. It is possible that iNOS impairs ETC complexes by post-translationally modifying complex subunits through nitrosylation and nitration leading to inactivation as seen in other models (Radi, 2018). It is possible that iNOS drives mitophagy by impairing mitochondrial energy production in addition to its observed regulation systemic inflammatory cytokines.

Mitochondrial fission and fusion are also key regulatory processes dictating mitophagy levels, with increases in fission and mitochondrial fragmentation often

preceding mitophagy (Romanello & Sandri, 2022). Indeed, mitochondrial fission is reportedly elevated in cachectic muscle with increases in fission factors such as dynamin-related protein 1 (DRP-1), while fusion is impaired with mitofusin (MFN) proteins MFN-1 and -2 and optic atrophy protein 1 (OPA1) decreasing (Brown *et al.*, 2017; VanderVeen *et al.*, 2017; White *et al.*, 2012). Work studying macrophage activation from naïve to M1 state showed that M1 macrophages had fragmented mitochondria (Gao *et al*, 2017; Li *et al.*, 2020). This fragmentation was attributed to decreases in fusion proteins and increases in DRP-1 activity, similar to what occurs in cachectic muscle (Gao *et al.*, 2017). Interestingly, iNOS inhibition in M1 macrophages prevented mitochondrial fragmentation (Li *et al.*, 2020). Potentially explaining the reduction of fission in NO-deficient M1 macrophages, S-nitrosylation and activation of DRP-1 by NO has been implicated in increasing mitochondrial fission in models of neuronal injury (Cho *et al*, 2009; Li *et al.*, 2020). Exploring whether iNOS promotes mitophagy in cachectic muscle by inducing fragmentation through DRP-1 S-nitrosylation could prove fruitful.

On the other hand, iNOS could also promote fragmentation and mitophagy through impairment of fusion protein such as OPA1. In addition to its roles in fusion, OPA1 is also a key structural protein in the IMM that controls cristae remodeling and architecture (Cogliati *et al.*, 2016). As we observed iNOS-associated disruption of cristae and the IMM, exploring whether iNOS alters cristae architecture through OPA1 and whether this affects mitochondrial dynamics and levels remains promising. Indeed, S-nitrosylation of the pro-fusion protein OPA1 has also been reported, although the functional effect of this modification is not yet determined (Montagna *et al*, 2020). Future work should

assess whether OPA1 is nitrosylated in cachectic muscle and if this iNOS-mediated effect disrupts fusion of mitochondria and their membrane structure. Due to its extensive metabolic effects, iNOS likely disrupts several of the aforementioned metabolic processes. As eIF4A inhibition represses iNOS expression and activity, future studies can assess whether and how eIF4A inhibitors affect cachexia-induced metabolic defect.

5.3 How does iNOS impair the myogenic program?

As previously shown by our lab, iNOS and associated peroxynitrite production has been implicated in disrupting the myogenic program in cachectic muscle by reducing the expression of MRFs such as MyoD (Di Marco *et al.*, 2005). Indeed, a recent study has confirmed that iNOS impairs myoblast differentiation under cachectic conditions, impairing their proliferation and fusion into myotubes (Arneson-Wissink & Doles, 2021). Furthermore, other studies have reported cachexia-induced decreases in MRF expression (Brown *et al*, 2018; Di Marco *et al.*, 2012; Guttridge *et al.*, 2000; Hall *et al.*, 2018; He *et al.*, 2013). These iNOS-dependent myogenic defects likely contribute to accumulation of damage and disrupted muscle regenerative capacity that has been identified in mouse models of cachexia (Coletti *et al*, 2016; He *et al.*, 2013; Hogan *et al*, 2018; Inaba *et al*, 2018).

iNOS-mediated downregulation of MRF expression was correlated with decreased association of the RNA binding protein HuR to the MyoD and Myogenin mRNAs leading to their increased decay (Di Marco *et al.*, 2005). Simultaneously, HuR was also shown to have increased association with the iNOS mRNA, increasing its stability and facilitating the induction of the iNOS/NO pathway (Di Marco *et al.*, 2005). Taken together these cachexia-induced events suggest an iNOS-induced switch in HuR

association from pro-myogenic MRF mRNAs to pro-cachectic messages such as iNOS. Indeed, HuR has also been implicated in promoting the translation of the pro-cachectic factor STAT3 in wasting muscle (Mubaid *et al.*, 2019). Furthermore, genetically modified mice with muscle specific knockout of the HuR gene were protected against cancer cachexia-induced muscle wasting highlighting its importance as a pro-cachectic factor (Janice Sánchez *et al.*, 2019).

Interestingly, HuR has been shown to be sensitive to modification by RNS. Indeed, HuR RNA targeting has been shown to be altered by S-nitrosylation (Banadakoppa *et al*, 2013). Whether HuR targeting is altered by RNS in cachectic muscle is yet to be determined. We have therefore begun a study to address this question by assessing post-translational modification of HuR by RNS in models of muscle wasting. To this end, I found that HuR is susceptible to tyrosine nitration in an *in vitro* assay using recombinant, purified HuR treated directly with peroxynitrite (Figure 5.2A). As a follow up, the nitrated residues of HuR in the *in vitro* assay were identified through mass spectrometry which found 6 of 10 tyrosine residues were nitrate, 5 of which were on RNA recognition motif (RRM) 1 and RRM2 of the protein suggesting they can alter RNA binding (Figure 5.2B). Determining whether these sites are nitrated in cachectic muscle and if this nitration event is responsible for a functional switch of HuR can reinforce the notion that iNOS is a negative regulator of the myogenic program in wasting muscle.

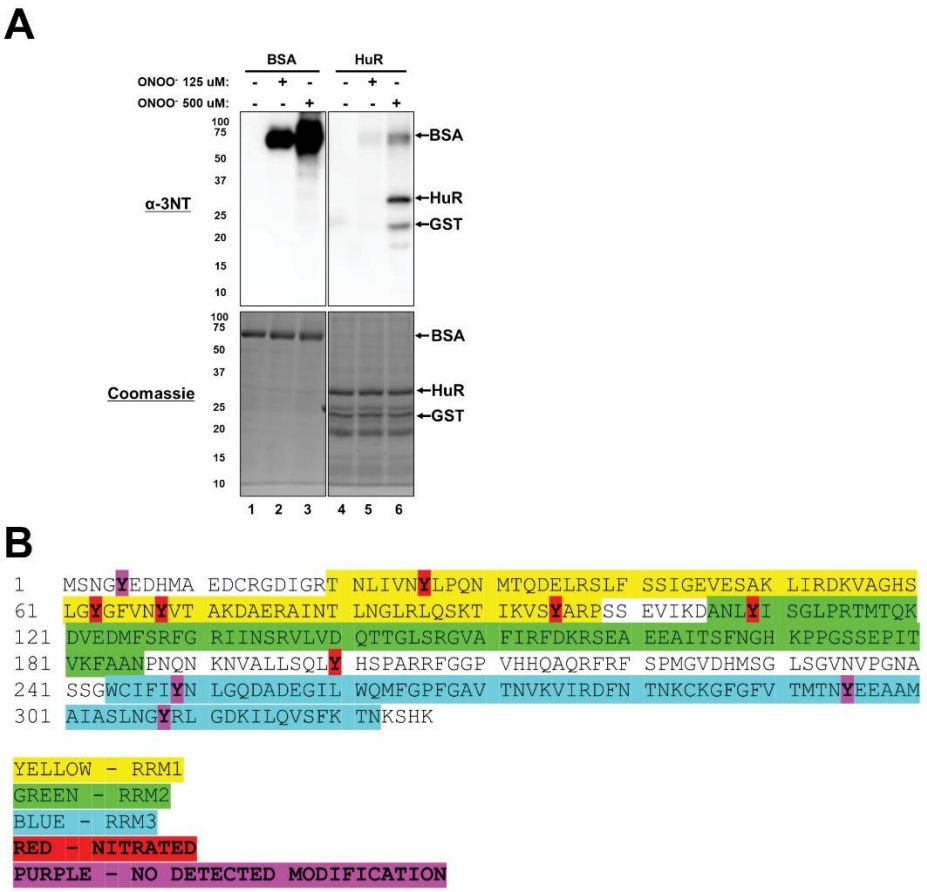

Figure 5.2*: In vitro* analysis of HuR nitration.

Recombinant HuR purified and cleaved from GST-HuR, recombinant GST, and BSA were treated with indicated doses of peroxynitrite.

(A) Representative image of Western blot analysis of untreated and peroxynitrite treated purified proteins samples probed for 3NT. BSA was included as a positive control for nitration. Coomassie blue was used to confirm equal loading.

(B) Amino acid sequence of HuR. Nitrated and unmodified tyrosine residues are highlighted as red and purple, respectively. RRM domains are highlighted in yellow, green, and blue.

5.4 How does iNOS and eIF4A inhibition affect inflammatory signaling?

The strong link between inflammation and cachexia initiation/progression encouraged our assessment of how GW and eIF4A inhibitors affect pro-inflammatory signaling and inflammatory cell population/function. iNOS expression and NO secretion from inflammatory cells in the muscle micro-environment are likely contributors to muscle wasting *in vivo*. In Chapter 2, the strategies utilized to perturb iNOS were not specific to muscle and inhibited iNOS in the whole body, including inflammatory compartments. Nevertheless, genetic and pharmacological inhibition of iNOS in our models of cachexia successfully disrupted iNOS activity in muscle as visualized by 3NT levels and associated wasting. Elucidation of the role of inflammatory cell iNOS and muscle-specific iNOS activity in cachectic contexts using tissue specific knockout models could provide interesting insight into the contribution of each cell type to muscle wasting. On a similar note, the work presented in Chapter 2 did not assess how other NOS isoforms, nNOS and eNOS, affect cachectic muscle wasting. Assessing the contribution of these NOS isoforms to cachectic muscle wasting could bolster our understanding of how nitric oxide metabolism promotes wasting. As other NOS isoforms are expressed in muscle, investigating how iNOS ablation affects their expression and activity should also be explored. Indeed, nNOS expression has been shown to increase significantly in diaphragm muscles of iNOS KO mice treated with LPS compared to WT counterparts (Comtois *et al*, 1999). Determining whether this occurs in limb muscles of iNOS KO mice and how this affects wasting phenotypes remains an important question.

Due to the prominent role of iNOS in immunity, it was likely that iNOS would affect immune cells in cachectic mice (Bogdan, 2001). The importance of assessing immune

cells in cachexia has been recognized as recent studies have investigated the role of cancer-cachexia induced macrophage populations in promoting muscle wasting and regulating adipose wasting (Erdem *et al*, 2019; Shukla *et al.*, 2020). Of note, one of these studies demonstrated a functional link between M2 polarized macrophages in the muscle microenvironment with induction of STAT3 signaling and muscle wasting (Shukla *et al.*, 2020). Our results demonstrated that iNOS inhibition significantly reduced secretion of pro-inflammatory cytokines; however, iNOS ablation did not affect splenomegaly, splenic macrophage polarization, levels of muscle macrophages, or tumor. eIF4A inhibitors had a similar effect in impairing cytokine secretion (IL-6), which was attributed to prevention of pro-inflammatory signaling within the cells through STAT3 repression. Assessing if iNOS affects activation of pro-inflammatory transcriptional programs in inflammatory cells (e.g., STAT3, NF-κB, and FOXO) could explain the discrepancy in function between cachexia-induced cell populations with or without iNOS. Future studies can also evaluate macrophage polarization and resident immune cells in cachectic muscle to understand how iNOS affects the muscle microenvironment to promote wasting. Furthermore, how eIF4A inhibitors affect cachexia-induced inflammatory changes *in vivo* should be tested as eIF4A inhibition has been shown to have broad anti-inflammatory effects.

5.5 Does eIF4A inhibition affect STAT3 translation?

The results presented in Chapter 3 demonstrate that PatA and Hipp decreased IFNγ/TNFα-induced IL-6 secretion and mRNA levels, which was correlated with significantly less STAT3 protein synthesis without a concurrent effect on STAT3 mRNA. These results suggest that eIF4A inhibitors impair the translation of the STAT3

transcript and the activity of the STAT3 pathway thereby lowering IL-6 transcription and secretion. Although STAT3 activation and protein levels are often correlated with serum IL-6 levels during cachexia (Bonetto *et al.*, 2012; Bonetto *et al.*, 2011; Zimmers *et al.*, 2016), it is unlikely that lower STAT3 levels are a result of decreased IL-6 secretion as previous work from our lab demonstrate that STAT3 induction in IFNγ/TNFα treated C2C12 myotubes does not depend on extracellular IL-6 (Ma *et al.*, 2017). In order to confirm this, polysome profiling can be performed to evaluate the fraction of STAT3 mRNA that is being actively translated vs. repressed. Indeed, our lab has used this approach to confirm the repression of iNOS translation and the recovery of MRFs MyoD and myogenin translation by PatA (Di Marco *et al.*, 2012).

5.6 Conclusion: Repurposing GW274150 and developing eIF4A inhibitors for the treatment of cachexia in clinic

This thesis provides novel mechanistic insight into how iNOS promotes muscle wasting and identifies the dependence of the pro-cachectic factor STAT3 on eIF4A for its expression. In addition, this thesis highlights the potential of two anti-cachectic treatment options (GW and eIF4A inhibitor Hipp) in preventing cachectic muscle wasting. However, the efficacy of iNOS or eIF4A inhibitors in treating cachexia in clinic is yet to be proven.

With a wide-ranging role in inflammation, iNOS has been explored as a therapeutic target in various conditions marked by high levels of inflammation. Indeed, the inhibitor used in our studies, GW274150, has been tested in clinical trials for the treatment of asthma, arthritis, and migraines (Víteček *et al.*, 2012). Although these trials were stopped due to GW not surpassing current treatment standards for these conditions, the

drug was non-toxic, potent at inhibiting iNOS, and had good pharmacokinetic characteristics (Víteček *et al.*, 2012). With these positive medicinal characteristics and the demonstrated anti-cachectic effects of GW in preclinical models presented in this thesis, repurposing of GW for the treatment of cachexia holds promise as there is no current approved treatment for this condition. iNOS induction in muscle has been reported in patients suffering from several cachexia causing diseases including cancer, AIDS, CHF, and COPD; therefore, GW may have a therapeutic benefit in the treatment of cachexia in various conditions (Adams *et al.*, 2003; Agusti *et al.*, 2004; Ramamoorthy *et al.*, 2009). Although not the focus of this research, GW may also benefit patients afflicted by cancer cachexia as iNOS inhibition has been reported to reduce tumor growth and metastasis (Garrido *et al.*, 2017; Granados-Principal *et al.*, 2015; Kostourou *et al.*, 2011). With further confirmation of the safety and efficacy of GW in preclinical models of cachexia, future clinical studies should be conducted to assess the therapeutic potential of iNOS inhibitors in treating this currently untreatable syndrome.

As highlighted in the introduction, a setback of monotherapies in clinic targeting pro-cachectic cytokines is the redundant function of these cytokines in activating pro-atrophic effectors. For example, the pro-cachectic transcription factors STAT3, NF-κB, and FOXOs can be activated by several humoral factors and intracellular stimuli counteracting individual cytokine blockades. To address this issue, our lab has evaluated targeting the downstream effectors that cause atrophy where cytokine signaling converge (e.g., iNOS). However, whether this strategy is effective in clinic is to be determined. In recent years use of multimodal strategies, including combining pharmaceutical agents, exercise, and dietary supplementation to treat cachexia and

address the multifactorial nature of its initiation and progression has gained traction (Arends *et al.*, 2021; Fearon *et al.*, 2011; Solheim *et al.*, 2018). Repurposing GW for use in these multimodal regimens could have significant benefits to their success and the health of patients.

Although the eIF4A inhibitors tested in Chapter 3 were employed as single agents, they mimic the benefits of multimodal approaches by targeting a wide subset of pro-cachectic factors from the initiating cytokines, transcription factors, the downstream effectors. This characteristic of eIF4A inhibitors has made it an attractive therapeutic option for the treatment of cancer and viral infections. Indeed, the rocaglate, Zotatifin, is being tested in clinic in clinical trials at the Phase I/II stage (Taroncher-Oldenburg *et al.*, 2021). Taken with the anti-cancer properties of eIF4A inhibitors, clinically translatable drugs such as Hipp can prove to be very effective in treating cancer cachexia.

The possibility of using iNOS and eIF4A inhibitors in tandem as a combinatorial therapy is yet to be tested; however, therapies utilizing both these strategies offer potential benefits. iNOS and eIF4A inhibitors have several overlapping functions that combat cachexia such as impairing the iNOS/NO pathway, IL-6 expression, and inflammatory signaling. If these strategies work synergistically in carrying out these anti-cachectic functions, treatments utilizing iNOS inhibitors and eIF4A inhibitors can have improved efficacy and greater patient tolerance as lower doses would be required to achieve the desired clinical outcome. On the other hand, if these strategies do not work in synergy or have no additive effects, employing them together would be futile due to the redundancy in function. In this case these drugs can be employed as a second-line treatment relative to each other in case of negative side effects or lack of recovery from

cachexia. For example, if a cachexia patient treated with iNOS inhibitors is not reaching desired clinical outcomes, clinicians can switch to eIF4A inhibitors to overcome these issues or vice versa. Nevertheless, future work should explore the possibility of combining these drugs in combating cachexia-driven muscle wasting.

This work has contributed to our knowledge of the anti-cachectic mechanisms of iNOS and eIF4A inhibition and uncovered new directions to investigate on how these therapeutics can contribute to mitochondrial function, immune system function, and overall muscle function. Elaboration of the mechanisms behind iNOS induced defects in metabolism, myogenesis, and inflammation during cachexia can inform the repurposing of GW as a therapeutic. Additionally, further testing of the efficacy of clinically amenable eIF4A inhibitors such as Hipp in animal models of cachexia can push the development of this promising class of drugs. As our understanding of the etiology of cachexia continues to advance, there is promise that cachexia will no longer be the deadly, incurable syndrome that it is today.

Appendices
Appendix Chapter 2

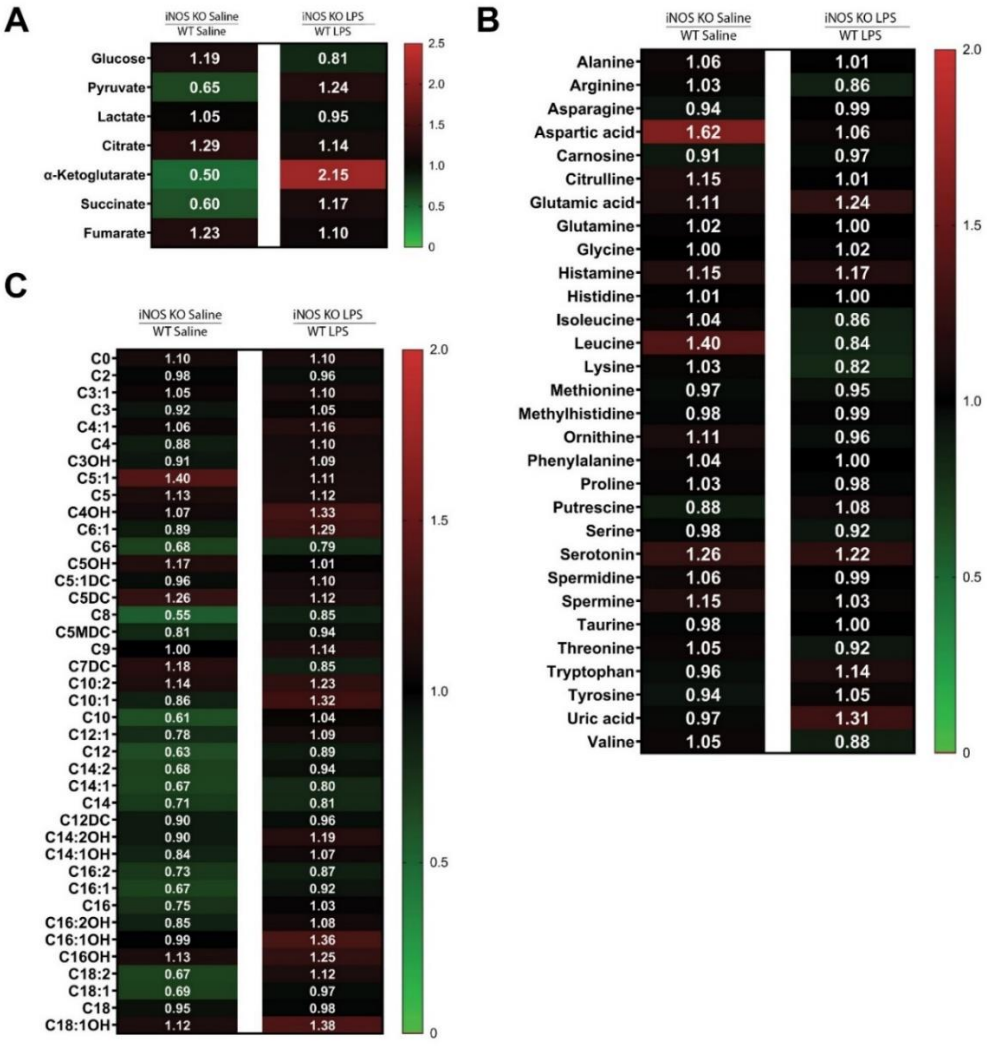

Appendix Figure 2.1: Metabolite levels of iNOS KO mice compared to WT mice.

Male C57BL/6 wildtype (WT) and iNOS knockout (KO) mice were intraperitoneally injected with 1mg kg^{-1} LPS or an equivalent volume of carrier solution. Saline treated WT and iNOS KO mice as well as the LPS-treated KO cohorts were pair-fed (PF) to the WT LPS-treated cohorts. After 18h, mice were euthanized, and the metabolome of tibialis anterior muscles was analyzed through LC-MS/MS.

(A-C)Heatmap visualizing mean concentration of (A) metabolites involved in

Glycolysis and TCA cycle (B) amino acids and amino acid derivatives and (C) acylcarnitines relative to WT of each treatment group. Red and green indicate an increase or decrease in metabolite levels, respectively.

Data information: Individual data points represent values from individual mice, with a total of six mice per cohort (n = 6). Plotted concentration data was relativized to WT of corresponding treatment.

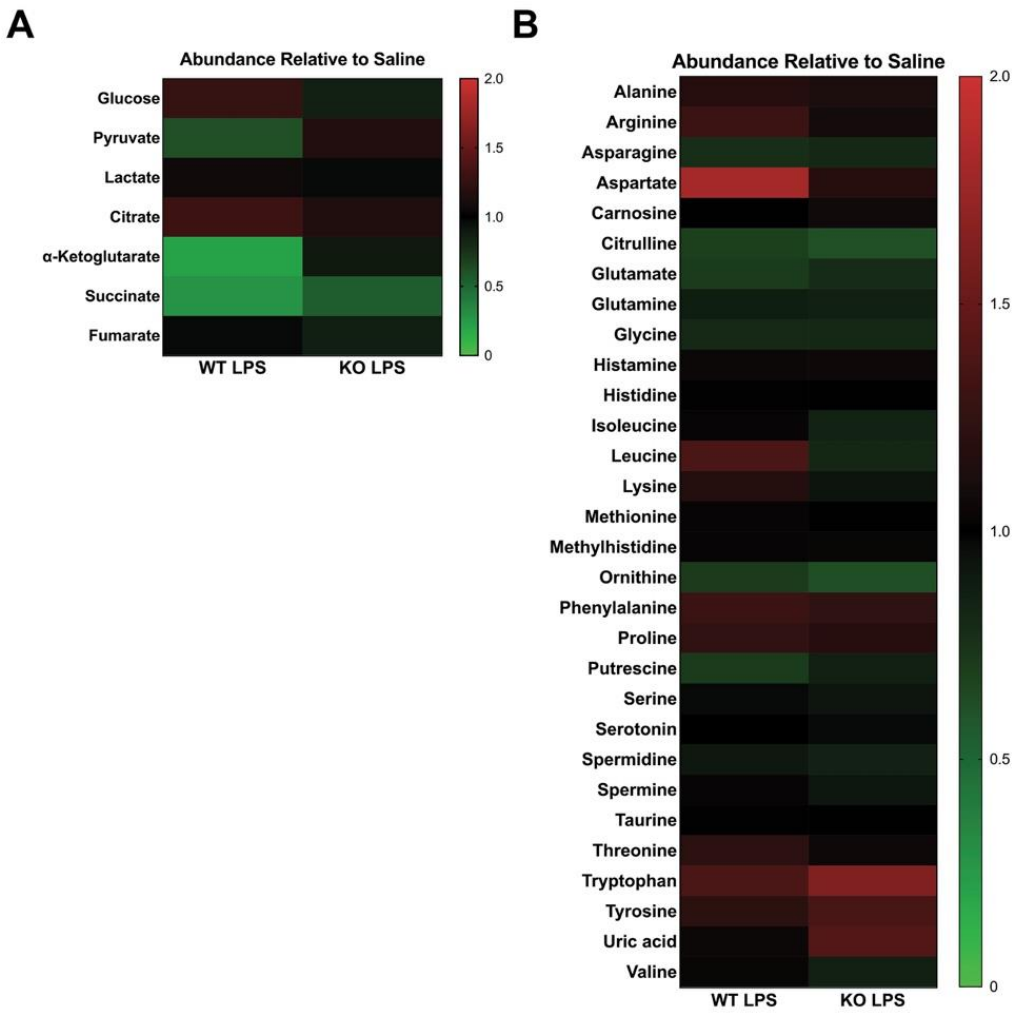

Appendix Figure 2.2: Genetic ablation of iNOS prevents LPS-driven deregulation of the TCA cycle and amino acid metabolism.

Male C57BL/6 wildtype (WT) and iNOS knockout (KO) mice were intraperitoneally injected with 1mg kg^{-1} LPS or an equivalent volume of carrier solution. Control WT, Control KO, and LPS-treated KO cohorts were pair-fed (PF) to the WT LPS-treated cohorts. After 18h, mice were euthanized, and the metabolome of tibialis anterior muscles was analyzed through LC-MS/MS.

(A) Heatmap visualizing mean concentration corresponding to metabolites involved in Glycolysis and TCA cycle relative to saline controls of each genotype. Red and green indicate an increase or decrease in metabolite levels, respectively.
(B) Heatmap visualizing mean concentration of amino acids and amino acid derivatives relative to saline controls of each genotype. Red and green indicate an increase or decrease in metabolite levels, respectively.

Data information: Individual data points represent values from individual mice, with a total of six mice per cohort (n = 6). Plotted concentration data was relativized to saline controls of corresponding genotype.

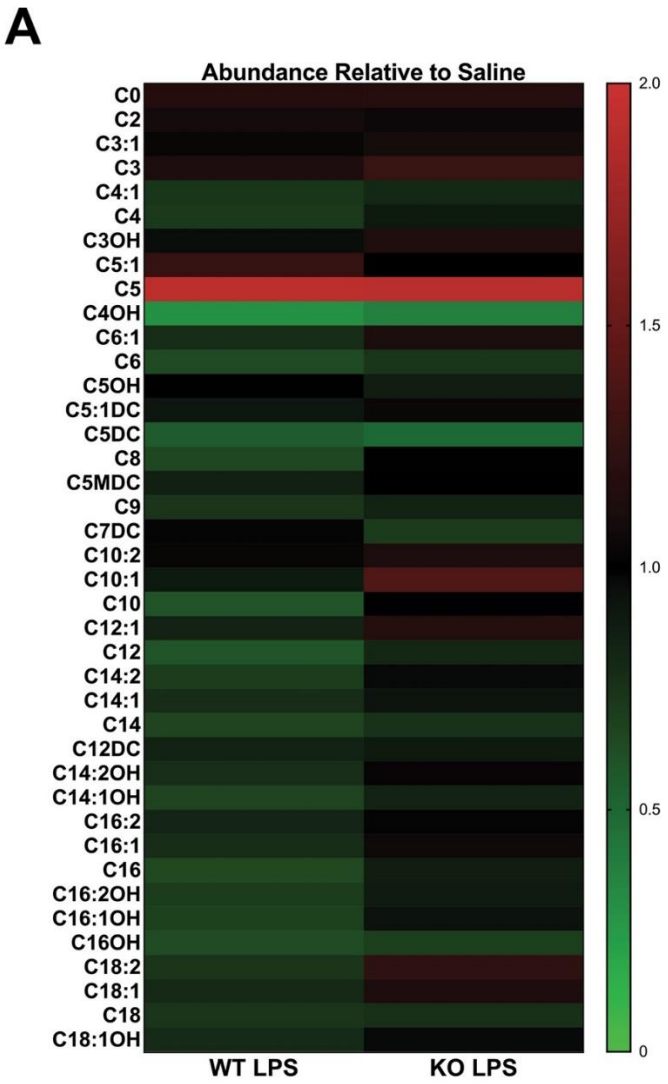

Appendix Figure 2.3: Genetic ablation of iNOS prevents LPS-driven deregulation of the acylcarnitine metabolism.

Male C57BL/6 wildtype (WT) and iNOS knockout (KO) mice were intraperitoneally injected with 1mg kg^{-1} LPS or an equivalent volume of carrier solution. Control WT, Control KO, and LPS-treated KO cohorts were pair-fed (PF) to the WT LPS-treated cohorts. After 18h, mice were euthanized, and the metabolome of tibialis anterior muscles was analyzed through LC-MS/MS.

(A) Heatmap visualizing mean concentration of acylcarnitines relative to saline controls of each genotype. Red and green indicate an increase or decrease in metabolite levels, respectively.

Data information: Individual data points represent values from individual mice, with a total of six mice per cohort (n = 6). Plotted concentration data was relativized to saline controls of corresponding genotype.

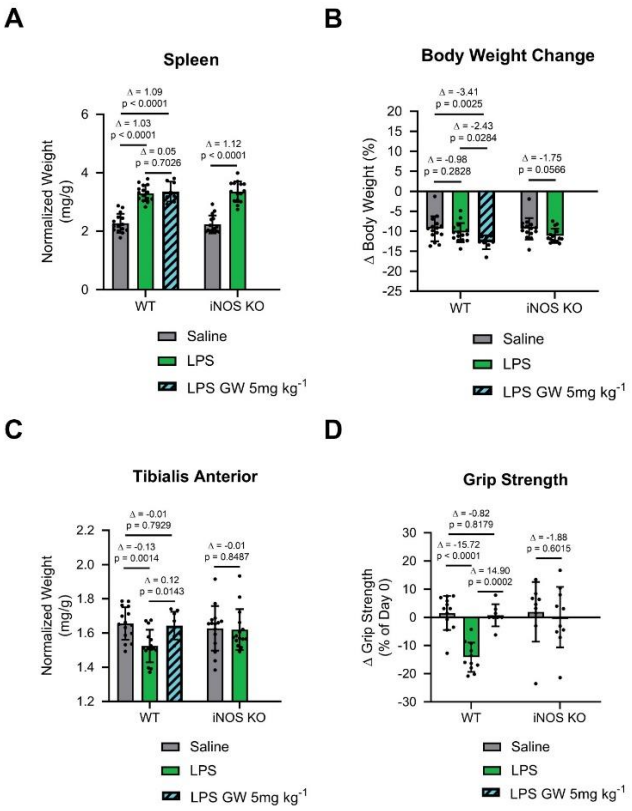

Appendix Figure 2.4: Pharmacological inhibition of iNOS prevents LPS-driven muscle wasting.

Male C57BL/6 wildtype (WT) and iNOS knockout (KO) mice were intraperitoneally injected with saline, 1mg kg^{-1} LPS or 5mg kg^{-1} of GW and LPS. Data was compared to previously shown data in Figures 1D, 1H, EV1A, and EV2A from Control WT, Control KO, and LPS-treated WT and KO cohorts. After 18h, mice were euthanized, and tissue samples were analyzed.

(A) Spleen weight normalized to initial body weight. (WT saline n=15, WT LPS n=15, WT LPS+GW n=8, iNOS KO saline n=15, and iNOS KO LPS n=15).
(B) Percent body weight change from time of injection to endpoint of experiment. (WT saline n=15, WT LPS n=15, WT LPS+GW n=8, iNOS KO saline n=15, and iNOS KO LPS n=15).
(C) Tibialis anterior weight normalized to initial body weight. (WT saline n=15, WT LPS n=15, WT LPS+GW n=8, iNOS KO saline n=15, and iNOS KO LPS n=15).
(D) Change in grip strength from before injection and before endpoint collection. (WT saline n=12, WT LPS n=11, WT LPS+GW n=8, iNOS KO saline n=9, and iNOS KO LPS n=10).

Data information: Data from Control WT, Control KO, and LPS-treated WT and KO cohorts are those shown in Figures 1D, 1H, EV1A, and EV2A and compared to WT LPS and GW-treated mice. Individual data points represent values from individual mice. Error bars represent the standard deviation (SD) of the mean. For statistical comparisons, Δ indicates the difference of mean values and p-values were calculated with an ANOVA followed by Fisher's LSD test.

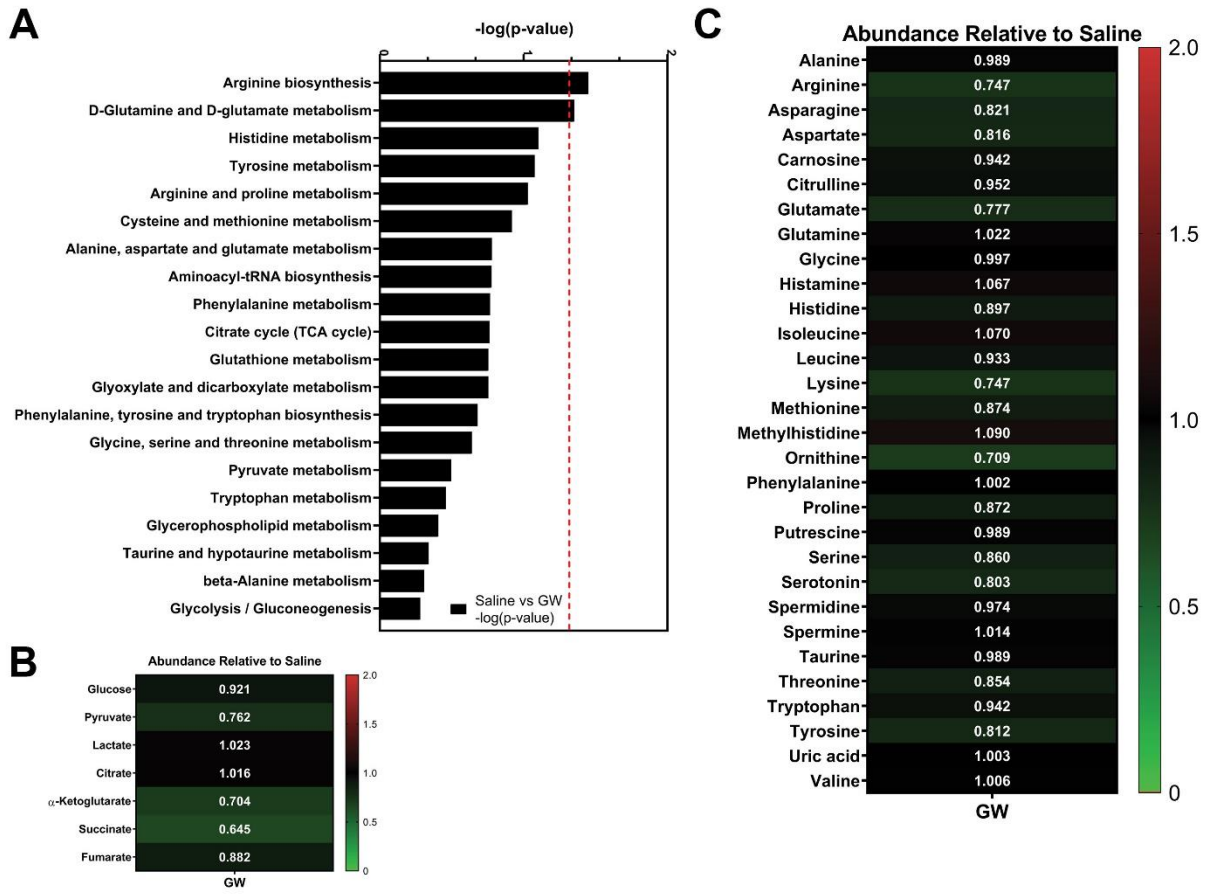

Appendix Figure 2.5: Characterization of GW-induced metabolome alterations.

Male BALB/C mice were injected subcutaneously with saline. After 5 days and everyday thereafter, the mice were injected with either saline or GW 5mg kg^{-1}. After 16 days, mice were euthanized, and the metabolome of tibialis anterior muscles was analyzed through LC-MS/MS.

(A) Pathway Analysis using MetaboAnalyst 4.0 Software comparing significantly altered pathways from saline to GW. Pathways are ranked by their significance and filtered based on a Pathway Impact Score >0.1. Metabolomic data were range-scaled and mean-centered.

(B-C) Heatmap visualizing mean concentration corresponding to (B) metabolites involved in Glycolysis and TCA cycle or (C) amino acids and amino acid derivatives in GW treated mice relative to saline controls. Red and green indicate an increase or decrease in metabolite levels, respectively.

Data information: Individual data points represent values from individual mice, with a total of six mice per cohort (n = 6).

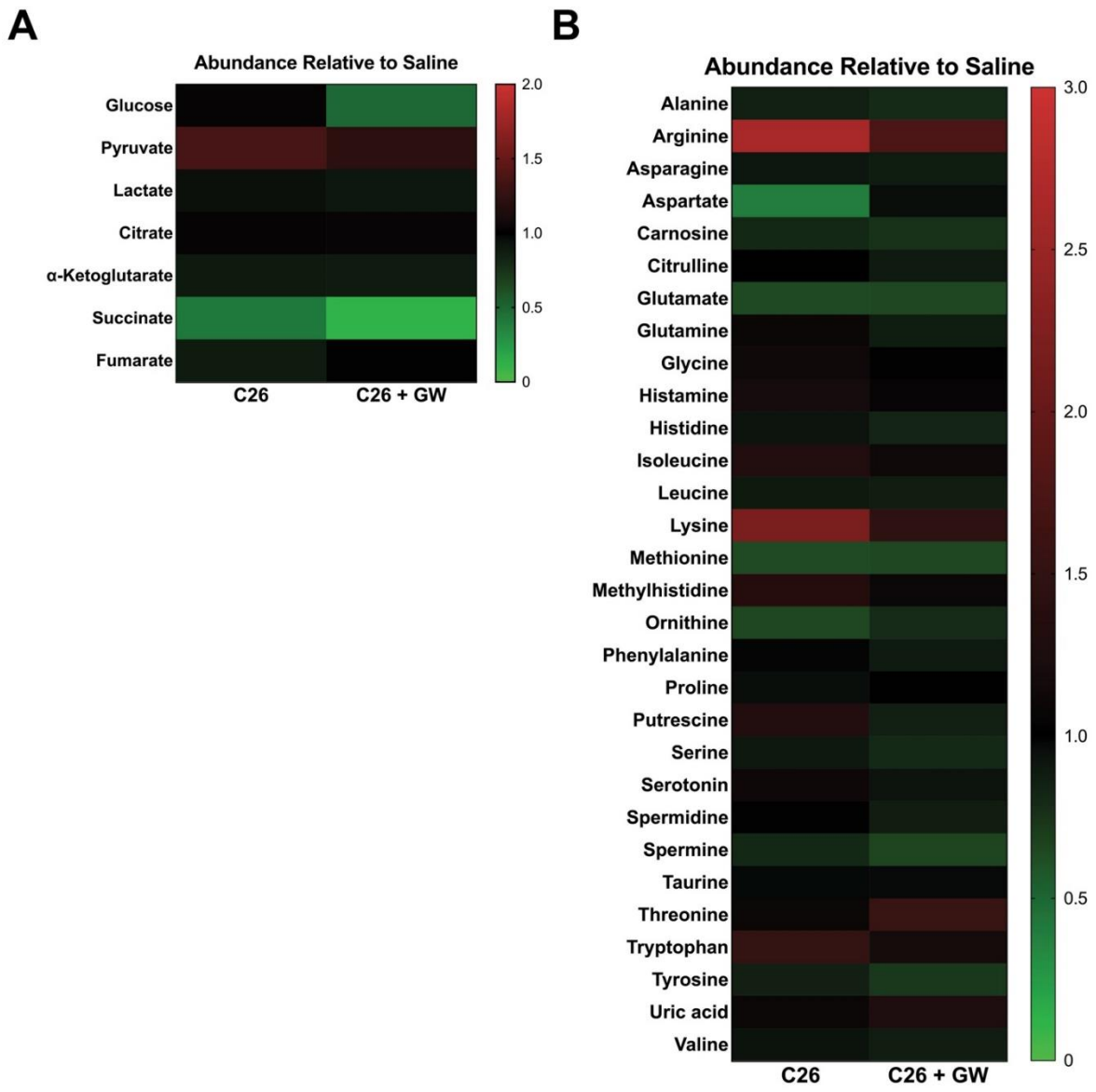

Appendix Figure 2.6: Pharmacological inhibition of iNOS prevents C26-driven deregulation of amino acid metabolism.

Male BALB/C mice were injected subcutaneously with C26 cells ($1.25x10^6$ cells) or an equivalent volume of saline. After 5 days and everyday thereafter, the mice injected with C26 cells were injected with either saline or GW 5mg kg^{-1}. After 16 days, mice were euthanized, and the metabolome of tibialis anterior muscles was analyzed through LC-MS/MS.

(A-B) Heatmap visualizing mean concentration corresponding to (A) metabolites involved in Glycolysis and TCA cycle or (B) amino acids and amino acid derivatives relative to saline controls. Red and green indicate an increase or decrease in metabolite levels, respectively.

Data information: Individual data points represent values from individual mice, with a total of six mice per cohort (n = 6).

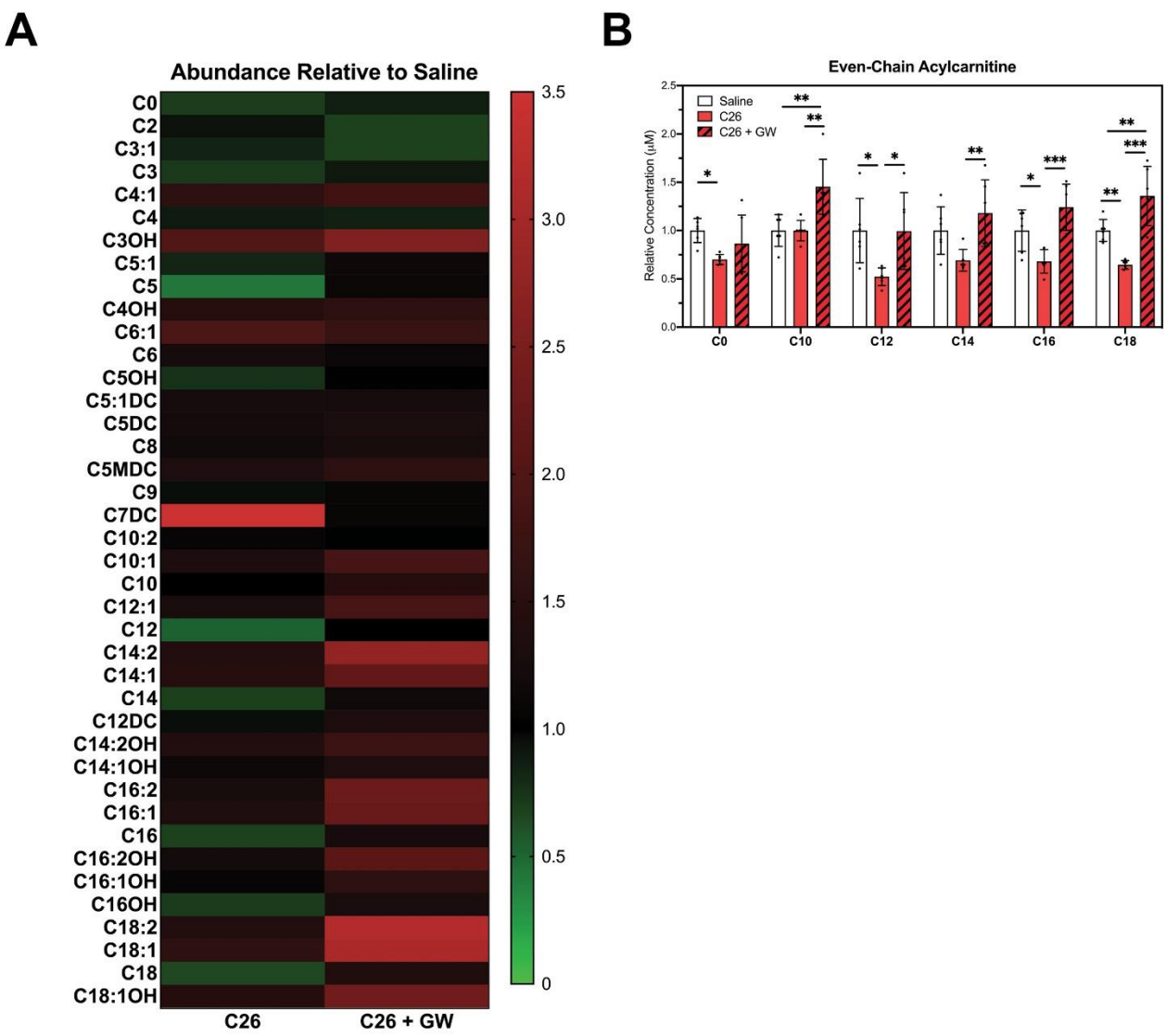

Appendix Figure 2.7: Pharmacological inhibition of iNOS prevents C26-driven deregulation of acylcarnitine metabolism.

Male BALB/C mice were injected subcutaneously with C26 cells ($1.25x10^6$ cells) or an equivalent volume of saline. After 5 days and everyday thereafter, the mice injected with C26 cells were injected with either saline or GW (5mg kg^{-1}). After 16 days, mice were euthanized, and the metabolome of tibialis anterior muscles was analyzed through LC-MS/MS.

(A) Heatmap visualizing mean concentration of acylcarnitines relative to saline controls. Red and green indicate an increase or decrease in metabolite levels, respectively.
(B) Relative concentrations of even-chain acylcarnitines.

Data information: Individual data points represent values from individual mice, with a total of six mice per cohort (n = 6). Error bars represent the standard deviation (SD) of the mean. p-values were calculated with an ANOVA followed by Fisher's LSD test (*P < 0.05; **P < 0.01; ***P < 0.001).

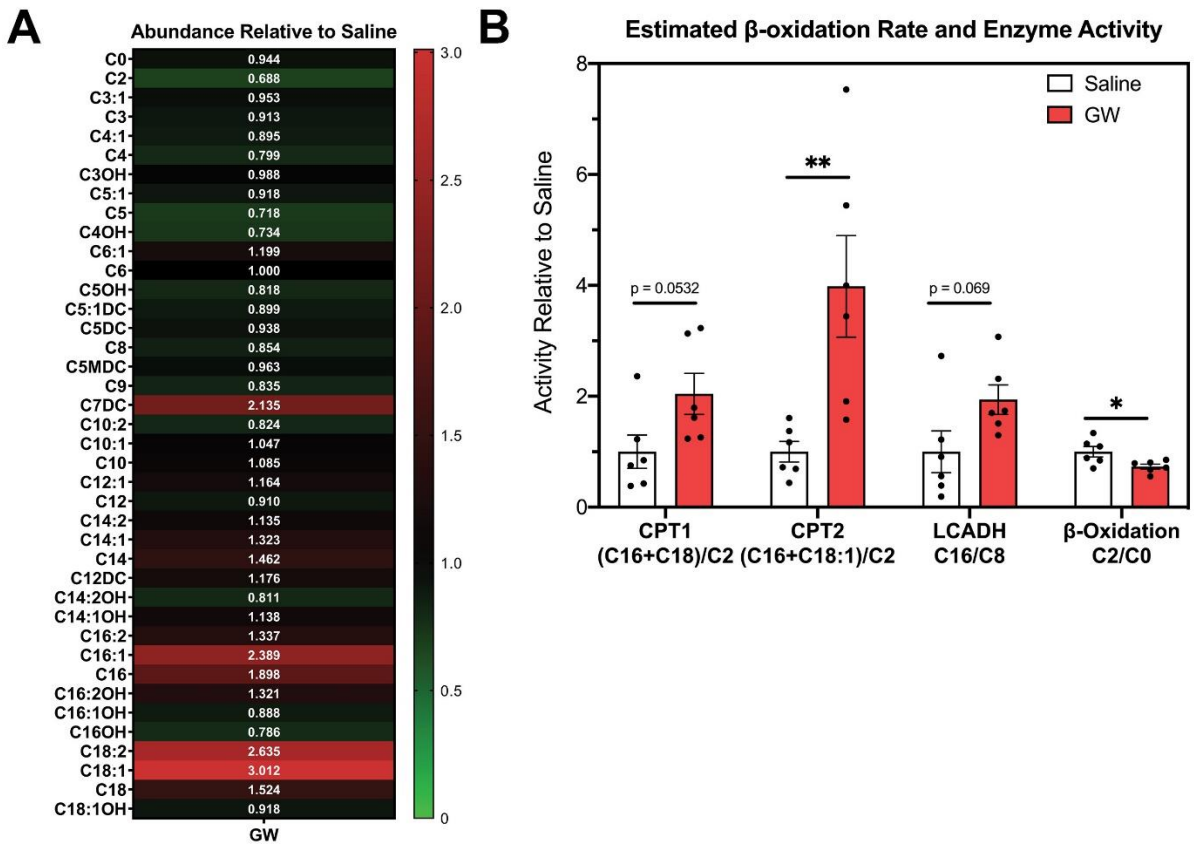

Appendix Figure 2.8: GW alters acylcarnitine metabolism and β-oxidation in mice.

Male BALB/C mice were injected subcutaneously with saline. After 5 days and everyday thereafter, the mice were injected with either saline or GW 5mg kg^{-1}. After 16 days, mice were euthanized, and the metabolome of tibialis anterior muscles was analyzed through LC-MS/MS.

(A) Heatmap visualizing mean concentration of acylcarnitines relative to saline controls. Red and green indicate an increase or decrease in metabolite levels, respectively.
(B) Relative estimated activity of CPT1, CPT2, LCADH, and β-oxidation.

Data information: Individual data points represent values from individual mice, with a total of six mice per cohort (n = 6) Error bars represent the standard deviation (SD) of the mean. p-values were calculated with an ANOVA followed by Fisher's LSD test (*P < 0.05; **P < 0.01; ***P < 0.001).

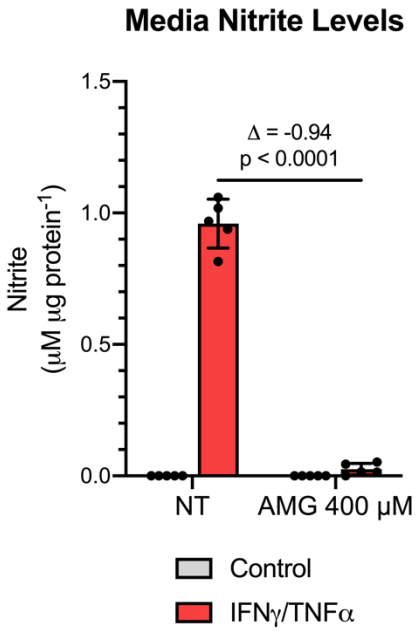

Appendix Figure 2.9: AMG prevents nitric oxide production in cytokine-treated myotubes.

C2C12 myotubes were treated with or without IFNγ (100U/mL) and TNFα (20ng/mL) and the indicated dose of aminoguanidine (AMG). Media nitrite levels were then measured 24h after treatment.

Data Information: Individual data points represent five independent experimental replicates (n=5). Error bars represent the standard deviation (SD) of the mean. For statistical comparisons, Δ indicates the difference of mean values and p-values were calculated with an ANOVA followed by Fisher's LSD test.

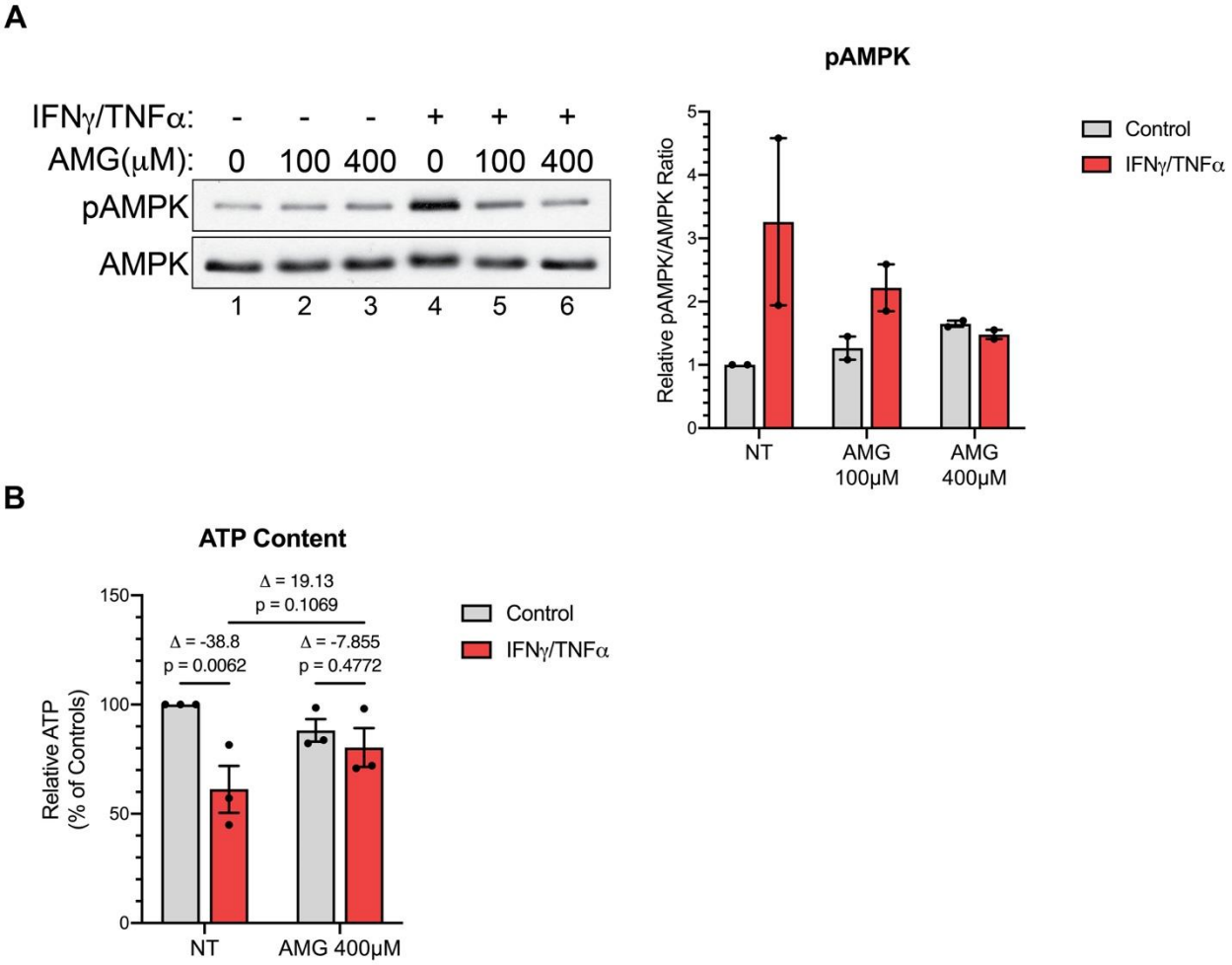

Appendix Figure 2.10: AMG recovers cellular ATP levels and reduces AMPK activation in cytokine-treated myotubes.

C2C12 myotubes were treated with or without IFNγ (100U/mL) and TNFα (20ng/mL) and the indicated doses aminoguanidine (AMG) for 24h.

(A) (*left*) Western blot analysis for pThr172-AMPK (pAMPK) and total AMPK (AMPK). (*right*) Quantification of the pAMPK to AMPK ratio relative to the untreated control (n=2).
(B) Cellular ATP content in myotubes treated with or without IFNγ and TNFα in the presence or absence of AMG. ATP content is shown as a percentage of the corresponding untreated control (n=3).

Data information: Individual data points are from two to three independent experimental replicates (n = 2-3). Error bars represent the standard deviation (SD) of the mean. For statistical comparisons, Δ indicates the difference of mean values and p-values were calculated with an ANOVA followed by Fisher's LSD test.

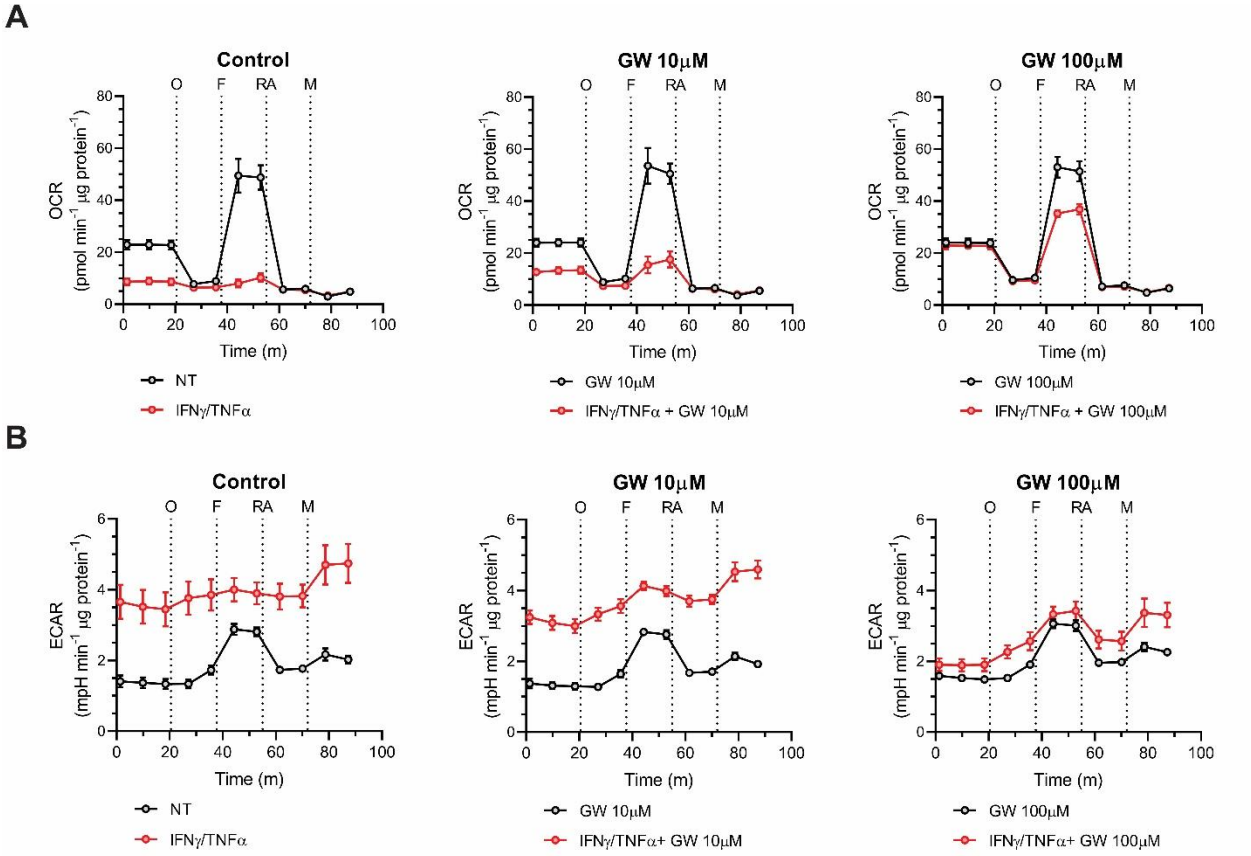

Appendix Figure 2.11: GW274150 reverses IFNγ/TNFα-induced suppression of OCR and elevation of ECAR.

C2C12 myotubes were treated with or without IFNγ (100U/mL) and TNFα (20ng/mL) and the indicated doses of GW274150 (GW). Extracellular flux was measured after 24h with a Seahorse XF Analyzer. Sequential injections of oligomycin (O, 1μM), FCCP (F, 1.5μM), Rotenone + Antimycin A (RA, 1μM), and monensin (M, 20μM) were performed to assess the bioenergetic profile.

(A) Oxygen consumption rate (OCR).

(B) Extracellular acidification rate (ECAR).

Data Information: Results are a representative example of three independent experiments (n = 3). Error bars represent the standard deviation of technical triplicates.

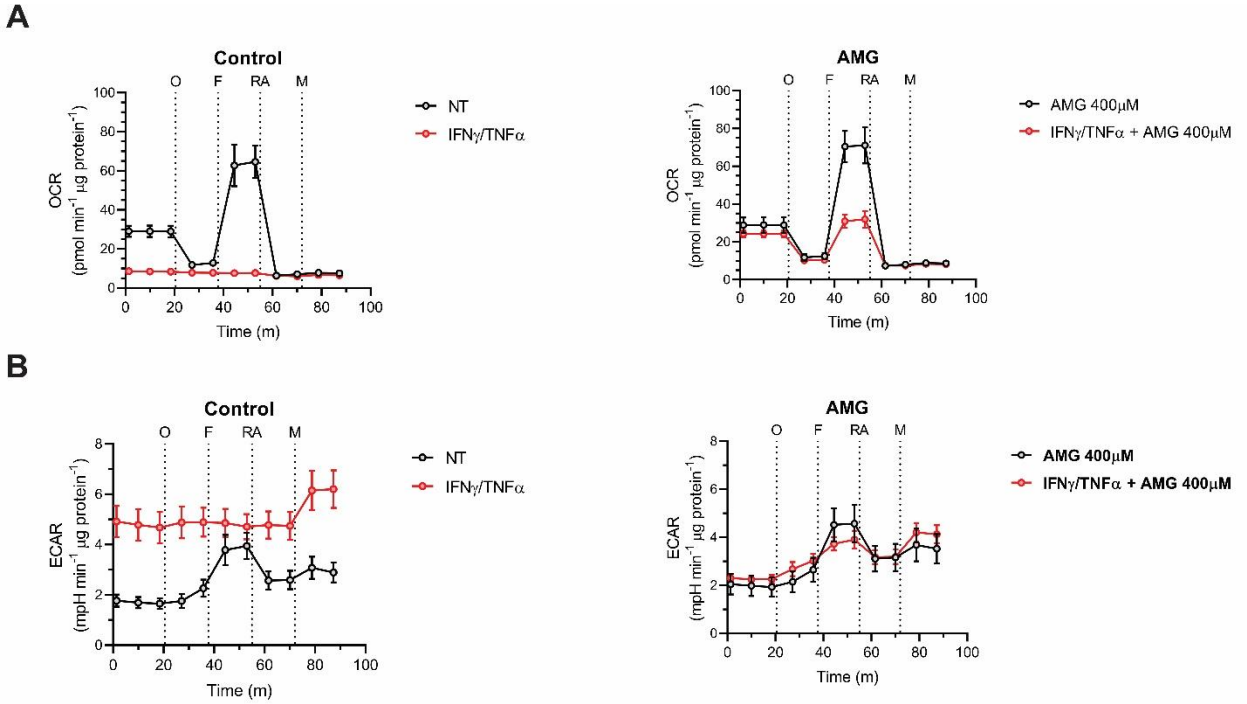

Appendix Figure 2.12: Aminoguanidine reverses IFNγ/TNFα-induced suppression of OCR and elevation of ECAR.

C2C12 myotubes were treated with or without IFNγ (100U/mL) and TNFα (20ng/mL) and aminoguanidine (AMG; 400µM). Extracellular flux was measured after 24h with a Seahorse XF analyzer. Sequential injections of oligomycin (O, 1µM), FCCP (F, 1.5µM), Rotenone + Antimycin A (RA, 1µM), and monensin (M, 20µM) were performed to assess the bioenergetic profile.

(A) Oxygen consumption rate (OCR).

(B) Extracellular acidification rate (ECAR).

Data Information: Results are a representative example of three independent experiments (n = 3). Error bars represent the standard deviation of technical replicates.

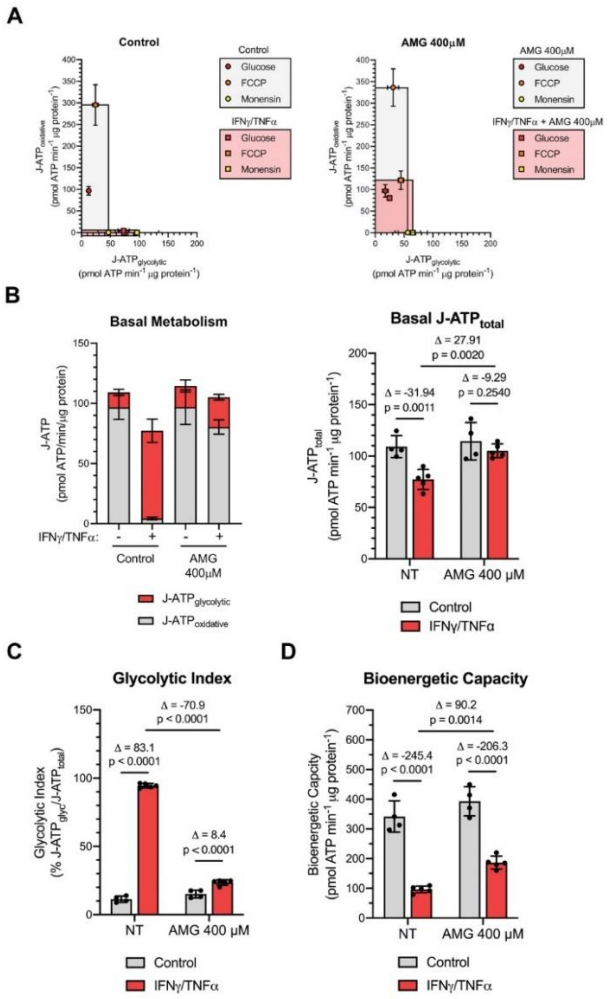

Appendix Figure 2.13: Aminoguanidine prevents a cytokine-induced shift to aerobic glycolysis in C2C12.

C2C12 myotubes were treated with or without IFNγ (100U/mL) and TNFα (20ng/mL) and aminoguanidine (AMG; 400µM). ATP production rates (J-ATP) from oxidative phosphorylation (oxidative) and glycolysis (glycolytic) were determined from measurements of extracellular flux 24h after treatment.

(A) Bioenergetic profiles. Highlighted squares are defined by the theoretical maximal J-ATP$_{oxidative}$ and J-ATP$_{glycolytic}$ rates.

(B) (*left)* Basal J-ATP$_{glycolytic}$ and J-ATP$_{oxidative}$ rates. (*right*) Total basal J-ATP rate.

(C) Glycolytic index of basal metabolism.

(D) Total bioenergetic capacity.

Data Information: Individual data points represent technical replicates. The data is representative of three independent experiments (n = 3). Error bars represent the standard deviation (SD) of the mean of technical replicates. For statistical comparisons, Δ indicates the difference of mean values of technical replicates and p-values were calculated with an ANOVA followed by Fisher's LSD test.

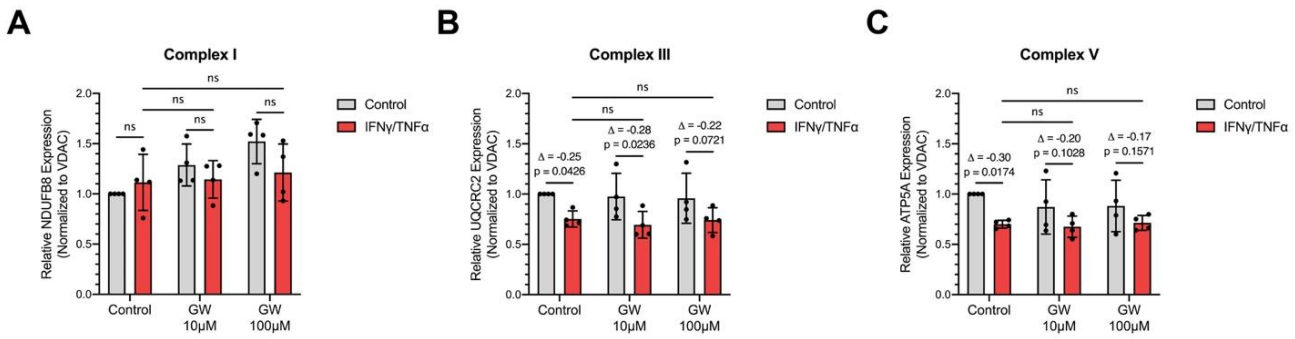

Appendix Figure 2.14: Effect of cytokine-induced muscle wasting on complex integrity.

C2C12 myotubes were treated with or without IFNγ (100U/mL) and TNFα (20ng/mL) and the indicated doses of GW274150 (GW). Protein content was extracted 24h after treatment.

(A-C) Quantification of complex subunits normalized to VDAC (Outer Mitochondrial Membrane; OMM) and relative to untreated control. (A) NDUFB8 (Complex I; CI) (B) UQCRC2 (Complex III; CIII) (C) ATP5A (Complex V; CV).

Data information: Individual data points are from four independent experimental replicates (n = 4). Error bars represent the standard deviation (SD) of the mean. For statistical comparisons, Δ indicates the difference of mean values and p-values were calculated with an ANOVA followed by Fisher's LSD test. Non statistically significant comparisons (P > 0.05) are indicated as non-significant (ns).

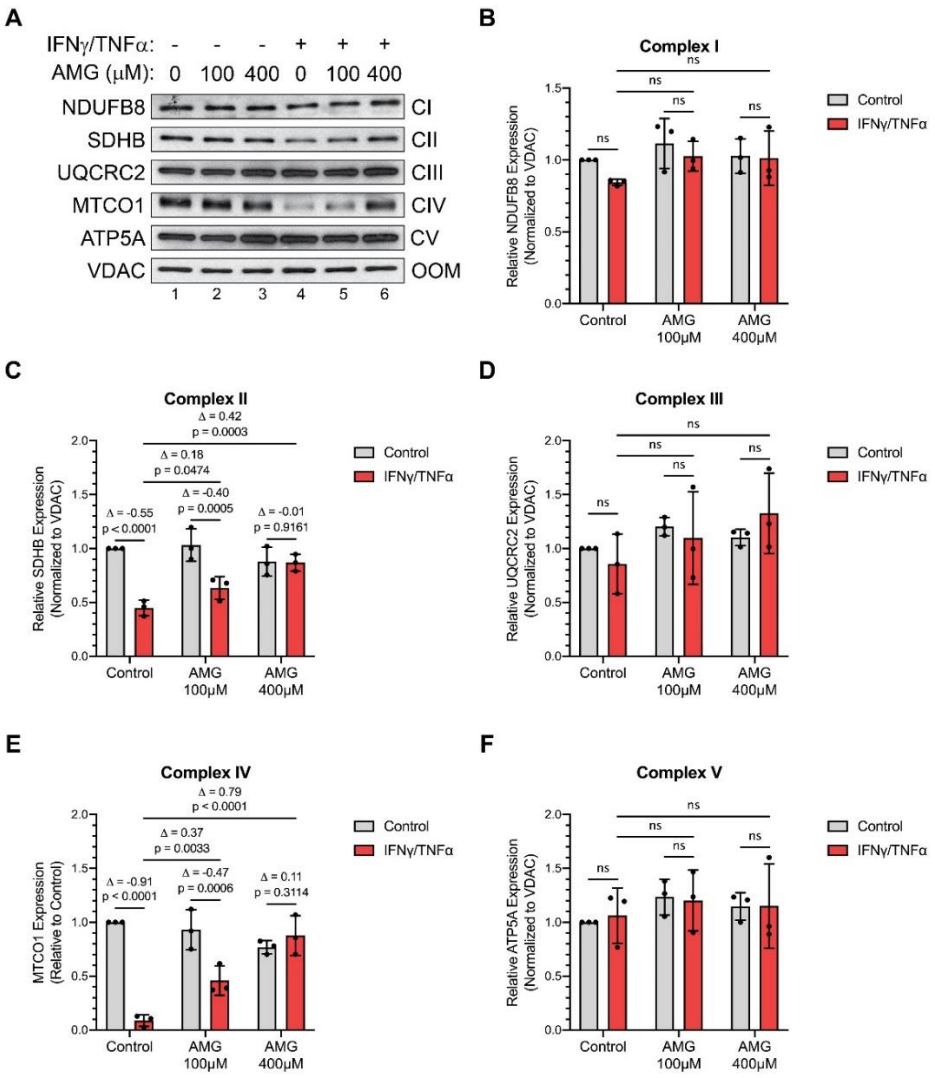

Appendix Figure 2.15: Cytokine-mediated loss of Complex II and IV integrity are reversed with aminoguanidine.

C2C12 myotubes were treated with or without IFNγ (100U/mL) and TNFα (20ng/mL) and the indicated doses of aminoguanidine (AMG). Protein content was extracted 24h after treatment.

(A) Western blot analysis for ETC protein complex subunits.

(B-F) Quantification of complex subunits normalized to VDAC (Outer Mitochondrial Membrane; OMM) and relative to untreated control. (B) NDUFB8 (Complex I; CI) (C) SDHB (Complex II; CII) (D) UQCRC2 (Complex III; CIII) (E) MTCO1 (Complex IV; CIV) (F) ATP5A (Complex V; CV).

Data information: Individual data points are from three independent experimental replicates (n = 3). Error bars represent the standard deviation (SD) of the mean. For statistical comparisons, Δ indicates the difference of mean values and p-values were calculated with an ANOVA followed by Fisher's LSD test. Non statistically significant comparisons (P > 0.05) are indicated as non-significant (ns).

References

Ábrigo J, Elorza AA, Riedel CA, Vilos C, Simon F, Cabrera D, Estrada L, Cabello-Verrugio C (2018) Role of oxidative stress as key regulator of muscle wasting during cachexia. *Oxidative medicine and cellular longevity* 2018

Acharyya S, Ladner KJ, Nelsen LL, Damrauer J, Reiser PJ, Swoap S, Guttridge DC (2004) Cancer cachexia is regulated by selective targeting of skeletal muscle gene products. *The Journal of clinical investigation* 114: 370-378

Adams V, Gußen V, Zozulya S, Cruz A, Moriscot A, Linke A, Labeit S (2020) Small-molecule chemical knockdown of MuRF1 in melanoma bearing mice attenuates tumor cachexia associated myopathy. *Cells* 9: 2272

Adams V, Späte U, Kränkel N, Christian SP, Linke A, Schuler G, Hambrecht R (2003) Nuclear factor-kappa B activation in skeletal muscle of patients with chronic heart failure: correlation with the expression of inducible nitric oxide synthase. *European Journal of Preventive Cardiology* 10: 273-277

Agrawal A, Rathor R, Kumar R, Suryakumar G, Singh SN, Kumar B (2020) Redox modification of ryanodine receptor contributes to impaired Ca2+ homeostasis and exacerbates muscle atrophy under high altitude. *Free Radical Biology and Medicine* 160: 643-656

Agusti A, Morla M, Sauleda J, Saus C, Busquets X (2004) NF-κB activation and iNOS upregulation in skeletal muscle of patients with COPD and low body weight. *Thorax* 59: 483-487

Ahsan H (2013) 3-Nitrotyrosine: A biomarker of nitrogen free radical species modified proteins in systemic autoimmunogenic conditions. *Human immunology* 74: 1392-1399

Albrecht JT (1996) Cachexia and anorexia in malignancy. *Hematology/Oncology Clinics* 10: 791-800

Alvarez S, Boveris A (2004) Mitochondrial nitric oxide metabolism in rat muscle during endotoxemia. *Free Radical Biology and Medicine* 37: 1472-1478

Anavi S, Tirosh O (2020) iNOS as a metabolic enzyme under stress conditions. *Free Radical Biology and Medicine* 146: 16-35

Ando K, Takahashi F, Motojima S, Nakashima K, Kaneko N, Hoshi K, Takahashi K (2013) Possible Role for Tocilizumab, an Anti–Interleukin-6 Receptor Antibody, in Treating Cancer Cachexia. *Journal of Clinical Oncology* 31: e69-e72

Anker SD, Ponikowski P, Varney S, Chua TP, Clark AL, Webb-Peploe KM, Harrington D, Kox WJ, Poole-Wilson PA, Coats AJ (1997) Wasting as independent risk factor for mortality in chronic heart failure. *The Lancet* 349: 1050-1053

Antunes D, Padrão AI, Maciel E, Santinha D, Oliveira P, Vitorino R, Moreira-Gonçalves D, Colaço B, Pires MJ, Nunes C (2014) Molecular insights into mitochondrial dysfunction in cancer-related muscle wasting. *Biochimica et Biophysica Acta (BBA)-Molecular and Cell Biology of Lipids* 1841: 896-905

Arends J, Strasser F, Gonella S, Solheim T, Madeddu C, Ravasco P, Buonaccorso L, de van der Schueren M, Baldwin C, Chasen M (2021) Cancer cachexia in adult patients: ESMO Clinical Practice Guidelines☆. *ESMO open* 6

Argilés JM, Betancourt A, Guàrdia-Olmos J, Peró-Cebollero M, López-Soriano FJ, Madeddu C, Serpe R, Busquets S (2017) Validation of the CAchexia SCOre (CASCO). Staging cancer patients: the use of miniCASCO as a simplified tool. *Frontiers in physiology* 8: 92

Argilés JM, López-Soriano FJ, Toledo M, Betancourt A, Serpe R, Busquets S (2011) The cachexia score (CASCO): a new tool for staging cachectic cancer patients. *Journal of cachexia, sarcopenia and muscle* 2: 87-93

Argilés JM, Orpí M, Busquets S, López-Soriano FJ (2012) Myostatin: more than just a regulator of muscle mass. *Drug discovery today* 17: 702-709

Arneson-Wissink PC, Doles JD (2021) Disrupted NOS2 metabolism drives myoblast response to wasting-associated cytokines. *Experimental Cell Research* 407: 112779

Arora G, Gupta A, Guo T, Gandhi A, Laine A, Williams D, Ahn C, Iyengar P, Infante R (2020) JAK Inhibitors Suppress Cancer Cachexia-Associated Anorexia and Adipose Wasting in Mice. *JCSM Rapid Commun* 3: 115-128

Arora GK, Gupta A, Narayanan S, Guo T, Iyengar P, Infante RE (2018) Cachexia-associated adipose loss induced by tumor-secreted leukemia inhibitory factor is counterbalanced by decreased leptin. *JCI insight* 3

Bailey JD, Diotallevi M, Nicol T, McNeill E, Shaw A, Chuaiphichai S, Hale A, Starr A, Nandi M, Stylianou E (2019) Nitric oxide modulates metabolic remodeling in inflammatory macrophages through TCA cycle regulation and itaconate accumulation. *Cell reports* 28: 218-230. e217

Baltgalvis KA, Berger FG, Pena MMO, Davis JM, Muga SJ, Carson JA (2008) Interleukin-6 and cachexia in Apc Min/+ mice. *American journal of physiology-Regulatory, integrative and comparative physiology* 294: R393-R401

Baltgalvis KA, Berger FG, Peña MMO, Davis JM, White JP, Carson JA (2009) Muscle wasting and interleukin-6-induced atrogin-I expression in the cachectic Apc Min/+ mouse. *Pflügers Archiv-European Journal of Physiology* 457: 989-1001

Banadakoppa M, Liebenthal D, Nowak DE, Urvil P, Yallampalli U, Wilson GM, Kishor A, Yallampalli C (2013) Role of transcription factor S p1 and RNA binding protein H u R in the downregulation of D r+ E scherichia coli receptor protein decay accelerating factor (DAF or CD 55) by nitric oxide. *The FEBS journal* 280: 840-854

Baracos VE, Martin L, Korc M, Guttridge DC, Fearon KC (2018) Cancer-associated cachexia. *Nature reviews Disease primers* 4: 1-18

Barreiro E, de la Puente B, Busquets S, López-Soriano FJ, Gea J, Argilés JM (2005) Both oxidative and nitrosative stress are associated with muscle wasting in tumour-bearing rats. *FEBS letters* 579: 1646-1652

Bayliss TJ, Smith JT, Schuster M, Dragnev KH, Rigas JR (2011) A humanized anti-IL-6 antibody (ALD518) in non-small cell lung cancer. *Expert opinion on biological therapy* 11: 1663-1668

Beutler B, Cerami A (1986) Cachectin and tumour necrosis factor as two sides of the same biological coin. *Nature* 320: 584-588

Beutler B, Greenwald D, Hulmes J, Chang M, Pan Y-C, Mathison J, Ulevitch R, Cerami A (1985) Identity of tumour necrosis factor and the macrophage-secreted factor cachectin. *Nature* 316: 552-554

Blum D, Stene G, Solheim T, Fayers P, Hjermstad M, Baracos V, Fearon K, Strasser F, Kaasa S, Koen M (2014) Validation of the Consensus-Definition for Cancer Cachexia and evaluation of a classification model—a study based on data from an international multicentre project (EPCRC-CSA). *Annals of oncology* 25: 1635-1642

Bodine SC, Latres E, Baumhueter S, Lai VK-M, Nunez L, Clarke BA, Poueymirou WT, Panaro FJ, Na E, Dharmarajan K (2001) Identification of ubiquitin ligases required for skeletal muscle atrophy. *Science* 294: 1704-1708

Bogdan C (2001) Nitric oxide and the immune response. *Nature immunology* 2: 907-916

Bonetto A, Aydogdu T, Jin X, Zhang Z, Zhan R, Puzis L, Koniaris LG, Zimmers TA (2012) JAK/STAT3 pathway inhibition blocks skeletal muscle wasting downstream of IL-6 and in experimental cancer cachexia. *American Journal of Physiology-Endocrinology and Metabolism* 303: E410-E421

Bonetto A, Aydogdu T, Kunzevitzky N, Guttridge DC, Khuri S, Koniaris LG, Zimmers TA (2011) STAT3 activation in skeletal muscle links muscle wasting and the acute phase response in cancer cachexia. *PloS one* 6: e22538

Bonetto A, Rupert JE, Barreto R, Zimmers TA (2016) The colon-26 carcinoma tumor-bearing mouse as a model for the study of cancer cachexia. *JoVE (Journal of Visualized Experiments)*: e54893

Bordeleau M-E, Robert F, Gerard B, Lindqvist L, Chen SM, Wendel H-G, Brem B, Greger H, Lowe SW, Porco JA (2008) Therapeutic suppression of translation initiation modulates chemosensitivity in a mouse lymphoma model. *The Journal of clinical investigation* 118: 2651-2660

Braun TP, Grossberg AJ, Krasnow SM, Levasseur PR, Szumowski M, Zhu XX, Maxson JE, Knoll JG, Barnes AP, Marks DL (2013) Cancer-and endotoxin-induced cachexia require intact glucocorticoid signaling in skeletal muscle. *The FASEB Journal* 27: 3572-3582

Brown JL, Lee DE, Rosa-Caldwell ME, Brown LA, Perry RA, Haynie WS, Huseman K, Sataranatarajan K, Van Remmen H, Washington TA (2018) Protein imbalance in the development of skeletal muscle wasting in tumour-bearing mice. *Journal of cachexia, sarcopenia and muscle* 9: 987-1002

Brown JL, Rosa-Caldwell ME, Lee DE, Blackwell TA, Brown LA, Perry RA, Haynie WS, Hardee JP, Carson JA, Wiggs MP (2017) Mitochondrial degeneration precedes the development of muscle atrophy in progression of cancer cachexia in tumour-bearing mice. *Journal of cachexia, sarcopenia and muscle* 8: 926-938

Brun CE, Rudnicki MA (2015) GDF11 and the mythical fountain of youth. *Cell Metabolism* 22: 54-56

Brunengraber H, Roe CR (2006) Anaplerotic molecules: current and future. *Journal of inherited metabolic disease* 29: 327-331

Buck M, Chojkier M (1996) Muscle wasting and dedifferentiation induced by oxidative stress in a murine model of cachexia is prevented by inhibitors of nitric oxide synthesis and antioxidants. *The EMBO journal* 15: 1753-1765

Busquets S, Toledo M, Orpí M, Massa D, Porta M, Capdevila E, Padilla N, Frailis V, López-Soriano FJ, Han H (2012) Myostatin blockage using actRIIB antagonism in mice bearing the Lewis lung carcinoma results in the improvement of muscle wasting and physical performance. *Journal of cachexia, sarcopenia and muscle* 3: 37-43

Cai D, Frantz JD, Tawa Jr NE, Melendez PA, Oh B-C, Lidov HG, Hasselgren P-O, Frontera WR, Lee J, Glass DJ (2004) IKKβ/NF-κB activation causes severe muscle wasting in mice. *Cell* 119: 285-298

Cala MP, Agulló-Ortuño MT, Prieto-García E, González-Riano C, Parrilla-Rubio L, Barbas C, Díaz-García CV, García A, Pernaut C, Adeva J (2018) Multiplatform plasma fingerprinting in cancer cachexia: a pilot observational and translational study. *Journal of cachexia, sarcopenia and muscle* 9: 348-357

Carson JA, Baltgalvis KA (2010) Interleukin-6 as a key regulator of muscle mass during cachexia. *Exercise and sport sciences reviews* 38: 168

Chatterjee PK, Patel NS, Sivarajah A, Kvale EO, Dugo L, Cuzzocrea S, Brown PA, Stewart KN, Mota-Filipe H, Britti D (2003) GW274150, a potent and highly selective inhibitor of iNOS, reduces experimental renal ischemia/reperfusion injury. *Kidney international* 63: 853-865

Chaturvedi R, Asim M, Lewis ND, Algood HMS, Cover TL, Kim PY, Wilson KT (2007) L-arginine availability regulates inducible nitric oxide synthase-dependent host defense against Helicobacter pylori. *Infection and immunity* 75: 4305-4315

Chen JL, Walton KL, Hagg A, Colgan TD, Johnson K, Qian H, Gregorevic P, Harrison CA (2017) Specific targeting of TGF-β family ligands demonstrates distinct roles in the regulation of muscle mass in health and disease. *Proceedings of the National Academy of Sciences* 114: E5266-E5275

Chen JL, Walton KL, Winbanks CE, Murphy KT, Thomson RE, Makanji Y, Qian H, Lynch GS, Harrison CA, Gregorevic P (2014) Elevated expression of activins promotes muscle wasting and cachexia. *The FASEB Journal* 28: 1711-1723

Chen S-E, Jin B, Li Y-P (2007) TNF-α regulates myogenesis and muscle regeneration by activating p38 MAPK. *American Journal of Physiology-Cell Physiology* 292: C1660-C1671

Chiocchetti GdMe, Lopes-Aguiar L, Miyaguti NAdS, Viana LR, Salgado CdM, Orvoën OO, Florindo D, Santos RWd, Cintra Gomes-Marcondes MC (2021) A Time-Course Comparison of Skeletal Muscle Metabolomic Alterations in Walker-256 Tumour-Bearing Rats at Different Stages of Life. *Metabolites* 11: 404

Cho D-H, Nakamura T, Fang J, Cieplak P, Godzik A, Gu Z, Lipton SA (2009) S-nitrosylation of Drp1 mediates β-amyloid-related mitochondrial fission and neuronal injury. *Science* 324: 102-105

Chu J, Pelletier J (2015) Targeting the eIF4A RNA helicase as an anti-neoplastic approach. *Biochimica et Biophysica Acta (BBA)-Gene Regulatory Mechanisms* 1849: 781-791

Cogliati S, Enriquez JA, Scorrano L (2016) Mitochondrial cristae: where beauty meets functionality. *Trends in biochemical sciences* 41: 261-273

Cohen S, Nathan JA, Goldberg AL (2015) Muscle wasting in disease: molecular mechanisms and promising therapies. *Nature reviews Drug discovery* 14: 58-74

Coletti D, Aulino P, Pigna E, Barteri F, Moresi V, Annibali D, Adamo S, Berardi E (2016) Spontaneous physical activity downregulates Pax7 in cancer cachexia. *Stem cells international* 2016

Comtois AS, El-Dwairi Q, Laubach VE, Hussain SN (1999) Lipopolysaccharide-induced diaphragmatic contractile dysfunction in mice lacking the inducible nitric oxide synthase. *American journal of respiratory and critical care medicine* 159: 1975-1980

Constantinou C, Fontes de Oliveira CC, Mintzopoulos D, Busquets S, He J, Kesarwani M, Mindrinos M, Rahme LG, Argilés JM, Tzika AA (2011) Nuclear magnetic resonance in conjunction with functional genomics suggests mitochondrial dysfunction in a murine model of cancer cachexia. *International journal of molecular medicine* 27: 15-24

Costelli P, Muscaritoli M, Bonetto A, Penna F, Reffo P, Bossola M, Bonelli G, Doglietto G, Baccino FM, Fanelli FR (2008) Muscle myostatin signalling is enhanced in experimental cancer cachexia. *European journal of clinical investigation* 38: 531-538

Cui P, Huang C, Guo J, Wang Q, Liu Z, Zhuo H, Lin D (2019a) Metabolic profiling of tumors, sera, and skeletal muscles from an orthotopic murine model of gastric cancer associated-cachexia. *Journal of proteome research* 18: 1880-1892

Cui P, Li X, Huang C, Li Q, Lin D (2022) Metabolomics and its Applications in Cancer Cachexia. *Frontiers in Molecular Biosciences* 9

Cui P, Shao W, Huang C, Wu C-J, Jiang B, Lin D (2019b) Metabolic derangements of skeletal muscle from a murine model of glioma cachexia. *Skeletal muscle* 9: 1-13

Cuzzocrea S, Chatterjee PK, Mazzon E, McDonald MC, Dugo L, Di Paola R, Serraino I, Britti D, Caputi AP, Thiemermann C (2002) Beneficial effects of GW274150, a novel, potent and selective inhibitor of iNOS activity, in a rodent model of collagen-induced arthritis. *European Journal of Pharmacology* 453: 119-129

Demicheli V, Moreno DM, Jara GE, Lima A, Carballal S, Rios N, Batthyany C, Ferrer-Sueta G, Quijano C, Estrín DA (2016) Mechanism of the reaction of human manganese superoxide dismutase with peroxynitrite: nitration of critical tyrosine 34. *Biochemistry* 55: 3403-3417

Der-Torossian H, Asher SA, Winnike JH, Wysong A, Yin X, Willis MS, O'Connell TM, Couch ME (2013a) Cancer cachexia's metabolic signature in a murine model confirms a distinct entity. *Metabolomics* 9: 730-739

Der-Torossian H, Wysong A, Shadfar S, Willis MS, McDunn J, Couch ME (2013b) Metabolic derangements in the gastrocnemius and the effect of Compound A therapy in a murine model of cancer cachexia. *Journal of Cachexia, Sarcopenia and Muscle* 4: 145-155

Di Marco S, Cammas A, Lian XJ, Kovacs EN, Ma JF, Hall DT, Mazroui R, Richardson J, Pelletier J, Gallouzi IE (2012) The translation inhibitor pateamine A prevents cachexia-induced muscle wasting in mice. *Nature communications* 3: 1-12

Di Marco S, Mazroui R, Dallaire P, Chittur S, Tenenbaum SA, Radzioch D, Marette A, Gallouzi I-E (2005) NF-κB-mediated MyoD decay during muscle wasting requires nitric oxide synthase mRNA stabilization, HuR protein, and nitric oxide release. *Molecular and cellular biology* 25: 6533-6545

Dufner A, Thomas G (1999) Ribosomal S6 kinase signaling and the control of translation. *Experimental cell research* 253: 100-109

Egerman MA, Cadena SM, Gilbert JA, Meyer A, Nelson HN, Swalley SE, Mallozzi C, Jacobi C, Jennings LL, Clay I (2015) GDF11 increases with age and inhibits skeletal muscle regeneration. *Cell metabolism* 22: 164-174

Egerman MA, Glass DJ (2014) Signaling pathways controlling skeletal muscle mass. *Critical reviews in biochemistry and molecular biology* 49: 59-68

Egerman MA, Glass DJ (2019) The role of GDF11 in aging and skeletal muscle, cardiac and bone homeostasis. *Critical reviews in biochemistry and molecular biology* 54: 174-183

Eisner R, Stretch C, Eastman T, Xia J, Hau D, Damaraju S, Greiner R, Wishart DS, Baracos VE (2011) Learning to predict cancer-associated skeletal muscle wasting from 1H-NMR profiles of urinary metabolites. *Metabolomics* 7: 25-34

El-Dwairi Q, Comtois A, Guo Y, Hussain S (1998) Endotoxin-induced skeletal muscle contractile dysfunction: contribution of nitric oxide synthases. *American Journal of Physiology-Cell Physiology* 274: C770-C779

El-Gayar S, Thüring-Nahler H, Pfeilschifter J, Röllinghoff M, Bogdan C (2003) Translational control of inducible nitric oxide synthase by IL-13 and arginine availability in inflammatory macrophages. *The Journal of Immunology* 171: 4561-4568

Elkina Y, von Haehling S, Anker SD, Springer J (2011) The role of myostatin in muscle wasting: an overview. *Journal of cachexia, sarcopenia and muscle* 2: 143-151

Erdem M, Möckel D, Jumpertz S, John C, Fragoulis A, Rudolph I, Wulfmeier J, Springer J, Horn H, Koch M (2019) Macrophages protect against loss of adipose tissue during cancer cachexia. *Journal of cachexia, sarcopenia and muscle* 10: 1128-1142

Evans WJ, Morley JE, Argilés J, Bales C, Baracos V, Guttridge D, Jatoi A, Kalantar-Zadeh K, Lochs H, Mantovani G (2008) Cachexia: a new definition. *Clinical nutrition* 27: 793-799

Fan M, Sun W, Gu X, Lu S, Shen Q, Liu X, Zhang X (2022) The critical role of STAT3 in biogenesis of tumor-derived exosomes with potency of inducing cancer cachexia in vitro and in vivo. *Oncogene*: 1-13

Fearon K, Strasser F, Anker SD, Bosaeus I, Bruera E, Fainsinger RL, Jatoi A, Loprinzi C, MacDonald N, Mantovani G (2011) Definition and classification of cancer cachexia: an international consensus. *The lancet oncology* 12: 489-495

Fearon KC, Glass DJ, Guttridge DC (2012) Cancer cachexia: mediators, signaling, and metabolic pathways. *Cell metabolism* 16: 153-166

Fontes-Oliveira CC, Busquets S, Toledo M, Penna F, Aylwin MP, Sirisi S, Silva AP, Orpí M, García A, Sette A (2013) Mitochondrial and sarcoplasmic reticulum abnormalities in cancer cachexia: altered energetic efficiency? *Biochimica et Biophysica Acta (BBA)-General Subjects* 1830: 2770-2778

Franco-Romero A, Sandri M (2021) Role of autophagy in muscle disease. *Molecular aspects of medicine* 82: 101041

Fujiwara Y, Kobayashi T, Chayahara N, Imamura Y, Toyoda M, Kiyota N, Mukohara T, Nishiumi S, Azuma T, Yoshida M (2014) Metabolomics evaluation of serum markers for cachexia and their intra-day variation in patients with advanced pancreatic cancer. *PloS one* 9: e113259

Fukawa T, Yan-Jiang BC, Min-Wen JC, Jun-Hao ET, Huang D, Qian C-N, Ong P, Li Z, Chen S, Mak SY (2016) Excessive fatty acid oxidation induces muscle atrophy in cancer cachexia. *Nature medicine* 22: 666-671

Gallot YS, Durieux A-C, Castells J, Desgeorges MM, Vernus B, Plantureux L, Rémond D, Jahnke VE, Lefai E, Dardevet D (2014) Myostatin gene inactivation prevents skeletal muscle wasting in cancer. *Cancer research* 74: 7344-7356

Gao Z, Li Y, Wang F, Huang T, Fan K, Zhang Y, Zhong J, Cao Q, Chao T, Jia J (2017) Mitochondrial dynamics controls anti-tumour innate immunity by regulating CHIP-IRF1 axis stability. *Nature communications* 8: 1-13

Garcia JM, Dunne RF, Santiago K, Martin L, Birnbaum MJ, Crawford J, Hendifar AE, Kochanczyk M, Moravek C, Piccinin D, 2022. Addressing unmet needs for people with cancer cachexia: recommendations from a multistakeholder workshop.

Garrido P, Shalaby A, Walsh EM, Keane N, Webber M, Keane MM, Sullivan FJ, Kerin MJ, Callagy G, Ryan AE (2017) Impact of inducible nitric oxide synthase (iNOS) expression on triple

negative breast cancer outcome and activation of EGFR and ERK signaling pathways. *Oncotarget* 8: 80568

Glass DJ (2010) Signaling pathways perturbing muscle mass. *Current opinion in clinical nutrition & metabolic care* 13: 225-229

Golan T, Geva R, Richards D, Madhusudan S, Lin BK, Wang HT, Walgren RA, Stemmer SM (2018) LY2495655, an antimyostatin antibody, in pancreatic cancer: a randomized, phase 2 trial. *Journal of cachexia, sarcopenia and muscle* 9: 871-879

Gouspillou G, Godin R, Piquereau J, Picard M, Mofarrahi M, Mathew J, Purves-Smith FM, Sgarioto N, Hepple RT, Burelle Y (2018) Protective role of Parkin in skeletal muscle contractile and mitochondrial function. *The Journal of physiology* 596: 2565-2579

Granados-Principal S, Liu Y, Guevara ML, Blanco E, Choi DS, Qian W, Patel T, Rodriguez AA, Cusimano J, Weiss HL (2015) Inhibition of iNOS as a novel effective targeted therapy against triple-negative breast cancer. *Breast cancer research* 17: 1-16

Guttridge DC (2004) Signaling pathways weigh in on decisions to make or break skeletal muscle. *Current Opinion in Clinical Nutrition & Metabolic Care* 7: 443-450

Guttridge DC, Mayo MW, Madrid LV, Wang C-Y, Baldwin Jr AS (2000) NF-κB-induced loss of MyoD messenger RNA: possible role in muscle decay and cachexia. *Science* 289: 2363-2366

Hall DT, Griss T, Ma JF, Sanchez BJ, Sadek J, Tremblay AMK, Mubaid S, Omer A, Ford RJ, Bedard N *et al* (2018) The AMPK agonist 5-aminoimidazole-4-carboxamide ribonucleotide (AICAR), but not metformin, prevents inflammation-associated cachectic muscle wasting. *EMBO Molecular Medicine* 10: e8307

Hall DT, Ma JF, Di Marco S, Gallouzi I-E (2011) Inducible nitric oxide synthase (iNOS) in muscle wasting syndrome, sarcopenia, and cachexia. *Aging (Albany NY)* 3: 702

Hammers DW, Merscham-Banda M, Hsiao JY, Engst S, Hartman JJ, Sweeney HL (2017) Supraphysiological levels of GDF 11 induce striated muscle atrophy. *EMBO molecular medicine* 9: 531-544

Han J, Meng Q, Shen L, Wu G (2018) Interleukin-6 induces fat loss in cancer cachexia by promoting white adipose tissue lipolysis and browning. *Lipids in Health and Disease* 17: 1-8

Hardee JP, Montalvo RN, Carson JA (2017) Linking cancer cachexia-induced anabolic resistance to skeletal muscle oxidative metabolism. *Oxidative medicine and cellular longevity* 2017

Hardie DG, Ross FA, Hawley SA (2012) AMPK: a nutrient and energy sensor that maintains energy homeostasis. *Nature reviews Molecular cell biology* 13: 251-262

Hatakeyama S, Summermatter S, Jourdain M, Melly S, Minetti GC, Lach-Trifilieff E (2016) ActRII blockade protects mice from cancer cachexia and prolongs survival in the presence of anti-cancer treatments. *Skeletal muscle* 6: 1-12

He WA, Berardi E, Cardillo VM, Acharyya S, Aulino P, Thomas-Ahner J, Wang J, Bloomston M, Muscarella P, Nau P (2013) NF-κB–mediated Pax7 dysregulation in the muscle microenvironment promotes cancer cachexia. *The Journal of clinical investigation* 123: 4821-4835

Hershey JW, Sonenberg N, Mathews MB (2012) Principles of translational control: an overview. *Cold Spring Harbor perspectives in biology* 4: a011528

Hnisz D, Abraham BJ, Lee TI, Lau A, Saint-André V, Sigova AA, Hoke HA, Young RA (2013) Super-enhancers in the control of cell identity and disease. *Cell* 155: 934-947

Hogan KA, Cho DS, Arneson PC, Samani A, Palines P, Yang Y, Doles JD (2018) Tumor-derived cytokines impair myogenesis and alter the skeletal muscle immune microenvironment. *Cytokine* 107: 9-17

Høivik HO, Laurijssens BE, Harnisch LO, Twomey CK, Dixon RM, Kirkham AJ, Williams PM, Wentz AL, Lunnon MW (2010) Lack of efficacy of the selective iNOS inhibitor GW274150 in prophylaxis of migraine headache. *Cephalalgia* 30: 1458-1467

Hu W, Ru Z, Zhou Y, Xiao W, Sun R, Zhang S, Gao Y, Li X, Zhang X, Yang H (2019) Lung cancer-derived extracellular vesicles induced myotube atrophy and adipocyte lipolysis via the extracellular IL-6-mediated STAT3 pathway. *Biochimica et Biophysica Acta (BBA)-Molecular and Cell Biology of Lipids* 1864: 1091-1102

Hurwitz H, Van Cutsem E, Bendell J, Hidalgo M, Li C-P, Salvo MG, Macarulla T, Sahai V, Sama A, Greeno E (2018) Ruxolitinib+ capecitabine in advanced/metastatic pancreatic cancer after disease progression/intolerance to first-line therapy: JANUS 1 and 2 randomized phase III studies. *Investigational new drugs* 36: 683-695

Hussain SN, Giaid A, Dawiri QE, Sakkal D, Hattori R, Guo Y (1997) Expression of nitric oxide synthases and GTP cyclohydrolase I in the ventilatory and limb muscles during endotoxemia. *American Journal of Respiratory Cell and Molecular Biology* 17: 173-180

Inaba S, Hinohara A, Tachibana M, Tsujikawa K, Fukada S-i (2018) Muscle regeneration is disrupted by cancer cachexia without loss of muscle stem cell potential. *PloS one* 13: e0205467

Janice Sánchez B, Tremblay A-MK, Leduc-Gaudet J-P, Hall DT, Kovacs E, Ma JF, Mubaid S, Hallauer PL, Phillips BL, Vest KE *et al* (2019) Depletion of HuR in murine skeletal muscle enhances exercise endurance and prevents cancer-induced muscle atrophy. *Nature Communications* 10: 4171

Jatoi A, Ritter HL, Dueck A, Nguyen PL, Nikcevich DA, Luyun RF, Mattar BI, Loprinzi CL (2010) A placebo-controlled, double-blind trial of infliximab for cancer-associated weight loss in elderly and/or poor performance non-small cell lung cancer patients (N01C9). *Lung cancer* 68: 234-239

Jin B, Li YP (2007) Curcumin prevents lipopolysaccharide-induced atrogin-1/MAFbx upregulation and muscle mass loss. *Journal of cellular biochemistry* 100: 960-969

Jones JE, Cadena SM, Gong C, Wang X, Chen Z, Wang SX, Vickers C, Chen H, Lach-Trifilieff E, Hadcock JR (2018) Supraphysiologic administration of GDF11 induces cachexia in part by upregulating GDF15. *Cell reports* 22: 1522-1530

Jorgensen MM, de la Puente P (2022) Leukemia Inhibitory Factor: An Important Cytokine in Pathologies and Cancer. *Biomolecules* 12: 217

Julienne CM, Dumas J-F, Goupille C, Pinault M, Berri C, Collin A, Tesseraud S, Couet C, Servais S (2012) Cancer cachexia is associated with a decrease in skeletal muscle mitochondrial oxidative capacities without alteration of ATP production efficiency. *Journal of cachexia, sarcopenia and muscle* 3: 265-275

Kalantar-Zadeh K, Rhee C, Sim JJ, Stenvinkel P, Anker SD, Kovesdy CP, 2013. Why cachexia kills: examining the causality of poor outcomes in wasting conditions. Wiley Online Library, pp. 89-94.

Kandarian SC, Nosacka RL, Delitto AE, Judge AR, Judge SM, Ganey JD, Moreira JD, Jackman RW (2018) Tumour-derived leukaemia inhibitory factor is a major driver of cancer cachexia and

morbidity in C26 tumour-bearing mice. *Journal of cachexia, sarcopenia and muscle* 9: 1109-1120

Kanski J, Behring A, Pelling J, Schoneich C (2005) Proteomic identification of 3-nitrotyrosine-containing rat cardiac proteins: effects of biological aging. *American Journal of Physiology-Heart and Circulatory Physiology* 288: H371-H381

Kayacan O, Karnak D, Beder S, Güllü E, Tutkak H, Senler FÇ, Köksal D (2006) Impact of TNF-α and IL-6 levels on development of cachexia in newly diagnosed NSCLC patients. *American journal of clinical oncology* 29: 328-335

Kazemi-Bajestani SMR, Mazurak VC, Baracos V, 2016. Computed tomography-defined muscle and fat wasting are associated with cancer clinical outcomes, Seminars in cell & developmental biology. Elsevier, pp. 2-10.

Klimek MEB, Aydogdu T, Link MJ, Pons M, Koniaris LG, Zimmers TA (2010) Acute inhibition of myostatin-family proteins preserves skeletal muscle in mouse models of cancer cachexia. *Biochemical and biophysical research communications* 391: 1548-1554

Kostourou V, Cartwright J, Johnstone A, Boult J, Cullis E, Whitley G, Robinson S (2011) The role of tumour-derived iNOS in tumour progression and angiogenesis. *British journal of cancer* 104: 83-90

Kuang S, Chargé SB, Seale P, Huh M, Rudnicki MA (2006) Distinct roles for Pax7 and Pax3 in adult regenerative myogenesis. *The Journal of cell biology* 172: 103-113

Kunzke T, Buck A, Prade VM, Feuchtinger A, Prokopchuk O, Martignoni ME, Heisz S, Hauner H, Janssen KP, Walch A (2020) Derangements of amino acids in cachectic skeletal muscle are caused by mitochondrial dysfunction. *Journal of cachexia, sarcopenia and muscle* 11: 226-240

Kuroda K, Nakashima J, Kanao K, Kikuchi E, Miyajima A, Horiguchi Y, Nakagawa K, Oya M, Ohigashi T, Murai M (2007) Interleukin 6 is associated with cachexia in patients with prostate cancer. *Urology* 69: 113-117

Lach-Trifilieff E, Minetti GC, Sheppard K, Ibebunjo C, Feige JN, Hartmann S, Brachat S, Rivet H, Koelbing C, Morvan F *et al* (2014) An Antibody Blocking Activin Type II Receptors Induces Strong Skeletal Muscle Hypertrophy and Protects from Atrophy. *Molecular and Cellular Biology* 34: 606-618

Laird BJ, McMillan D, Skipworth RJ, Fallon MT, Paval DR, McNeish I, Gallagher IJ (2021) The emerging role of interleukin 1β (IL-1β) in cancer cachexia. *Inflammation* 44: 1223-1228

Lang CH, Frost RA, Nairn AC, MacLean DA, Vary TC (2002) TNF-α impairs heart and skeletal muscle protein synthesis by altering translation initiation. *American Journal of Physiology-Endocrinology and Metabolism* 282: E336-E347

Lautaoja JH, Lalowski M, Nissinen TA, Hentilä J, Shi Y, Ritvos O, Cheng S, Hulmi JJ (2019) Muscle and serum metabolomes are dysregulated in colon-26 tumor-bearing mice despite amelioration of cachexia with activin receptor type 2B ligand blockade. *American Journal of Physiology-Endocrinology And Metabolism* 316: E852-E865

Lecker SH, Goldberg AL, Mitch WE (2006) Protein degradation by the ubiquitin–proteasome pathway in normal and disease states. *Journal of the American society of nephrology* 17: 1807-1819

Leduc-Gaudet J-P, Mayaki D, Reynaud O, Broering FE, Chaffer TJ, Hussain SN, Gouspillou G (2020) Parkin overexpression attenuates sepsis-induced muscle wasting. *Cells* 9: 1454

Leduc-Gaudet JP, Reynaud O, Hussain SN, Gouspillou G (2019) Parkin overexpression protects from ageing-related loss of muscle mass and strength. *The Journal of physiology* 597: 1975-1991

Lee D, Goldberg AL (2013) SIRT1 Protein, by Blocking the Activities of Transcription Factors FoxO1 and FoxO3, Inhibits Muscle Atrophy and Promotes Muscle Growth*. *Journal of Biological Chemistry* 288: 30515-30526

Lee J, Ryu H, Ferrante RJ, Morris Jr SM, Ratan RR (2003) Translational control of inducible nitric oxide synthase expression by arginine can explain the arginine paradox. *Proceedings of the National Academy of Sciences* 100: 4843-4848

Li S, Gao D, Jiang Y (2019) Function, detection and alteration of acylcarnitine metabolism in hepatocellular carcinoma. *Metabolites* 9: 36

Li Y-P, Chen Y, John J, Moylan J, Jin B, Mann DL, Reid MB (2005) TNF-α acts via p38 MAPK to stimulate expression of the ubiquitin ligase atrogin1/MAFbx in skeletal muscle. *The FASEB Journal* 19: 362-370

Li Y-P, Reid MB (2000) NF-κB mediates the protein loss induced by TNF-α in differentiated skeletal muscle myotubes. *American Journal of Physiology-Regulatory, Integrative and Comparative Physiology* 279: R1165-R1170

Li Y, He Y, Miao K, Zheng Y, Deng C, Liu T-M (2020) Imaging of macrophage mitochondria dynamics in vivo reveals cellular activation phenotype for diagnosis. *Theranostics* 10: 2897

Liu T, Zhang L, Joo D, Sun S-C (2017) NF-κB signaling in inflammation. *Signal transduction and targeted therapy* 2: 1-9

Llovera M, Carbó N, López-Soriano Jn, García-Martínez C, Busquets Sl, Alvarez B, Agell N, Costelli P, López-Soriano FJ, Celada A (1998) Different cytokines modulate ubiquitin gene expression in rat skeletal muscle. *Cancer letters* 133: 83-87

Loumaye A, de Barsy M, Nachit M, Lause P, Frateur L, van Maanen A, Trefois P, Gruson D, Thissen J-P (2015) Role of Activin A and myostatin in human cancer cachexia. *The Journal of Clinical Endocrinology & Metabolism* 100: 2030-2038

Loumaye A, de Barsy M, Nachit M, Lause P, van Maanen A, Trefois P, Gruson D, Thissen JP (2017) Circulating Activin A predicts survival in cancer patients. *Journal of cachexia, sarcopenia and muscle* 8: 768-777

Loumaye A, Thissen J-P (2017) Biomarkers of cancer cachexia. *Clinical biochemistry* 50: 1281-1288

Ma JF, Sanchez BJ, Hall DT, Tremblay AMK, Di Marco S, Gallouzi IE (2017) STAT 3 promotes IFN γ/TNF α-induced muscle wasting in an NF-κB-dependent and IL-6-independent manner. *EMBO molecular medicine* 9: 622-637

MacMillan-Crow L, Crow JP, Kerby JD, Beckman JS, Thompson JA (1996) Nitration and inactivation of manganese superoxide dismutase in chronic rejection of human renal allografts. *Proceedings of the National Academy of Sciences* 93: 11853-11858

Mamane Y, Petroulakis E, LeBacquer O, Sonenberg N (2006) mTOR, translation initiation and cancer. *Oncogene* 25: 6416-6422

Martin L, Senesse P, Gioulbasanis I, Antoun S, Bozzetti F, Deans C, Strasser F, Thoresen L, Jagoe RT, Chasen M (2015) Diagnostic criteria for the classification of cancer-associated weight loss. *Journal of Clinical Oncology* 33: 90-99

Matthys P, Dukmans R, Proost P, Van Damme J, Heremans H, Sobis H, Billiau A (1991a) Severe cachexia in mice inoculated with interferon-γ-producing tumor cells. *International journal of cancer* 49: 77-82

Matthys P, Heremans H, Opdenakker G, Billiau A (1991b) Anti-interferon-γ antibody treatment, growth of Lewis lung tumours in mice and tumour-associated cachexia. *European Journal of Cancer and Clinical Oncology* 27: 182-187

McDonald JJ, McMillan DC, Laird BJ (2018) Targeting IL-1α in cancer cachexia: a narrative review. *Current opinion in supportive and palliative care* 12: 453-459

McGuirk S, Gravel S-P, Deblois G, Papadopoli DJ, Faubert B, Wegner A, Hiller K, Avizonis D, Akavia UD, Jones RG (2013) PGC-1α supports glutamine metabolism in breast cancer. *Cancer & metabolism* 1: 1-11

McLean JB, Moylan JS, Andrade FH (2014) Mitochondria dysfunction in lung cancer-induced muscle wasting in C2C12 myotubes. *Frontiers in physiology* 5: 503

Mesa RA, Verstovsek S, Gupta V, Mascarenhas JO, Atallah E, Burn T, Sun W, Sandor V, Gotlib J (2015) Effects of ruxolitinib treatment on metabolic and nutritional parameters in patients with myelofibrosis from COMFORT-I. *Clinical Lymphoma Myeloma and Leukemia* 15: 214-221. e211

Miller A, McLeod L, Alhayyani S, Szczepny A, Watkins D, Chen W, Enriori P, Ferlin W, Ruwanpura S, Jenkins B (2017) Blockade of the IL-6 trans-signalling/STAT3 axis suppresses cachexia in Kras-induced lung adenocarcinoma. *Oncogene* 36: 3059-3066

Miller J, Alshehri A, Ramage MI, Stephens NA, Mullen AB, Boyd M, Ross JA, Wigmore SJ, Watson DG, Skipworth RJ (2019) Plasma metabolomics identifies lipid and amino acid markers of weight loss in patients with upper gastrointestinal cancer. *Cancers* 11: 1594

Moarbes V, Mayaki D, Huck L, Leblanc P, Vassilakopoulos T, Petrof BJ, Hussain SN (2019) Differential regulation of myofibrillar proteins in skeletal muscles of septic mice. *Physiological Reports* 7: e14248

Mofarrahi M, Sigala I, Guo Y, Godin R, Davis EC, Petrof B, Sandri M, Burelle Y, Hussain SN (2012) Autophagy and skeletal muscles in sepsis.

Montagna C, Cirotti C, Rizza S, Filomeni G (2020) When S-nitrosylation gets to mitochondria: From signaling to age-related diseases. *Antioxidants & Redox Signaling* 32: 884-905

Mookerjee SA, Gerencser AA, Nicholls DG, Brand MD (2017) Quantifying intracellular rates of glycolytic and oxidative ATP production and consumption using extracellular flux measurements. *Journal of Biological Chemistry* 292: 7189-7207

Mookerjee SA, Gerencser AA, Nicholls DG, Brand MD (2018) Quantifying intracellular rates of glycolytic and oxidative ATP production and consumption using extracellular flux measurements. *Journal of Biological Chemistry* 293: 12649-12652

Mubaid S, Ma JF, Omer A, Ashour K, Lian XJ, Sanchez BJ, Robinson S, Cammas A, Dormoy-Raclet V, Di Marco S (2019) HuR counteracts miR-330 to promote STAT3 translation during inflammation-induced muscle wasting. *Proceedings of the National Academy of Sciences* 116: 17261-17270

Murphy KT, Chee A, Trieu J, Naim T, Lynch GS (2012) Importance of functional and metabolic impairments in the characterization of the C-26 murine model of cancer cachexia. *Disease models & mechanisms* 5: 533-545

Muscaritoli M, Anker S, Argiles J, Aversa Z, Bauer J, Biolo G, Boirie Y, Bosaeus I, Cederholm T, Costelli P (2010) Consensus definition of sarcopenia, cachexia and pre-cachexia: joint

document elaborated by Special Interest Groups (SIG)“cachexia-anorexia in chronic wasting diseases” and “nutrition in geriatrics”. *Clinical nutrition* 29: 154-159

Nakazawa H, Chang K, Shinozaki S, Yasukawa T, Ishimaru K, Yasuhara S, Yu Y-M, Martyn JJ, Tompkins RG, Shimokado K (2017) iNOS as a driver of inflammation and apoptosis in mouse skeletal muscle after burn injury: possible involvement of Sirt1 S-nitrosylation-mediated acetylation of p65 NF-κB and p53. *PloS one* 12: e0170391

Ni Y, Lohinai Z, Heshiki Y, Dome B, Moldvay J, Dulka E, Galffy G, Berta J, Weiss GJ, Sommer MO (2021) Distinct composition and metabolic functions of human gut microbiota are associated with cachexia in lung cancer patients. *The ISME journal* 15: 3207-3220

Nicolini A, Ferrari P, Masoni MC, Fini M, Pagani S, Giampietro O, Carpi A (2013) Malnutrition, anorexia and cachexia in cancer patients: a mini-review on pathogenesis and treatment. *Biomedicine & Pharmacotherapy* 67: 807-817

Nielsen TL, Vissing J, Krag TO (2021) Antimyostatin treatment in health and disease: The story of great expectations and limited success. *Cells* 10: 533

O’Connell TM, Ardeshirpour F, Asher SA, Winnike JH, Yin X, George J, Guttridge DC, He W, Wysong A, Willis MS (2008) Metabolomic analysis of cancer cachexia reveals distinct lipid and glucose alterations. *Metabolomics* 4: 216-225

Owen AM, Patel SP, Smith JD, Balasuriya BK, Mori SF, Hawk GS, Stromberg AJ, Kuriyama N, Kaneki M, Rabchevsky AG (2019) Chronic muscle weakness and mitochondrial dysfunction in the absence of sustained atrophy in a preclinical sepsis model. *Elife* 8: e49920

Padrão AI, Oliveira P, Vitorino R, Colaço B, Pires MJ, Márquez M, Castellanos E, Neuparth MJ, Teixeira C, Costa C (2013) Bladder cancer-induced skeletal muscle wasting: disclosing the role of mitochondria plasticity. *The international journal of biochemistry & cell biology* 45: 1399-1409

Palmieri EM, Gonzalez-Cotto M, Baseler WA, Davies LC, Ghesquière B, Maio N, Rice CM, Rouault TA, Cassel T, Higashi RM (2020) Nitric oxide orchestrates metabolic rewiring in M1 macrophages by targeting aconitase 2 and pyruvate dehydrogenase. *Nature communications* 11: 1-17

Patel HJ, Patel BM (2017) TNF-α and cancer cachexia: Molecular insights and clinical implications. *Life sciences* 170: 56-63

Peixoto da Silva S, Santos JM, Costa e Silva MP, Gil da Costa RM, Medeiros R (2020) Cancer cachexia and its pathophysiology: Links with sarcopenia, anorexia and asthenia. *Journal of cachexia, sarcopenia and muscle* 11: 619-635

Pelletier J, Graff J, Ruggero D, Sonenberg N (2015) Targeting the eIF4F translation initiation complex: a critical nexus for cancer development. *Cancer research* 75: 250-263

Penna F, Ballarò R, Beltrà M, De Lucia S, García Castillo L, Costelli P (2019a) The skeletal muscle as an active player against cancer cachexia. *Frontiers in physiology* 10: 41

Penna F, Ballaro R, Costelli P (2020) The redox balance: a target for interventions against muscle wasting in cancer cachexia? *Antioxidants & Redox Signaling* 33: 542-558

Penna F, Ballarò R, Martinez-Cristobal P, Sala D, Sebastian D, Busquets S, Muscaritoli M, Argilés JM, Costelli P, Zorzano A (2019b) Autophagy exacerbates muscle wasting in cancer cachexia and impairs mitochondrial function. *Journal of molecular biology* 431: 2674-2686

Petruzzelli M, Schweiger M, Schreiber R, Campos-Olivas R, Tsoli M, Allen J, Swarbrick M, Rose-John S, Rincon M, Robertson G (2014) A switch from white to brown fat increases energy expenditure in cancer-associated cachexia. *Cell metabolism* 20: 433-447

Pin F, Barreto R, Couch ME, Bonetto A, O'Connell TM (2019a) Cachexia induced by cancer and chemotherapy yield distinct perturbations to energy metabolism. *Journal of cachexia, sarcopenia and muscle* 10: 140-154

Pin F, Beltrà M, Garcia-Castillo L, Pardini B, Birolo G, Matullo G, Penna F, Guttridge D, Costelli P (2022) Extracellular vesicles derived from tumour cells as a trigger of energy crisis in the skeletal muscle. *Journal of cachexia, sarcopenia and muscle* 13: 481-494

Pin F, Novinger LJ, Huot JR, Harris RA, Couch ME, O'Connell TM, Bonetto A (2019b) PDK4 drives metabolic alterations and muscle atrophy in cancer cachexia. *The FASEB Journal* 33: 7778-7790

Porporato P (2016) Understanding cachexia as a cancer metabolism syndrome. *Oncogenesis* 5: e200-e200

Pötgens SA, Thibaut MM, Joudiou N, Sboarina M, Neyrinck AM, Cani PD, Claus SP, Delzenne NM, Bindels LB (2021) Multi-compartment metabolomics and metagenomics reveal major hepatic and intestinal disturbances in cancer cachectic mice. *Journal of cachexia, sarcopenia and muscle* 12: 456-475

Powers SK, Morton AB, Ahn B, Smuder AJ (2016) Redox control of skeletal muscle atrophy. *Free Radical Biology and Medicine* 98: 208-217

QuanJun Y, GenJin Y, LiLi W, Yan H, YongLong H, Jin L, Jie L, JinLu H, Cheng G (2015) Integrated analysis of serum and intact muscle metabonomics identify metabolic profiles of cancer cachexia in a dynamic mouse model. *RSC advances* 5: 92438-92448

Radi R (2018) Oxygen radicals, nitric oxide, and peroxynitrite: Redox pathways in molecular medicine. *Proceedings of the National Academy of Sciences* 115: 5839-5848

Ramamoorthy S, Donohue M, Buck M (2009) Decreased Jun-D and myogenin expression in muscle wasting of human cachexia. *American Journal of Physiology-Endocrinology and Metabolism* 297: E392-E401

Ramsey ML, Talbert E, Ahn D, Bekaii-Saab T, Badi N, Bloomston PM, Conwell DL, Cruz-Monserrate Z, Dillhoff M, Farren MR (2019) Circulating interleukin-6 is associated with disease progression, but not cachexia in pancreatic cancer. *Pancreatology* 19: 80-87

Remels A, Gosker H, Schrauwen P, Hommelberg P, Sliwinski P, Polkey M, Galdiz J, Wouters E, Langen R, Schols A (2010) TNF-α impairs regulation of muscle oxidative phenotype: implications for cachexia? *The FASEB Journal* 24: 5052-5062

Riccardi DMDR, das Neves RX, de Matos-Neto EM, Camargo RG, Lima JDCC, Radloff K, Alves MJ, Costa RGF, Tokeshi F, Otoch JP (2020) Plasma lipid profile and systemic inflammation in patients with cancer cachexia. *Frontiers in Nutrition*: 4

Roeland EJ, Bohlke K, Baracos VE, Bruera E, Del Fabbro E, Dixon S, Fallon M, Herrstedt J, Lau H, Platek M (2020) Management of cancer cachexia: ASCO guideline. *Journal of Clinical Oncology* 38: 2438-2453

Romanello V, Sandri M, 2022. Implications of mitochondrial fusion and fission in skeletal muscle mass and health, Seminars in Cell & Developmental Biology. Elsevier.

Romo D, Choi NS, Li S, Buchler I, Shi Z, Liu JO (2004) Evidence for separate binding and scaffolding domains in the immunosuppressive and antitumor marine natural product, pateamine a: design, synthesis, and activity studies leading to a potent simplified derivative. *Journal of the American Chemical Society* 126: 10582-10588

Rosca MG, Vazquez EJ, Chen Q, Kerner J, Kern TS, Hoppel CL (2012) Oxidation of fatty acids is the source of increased mitochondrial reactive oxygen species production in kidney cortical tubules in early diabetes. *Diabetes* 61: 2074-2083

Rose-John S (2018) Interleukin-6 family cytokines. *Cold Spring Harbor perspectives in biology* 10: a028415

Sadeghi M, Keshavarz-Fathi M, Baracos V, Arends J, Mahmoudi M, Rezaei N (2018) Cancer cachexia: Diagnosis, assessment, and treatment. *Critical reviews in oncology/hematology* 127: 91-104

Sakuma K, Aoi W, Yamaguchi A (2017) Molecular mechanism of sarcopenia and cachexia: recent research advances. *Pflügers Archiv-European Journal of Physiology* 469: 573-591

Sandri M, 2016. Protein breakdown in cancer cachexia, Seminars in cell & developmental biology. Elsevier, pp. 11-19.

Sartori R, Milan G, Patron M, Mammucari C, Blaauw B, Abraham R, Sandri M (2009) Smad2 and 3 transcription factors control muscle mass in adulthood. *American journal of physiology-cell physiology* 296: C1248-C1257

Sartori R, Romanello V, Sandri M (2021) Mechanisms of muscle atrophy and hypertrophy: Implications in health and disease. *Nature communications* 12: 1-12

Scherbakov N, Doehner W (2018) Cachexia as a common characteristic in multiple chronic disease. *Journal of cachexia, sarcopenia and muscle* 9: 1189

Seifert EL, Estey C, Xuan JY, Harper M-E (2010) Electron transport chain-dependent and-independent mechanisms of mitochondrial H2O2 emission during long-chain fatty acid oxidation. *Journal of Biological Chemistry* 285: 5748-5758

Seto DN, Kandarian SC, Jackman RW (2015) A key role for leukemia inhibitory factor in C26 cancer cachexia. *Journal of Biological Chemistry* 290: 19976-19986

Seymour M, Pétavy F, Chiesa F, Perry H, Lukey PT, Binks M, Donatien PD, Freidin AJ, Eckersley RJ, McClinton C (2012) Ultrasonographic measures of synovitis in an early phase clinical trial: a double-blind, randomised, placebo and comparator controlled phase IIa clinical trial of GW274150 (a selective inducible nitric oxide synthase inhibitor) in rheumatoid arthritis. *Clinical and Experimental Rheumatology-Incl Supplements* 30: 254

Shinozaki S, Chang K, Sakai M, Shimizu N, Yamada M, Tanaka T, Nakazawa H, Ichinose F, Yamada Y, Ishigami A (2014) Inflammatory stimuli induce inhibitory S-nitrosylation of the deacetylase SIRT1 to increase acetylation and activation of p53 and p65. *Science signaling* 7: ra106-ra106

Shukla SK, Markov SD, Attri KS, Vernucci E, King RJ, Dasgupta A, Grandgenett PM, Hollingsworth MA, Singh PK, Yu F (2020) Macrophages potentiate STAT3 signaling in skeletal muscles and regulate pancreatic cancer cachexia. *Cancer letters* 484: 29-39

Shum AM, Mahendradatta T, Taylor RJ, Painter AB, Moore MM, Tsoli M, Tan TC, Clarke SJ, Robertson GR, Polly P (2012) Disruption of MEF2C signaling and loss of sarcomeric and mitochondrial integrity in cancer-induced skeletal muscle wasting. *Aging (Albany NY)* 4: 133

Shyh-Chang N (2017) Metabolic changes during cancer cachexia pathogenesis. *Translational Research in Breast Cancer*: 233-249

Siddiqui JA, Pothuraju R, Jain M, Batra SK, Nasser MW (2020) Advances in cancer cachexia: Intersection between affected organs, mediators, and pharmacological interventions. *Biochimica et Biophysica Acta (BBA)-Reviews on Cancer* 1873: 188359

Silva KAS, Dong J, Dong Y, Dong Y, Schor N, Tweardy DJ, Zhang L, Mitch WE (2015) Inhibition of Stat3 activation suppresses caspase-3 and the ubiquitin-proteasome system, leading to preservation of muscle mass in cancer cachexia. *Journal of Biological Chemistry* 290: 11177-11187

Singh K, Lin J, Lecomte N, Mohan P, Gokce A, Sanghvi VR, Jiang M, Grbovic-Huezo O, Burčul A, Stark SG (2021) Targeting eIF4A-dependent translation of KRAS signaling molecules. *Cancer research* 81: 2002-2014

Smith RC, Cramer MS, Mitchell PJ, Capen A, Huber L, Wang R, Myers L, Jones BE, Eastwood BJ, Ballard D (2015) Myostatin neutralization results in preservation of muscle mass and strength in preclinical models of tumor-induced muscle wasting. *Molecular Cancer Therapeutics* 14: 1661-1670

Socher SH, Martinez D, Craig JB, Kuhn JG, Oliff A (1988) Tumor necrosis factor not detectable in patients with clinical cancer cachexia. *JNCI: Journal of the National Cancer Institute* 80: 595-598

Soda K, Kawakami M, Kashii A, Miyata M (1995) Manifestations of cancer cachexia induced by colon 26 adenocarcinoma are not fully ascribable to interleukin-6. *International journal of cancer* 62: 332-336

Solheim TS, Laird BJ, Balstad TR, Bye A, Stene G, Baracos V, Strasser F, Griffiths G, Maddocks M, Fallon M (2018) Cancer cachexia: rationale for the MENAC (Multimodal—Exercise, Nutrition and Anti-inflammatory medication for Cachexia) trial. *BMJ supportive & palliative care* 8: 258-265

Springer J, Von Haehling S, Anker SD (2006) The need for a standardized definition for cachexia in chronic illness. *Nature clinical practice Endocrinology & metabolism* 2: 416-417

Stana F, Vujovic M, Mayaki D, Leduc-Gaudet J-P, Leblanc P, Huck L, Hussain SN (2017) Differential regulation of the autophagy and proteasome pathways in skeletal muscles in sepsis. *Critical Care Medicine* 45: e971-e979

Stein SC, Woods A, Jones NA, Davison MD, Carling D (2000) The regulation of AMP-activated protein kinase by phosphorylation. *Biochemical Journal* 345: 437-443

Stephens NA, Skipworth RJ, Fearon KC (2008) Cachexia, survival and the acute phase response. *Current opinion in supportive and palliative care* 2: 267-274

Strassmann G, Fong M, Kenney J, Jacob C (1992) Evidence for the involvement of interleukin 6 in experimental cancer cachexia. *The Journal of clinical investigation* 89: 1681-1684

Stretch C, Eastman T, Mandal R, Eisner R, Wishart DS, Mourtzakis M, Prado CM, Damaraju S, Ball RO, Greiner R (2012) Prediction of skeletal muscle and fat mass in patients with advanced cancer using a metabolomic approach. *The Journal of nutrition* 142: 14-21

Suh J, Lee Y-S (2020) Similar sequences but dissimilar biological functions of GDF11 and myostatin. *Experimental & molecular medicine* 52: 1673-1693

Taroncher-Oldenburg G, Müller C, Obermann W, Ziebuhr J, Hartmann RK, Grünweller A (2021) Targeting the DEAD-box RNA helicase eIF4A with rocaglates—a pan-antiviral strategy for minimizing the impact of future RNA virus pandemics. *Microorganisms* 9: 540

Thornalley PJ (2003) Use of aminoguanidine (Pimagedine) to prevent the formation of advanced glycation endproducts. *Archives of biochemistry and biophysics* 419: 31-40

Tisdale MJ (1997) Biology of cachexia. *Journal of the National Cancer Institute* 89: 1763-1773

Tisdale MJ (2008) Catabolic mediators of cancer cachexia. *Current opinion in supportive and palliative care* 2: 256-261

Tisdale MJ (2009) Mechanisms of cancer cachexia. *Physiological reviews* 89: 381-410

Tomasin R, Martin ACBM, Cominetti MR (2019) Metastasis and cachexia: alongside in clinics, but not so in animal models. *Journal of cachexia, sarcopenia and muscle* 10: 1183-1194

Tseng Y-C, Kulp SK, Lai I-L, Hsu E-C, He WA, Frankhouser DE, Yan PS, Mo X, Bloomston M, Lesinski GB (2015) Preclinical investigation of the novel histone deacetylase inhibitor AR-42 in the treatment of cancer-induced cachexia. *Journal of the National Cancer Institute* 107: djv274

Vander Heiden MG, Cantley LC, Thompson CB (2009) Understanding the Warburg effect: the metabolic requirements of cell proliferation. *science* 324: 1029-1033

VanderVeen BN, Fix DK, Carson JA (2017) Disrupted skeletal muscle mitochondrial dynamics, mitophagy, and biogenesis during cancer cachexia: a role for inflammation. *Oxidative medicine and cellular longevity* 2017

VanderVeen BN, Fix DK, Montalvo RN, Counts BR, Smuder AJ, Murphy EA, Koh Hj, Carson JA (2019) The regulation of skeletal muscle fatigability and mitochondrial function by chronically elevated interleukin-6. *Experimental physiology* 104: 385-397

VanderVeen BN, Hardee JP, Fix DK, Carson JA (2018) Skeletal muscle function during the progression of cancer cachexia in the male ApcMin/+ mouse. *Journal of applied physiology* 124: 684-695

Verstovsek S, Gotlib J, Mesa RA, Vannucchi AM, Kiladjian J-J, Cervantes F, Harrison CN, Paquette R, Sun W, Naim A (2017) Long-term survival in patients treated with ruxolitinib for myelofibrosis: COMFORT-I and-II pooled analyses. *Journal of hematology & oncology* 10: 1-6

Vigano A, Del Fabbro E, Bruera E, Borod M (2012) The cachexia clinic: from staging to managing nutritional and functional problems in advanced cancer patients. *Critical Reviews™ in Oncogenesis* 17

Vigano AA, Morais JA, Ciutto L, Rosenthall L, di Tomasso J, Khan S, Olders H, Borod M, Kilgour RD (2017) Use of routinely available clinical, nutritional, and functional criteria to classify cachexia in advanced cancer patients. *Clinical nutrition* 36: 1378-1390

Víteček J, Lojek A, Valacchi G, Kubala L (2012) Arginine-based inhibitors of nitric oxide synthase: therapeutic potential and challenges. *Mediators of inflammation* 2012

von Haehling S, Anker MS, Anker SD, 2016. Prevalence and clinical impact of cachexia in chronic illness in Europe, USA, and Japan: facts and numbers update 2016. Wiley Online Library, pp. 507-509.

von Haehling S, Genth-Zotz S, Anker S, Volk H (2002) Cachexia: a therapeutic approach beyond cytokine antagonism. *International journal of cardiology* 85: 173-183

Voronov E, Dotan S, Krelin Y, Song X, Elkabets M, Carmi Y, Rider P, Cohen I, Romzova M, Kaplanov I *et al* (2013) Unique Versus Redundant Functions of IL-1α and IL-1β in the Tumor Microenvironment. *Frontiers in Immunology* 4

Webster JM, Kempen LJ, Hardy RS, Langen RC (2020) Inflammation and skeletal muscle wasting during cachexia. *Frontiers in physiology*: 1449

White JP, Puppa MJ, Gao S, Sato S, Welle SL, Carson JA (2013) Muscle mTORC1 suppression by IL-6 during cancer cachexia: a role for AMPK. *American Journal of Physiology-Endocrinology and Metabolism* 304: E1042-E1052

White JP, Puppa MJ, Sato S, Gao S, Price RL, Baynes JW, Kostek MC, Matesic LE, Carson JA (2012) IL-6 regulation on skeletal muscle mitochondrial remodeling during cancer cachexia in the Apc Min/+ mouse. *Skeletal muscle* 2: 1-16

Wiedenmann B, Malfertheiner P, Friess H, Ritch P, Arseneau J, Mantovani G, Caprioni F, Van Cutsem E, Richel D, DeWitte M (2008) A multicenter, phase II study of infliximab plus gemcitabine in pancreatic cancer cachexia. *The journal of supportive oncology* 6: 18-25

Wolfe AL, Singh K, Zhong Y, Drewe P, Rajasekhar VK, Sanghvi VR, Mavrakis KJ, Jiang M, Roderick JE, Van der Meulen J (2014) RNA G-quadruplexes cause eIF4A-dependent oncogene translation in cancer. *Nature* 513: 65-70

Wyart E, Hsu MY, Sartori R, Mina E, Rausch V, Pierobon ES, Mezzanotte M, Pezzini C, Bindels LB, Lauria A (2022) Iron supplementation is sufficient to rescue skeletal muscle mass and function in cancer cachexia. *EMBO reports* 23: e53746

Wyke SM, Tisdale MJ (2005) NF-κB mediates proteolysis-inducing factor induced protein degradation and expression of the ubiquitin–proteasome system in skeletal muscle. *British journal of cancer* 92: 711-721

Wysong A, Couch M, Shadfar S, Li L, Rodriguez JE, Asher S, Yin X, Gore M, Baldwin A, Patterson C (2011) NF-κB inhibition protects against tumor-induced cardiac atrophy in vivo. *The American journal of pathology* 178: 1059-1068

Xie K, Xiong H, Xiao W, Xiong Z, Hu W, Ye J, Xu N, Shi J, Yuan C, Chen Z (2021) Downregulation of miR-29c promotes muscle wasting by modulating the activity of leukemia inhibitory factor in lung cancer cachexia. *Cancer cell international* 21: 1-14

Xu W, Ghosh S, Comhair SA, Asosingh K, Janocha AJ, Mavrakis DA, Bennett CD, Gruca LL, Graham BB, Queisser KA (2016) Increased mitochondrial arginine metabolism supports bioenergetics in asthma. *The Journal of clinical investigation* 126: 2465-2481

Yang QJ, Zhao JR, Hao J, Li B, Huo Y, Han YL, Wan LL, Li J, Huang J, Lu J (2018) Serum and urine metabolomics study reveals a distinct diagnostic model for cancer cachexia. *Journal of cachexia, sarcopenia and muscle* 9: 71-85

Ye Z, Wang S, Zhang C, Zhao Y (2020) Coordinated modulation of energy metabolism and inflammation by branched-chain amino acids and fatty acids. *Frontiers in endocrinology*: 617

Yoon S, Woo S, Kang J, Kim K, Shin H, Gwak H, Park S, Chwae Y (2012) NF-κB and STAT3 cooperatively induce IL6 in starved cancer cells. *Oncogene* 31: 3467-3481

Yu H, Pardoll D, Jove R (2009) STATs in cancer inflammation and immunity: a leading role for STAT3. *Nature reviews cancer* 9: 798-809

Zhang C, Liu J, Wang J, Hu W, Feng Z (2021) The emerging role of leukemia inhibitory factor in cancer and therapy. *Pharmacology & Therapeutics* 221: 107754

Zhang L, Pan J, Dong Y, Tweardy DJ, Dong Y, Garibotto G, Mitch WE (2013) Stat3 activation links a C/EBPδ to myostatin pathway to stimulate loss of muscle mass. *Cell metabolism* 18: 368-379

Zhang S, Hulver MW, McMillan RP, Cline MA, Gilbert ER (2014) The pivotal role of pyruvate dehydrogenase kinases in metabolic flexibility. *Nutrition & Metabolism* 11: 10

Zhang X, Bi C, Lu T, Zhang W, Yue T, Wang C, Tian T, Zhang X, Huang Y, Lunning M (2020) Targeting translation initiation by synthetic rocaglates for treating MYC-driven lymphomas. *Leukemia* 34: 138-150

Zhou L, Zhang T, Shao W, Lu R, Wang L, Liu H, Jiang B, Li S, Zhuo H, Wang S (2021) Amiloride ameliorates muscle wasting in cancer cachexia through inhibiting tumor-derived exosome release. *Skeletal muscle* 11: 1-16

Zhou T, Wang B, Liu H, Yang K, Thapa S, Zhang H, Li L, Yu S (2018) Development and validation of a clinically applicable score to classify cachexia stages in advanced cancer patients. *Journal of Cachexia, Sarcopenia and Muscle* 9: 306-314

Zhou W, Jiang Z-W, Tian J, Jiang J, Li N, Li J-S (2003) Role of NF-κB and cytokine in experimental cancer cachexia. *World Journal of Gastroenterology: WJG* 9: 1567

Zhou X, Wang JL, Lu J, Song Y, Kwak KS, Jiao Q, Rosenfeld R, Chen Q, Boone T, Simonet WS (2010) Reversal of cancer cachexia and muscle wasting by ActRIIB antagonism leads to prolonged survival. *Cell* 142: 531-543

Zimmers TA, Davies MV, Koniaris LG, Haynes P, Esquela AF, Tomkinson KN, McPherron AC, Wolfman NM, Lee S-J (2002) Induction of cachexia in mice by systemically administered myostatin. *Science* 296: 1486-1488

Zimmers TA, Fishel ML, Bonetto A, 2016. STAT3 in the systemic inflammation of cancer cachexia, Seminars in cell & developmental biology. Elsevier, pp. 28-41.

Zimmers TA, Jiang Y, Wang M, Liang TW, Rupert JE, Au ED, Marino FE, Couch ME, Koniaris LG (2017) Exogenous GDF11 induces cardiac and skeletal muscle dysfunction and wasting. *Basic research in cardiology* 112: 1-12